

PB86152089



# BEHAVIOR OF PILES AND PILE GROUPS IN COHESIONLESS SOILS

Research, Development,  
and Technology

Turner-Fairbank Highway  
Research Center  
6300 Georgetown Pike  
McLean, Virginia 22101

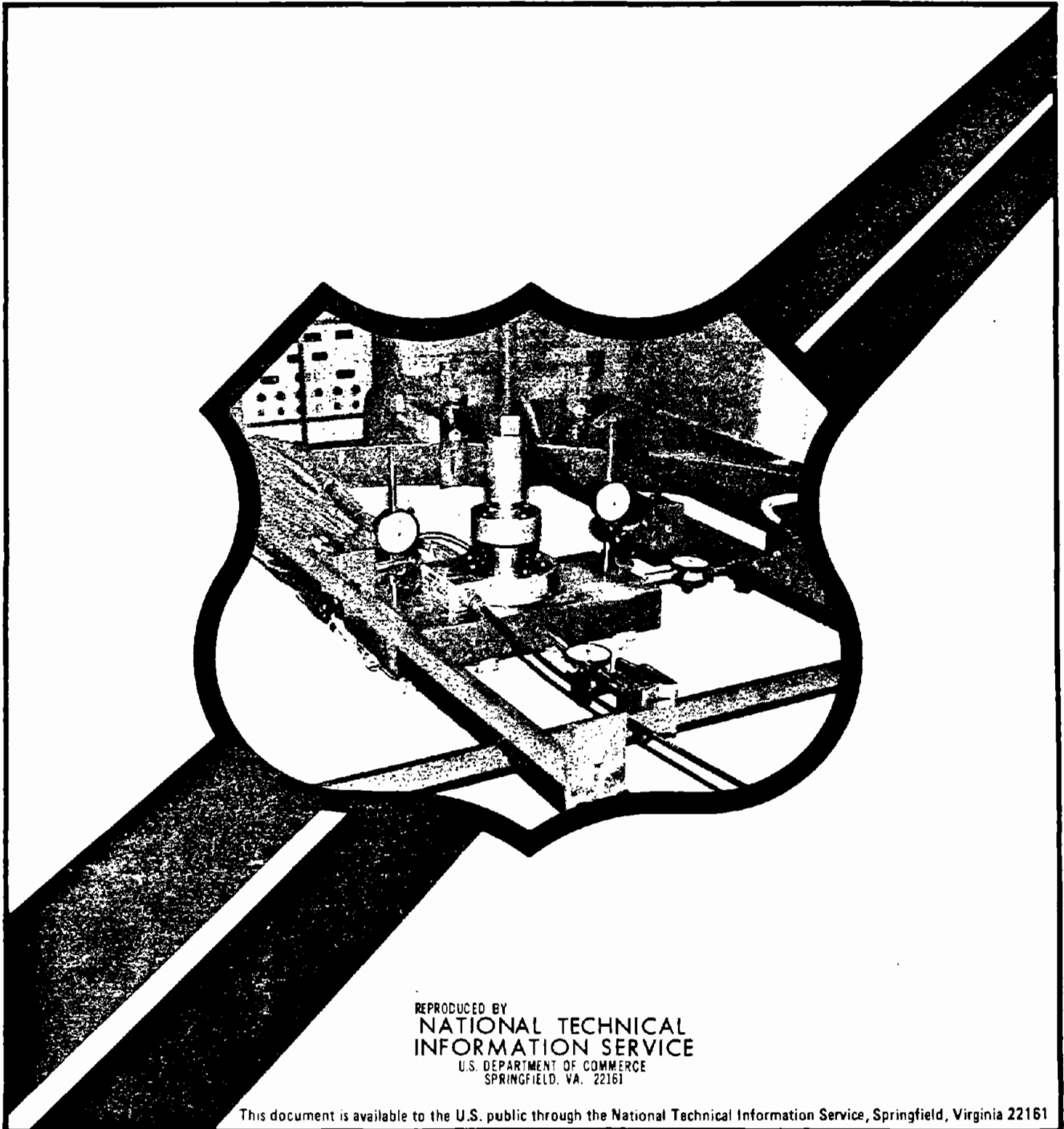


U.S. Department  
of Transportation

**Federal Highway  
Administration**

Report No.  
FHWA/RD-83/038

Final Report  
July 1985



REPRODUCED BY  
**NATIONAL TECHNICAL  
INFORMATION SERVICE**  
U.S. DEPARTMENT OF COMMERCE  
SPRINGFIELD, VA. 22161

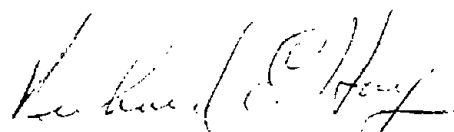
This document is available to the U.S. public through the National Technical Information Service, Springfield, Virginia 22161

## FOREWORD

This report describes the results of an in-depth study of pile load test data to determine the behavior of piles and pile groups in cohesionless soils. The report will be of interest to other researchers concerned with load transfer characteristics of piles in cohesionless soils beneath bridge foundations and other structural foundations.

This report presents the results of a Texas A&M University research project, "Behavior of Piles and Pile Groups in Cohesionless Soils." The program was conducted for the Federal Highway Administration, Office of Engineering and Highway Operations Research and Development, Washington, D.C., under contract DTFH61-82-C-0038. The study was jointly sponsored by the U.S. Geological Survey, Reston, Virginia. The final report covers the period from October 1, 1982 to October 26, 1983.

The problem of residual driving stresses was analyzed to determine the relevant importance in load transfer behavior and the formulation of pile capacity design methods. A new predictive method which considers residual driving stresses was developed and presented in this report. Actual field load tests on piles in cohesionless soils will be conducted in a follow-on study to investigate the new design method and residual stress theory. This report is being distributed to research and development audiences. Additional copies are available from the National Technical Information Service (NTIS), U.S. Department of Commerce, 5285 Port Royal Road, Springfield, Virginia 22161. A small charge is imposed for copies provided by NTIS.



Richard E. Hay, Director  
Office of Engineering  
and Highway Operations  
Research and Development

## NOTICE

This document is disseminated under the sponsorship of the Department of Transportation in the interest of information exchange. The United States Government assumes no liability for its contents or use thereof. The contents of this report reflect the views of the contractor, who is responsible for the accuracy of the data presented herein. The contents do not necessarily reflect the official policy of the Department of Transportation. This report does not constitute a standard, specification, or regulation.

The United States Government does not endorse products or manufacturers. Trade or manufacturers' names appear herein only because they are considered essential to the object of this document.

1. Report No. FHWA/RD-83/038		2. Government Accession No.		3. Report's Catalog No. PB86 152089 VAS	
4. Title and Subtitle BEHAVIOR OF PILES AND PILE GROUPS IN COHESIONLESS SOILS.				5. Report Date July 1985	
				6. Performing Organization Code	
7. Author(s) J.-L Briaud, L. Tucker, R.L. Lytton, H.M. Coyle				8. Performing Organization Report No.	
9. Performing Organization Name and Address Texas Transportation Institute and Civil Engineering Department Texas A&M University College Station, TX 77843				10. Work Unit No. FCP No. 35P1182	
				11. Contract or Grant No. DTFH61- 82 - C - 0038	
12. Sponsoring Agency Name and Address Federal Highway Administration Office of Research - Materials Division Washington, D.C. 20590				13. Type of Report and Period Covered Final Report on Task A	
				14. Sponsoring Agency Code CME-0150	
15. Supplementary Notes FHWA Technical Contact: Carl Ealy (HNR-30) Special Consultants: R.A. Hawkins, Lee L. Lowery, Jr., M. W. O'Neill					
16. Abstract  In order to gain a better understanding of the behavior of piles in sand, an extensive search of the literature has been performed to collect data on instrumented piles driven in sand and tested under vertical loads. The load transfer characteristics of the piles were then analyzed without considering residual stresses. Wherever the data allowed it, the load transfer analysis was repeated after considering residual stresses. The results of this analysis were correlated with the available soil data to obtain a predictive method which considers residual driving stresses. The results of this method as well as conventional and new in situ tests methods were then compared to actual load test results. Areas of critical need for further research are pointed out and recommendations are made for their implementation.					
17. Key Words Piles-Driven-Sand-Residual Stresses- Deep Foundations-Ultimate Capacity-Wave Equation-Standard Penetration Test- Pressuremeter-Cone Penetrometer.			18. Distribution Statement No restriction. This document is available to the U.S. Public through the National Technical Information Service, Springfield, Virginia, 22161		
19. Security Classif. (of this report) Unclassified		20. Security Classif. (of this page) Unclassified		21. No. of Pages 237	22. Price

CONVERSION FACTORS, U. S. CUSTOMARY TO METRIC (SI)  
UNITS OF MEASUREMENT

U. S. customary units of measurement used in this report can be converted to metric (SI) units as follows:

Multiply	by	To Obtain
Angstroms	0.0000001 ( $10^{-7}$ )	millimetres
inches	2.54	centimetres
feet	0.3048	metres
miles (U.S. Statute)	1.609344	kilometres
square inches	0.00064516	square metres
square feet	0.09290304	square metres
cubic feet	0.02831685	cubic metres
cubic yards	0.7645549	cubic metres
grams	0.001	kilograms
pounds (mass)	0.4535924	kilograms
tons (2000 pounds)	907.1847	kilograms
pounds (mass) per cubic foot	16.01846	kilograms per cubic metre
pounds (mass) per cubic yard	0.59327631	kilograms per cubic metre
pounds (force)	4.448222	newtons
pounds (force) per square inch	6894.757	pascals
pounds (force) per square foot	4.882428	kilograms per square metre
miles per hour	1.609344	kilometres per hour
degrees (angle)	0.01745329	radians
Fahrenheit degrees	5/9	Celsius degrees or Kelvins*

---

\* To obtain Celsius (c) temperature readings from Fahrenheit (f) readings, use the following formula:  $C = (5/9)(F - 32)$ . To obtain Kelvin (K) readings, use:  $K = (5/9)(F - 32) + 273.15$ .

TABLE OF CONTENTS

	<u>Page</u>
CHAPTER I INTRODUCTION . . . . .	1
CHAPTER II PILE LOAD TESTS SELECTED . . . . .	2
Load Tests and Instrumentation . . . . .	2
Failure Criteria . . . . .	7
CHAPTER III CONVENTIONAL LOAD TRANSFER ANALYSIS . . . . .	12
Incremental Method . . . . .	12
Average Method . . . . .	14
Analysis . . . . .	14
Hyperbolic Regression . . . . .	30
CHAPTER IV RESIDUAL STRESSES: BASIC CONSIDERATIONS . . . . .	34
The Phenomenon . . . . .	34
Influencing Factors . . . . .	34
Theoretical Formulation . . . . .	36
Discussion of the Theoretical Formulation . . . . .	42
Example of Theoretical Residual Loads . . . . .	42
Extension of the Results to the Tension Test . . . . .	44
Conclusions . . . . .	47
CHAPTER V OBTAINING RESIDUAL STRESSES FROM LOAD TESTS. . . . .	48
Conventional Load Tests . . . . .	48
Existence of Residual Stresses . . . . .	48
Measuring Residual Stresses . . . . .	52
<u>Method 1: Read Instrumentation Before and</u>	
<u>After Driving</u> . . . . .	52
<u>Method 2. Hunter-Davisson Method</u> . . . . .	53
<u>Method 3: No Unloading Reading Method</u> . . . . .	55
<u>Method 4: No Instrumentation Method</u> . . . . .	55
Residual Stresses: Load Test Results . . . . .	56
CHAPTER VI OBTAINING RESIDUAL STRESSES FROM THE WAVE EQUATION . . . . .	59
General . . . . .	59
The Model . . . . .	59
Obtaining Residual Stresses . . . . .	59
Results . . . . .	62
Hyperbolic Soil Model . . . . .	68
CHAPTER VII LOAD TRANSFER ANALYSIS BY FINITE DIFFERENCE-PATTERN SEARCH APPROACH . . . . .	70
Introduction . . . . .	70
Numerical Approximation of Differential Equation . . . . .	70

TABLE OF CONTENTS (Continued)

	<u>Page</u>
Summary of Pile Analysis . . . . .	75
<u>Residual Stress Properties</u> . . . . .	75
<u>Soil-Pile Shear Stiffness and</u>	
<u>Strength Properties</u> . . . . .	77
<u>Pile Point-Soil Stiffness and</u>	
<u>Strength Properties</u> . . . . .	77
Conclusions . . . . .	79
 CHAPTER VIII A NEW DESIGN METHOD CONSIDERING RESIDUAL STRESSES . . . . .	 82
General . . . . .	82
The Real Meaning of Residual Stresses . . . . .	82
Correlations . . . . .	84
<u>Residual Driving Stresses</u> . . . . .	84
<u>Point Load - Point Movement Characteristics</u> . .	86
<u>Side Friction - Pile Movement Characteristics</u> . .	89
Low Displacement Piles (H-Piles). . . . .	93
A New Design Method . . . . .	93
<u>Ultimate Capacity</u> . . . . .	93
<u>Load Transfer Curves</u> . . . . .	95
Axially Loaded Pile Program . . . . .	96
 CHAPTER IX PREDICTIONS BY CONVENTIONAL METHODS . . . . .	 100
Predictions of Ultimate Capacity . . . . .	100
<u>API Method</u> . . . . .	101
<u>Meyerhof Method</u> . . . . .	101
<u>Coyle-Castello Method</u> . . . . .	103
<u>Comparison of Ultimate Capacity Predictions</u> . .	107
Predictions of Load-Settlement Behavior . . . . .	115
<u>Coyle t-z Curve Method</u> . . . . .	115
<u>Briaud-Tucker Method</u> . . . . .	117
<u>Comparison of the Results</u> . . . . .	118
 CHAPTER X PREDICTION BY THE CONE PENETROMETER AND PRESSUREMETER METHODS . . . . .	 142
Pressuremeter Methods . . . . .	142
<u>Ultimate Capacity</u> . . . . .	142
<u>Load-Settlement Curve</u> . . . . .	151
Cone Penetrometer Methods . . . . .	160
<u>Ultimate Capacity</u> . . . . .	160
<u>Load-Settlement Curve</u> . . . . .	167
Comparison of the Results . . . . .	169
 CHAPTER XI IMPROVING THE STATE OF THE PRACTICE . . . . .	 193
Results of Interviews . . . . .	193
Precision on the Soil Parameters . . . . .	196
Cost Saving Aspect . . . . .	197

TABLE OF CONTENTS (Continued)

	<u>Page</u>
<u>Considering Residual Stresses</u> . . . . .	197
<u>Developing an Optimum Method of Design</u> . . . . .	199
CHAPTER XII SUMMARY, CONCLUSIONS AND RECOMMENDATIONS . . . . .	204
Summary and Conclusion . . . . .	204
<u>Pile Load Tests Selected</u> . . . . .	204
<u>Conventional Load Transfer Analysis</u> . . . . .	205
<u>Residual Stresses: Basic Considerations</u> . . . . .	206
<u>Obtaining Residual Stresses from Load Tests</u> . . . . .	206
<u>Obtaining Residual Stresses with the Wave</u>	
<u>Equation</u> . . . . .	207
<u>Load Transfer Analysis by Finite</u>	
<u>Difference-Pattern Search Approach</u> . . . . .	207
<u>A New Design Method Considering Residual</u>	
<u>Stresses</u> . . . . .	208
<u>Predictions by Conventional Methods</u> . . . . .	210
<u>Prediction by the Cone Penetrometer</u>	
<u>and the Pressuremeter Methods</u> . . . . .	210
<u>Improving the State of the Practice</u> . . . . .	211
Recommendations for Further Research . . . . .	212
REFERENCES . . . . .	214

LIST OF FIGURES

1. Example of Pile Instrumentation . . . . .	6
2. Example of Davisson and $0.1xD$ Failure Criteria . . . . .	8
3. Segmentation of Pile for Incremental Load Transfer Analysis . . . . .	13
4. Arkansas River Pile 1 Compression Test: Load Distribution, Incremental Analyses . . . . .	15
5. Arkansas River Pile 1 Compression Test: f-z Curves, Incremental Analysis . . . . .	16
6. Arkansas River Pile 1 Compression Test: Percent Point Load Versus Top Load, Incremental Analysis . . . . .	17
7. Arkansas River Pile 1 Compression Test: f-w Curves, Incremental Analysis . . . . .	18
8. Arkansas River Pile 1 Compression Test: Q-w Curve, Incremental Analysis . . . . .	19

LIST OF FIGURES (Continued)

	<u>Page</u>
9. Arkansas River Pile 1 Compression Test: $f/f_{\max}$ - w Curves, Incremental Analysis . . . . .	20
10. Arkansas River Pile 1 Compression Test: $f/f_{\max}$ - w/R Curves, Incremental Analysis . . . . .	21
11. Ogeechee River Site: Comparison of Incremental and Average Analyses . . . . .	23
12. Arkansas River Pile 1 Compression Test: Load Distribution, Average Analysis . . . . .	24
13. Arkansas River Pile 1 Compression Test: Percent Point Load Versus Top Load, Average Analysis . . . . .	25
14. Arkansas River Pile 1 Compression Test: f-w Curve, Average Analysis . . . . .	26
15. Arkansas River Pile 1 Compression Test: Q-w Curve, Average Analysis . . . . .	27
16. Arkansas River Pile 1 Compression Test: $f/f_{\max}$ - w Curve, Average Analysis . . . . .	28
17. Arkansas River Pile 1 Compression Test: $f/f_{\max}$ - w/R Curve, Average Analysis . . . . .	29
18. Arkansas River Pile 1: Hyperbolic Regression for f-w Curve . . . . .	31
19. Ultimate Loads and Residual Loads . . . . .	35
20. Unloading Process for Residual Loads . . . . .	38
21. Sign Convention for Theoretical Formulation . . . . .	39
22. Example of Theoretical Residual Loads . . . . .	45
23. Example of Theoretical Residual Load after a Tension Test . . . . .	46
24. Load in Pile During Compression Test . . . . .	49
25. Load in Pile During Tension Test . . . . .	50
26. Comparison of Residual Loads in Vibrated and Driven Piles . . . . .	51
27. Hunter-Davisson Method for Residual Load Correction . . . . .	54



LIST OF FIGURES (Continued)

	<u>Page</u>
28. Comparison of the Friction Load in Tension and in Compression . . . . .	58
29. Pile and Soil Idealization for Use in the Wave Equation . . . . .	60
30. Smith's Soil Model . . . . .	61
31. Variation of Point Load with Time for Six Hammer Blows . . . . .	63
32. Obtaining Residual Point load from Wave Equation Results . . . . .	64
33. Residual Point Load Versus Blowcount . . . . .	65
34. Comparison of Predicted Versus Measured Residual Point Load Using Blowcount Correlation . . . . .	66
35. Arkansas River Pile 3: Residual Point Load Versus Static Soil Resistance . . . . .	67
36. Comparison of Predicted Versus Measured Residual Point Load Using Ultimate Resistance Correlation . . . . .	69
37. Loads in a Pile Before and After Loading . . . . .	71
38. Differential Element for a Pile . . . . .	72
39. Illustration of Soil Constitutive Equation . . . . .	73
40. Residual Point Pressure Versus $L\beta$ . . . . .	85
41. $q/N_{pt}$ Versus $(w/D \times 100)$ . . . . .	88
42. $\text{Log}(q_{\max})$ Versus $\text{Log}(N_{pt})$ . . . . .	90
43. $\text{Log}(K_p)$ Versus $\text{Log}(N_{pt})$ . . . . .	91
44. $\text{Log}(f_{\max})$ Versus $\text{Log}(N_{\text{side}})$ . . . . .	92
45. $\text{Log}(K_t)$ Versus $\text{Log}(N_{\text{side}})$ . . . . .	94
46. Examples of Hyperbolic Load Transfer Curves . . . . .	97
47. Elastic Compression of Pile Under Residual State of Stress . . . . .	99
48. Coyle-Castello Method: $f_s$ Versus $L/D$ . . . . .	104
49. Coyle-Castello Method: $q_0$ Versus $L/D$ . . . . .	105

LIST OF FIGURES (Continued)

		<u>Page</u>
50.	Frequency Distribution . API Code . Total Load . . . . .	110
51.	Frequency Distribution . Meyerhof Method . Total Load . . . . .	111
52.	Frequency Distribution . Coyle-Castello Method. Total Load . . . . .	112
53.	Frequency Distribution . Coyle-Castello Method . Total Load . . . . .	113
54.	Arkansas River Pile 1: Load-Settlement Predictions by Coyle and Briaud-Tucker Methods . . . . .	119
55.	Arkansas River Pile 2: Load-Settlement Predictions by Coyle and Briaud-Tucker Methods . . . . .	120
56.	Arkansas River Pile 3: Load-Settlement Predictions by Coyle and Briaud-Tucker Methods . . . . .	121
57.	Arkansas River Pile 10: Load-Settlement Predictions by Coyle and Briaud-Tucker Methods . . . . .	122
58.	Arkansas River Pile 16: Load-Settlement Predictions by Coyle and Briaud-Tucker Methods . . . . .	123
59.	Low Sill Structure Pile 2: Load-Settlement Predictions by Coyle and Briaud-Tucker Methods. . . . .	124
60.	Low Sill Structure Pile 4: Load-Settlement Predictions by Coyle and Briaud-Tucker Methods . . . . .	125
61.	Low Sill Structure Pile 5: Load-Settlement Predictions by Coyle and Briaud-Tucker Methods . . . . .	126
62.	Low Sill Structure Pile 6: Load-Settlement Predictions by Coyle and Briaud-Tucker Methods . . . . .	127
63.	Ogeechee River Pile H-11: Load-Settlement Predictions by Coyle and Briaud-Tucker Methods . . . . .	128
64.	Ogeechee River Pile H-12: Load-Settlement Predictions by Coyle and Briaud-Tucker Methods . . . . .	129
65.	Ogeechee River Pile H-13: Load-Settlement Predictions by Coyle and Briaud-Tucker Methods . . . . .	130
66.	Ogeechee River Pile H-14: Load-Settlement Predictions by Coyle and Briaud-Tucker Methods . . . . .	131
67.	Ogeechee River Pile H-15: Load-Settlement Predictions by Coyle and Briaud-Tucker Methods . . . . .	132

LIST OF FIGURES (Continued)

	<u>Page</u>
68. Corpus Christi Pile: Load-Settlement Predictions by Coyle and Briaud-Tucker Methods . . . . .	133
69. Tavenas Pile J-5: Load-Settlement Predictions by Coyle and Briaud-Tucker Methods . . . . .	134
70. Lock and Dam 26 Ellis Island Site Pile M6: Load-Settlement Predictions by Coyle and Briaud-Tucker Methods . . . . .	135
71. Gregersen Pile A: Load-Settlement Predictions by Coyle and Briaud-Tucker Methods . . . . .	136
72. Gregersen Pile D/A: Load-Settlement Predictions by Coyle and Briaud-Tucker Methods . . . . .	137
73. Gregersen Pile C: Load-Settlement Predictions by Coyle and Briaud-Tucker Methods . . . . .	138
74. Gregersen Pile B/C: Load-Settlement Predictions by Coyle and Briaud-Tucker Methods . . . . .	139
75. West Seattle Freeway Pile A: Load-Settlement Predictions by Coyle and Briaud-Tucker Methods . . . . .	140
76. West Seattle Freeway Pile B: Load-Settlement Predictions by Coyle and Briaud-Tucker Methods . . . . .	141
77. Bearing Capacity Factor Chart for Piles; for Use with Method A . . . . .	144
78. Skin Friction Design Chart for Piles; for Use with Method A . . . . .	145
79. Bearing Capacity Factor Charts for Bored Piles; for Use with Method B . . . . .	147
80. Bearing Capacity Factor Charts for Driven Piles; for Use with Method B . . . . .	149
81. Skin Friction Design Chart for Use with Method B . . . . .	150
82. Bearing Capacity Factor Chart for Use with Method C . . . . .	153
83. Skin Friction Design Chart for Use with Method C . . . . .	154
84. q-w and f-w Curves for Use with Method A . . . . .	156
85. q-w and f-w Curves for Use with Method B . . . . .	159
86. q-w and f-w Curves for Use with Method C . . . . .	161

LIST OF FIGURES (Continued)

	<u>Page</u>
87. Point Bearing of Piles in Sand . . . . .	163
88. Limit Values for Point Bearing of Piles in Sand . . . . .	164
89. Penetrometer Design Curves for Pile Side Friction In Sand . . . . .	166
90. Bjerrum's Field Vane Shear Strength Correction Curve . . . . .	168
91. Ogeechee River Pile H-11: Load-Settlement Prediction by CPT Method . . . . .	171
92. Ogeechee River Pile H-12: Load-Settlement Prediction by CPT Method . . . . .	172
93. Ogeechee River Pile H-13: Load-Settlement Prediction by CPT Method . . . . .	173
94. Ogeechee River Pile H-14: Load-Settlement Prediction by CPT Method . . . . .	174
95. Ogeechee River Pile H-15: Load-Settlement Prediction by CPT Method . . . . .	175
96. Tavenas Pile J-5: Load-Settlement Prediction by CPT Method . . . . .	176
97. West Seattle Freeway Pile A: Load-Settlement Predictions by CPT Method . . . . .	177
98. West Seattle Freeway Pile B: Load-Settlement Predictions by CPT Method . . . . .	178
99. Gregersen Pile A: Load-Settlement Predictions by CPT Method . . . . .	179
100. Gregersen Pile D/A: Load-Settlement Predictions by CPT Method . . . . .	180
101. Gregersen Pile C: Load-Settlement Predictions by CPT Method . . . . .	181
102. Gregersen Pile B/C: Load-Settlement Predictions by CPT Method . . . . .	182
103. Lock and Dam 26 Ellis Island Site Pile M6: Load-Settlement Predictions by PMT and CPT Methods . . . . .	183
104. Sellgren Pile AI: Load-Settlement Predictions by PMT and CPT Methods . . . . .	184

LIST OF FIGURES (Continued)

	<u>Page</u>
105. Frequency Distribution. Cone Penetrometer Method. Point Load . . . . .	186
106. Frequency Distribution. Cone Penetrometer Method. Side Load . . . . .	187
107. Frequency Distribution. Cone Penetrometer Method Total Load . . . . .	188
108. Frequency Distribution. Pressuremeter Method. Point Load . . . . .	189
109. Frequency Distribution. Pressuremeter Method. Side Load . . . . .	190
110. Frequency Distribution. Pressuremeter Method. Total Load . . . . .	191
111. Cost of Site Investigation Versus Cost of Installed Piles . . . . .	194
112. The Dynamic Pressio Penetrometer (DYPP). . . . .	201

LIST OF TABLES

1. Pile Load Test Information . . . . .	3
2. Ultimate Load by Various Failure Criteria . . . . .	10
3. Parameters from Hyperbolic Regression . . . . .	32
4. Ultimate Loads from Hyperbolic Asymptotes . . . . .	33
5. Distribution of Residual Loads after Driving . . . . .	43
6. Distribution of Residual Loads after Tension Test . . . . .	47
7. Comparison of Methods of Obtaining Residual Loads from Load Test Data . . . . .	57
8. Residual Stress Properties . . . . .	76
9. Soil Shear Stiffness and Strength Properties . . . . .	78
10. Pile Point - Soil Stiffness and Strengths Properties . . . . .	80
11. Ratio of Point Load to $N_{pt}$ for Various Pile Movements . . . . .	87
12. API Design Factors . . . . .	101

LIST OF TABLES (Continued)

	<u>Page</u>
13. API Code Predictions . . . . .	102
14. Meyerhof Predictions . . . . .	106
15. Coyle and Castello Predictions . . . . .	108
16. Comparison of Ultimate Loads . . . . .	109
17. Summary of Frequency Distribution Results . . . . .	114
18. Friction-Movement Curve . . . . .	116
19. Point Bearing-Movement Curve . . . . .	116
20. Soil Categories - Menard Method . . . . .	146
21. Soil Categories - Bustamante-Gianeselli Method . . . . .	152
22. Choosing the Skin Friction Design Curve for Bustamante-Gianeselli Method . . . . .	155
23. Values of the Parameter $\alpha$ . . . . .	158
24. Coefficient of Friction Mobilization, $C$ - Gambin Method . . . . .	158
25. CPT Pile Capacity Factor - Bustamante and Gianeselli Method . . . . .	165
26. Pile Capacity Predictions by CPT and PMT Methods . . . . .	170
27. Ratio of Predicted Loads over Measured Loads: CPT Methods . . . . .	170
28. Summary of Frequency Distribution Results for PMT and CPT Methods . . . . .	192

LIST OF SYMBOLS

- A pile cross-sectional area
- A constant to describe variation of soil shear stiffness
- $A_p$  area of pile point
- $A_S$  side surface area of pile
- B constant to describe variation of soil shear strength

LIST OF SYMBOLS (Continued)

B	pile width or diameter
C	constant used to describe distribution of residual shear stresses after driving
C	coefficient of friction mobilization used in pressuremeter Method A
C	coefficient in Davisson's failure criteria to account for displacement necessary for friction mobilization
D	pile diameter
D	constant to describe distribution of residual shear stresses after driving
D <sub>O</sub>	outside pile diameter
E	soil modulus of elasticity
E <sub>O</sub>	pressuremeter first load modulus
E <sub>P</sub>	pile modulus of elasticity
E <sub>R</sub>	pressuremeter reload modulus
f	soil-pile friction
f <sub>max</sub>	maximum soil-pile friction
f <sub>res</sub>	residual soil-pile friction due to driving
f <sub>s</sub>	soil-pile friction
h <sub>e</sub>	equivalent length of pile
k	pressuremeter bearing capacity factor
k	ratio of unit pile friction to CPT sleeve friction
k <sub>C</sub>	cone penetrometer bearing capacity factor
K	lateral earth pressure coefficient
K <sub>P</sub>	initial tangent modulus of loading point pressure-movement curve
K' <sub>P</sub>	initial tangent modulus of unloading point pressure-movement curve

LIST OF SYMBOLS (Continued)

$K_T$	initial tangent modulus of loading friction-movement curve
$K'_T$	initial tangent modulus of unloading friction-movement curve
$L$	pile length
$\Delta L$	incremental length of pile
$N$	blowcount from Standard Penetration Test (SPT)
$N_{side}, \bar{N}$	average SPT N value over length of pile
$N_{pt}$	average SPT N value near pile point
$N'$	SPT N value corrected for fine silty-sand below the water table
$N_q$	bearing capacity factor for sand
$m$	constant to describe variation of soil shear strength
$n$	constant to describe variation of soil shear stiffness
$p$	effective vertical pressure at any depth
$p_l$	pressuremeter limit pressure
$p_{le}^*$	equivalent net limit pressure near pile point
$p_o$	effective vertical pressure at pile point
$q$	pile point bearing pressure
$q_c$	cone penetration point resistance
$q_o$	pile point pressure
$q_{ov}$	total overburden pressure
$q_{res}$	residual point pressure due to driving
$Q$	load in pile
$Q_p$	point load on pile
$Q_{PU}$	ultimate load at point of pile
$Q_{PR}$	residual load at point of pile
$Q_R$	residual load in pile at any depth



LIST OF SYMBOLS (Continued)

$Q_S$	friction load on pile
$Q_T$	load applied to top of pile
$Q_{TU}$	ultimate load at top of pile
$Q_U$	ultimate load in pile at any depth
$Q_{ult}$	ultimate load on pile top
$R$	radius of pile
$R_O$	reference radius used in pressuremeter Method A
$S$	settlement of top of pile
$S_U$	undrained soil shear strength
$w$	movement of pile at station
$z$	depth
$\alpha$	coefficient of friction mobilization used in pressuremeter Method C
$\alpha$	friction coefficient for use in deRuiter and Beringens CPT method
$\alpha, \beta$	coefficients in solution to governing differential equation for pile under load
$\beta$	soil-pile relative stiffness parameter in loading
$\gamma$	constant used to describe distribution of residual shear stresses after driving
$\delta$	friction angle between pile and soil
$\Delta X$	change in parameter X
$\epsilon$	measured strain in pile
$\phi$	friction angle of soil
$\phi$	constant used to describe distribution of residual shear stresses after driving
$\lambda$	shape factor used in pressuremeter Method A

LIST OF SYMBOLS (Continued)

$\mu$	mean
$\mu$	Bjerrums field vane shear strength correction factor
$\nu$	Poisson's ratio
$\sigma$	Standard deviation
$\sigma$	normal stress in pile segment
$\tau_r$	residual soil shear stresses
$\Delta\tau_f$	asymptotic value of shear stress
$\Delta\tau_s$	shear stress at which slip occurs between soil and pile
$\Omega$	soil-pile relative stiffness parameter for unloading

## CHAPTER I - INTRODUCTION

In order to advance the state of knowledge on the behavior of piles and pile groups in cohesionless soils, an extensive review of the literature has been made. The study was limited to data on instrumented piles, hammer driven and load tested vertically. The resulting data base was analyzed to determine the load transfer characteristics of the soil, including the effects of residual driving stresses where the data was sufficient.

The problem of residual driving stresses has been analyzed in detail to determine their importance in the reduction of load test data, in the formulation of pile capacity design methods and in the load-settlement behavior of piles. The results of the load transfer analysis were then correlated with the available soil data to obtain a predictive method which considers residual driving stresses. The results of this method as well as conventional and new in situ tests methods were then compared to actual load test results. Areas of critical need for further research are pointed out and recommendations are made for their implementation.

## CHAPTER II - PILE LOAD TESTS SELECTED

### LOAD TESTS AND INSTRUMENTATION

This study was restricted to vertical pile load tests on instrumented piles hammer driven in sand. A review of the literature revealed 10 sites with a total of 33 instrumented piles. Details of the piles and soil data available at the sites are presented in Table 1.

The width of pile given in Table 1 is corrected for modifications to the pile for instrumentation. For example, Arkansas pile 1 is a 12.75-in. (32.4 cm) diameter pipe pile. However, two 4-in. (10.2 cm) wide channels were welded to the outside of the pile to protect the instrumentation, increasing the effective diameter of the pile to 14.4 in. (36.6 cm). For non-circular piles the diameter given is that of a circle with the same cross-sectional area as the pile. The assumption was made that H-piles fail along the rectangular cross section enclosing the pile. The equivalent diameter was then computed as for other non-circular piles. This diameter was used in all analyses presented later.

The piles were all instrumented with strain gages, strain rods, or both (Fig. 1). The strain rods measure the movement of the pile at certain levels or stations along the pile with respect to the top of the pile. Loads are then obtained indirectly at midpoints between two strain rods using the formula:

$$Q = \frac{(w_i - w_{i+1}) AE_p}{\Delta L} \dots \dots \dots (1)$$

where Q is the load in the pile,  $w_i$  is the movement at station i, A is the pile cross-sectional area,  $E_p$  is the modulus of elasticity of the pile, and  $\Delta L$  is the distance between the two stations. When strain gages are used to instrument the pile, the load is found at the strain gage level by:

TABLE 1.- Pile Load Test Information

SITE	PILE	SYMBOL	PILE TYPE AND MATERIAL	DIMENSIONS			MODULUS OF ELASTICITY psi x 10 <sup>-6</sup>	TYPE TEST	STRAIN RODS	STRAIN GAGES	SOIL DATA				REFERENCE
				DIA-METER ft	LENGTH ft	AREA in <sup>2</sup>					SPT	CPT	PMT	OTHER	
(1)	(2)	(3)	(4)	(5)	(6)	(7)	(8)	(9)	(10)	(11)	(12)	(13)	(14)	(15)	(16)
Lock and Dam 4, Arkansas River (1963)	1	1	Steel Pipe	1.20	53.1	17.12	29.0	C,T	X						17, 24
	2	2	Steel Pipe	1.50	52.8	23.86	29.0	C,T	X	X					
	3	3	Steel Pipe	1.70	53.0	27.36	29.0	C,T	X						
	6	4	Steel "H" HP 14x73	1.34	40.0	25.70	29.0	C	X						
	7	5	Steel "H" HP 14x73	1.34	52.1	29.33	29.0	C,T	X	X	X				
	9	6	Steel "H" HP 14x73	1.34	53.2	26.28	29.0	C	X						
	10	7	Steel Pipe	1.50	53.1	23.86	29.0	C,T	X	X					
	16	8	Steel Pipe	1.42	52.7	19.62	29.0	C,T		X					
Low Sill Structure, Old River, La. (1956)	1	9	Steel "H" HP 14x73	1.34	80.5	25.70	29.0	C	X						25
	2	10	Steel Pipe	1.75	65.1	27.36	29.0	C,T	X						
	3 <sup>a</sup>	11	Steel "H" HP 14x73	1.34	70.6	25.70	29.0	C	X		X				
	4	12	Steel Pipe	1.42	66.3	22.65	29.0	C,T	X						
	5	13	Steel Pipe	1.42	45.1	22.65	29.0	C,T	X						
	6	14	Steel Pipe	1.58	65.2	25.00	29.0	C,T	X						
Ogeechee River, (1969)	H-11	15	Steel Pipe	1.50	9.9	27.49	30.0	C		X					39, 41
	H-12	16	Steel Pipe	1.50	20.1	27.49	30.0	C		X				Dry Density, Total Density	
	H-13	17	Steel Pipe	1.50	29.1	27.49	30.0	C		X	X	X			
	H-14	18	Steel Pipe	1.50	39.3	27.49	30.0	C		X					
	H-15	19	Steel Pipe	1.50	49.3	27.49	30.0	C		X					

TABLE 1.- Pile Load Test Information (Continued)

(1)	(2)	(3)	(4)	(5)	(6)	(7)	(8)	(9)	(10)	(11)	(12)	(13)	(14)	(15)	(16)
Lock and Dam 26 Replacement Site (1972)	5IP-I	20	Steel "H" HP 14x73	1.34	80.1	21.40	29.0	T		X					18
	5IP-II	21	Steel "H" HP 14x73	1.34	54.4	21.40	29.0	T		X	X				
	3IP-IIIS	22	Steel "H" HP 14x73	1.34	54.0	21.40	29.0	C,T		X					
West Seattle Freeway Bridge (1980)	A	23	Octagonal Prestressed Concrete	2.05	98.0	477.20	5.56	C	X	X				Self-Boring PMT (partial)	33, 34
	B	24	Octagonal Prestressed Concrete	2.05	84.0	477.20	5.56	C	X	X		X			
Tavenas (1970)	H5	25	Steel "H" 12 BP 74	1.09	60.0	21.80	35.0	C		X				37	
	J5	26	Hexagonal Prestressed Concrete	1.05	60.0	127.00	3.94	C		X		X	X		
Gregersen (1969)	A	27	Circular Prestressed Concrete	0.92	26.2	95.45	3.15	C		X				20	
	D/A	28	Circular Prestressed Concrete	0.92	52.5	95.45	3.15	C		X					
	C	29	Tapered Circular Prestressed Concrete	Top 0.92 Bot. 0.66	26.2	varied	3.15	C		X		X	X		
	B/C	30	Straight Cir. to 26.3 ft. Tapered to bottom Pres. Conc.	Top 0.92 Bot. 0.66	52.5	varied	3.15	C		X					

TABLE 1.- Pile Load Test Information (Continued)

(1)	(2)	(3)	(4)	(5)	(6)	(7)	(8)	(9)	(10)	(11)	(12)	(13)	(14)	(15)	(16)
Corpus Christi (1971)	Init.	31	Square Prestressed Concrete	1.50	33.5	256.00	5.6	C		X				Texas Highway Dept. Cone	11
	Final	32	Square Prestressed Concrete	1.50	33.5	256.00	5.6	C		X					
Sellgren (1981)	A-I	33	Square Prestressed Concrete	1.00	35.4	113.00	3.15	C		X					32
	A-II	34	Square Prestressed Concrete	1.00	35.4	113.00	3.15	C		X			X		
Lock and Dam 26 Ellis Island Site (1978)	M6	35	Timber	Top 1.10 Bot. 0.92	35.0	varied	2.0	C	X	X	X	X	X	Shear Wave Velocity	43, 44

a Had a 3/4 in. (1.9 cm) thick square plate on the bottom.

Note: 1 ft = 0.305 m; 1 psi = 6.89 kN/m<sup>2</sup>

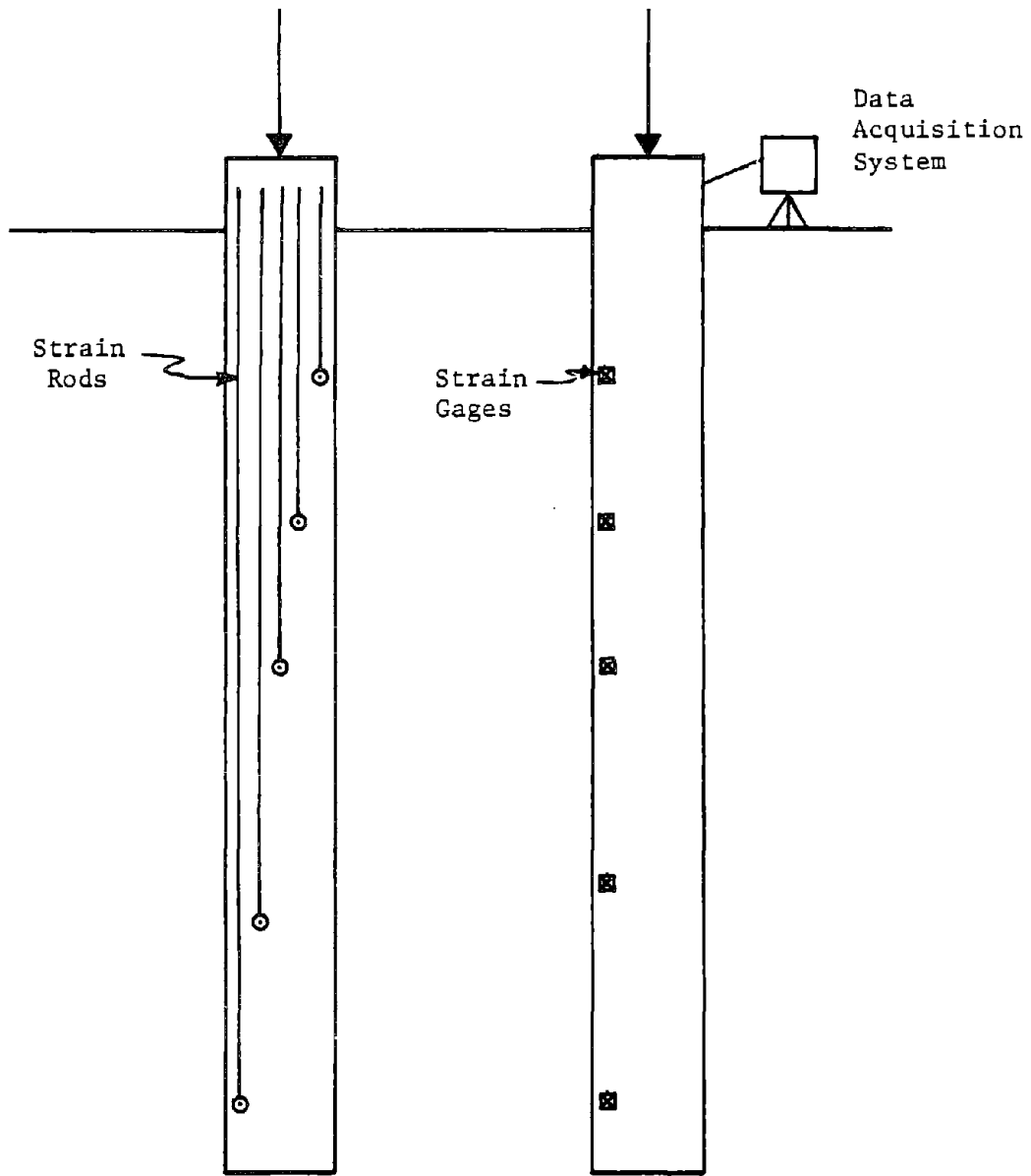


FIG. 1.- Example of Pile Instrumentation



$$Q = \epsilon E_p A \dots \dots \dots (2)$$

where  $\epsilon$  is the measured strain

#### FAILURE CRITERIA

Vertical load tests in sand rarely reach a plunging load where a large increase in settlement occurs for a small increase in load. Thus, various criteria have been proposed to define the failure load. The main reason for defining a failure load is for the purpose of formulating a design procedure or verifying an existing method. Any comparison of a predictive method to load test results should be based upon the failure criterion used to develop the method, otherwise incorrect conclusions will be made concerning the method.

Three failure criteria have been used on the selected tests. The first criterion selected was Davisson's criterion (14) which is the load corresponding to a settlement of the pile top, S, of

$$S = \frac{PL}{AE_p} + C + \frac{D}{120} \dots \dots \dots (3)$$

where P is the defined failure load, L is the pile length, C is a constant, and D is the pile tip diameter in inches.

The first term is the elastic compression of the pile under the defined failure load. The second term is a constant to account for the amount of displacement necessary to mobilize the skin friction and was taken to be 0.15 in. (0.38cm) as recommended by Davisson (14). The third term is to account for the amount of displacement needed to mobilize the point resistance.

The second criterion selected was the load corresponding to a settlement of one-tenth of the pile diameter (0.1 x D). An example showing the use of the two failure criteria is given in Fig. 2.

Of the 35 selected pile load tests the load-settlement curve had to be extrapolated to obtain results in 3 cases for Davisson's criterion

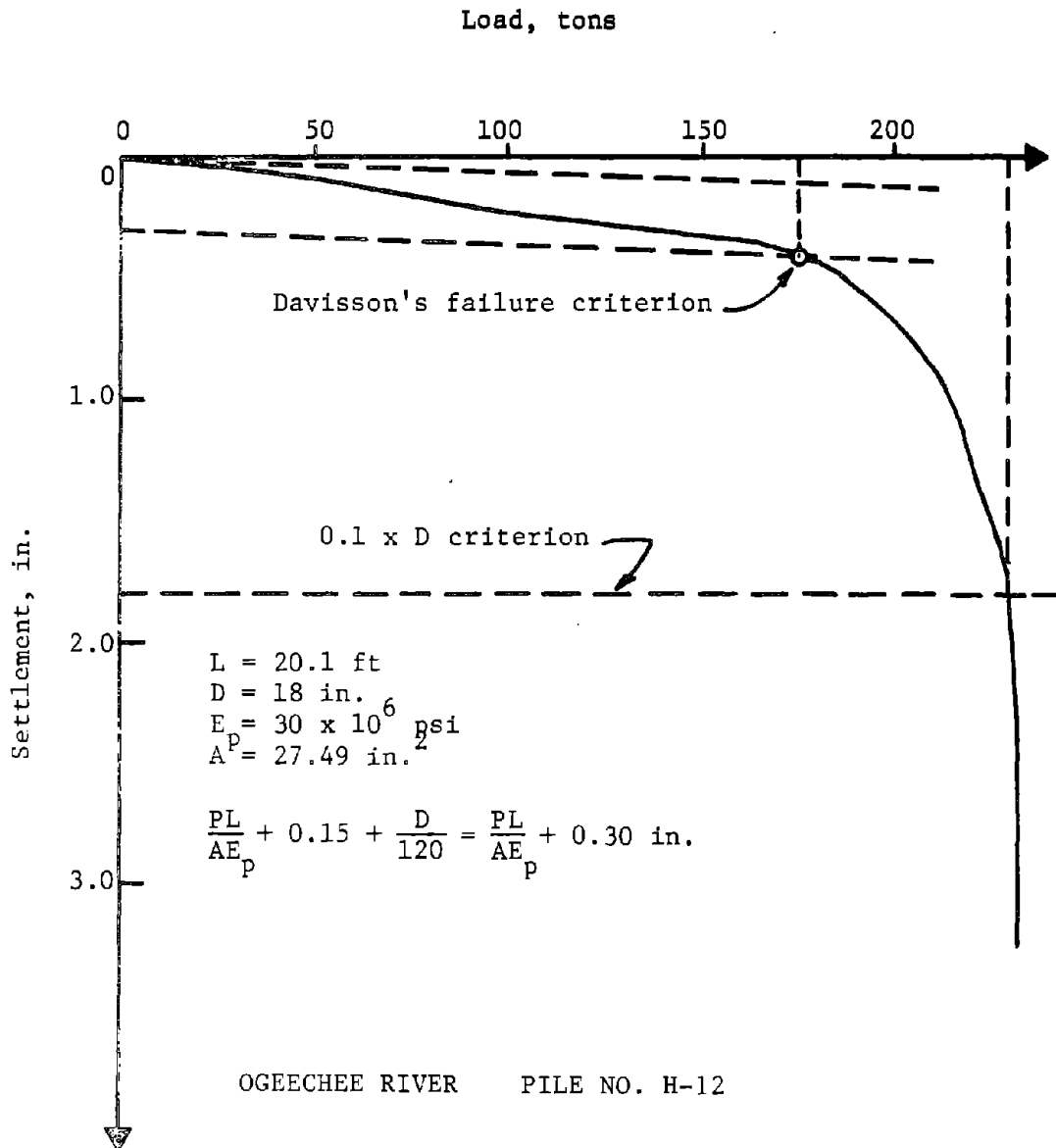


FIG. 2.- Example of Davisson and 0.1xD Failure Criteria  
 (1 in. = 2.54 cm; 1 ft = 0.305 m; 1 ton = 8.9 kN;  
 1 psi = 6.89 kPa)

and in 13 cases for the 0.1 x D criterion. In one case the load settlement curve could not be extrapolated with confidence to a settlement of 0.1 x D. The 0.1 x D criterion consistently gave ultimate loads higher than the Davisson criterion. The average difference was 23% with a maximum difference of over 100%. This emphasizes the importance of using the same failure criterion when analyzing a prediction method as was used to develop the method.

The third failure criterion was developed in an attempt to provide a uniform method for extrapolating the load test results to an ultimate load. The criterion requires instrumented pile load tests and consists of first performing a load transfer analysis to obtain the unit side friction versus pile movement (f-w) and unit point bearing pressure versus point movement (q-w) curves. A hyperbola is then fitted to these curves to obtain the asymptote for both the friction and the point bearing pressure. These values are then used to compute the ultimate pile capacity. The details of the load transfer analysis and curve fitting are given in Chapter III. This criterion generally resulted in higher values than the other two failure criteria. The only cases where this criterion yielded lower loads was when extrapolation of the load-settlement curve was required. This indicates that the extrapolation of the load test results by eye may overpredict the peak capacity. Table 2 gives a comparison of the failure loads determined by the three criteria along with the ultimate load applied during the load test.

Davisson's criterion yields a conservative estimate of the ultimate load for piles in sand due to the large settlements required to mobilize the point bearing. A combination of Davisson's criterion with the 0.1xD criterion would seem to provide a satisfactory failure criterion. The ultimate load would then be defined as the load corresponding to a top settlement of:

$$S = \frac{PL}{AE_p} + 0.1D \dots \dots \dots (4)$$

This would provide enough point movement to mobilize the tip bearing

TABLE 2.- Ultimate Loads by Various Failure Criteria

SITE	SOIL DESCRIPTION	PILE	ULTIMATE LOAD			MAXIMUM APPLIED LOAD ton
			DAVISSON ton	0.1xD ton	HYPERBOLIC ton	
Arkansas River	0-30 ft fine sand, SP below 30 ft fine sand with silt and clay, SP-SM	1	161	172 <sup>a</sup>	216	172
		2	207	242	322	250
		3	230	272 <sup>a</sup>	264	259
		6	132	183 <sup>a</sup>	257	183
		7	189	243	297	255
		9	222	250 <sup>a</sup>	268	250
		10	200	242 <sup>a</sup>	283	230
Low Sill Structure	0-50 ft silt below 50 ft fine and medium sand	1	358	390 <sup>a</sup>	346	358
		2	338	420 <sup>a</sup>	377	372
		3	185	240	255	240
		4	400 <sup>a</sup>	440 <sup>a</sup>	402	341
		5	135	145	158	145
		6	365 <sup>a</sup>	430 <sup>a</sup>	376	345
Ogeechee River	0-12 ft silty sand below 12 ft fine and medium sand, SW-SP	H-11	35	76	134	105
		H-12	173	232	245	238
		H-13	205	297	328	315
		H-14	290	347	418	400
		H-15	350	421	545	430
Lock and Dam 26 (1972)	0-80 ft coarse sand, SP w/ cobble layer at 58 ft below 80 ft limestone	JIP-IIIS	160 <sup>a</sup>	b	173	150
West Seattle Freeway Bridge	0-78 ft fine to medium sand with silt and clay lenses	A	525	525	608	535
	below 78 ft interbedded clayey sandy silt and silty fine sand	B	450	450	532	450
Tavenas	0-16 ft loose crushed stone	J5	120	163	177	163
	below 16 ft medium to fine uniform sand, SP	H5	109	150	171	150
Gregersen	0-5.6 ft sand	A	24.3	27	28.4	30
	5.6-9.8 ft fine sand, SP	D/A	44.5	51	c	52
	below 9.8 ft medium to coarse sand, SP	C	26.4	30	29.5	31
		B/C	42.7	48	c	52
Corpus Christi	0-8 ft fine sand, SP	Initial	108	150 <sup>a</sup>	217	134
	below 8 ft fine silty sand, SP and SM	Final	135	138 <sup>a</sup>	213	157
Sellgren	0-12 ft silt	AI	58	78	107	90
	below 12 ft fine sand	AII	129	143	189	158
Lock and Dam 26 (1978)	fine to coarse sand with trace gravel	M5	75	95	119	110
Average			192	228	264	222

<sup>a</sup> Load-settlement curve had to be extrapolated to obtain value  
<sup>b</sup> Load-settlement curve could not be extrapolated with confidence to obtain value  
<sup>c</sup> Not enough data available for regression  
 Note: 1 ton = 8.9 kN; 1 ft = 0.305 m

and would also include the elastic compression of the pile. The second term has been omitted because the movement needed to mobilize the friction is very small compared to that necessary to mobilize the point reaction. Thus, if the point moves  $0.1 \times D$  the friction will be fully mobilized. This criterion was not applied in this study since this would require even further extrapolation of the load-settlement curves. It is recommended, however, that future pile load tests in sand be carried to this amount of settlement to insure that a value close to a plunging load is obtained.

CHAPTER III - CONVENTIONAL LOAD TRANSFER ANALYSIS

INCREMENTAL METHOD

The incremental method of load transfer analysis allows one to obtain unit side friction versus pile movement (f-w) curves at various stations along a pile and the unit tip bearing versus tip movement (q-w) curve. This analysis requires the measurement of load and movement at the top of the pile and of load at various stations along the pile. The procedure has been detailed by Coyle and Reese (13) and is outlined here. Fig. 3 shows a pile divided into three segments, each of which is divided into two equal parts. The load in the pile has been measured at stations 2 and 4 and at the pile tip. The average side friction, f, in a segment is found by subtracting the load at the bottom of the segment from the load at the top and dividing by the circumferential area as follows:

$$f_i = \frac{(Q_{i-1} - Q_{i+1})}{\pi D_o (z_{i+1} - z_{i-1})} \dots \dots \dots (5)$$

where  $Q_i$  is the load at station  $i$ ,  $D_o$  is the pile outside diameter, and  $z_i$  is the depth to station  $i$ . The movements at the midpoints of the segments are found beginning from the known movement at the top of the pile and subtracting the elastic compression of the pile segments. The general equation for the movement of the pile at any station,  $w_i$ , is:

$$w_i = w_{i-1} - \frac{\frac{1}{2} (Q_{i-1} + Q_i) (z_{i+1} - z_{i-1})}{AE_p} \dots \dots \dots (9)$$

From this analysis are obtained the unit side friction versus movement curves. The unit tip bearing is obtained by dividing the tip load by the tip area. The tip movement is obtained in the same manner as the movement at the other stations.

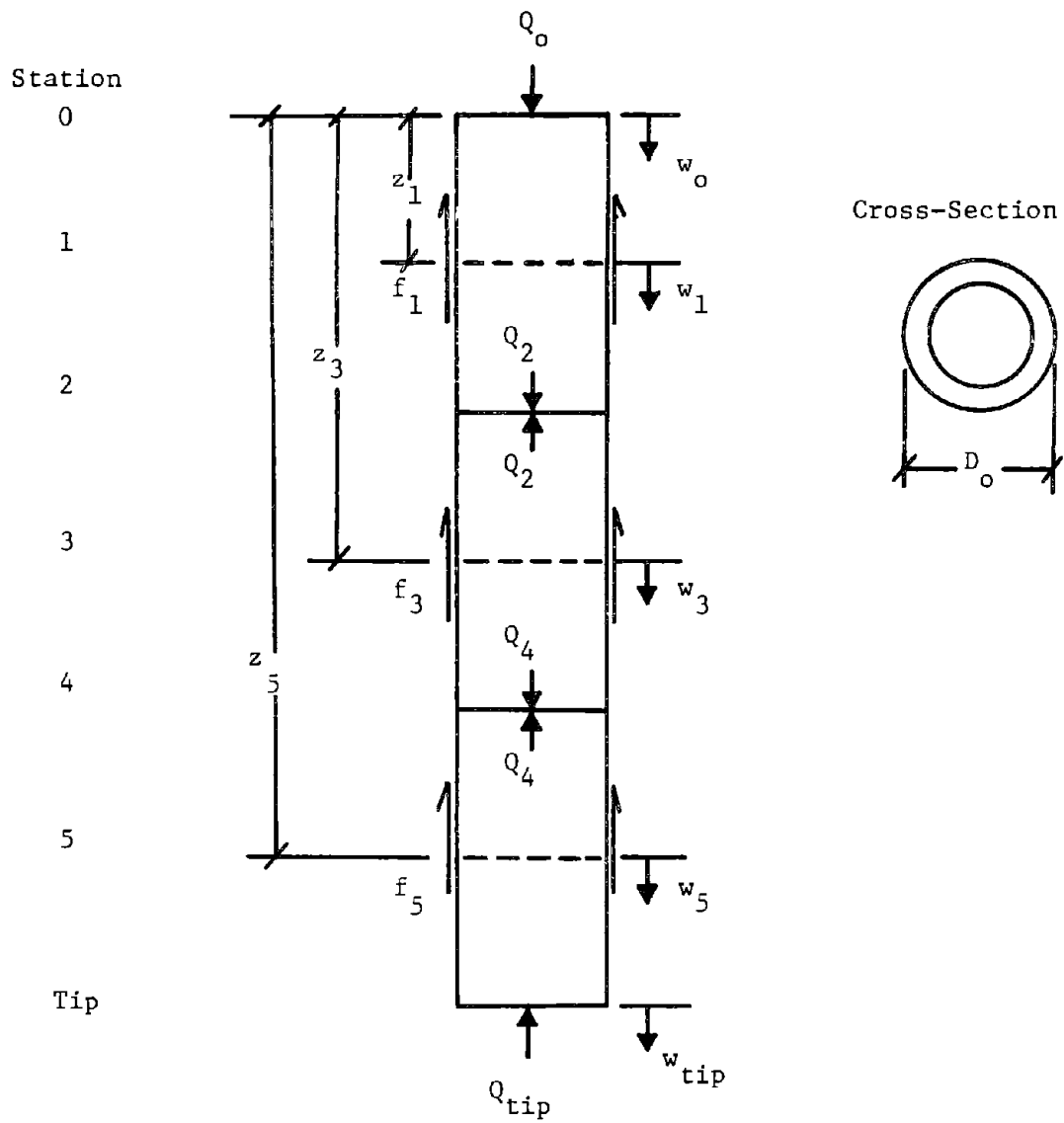


FIG. 3 .- Segmentation of Pile for Incremental Load Transfer Analysis

## AVERAGE METHOD

A second method of load transfer analysis is the average method. The analysis is carried out in the same way as the incremental analysis but considers the pile as only one segment. This results in only one average f-w curve and the q-w curve. This method has the advantage of being simple and requires less pile instrumentation than the incremental analysis. This method may also be applied to an uninstrumented pile if it is loaded in both compression and tension, the assumption being made that the friction is the same in both compression and tension. Thus, the data base for this method may be much larger than that for the incremental method.

Most of the piles selected did not have the load measured directly at the pile tip. For these piles the tip load was found by linear extrapolation from the last two load measurements. This extrapolation had the restrictions that the load could not be negative or higher than the last load measured.

## ANALYSIS

Both of the methods of analysis are readily adapted to computer solution. A computer program was written and used to analyze all the piles in this study. After the load transfer analysis was performed the following plots were made:

1. Side friction versus depth for each load step (f-z),
2. Ratio of point load to total load versus total load,
3. Unit side friction versus pile movement (f-w),
4. Tip load versus tip movement (q-w),
5. Ratio of side friction to maximum side friction versus pile movement ( $f/f_{\max}$ -w), and
6. Ratio of side friction to maximum friction versus the ratio of pile movement to pile radius ( $f/f_{\max}$ -w/R).

Fig. 4 shows a plot of load versus depth (Q-z) for Arkansas pile 1. A complete set of plots of the results of the incremental analysis are shown in Figs. 5 through 10. The side friction is directly proportional to the slope of the Q-z curve. As a result, the side friction is



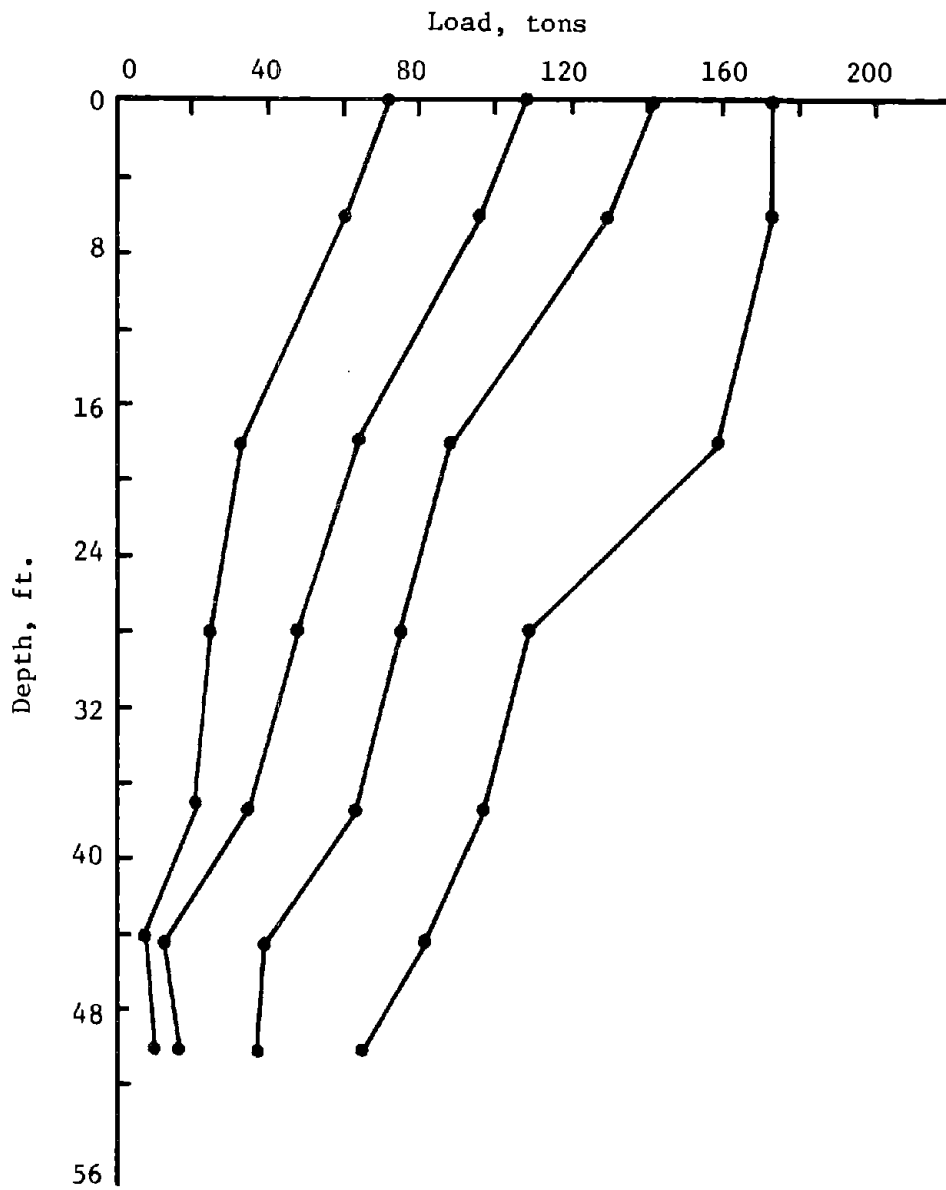


FIG. 4.- Arkansas River Pile 1 Compression Test: Load Distribution, Incremental Analysis (1 ft = 0.305 m; 1 ton = 8.9 kN)

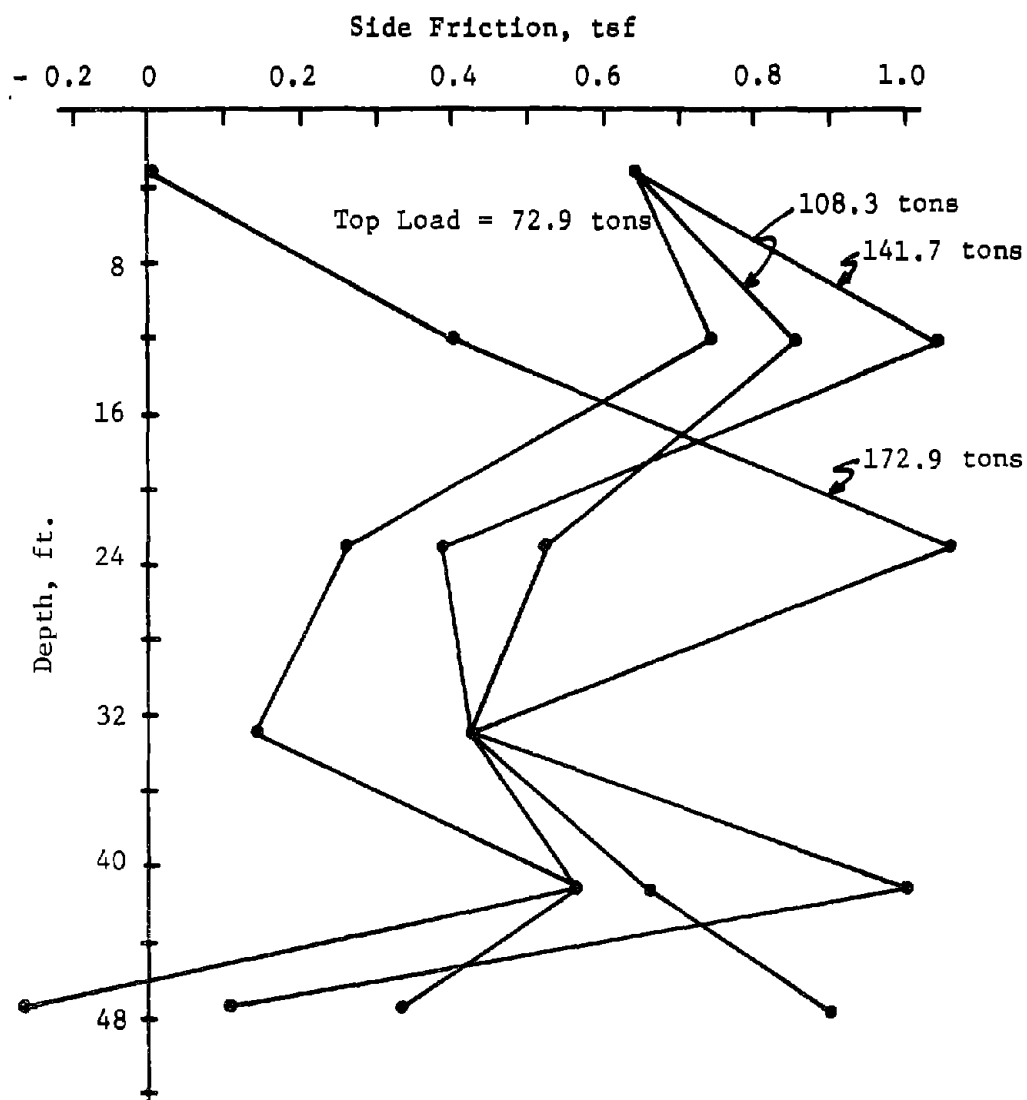


FIG. 5.- Arkansas River Pile 1 Compression Test: f-z Curves, Incremental Analysis (1 ft = 0.305 m; 1 tsf = 95.8 kPa; 1 ton = 8.9 kN)

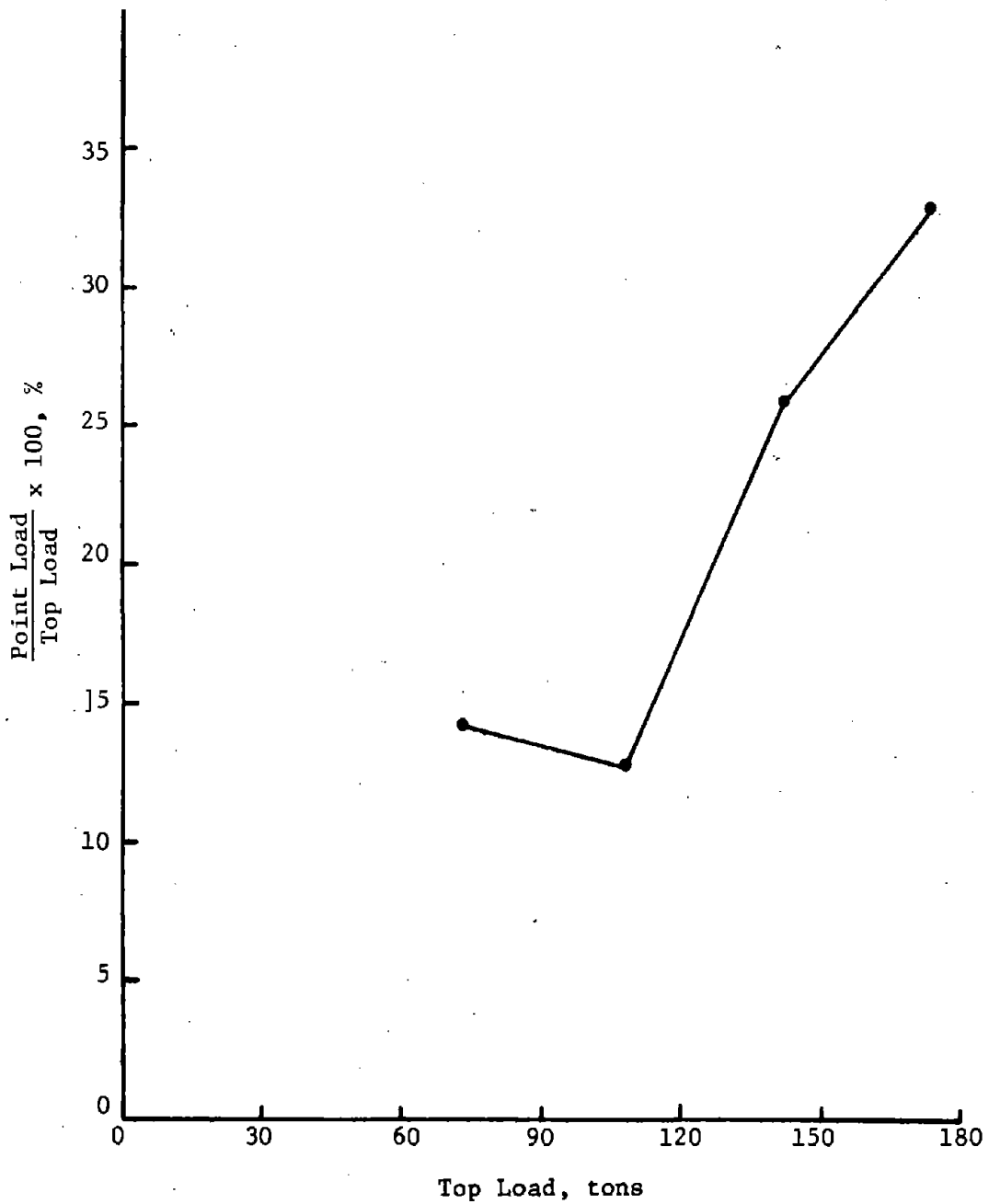


FIG. 6.- Arkansas River Pile 1 Compression Test: Percent Point Load Versus Top Load, Incremental Analysis (1 ton = 8.9 kN)

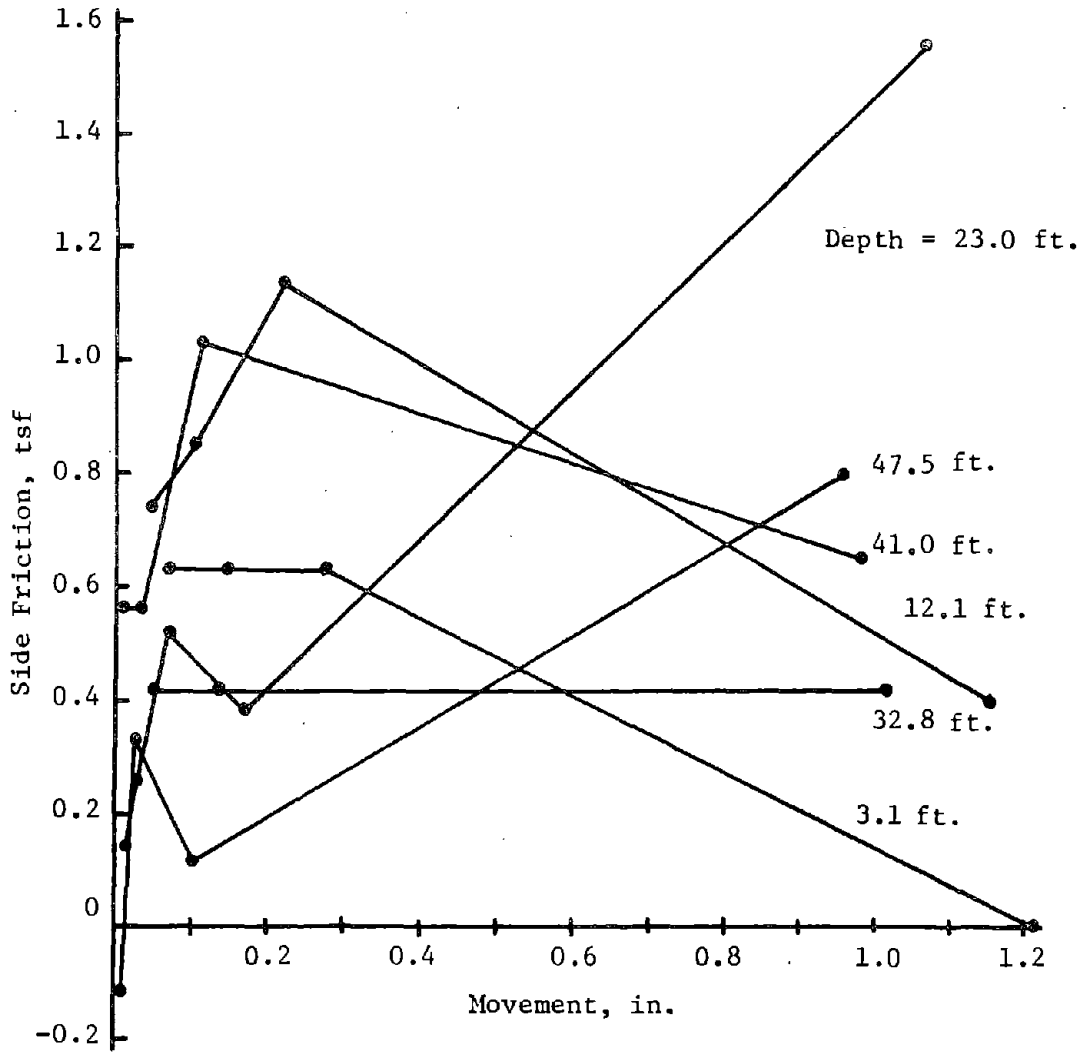


FIG. 7.- Arkansas River Pile 1 Compression Test: f-w Curves, Incremental Analysis (1 in. = 2.54 cm; 1 tsf = 95.8 kPa; 1 ft = 0.305 m)

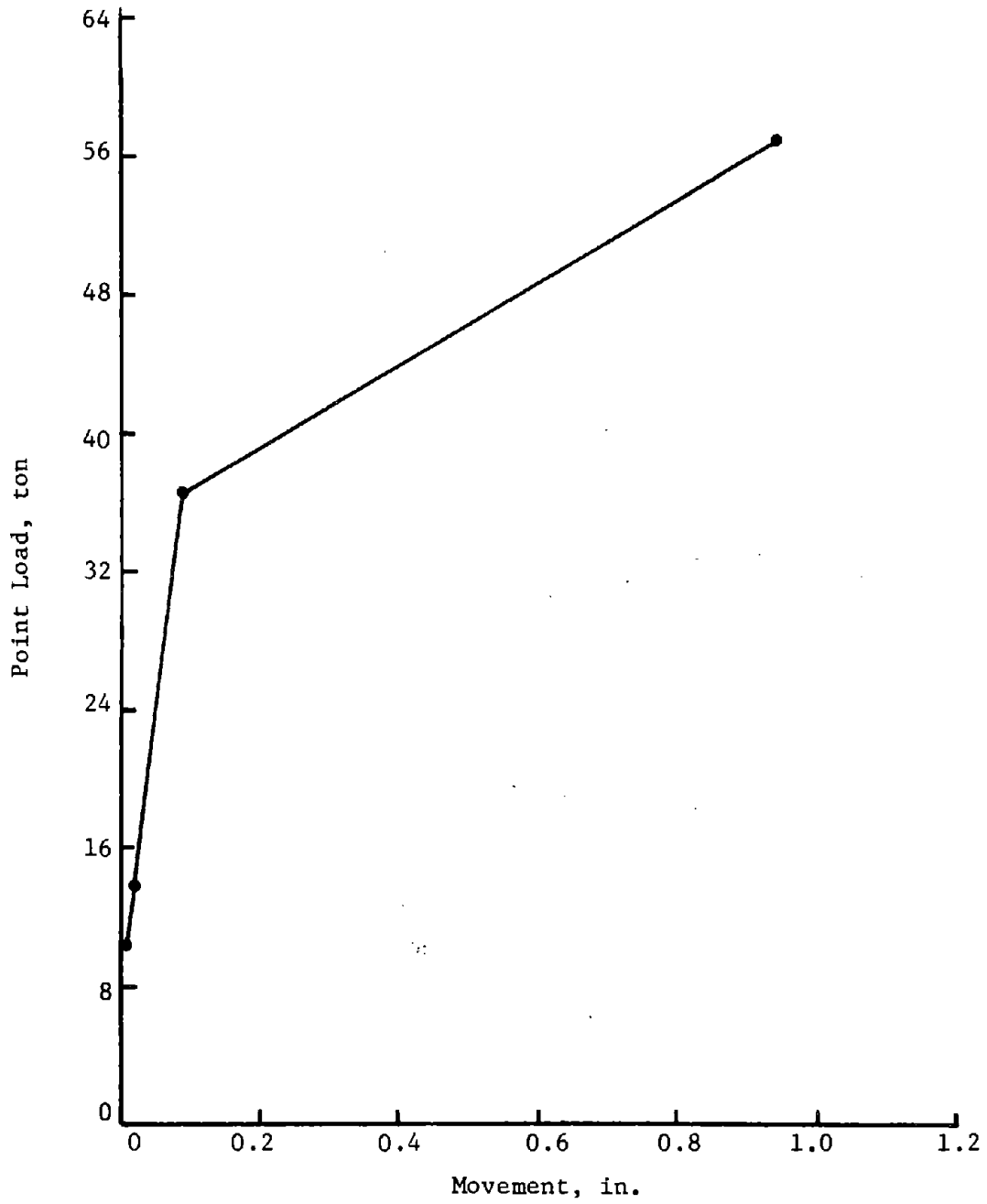


FIG. 8.- Arkansas River Pile 1 Compression Test: Q-w Curve  
Incremental Analysis (1 in. = 2.54 cm; 1 ton = 8.9 kN)

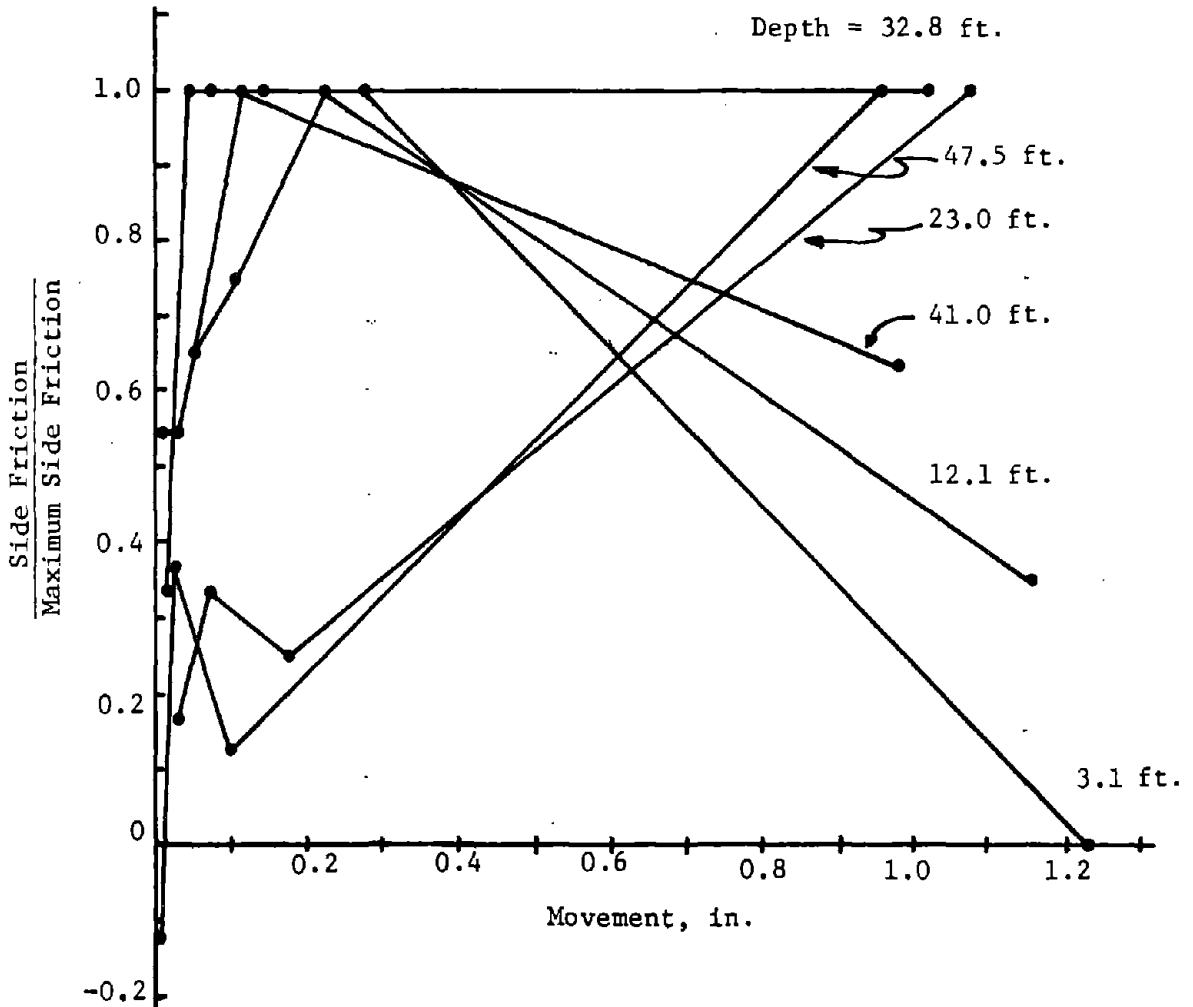


FIG. 9.- Arkansas River Pile 1 Compression Test:  $f/f_{max}$  - w Curves, Incremental Analysis (1 in. = 2.54 cm; 1 ft = 0.305 m)

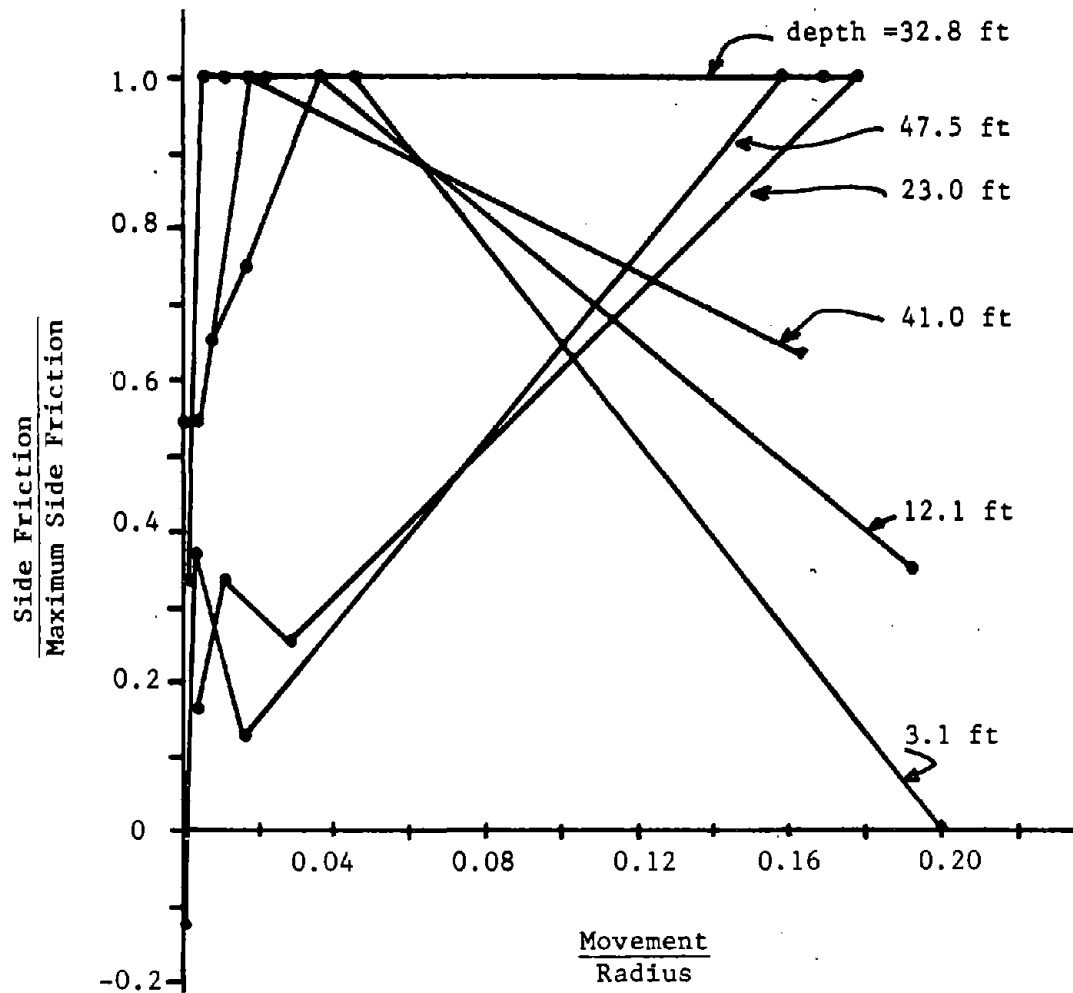


FIG. 10.- Arkansas River Pile 1 Compression Test:  $f/f_{max}$  - w/R Curve, Incremental Analysis (1 ft = 0.305 m)

very sensitive to error in the measurements and therefore showed some very erratic results. At some levels the friction decreases with increasing movement and for some piles, becomes negative at large loads. Fig. 11 compares the results of the incremental and average methods for the Ogeechee River site piles. These were actually one pile tested at five different embedment depths. The incremental analysis yielded a wide range of results. For example, at a depth of 10 ft the incremental analysis gave friction values ranging from 0.2 tsf to 1.0 tsf (19.2 kPa to 95.8 kPa). The results of the average analysis on the other hand show a definite trend of increasing friction with depth.

The results from the incremental analysis may be improved by fitting a smooth curve through the data points. This process should take into account the reliability of the instrumentation at each level. This process also includes some judgement which may vary between individuals. Since the published data was insufficient to determine the reliability of the instrumentation, and in order to avoid judgements which may be questionable, the actual data points were used in the incremental analysis. The results were too scattered for correlation and the results of the average analysis were used in correlations with soil parameters. For comparison, the complete set of plots for the average analysis of Arkansas pile 1 is shown in Figs. 12 through 17.

Another problem encountered in both methods of analysis is shown in Fig. 15. At the low load steps the computed movement of the pile tip is negative, indicating that the pile tip is moving up. This may be due to several things: incorrect pile modulus, incorrect pile cross-sectional area, or incorrect measurement of the pile top movements due to movement of the reference beam. The pile moduli and cross-sectional area used in this study were those reported in the literature and are felt to be accurate for the purpose of computing movements. These values would need to be in error by a factor of two or more to create the error observed in the computed pile movements. The error may then be attributed to measurement error. In order to correct for this the  $f$ - $w$  and  $q$ - $w$  curves were extrapolated back to zero  $f$  or  $q$ . The axes



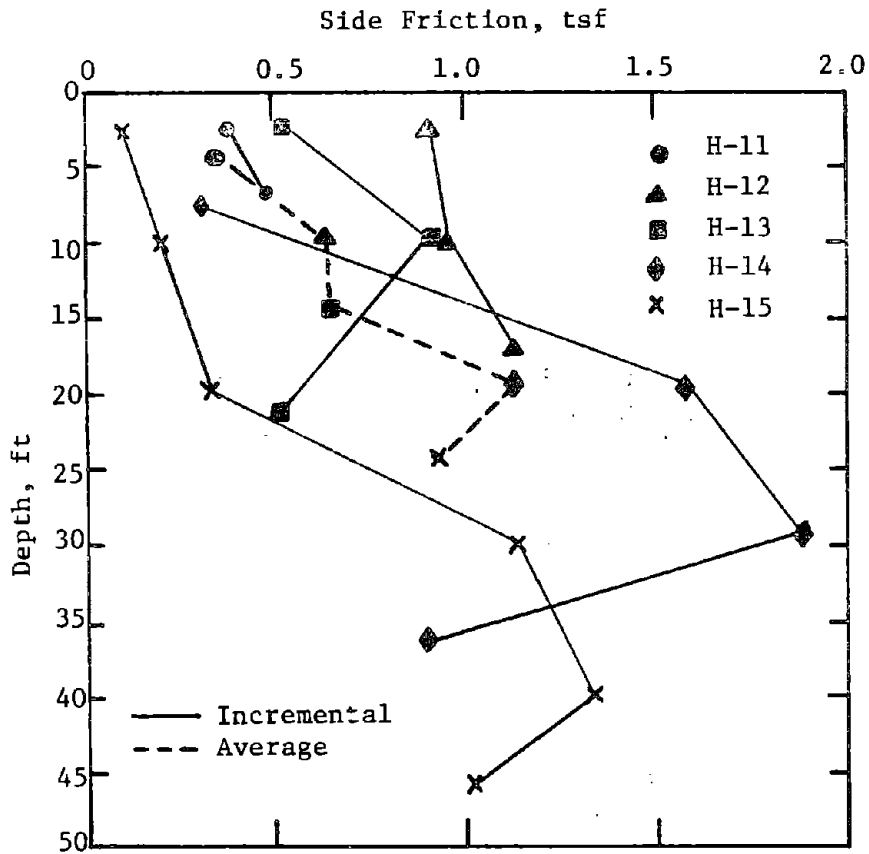


FIG. 11.- Ogeechee River Site: Comparison of Incremental and Average Analyses (1 ft = 0.305 m; 1 tsf = 95.8 kPa)

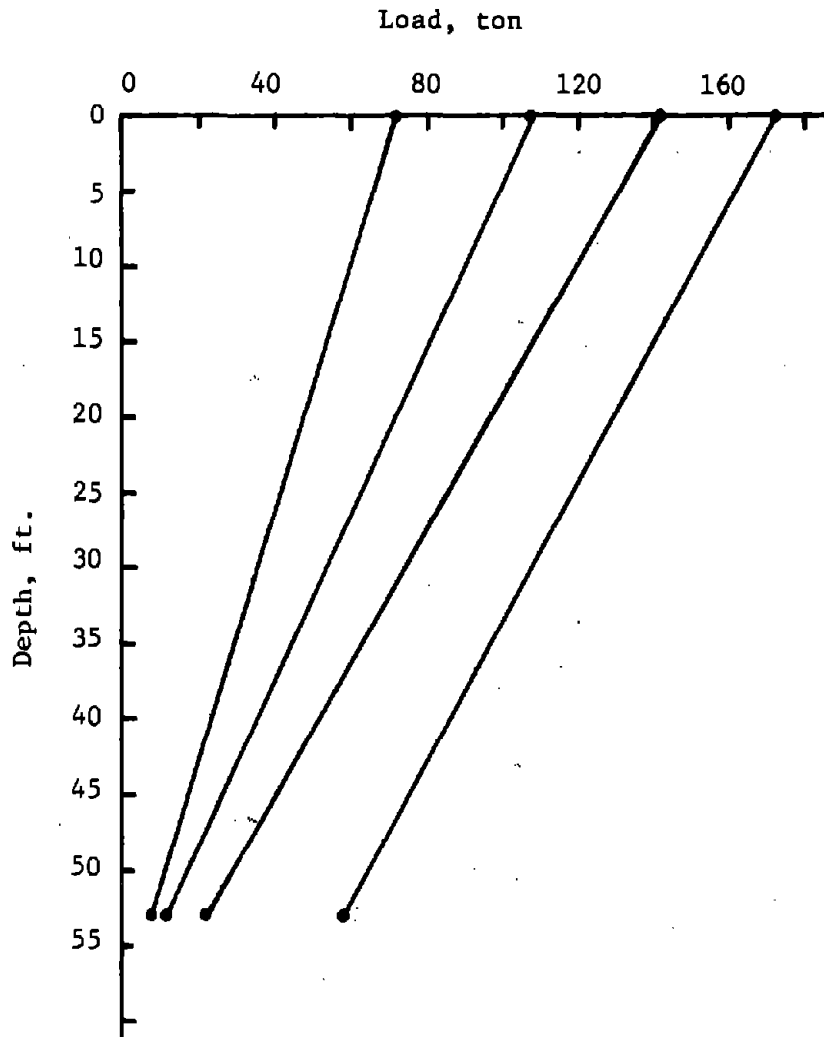


FIG. 12.- Arkansas River Pile 1 Compression Test: Load Distribution, Average Analysis (1 ft = 0.305 m; 1 ton = 8.9 kN)

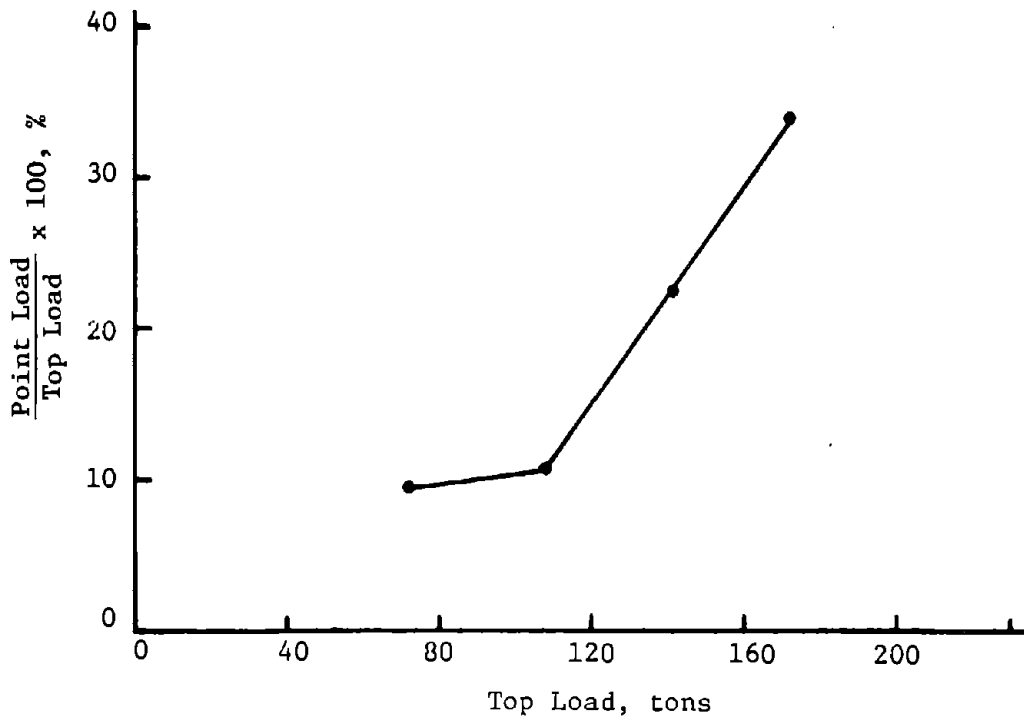


FIG. 13.- Arkansas River Pile 1 Compression Test: Percent Point Load Versus Top Load, Average Analysis (1 ton = 8.9 kN)

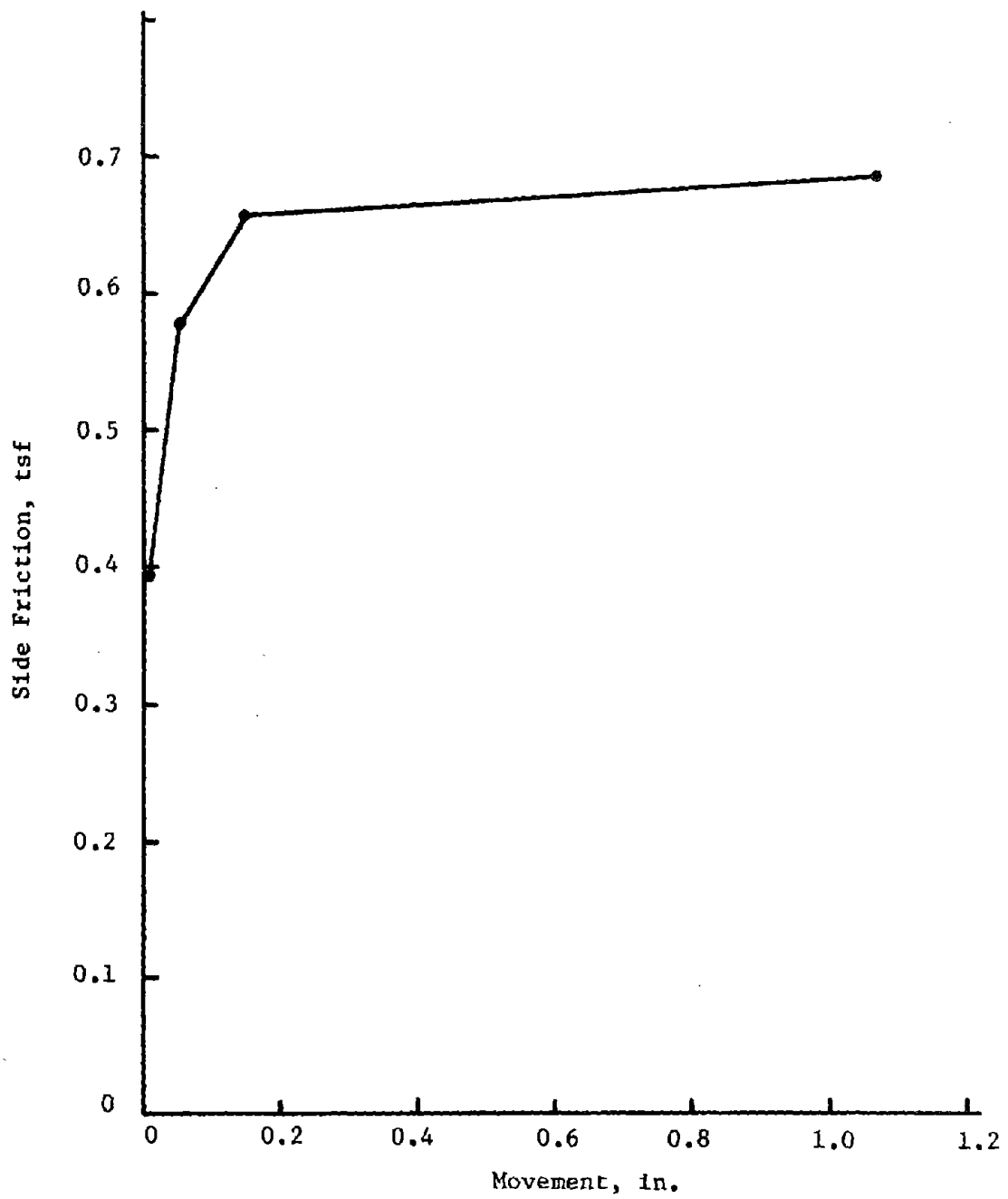


FIG. 14.- Arkansas River Pile 1 Compression Test: f-w Curve, Average Analysis  
(1 in. = 2.54 cm; 1 tsf = 95.8 kPa)

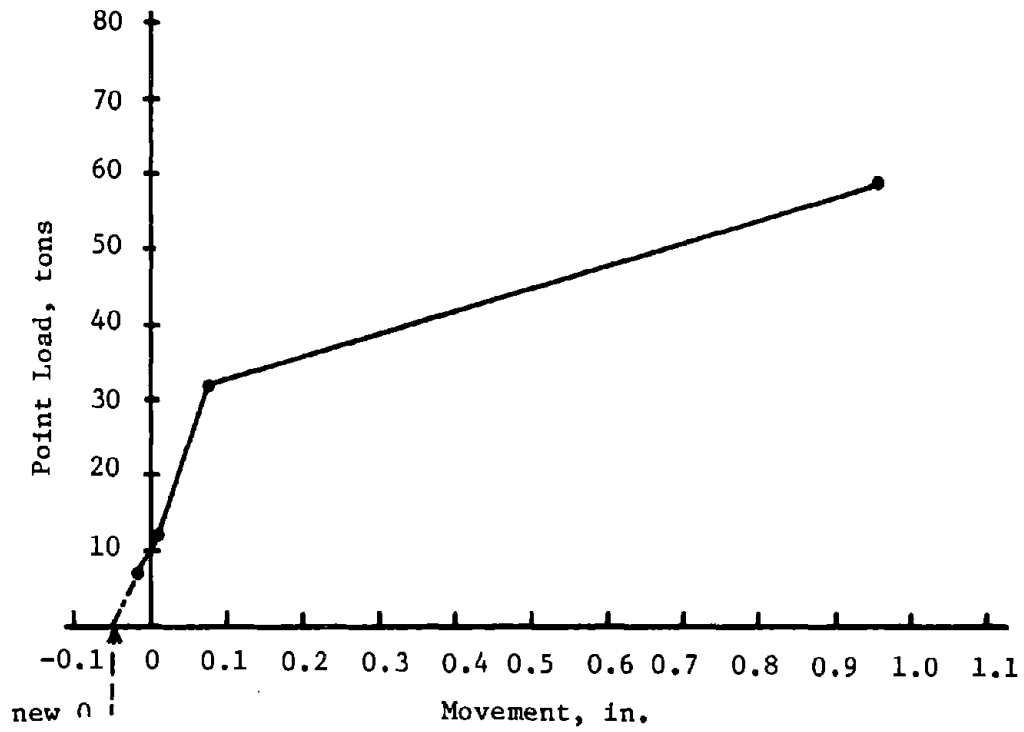


FIG. 15.- Arkansas River Pile 1 Compression Test: Q-w Curve, Average Analysis (1 in. = 2.54 cm; 1 ton = 8.9 kN)

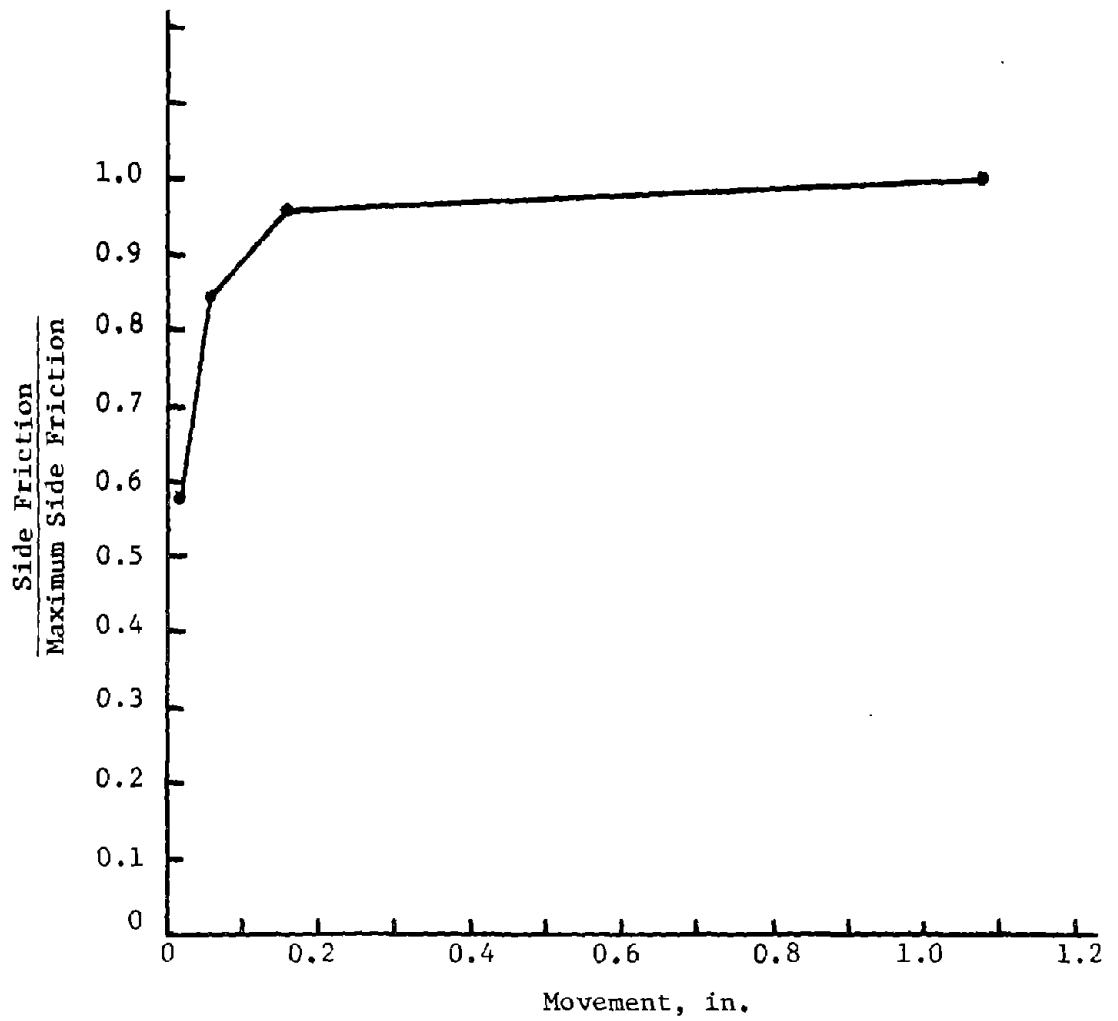


FIG. 16.- Arkansas River Pile 1 Compression Test:  $f/f_{\max}$  - w Curve, Average Analysis (1 in. = 2.54 cm)

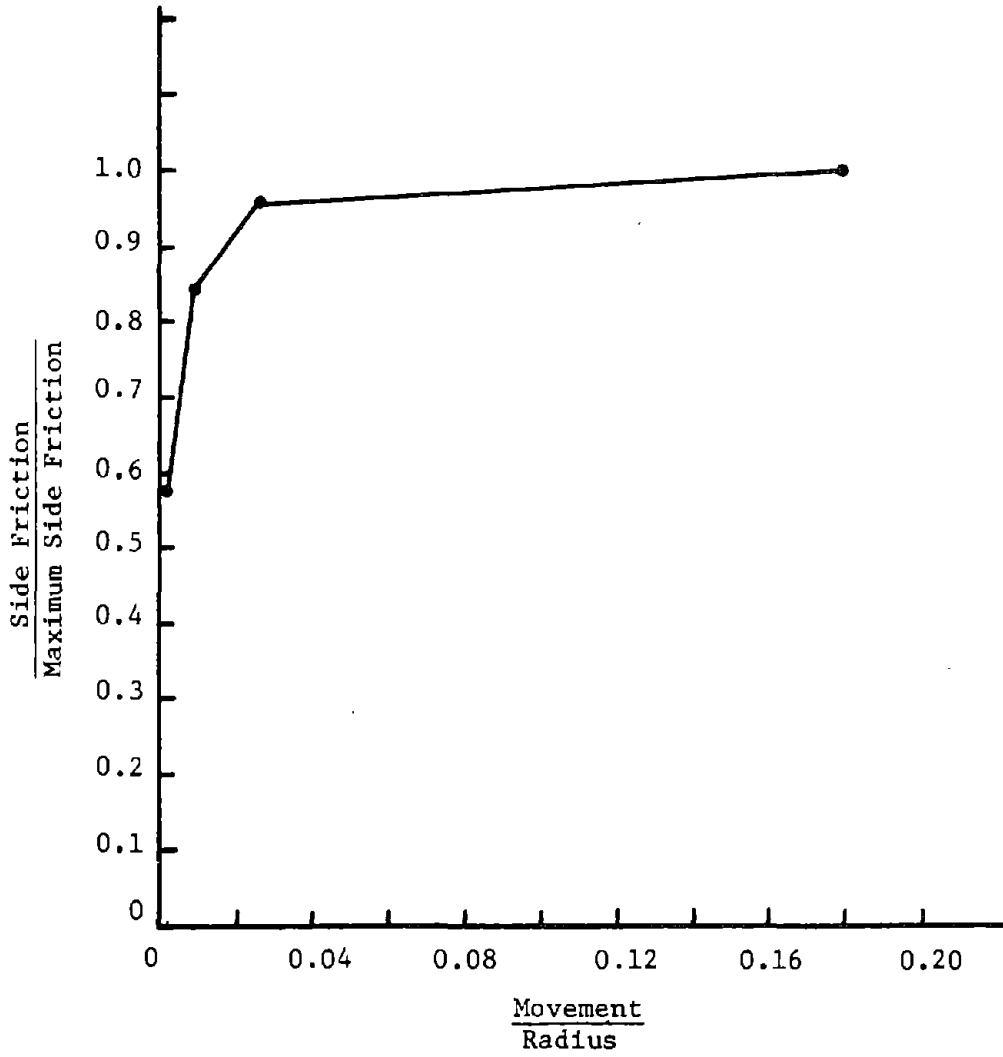


FIG. 17.- Arkansas River Pile 1 Compression Test:  $f/f_{\max} - w/R$   
Curve, Average Analysis

were then recentered at this point for further analysis as shown in Fig. 15.

#### HYPERBOLIC REGRESSION

The hyperbolic model for soil response has been proposed and used with success by various writers (22). The equation of the f-w and q-w curves for the hyperbolic model are

$$f = \frac{w}{\frac{1}{K_{\tau}} + \frac{w}{f_{\max} + f_{\text{res}}}} \dots \dots \dots (7)$$

and

$$q = \frac{w}{\frac{1}{K_p} + \frac{w}{q_{\max} - q_{\text{res}}}} \dots \dots \dots (8)$$

where  $K_{\tau}$  is the initial tangent modulus of the f-w curve,  $K_p$  is the initial tangent modulus for the q-w curve,  $f_{\max} + f_{\text{res}}$  is the hyperbolic asymptote of the f-w curve, and  $(q_{\max} - q_{\text{res}})$  is asymptotic of the q-w curve. These initial tangent moduli and the asymptote values may be obtained by plotting  $w/f$  or  $w/q$  versus  $w$  and performing a linear regression through these points. The y-intercept of these lines are then the initial tangent moduli and the slopes of these lines are the asymptotic values. The regression for the f-w curve of Arkansas pile 1 is shown in Fig. 18. When the pile was instrumented with both strain gages and strain rods the analyses were performed separately and then combined to obtain average values. The parameters for the load transfer curves for all the piles are given in Table 3. The values of point load, side friction load, and total load, using these parameters are shown in Table 4.



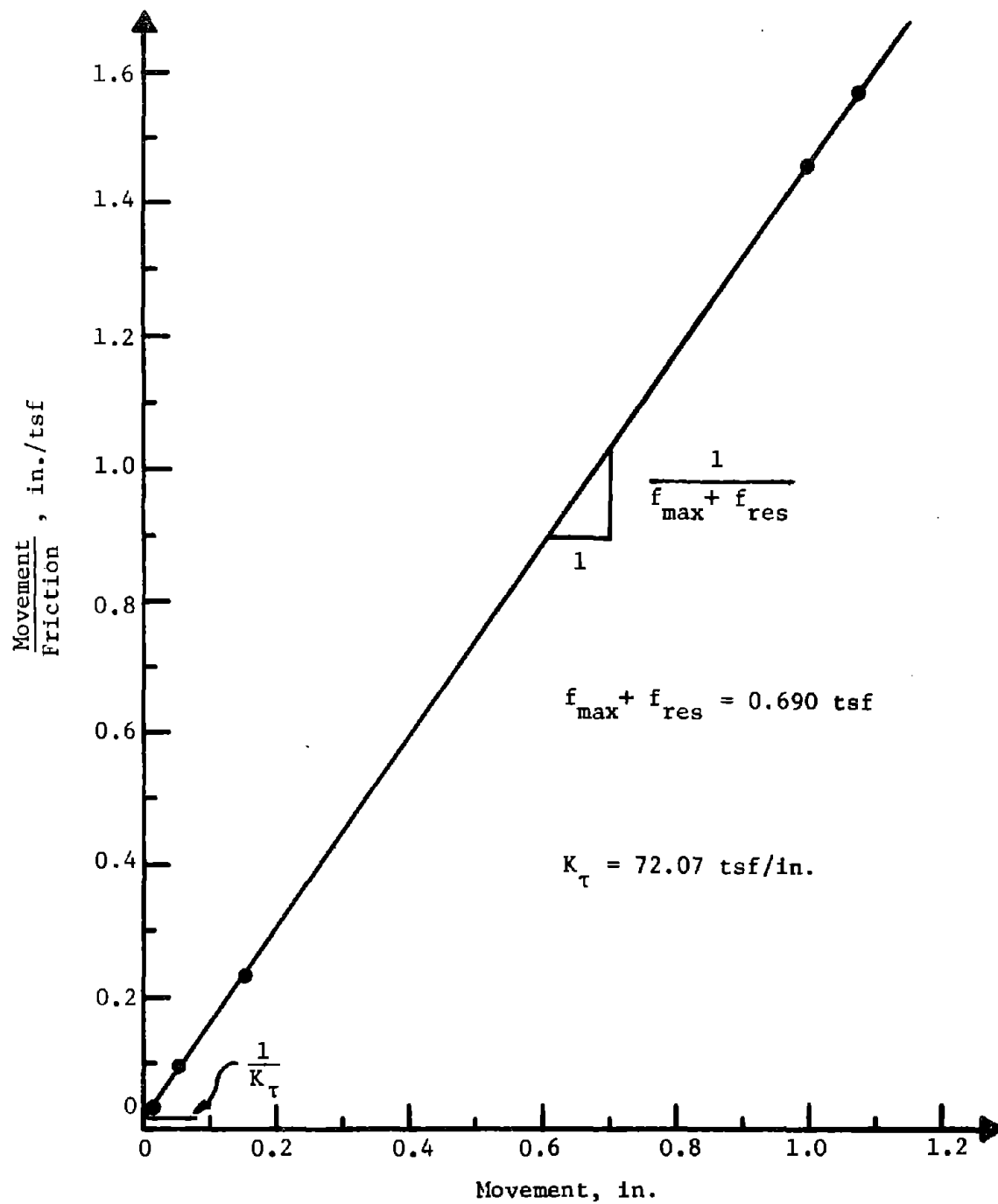


FIG. 18.- Arkansas River Pile 1: Hyperbolic Regression for f-w Curve  
 (1 in. = 2.54 cm; 1 tsf = 95.8 kPa; 1 tsf/in = 37.7 kPa/cm)

TABLE 3.- Parameters from Hyperbolic Regression

Site	Pile	$f_{\max} + f_{\text{res}}$ (tsf)	$K_T$ (tsf/in.)	$q_{\max} - q_{\text{res}}$ (tsf)	$K_p$ (tsf/in.)
Arkansas	1	0.690	72.07	69.4	1506.3
	2	0.752	10.84	76.6	462.5
	3	0.553	17.57	47.1	534.6
	6 <sup>b</sup>	1.174	3.05	25.9	63.4
	7 <sup>b</sup>	1.067	3.86	26.1	212.1
	9 <sup>b</sup>	1.004	4.89	12.6	35.4
	10	0.692	21.47	62.4	174.6
	16	0.471	28.74	22.4	1201.1
Low Sill	1b	0.624	20.70	79.5	1609.0
	2	0.794	22.67	38.2	490.6
	3 <sup>b</sup>	0.380	10.18	93.9	209.9
	4	1.032	34.47	61.5	832.7
	5	0.699	20.64	10.5	95.2
	6	0.872	43.96	49.2	1250.6
Ogeechee River	H-11	0.345	12.26	66.7	52.3
	H-12	0.636	6.75	104.5	659.6
	H-13	0.646	5.91	135.2	597.0
	H-14	1.130	2.60	118.0	1081.5
	H-15	0.930	2.01	186.0	493.5
West Seattle	A	0.743	6.99	37.6	385.5
	B	0.682	5.30	45.8	577.4
Tavenas	H5 <sup>b</sup>	0.392	2.02	86.0	250.2
	J5	0.539	3.36	80.6	802.8
Sellgren	AI	0.152	10.45	114.9	322.8
	AII	1.123	14.09	81.3	109.8
Corpus Christi	Initial	0.232	3.04	102.5	231.3
	Final	0.377	4.54	87.6	324.7
Gregersen	A	0.291	10.25	9.32	590.5
	D/A	a	a	a	a
	C	0.389	16.33	12.2	874.4
	B/C	a	a	a	a
Lock and Dam 26	M6	0.887	5.55	29.9	227.1
	3IP-111S <sup>b</sup>	0.503	7.00	32.7	512.2

a - Not enough data available for regression.

b - Analysis of H-piles used and perimeter of enclosing rectangle.

Note: 1 tsf = 95.8 kN/m<sup>2</sup>; 1 tsf/in. = 37.7 kPa/cm

TABLE 4.- Ultimate Loads from Hyperbolic Asymptote

Site	Pile	$Q_p$	$Q_s$	$Q_t$
		tons	tons	tons
Arkansas	1	78	138	216
	2	135	187	322
	3	107	157	264
	6	36	221	257
	7	36	261	297
	9	17	251	268
	10	110	173	283
	16	35	111	146
Low Sill	1	110	236	346
	2	92	285	377
	3	129	126	255
	4	97	305	402
	5	17	141	158
	6	96	282	378
Vesic	H-11	118	16	134
	H-12	185	60	245
	H-13	239	89	328
	H-14	209	209	418
	H-15	329	216	545
Seattle	A	125	483	608
	B	152	380	532
Tavenas	H-5	80	91	171
	J-5	70	107	177
Gregersen	A	3	25.4	28.4
	D/A	a	a	a
	C	2.9	26.6	29.5
	B/C	a	a	a
Corpusi	Initial	182	35	217
Christi	Final	156	57	213
Sellgren	AI	90	17	107
	AII	64	125	189
LD26 ELLIS	M6	20	99	119
LD26 REPL	31P-IIIS	45	128	173

a - Not enough data available for regression.

Note:- 1 ton = 8.9 kN

## CHAPTER IV - RESIDUAL STRESSES: BASIC CONSIDERATIONS

### THE PHENOMENON

During a hammer blow, a pile will move downward first, then rebound and then oscillate around a final position. At its final position the pile is in equilibrium under a certain point load and a certain friction load, which cancel out since the top load is zero. The process repeats itself during the full driving sequence of the pile and when the pile reaches final penetration the load distribution in the pile can be as shown on Fig. 19.

During the downward movement of the pile the pile-soil friction is acting upward on the pile to resist the penetration of the pile; the point soil resistance is also acting upward. During the rebound that follows, the soil under the point pushes the pile back up while the pile decompresses elastically. These two components of the rebound create enough upward movement to reverse the direction of the pile-soil friction which now acts downward at least in the upper portion of the pile. Equilibrium is reached when enough of the friction stresses have reversed themselves in order to keep the bottom of the pile prestressed against the soil.

It is clear that the residual stresses phenomenon is governed by the unloading characteristics of the point and friction transfer curves ( $q-w$  and the  $f-w$  curves) on one hand, and by the elastic characteristics of the pile on the other. In sands, a significant residual point load can exist because little movement is needed to unload the  $f-w$  curve, while much more movement is needed to unload the  $q-w$  curve. In clays, small, if any, residual point load will exist because the movement necessary to unload the  $f-w$  and  $q-w$  curves are of the same magnitude and the point load is usually small to start with.

### INFLUENCING FACTORS

If a short pile, about 10 ft (3 m) long, is driven in sand the point load will be high compared to the friction load. Since it is the

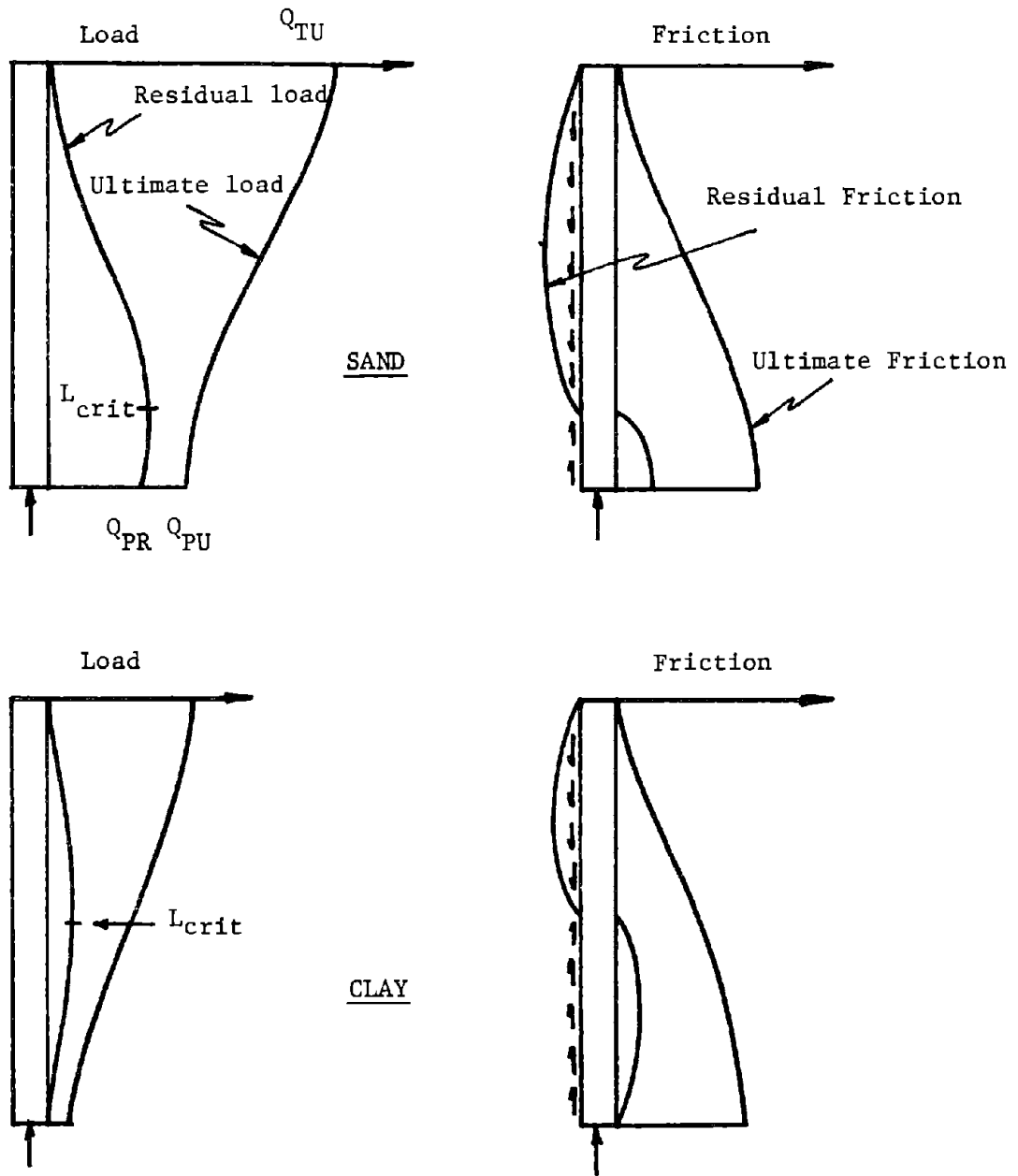


FIG. 19.- Ultimate Loads and Residual Loads

reversal of the friction which keeps the point pre-stressed against the soil, if there is little friction available there will be a small residual point load. Indeed, the residual point load cannot be larger than the total friction load. As the length of the pile increases, more friction is available and more residual point load is maintained. Beyond a certain length  $L_{critical}$  (Fig. 19) there is a sufficient amount of friction available to maintain a residual point load and this load is then controlled by the compatibility of unloading displacement. The length of the pile is an influencing factor.

If a stiff pile is driven in a soft soil the part of the rebound due to elastic decompression of the pile will be small compared to the upward movement necessary to reverse the friction stresses: residual point loads will be small. If on the other hand, a soft pile is driven in a stiff soil the part of the rebound due to elastic decompression of the pile will be large enough to reverse the friction stresses: residual point loads will be large. The pile-soil stiffness ratio is an influencing factor.

If the slope of the unloading portion of the  $f-w$  curve is much steeper than the slope of the unloading portion of the  $q-w$  curve, little movement will be needed to reverse the friction stresses and large residual point loads will exist. If, on the contrary the slope of the unloading portion of the  $q-w$  curve is much steeper than the slope of the unloading portion of the  $f-w$  curve, the point load will be completely unloaded before enough movement is generated to reverse the friction. The  $q-w/f-w$  unloading stiffness ratio is an influencing factor.

#### THEORETICAL FORMULATION

The theoretical formulation which follows makes a number of simplifying assumptions. The results are useful however, because they show theoretically the role of the various influencing factors which were discussed qualitatively in the previous section. The residual loads are loads that are locked in the pile upon unloading of the pile after the pile has been brought to the ultimate soil resistance. Therefore,

the theoretical analysis takes as an initial condition the stress and load distribution in the pile at failure. The ultimate skin friction is  $\tau_U$ , and the ultimate point resistance is  $q_U$  (Fig. 20). The top ultimate load is  $Q_{TU}$  and the point ultimate load is  $Q_{PU}$ . The load anywhere in the pile is  $Q_U$ .

The unloading of the friction is assumed to obey the linear elastic model (Fig. 20):

$$\Delta\tau = K'_T \Delta w \dots \dots \dots (9)$$

where  $\Delta\tau$  is the decrease in pile-soil friction stress at depth  $z$   
 $K'_T$  is the unloading stiffness in friction  
 $\Delta w$  is the upward movement of the pile upon unloading at depth  $z$ .

The conventions of sign and direction are shown on Fig. 21.

Similarly the unloading of the point follows:

$$\Delta q = K'_p \Delta w_p \dots \dots \dots (10)$$

where  $\Delta q$  is the decrease in point resistance  
 $K'_p$  is the unloading stiffness for the point.  
 $\Delta w_p$  is the upward movement of the pile at the point upon unloading.

Because the pile was in equilibrium at failure, any change in stress brought about by the unloading must also satisfy equilibrium if the pile is to be in equilibrium after complete unloading. Therefore, the equilibrium of the elementary pile element can be written incrementally as follows (Fig. 21):

$$-\frac{\partial \Delta\sigma}{\partial z} - \frac{P}{A} \Delta\tau = 0 \dots \dots \dots (11)$$

where  $\Delta\sigma$  = normal stresses decrease in pile at depth  $z$   
 $A$  = cross sectional area of pile.  
 $P$  = perimeter of pile.

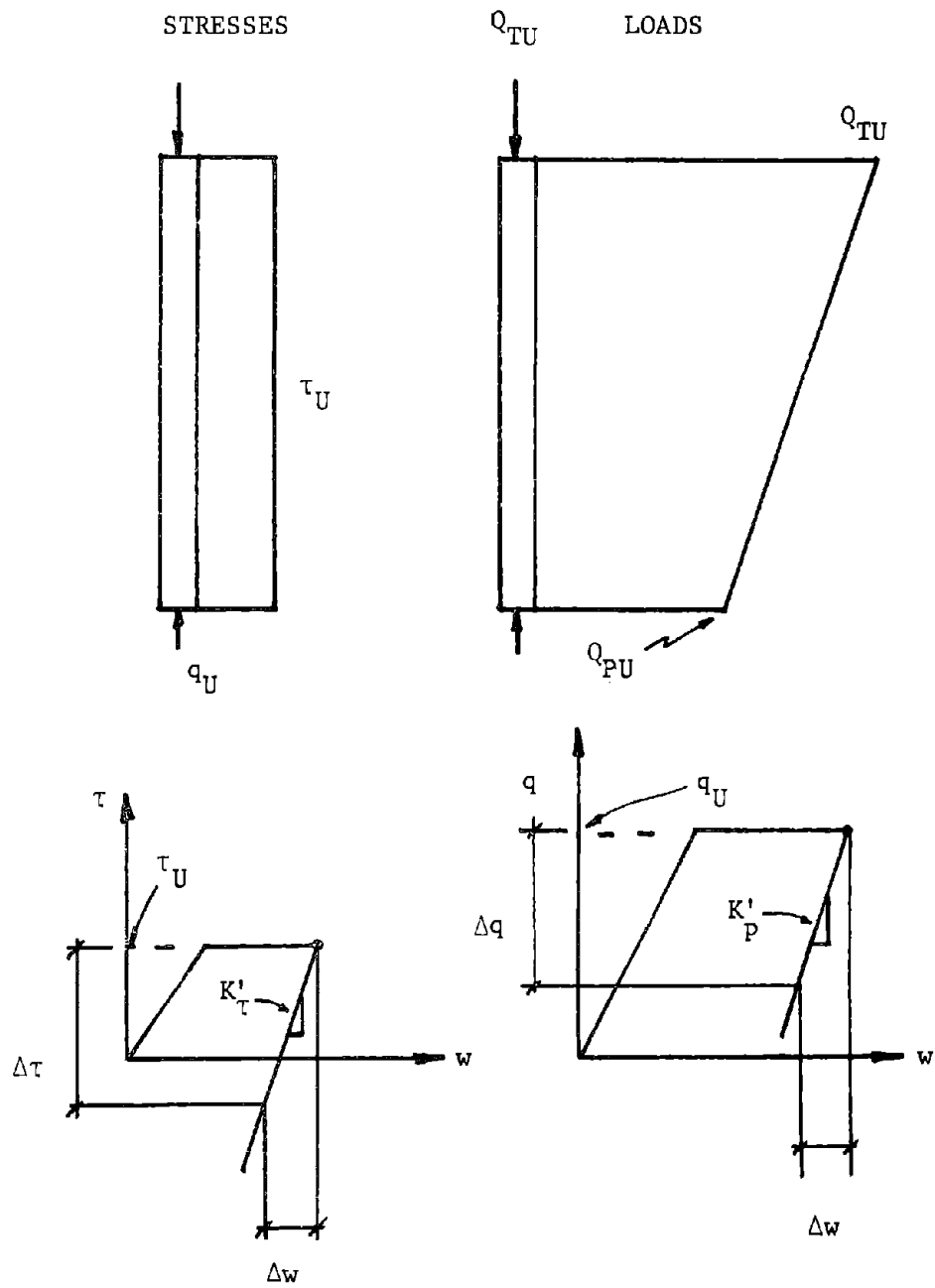


FIG. 20.- Unloading Process for Residual Loads



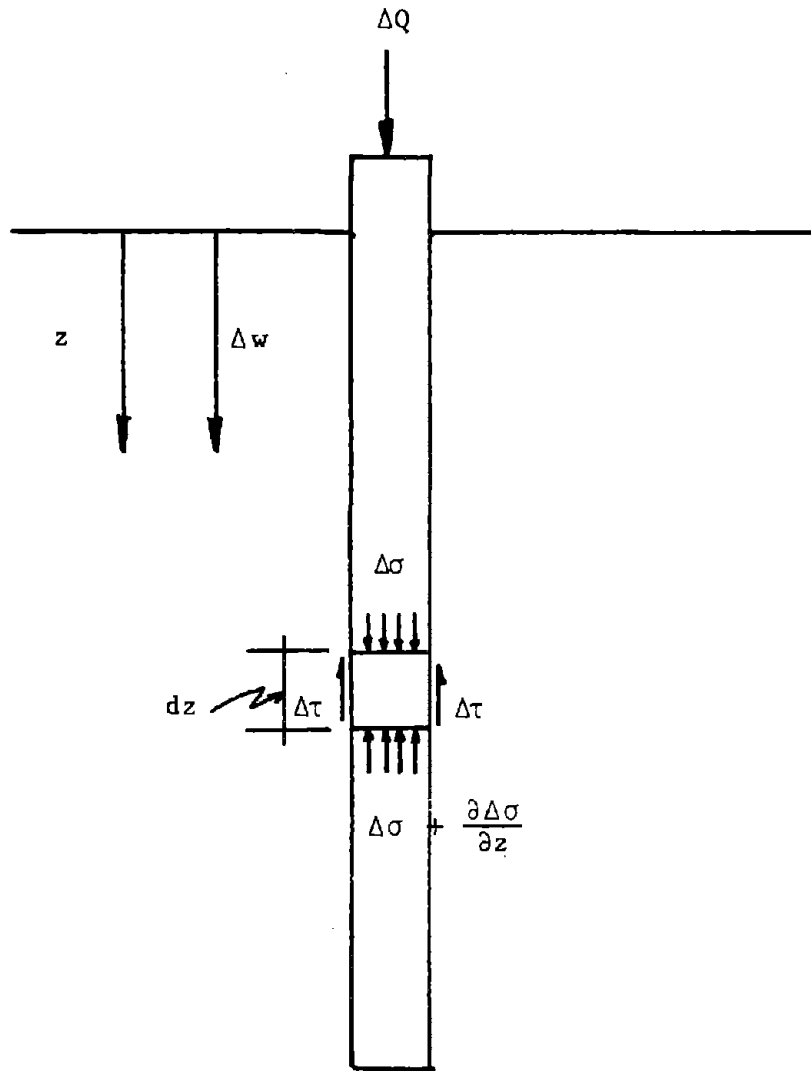


FIG. 21.- Sign Conventions for Theoretical Formulation

The constitutive equation for the pile is:

$$\Delta\sigma = -E_p \Delta\varepsilon = -E_p \frac{\partial\Delta w}{\partial z} \dots\dots\dots (12)$$

where  $E_p$  is the pile modulus  
 $\Delta\varepsilon$  is the decrease in normal strain at depth  $z$  due to unloading.

Combining the equations above leads to:

$$\frac{\partial^2 \Delta w}{\partial z^2} - \frac{PK'_T}{AE_p} \Delta w = 0 \dots\dots\dots (13)$$

for which the solution is:

$$\Delta w = \alpha e^{\Omega z} + \beta e^{-\Omega z} \dots\dots\dots (14)$$

with  $\Omega = \sqrt{\frac{K'_T P}{E_p A}}$

The decrease in load in the pile  $\Delta Q$  is:

$$\Delta Q = AE_p \frac{\partial\Delta w}{\partial z} \dots\dots\dots (15)$$

or  $\Delta Q = -AE_p \Omega (\alpha e^{\Omega z} - \beta e^{-\Omega z}) \dots\dots\dots (16)$

with  $\Delta Q = - (Q_U - Q_R)$

where  $Q_R$  is the residual load in the pile at a depth  $z$ .

The boundary conditions can be written as follows:

for $z = 0$	$\Delta Q = - Q_{TU}$
for $z = L$	$\Delta Q = - (Q_{PU} - Q_{PR})$

where  $Q_{PR}$  is the residual point load.

It is also known that:

$$\begin{aligned} \text{for } z = L & \quad \Delta w = \Delta w_p \\ \text{and} & \quad - (Q_{PU} - Q_{PR}) = K'_p \Delta w_p A \end{aligned}$$

These last four equations involve four unknowns ( $\alpha, \beta, Q_{PR}, \Delta w_p$ ) which can therefore be obtained. The result is:

$$Q_R = Q_U - Q_{TU} \left( \frac{(E_p \Omega + K'_p) e^{\Omega(L-z)} - (E_p \Omega - K'_p) e^{-\Omega(L-z)}}{(E_p \Omega + K'_p) e^{\Omega L} - (E_p \Omega - K'_p) e^{-\Omega L}} \right) \dots (17)$$

which can be simplified to

$$Q_R = Q_U - Q_{TU} \left( \frac{\text{Cosh } (\partial + \Omega(L-z))}{\text{Cosh } (\partial + \Omega L)} \right) \dots (18)$$

with  $\tanh \partial = \frac{E_p \Omega}{K'_p}$

This equation which gives the distribution of the residual load in the pile can be used to express the residual load at the point  $Q_{PR}$ .

$$Q_{PR} = Q_{PU} - \frac{2Q_{TU}}{\left(1 + \frac{E_p \Omega}{K'_p}\right) e^{\Omega L} + \left(1 - \frac{E_p \Omega}{K'_p}\right) e^{-\Omega L}} \dots (19.a)$$

or,

$$Q_{PR} = Q_{PU} - Q_{TU} \frac{\cosh \partial}{\cosh (\partial + \Omega L)} \dots (19.b)$$

The residual friction stresses along the pile are:

$$\tau_R = \tau_U - Q_{TU} \frac{\Omega}{P} \left( \frac{(E_p \Omega + K'_p) e^{\Omega(L-z)} + (E_p \Omega - K'_p) e^{-\Omega(L-z)}}{(E_p \Omega + K'_p) e^{\Omega L} - (E_p \Omega - K'_p) e^{-\Omega L}} \right) \dots (20)$$

## DISCUSSION OF THE THEORETICAL FORMULATION

If the pile is infinitely short, the total load on the pile  $Q_{TU}$  is equal to the point load  $Q_{PU}$ . For  $L$  equal zero the above equations show that  $Q_{PR}$  is zero. No residual point load can exist since no shaft friction can be reversed to maintain any residual point load.

If the pile is infinitely long then the equations give a residual point load equal to the ultimate point load. Indeed, there is an infinite amount of friction available to maintain the full ultimate point load and the unloading of the top of the infinitely long pile does not generate any unloading movement at the pile tip.

If the value of  $K'_p$  is low,  $E_p \Omega / K'_p$  is large compared to 1 and the residual point load is large. Indeed if the value of  $K'_p$  is low, it takes a large unloading displacement to unload the point load; before the point load is unloaded significantly the friction is reversed and residual load equilibrium is reached.

If the value of  $\Omega$  is large, again the equations point to a large residual point load. Indeed if the value of  $\Omega$  is large,  $K'_p$  is large compared to  $E_p$ . This means that it takes little displacement to reverse the friction but that the elastic decompression of the pile is large. Therefore, friction is reversed early and a large residual point load is maintained.

The equations derived show theoretically what was expected physically. It is important to note that the distribution of residual loads is dependent upon the load distribution at ultimate load. Indeed, different ultimate load distribution will lead to different residual load distribution. The same comment applies to the distribution of residual stresses.

## EXAMPLE OF THEORETICAL RESIDUAL LOADS

The following example is given to illustrate the results of the theoretical formulation. The pile was chosen as being an "average" pile for normal onshore conditions. The following values are considered:

Pile  $A = 144 \text{ in.}^2 (0.093 \text{ m}^2)$   
 $P = 48 \text{ in.} (1.22 \text{ m})$   
 $E_p = 3 \times 10^6 \text{ lb/in.}^2 (2.07 \times 10^7 \text{ kN/m}^2)$   
 $L = 600 \text{ in.} (15.24 \text{ m})$

Soil  $K_T = 40 \text{ lb/in.}^3 (10840 \text{ kN/m}^3)$   
 $K_p = 2300 \text{ lb/in.}^3 (623,300 \text{ kN/m}^3)$   
 $Q_{TU} = 200,000 \text{ lbs.} (44.94 \text{ kN})$   
 $Q_{pU} = 100,000 \text{ lbs.} (22.47 \text{ kN})$

The theoretical parameters are obtained:

$$\Omega = 2.1 \times 10^{-3} \text{ in.}^{-1} (8.3 \times 10^{-4} \text{ cm}^{-1})$$

$$E_p \Omega - K'_p = 4,000 \text{ lb/in.}^3 (1.08 \times 10^6 \text{ kN/m}^3)$$

$$E_p \Omega + K'_p = 8,600 \text{ lb/in.}^3 (2.33 \times 10^6 \text{ kN/m}^3)$$

$$\Omega L = 1.26$$

Table 5 gives the residual loads and residual friction stresses as a function of depth.

TABLE 5.-Distribution of Residual Loads After Driving

Depth ft	Ultimate Load tons	Residual Load tons	Ultimate Friction tsf	Residual Friction tsf
0	100	0	0.25	- 0.38
10	90	14	0.25	- 0.29
20	80	24	0.25	- 0.18
30	70	30	0.25	- 0.11
40	60	33	0.25	- 0.06
50	50	34	0.25	- 0.02

Note: 1 ft = 0.305 m; 1 ton = 8.9 kN; 1 tsf = 95.8 kN/m<sup>2</sup>

The results are plotted on Fig. 22. The profile of the residual friction stresses  $\tau_R$  shows a friction at the surface which is larger than the ultimate friction  $\tau_U$ . This is due to the elastic analysis which did not consider an ultimate value. In reality the ultimate friction at the surface is zero and a possible real profile is shown in dotted line on Fig. 22. The corresponding real profile for load distribution is shown.

#### EXTENSION OF THE RESULTS TO THE TENSION TEST

All the theory and discussion presented above pertain to the case of a hammer blow or a compression test. The results can be extended to the case of the residual loads that exist in a pile after a tension test. The theoretical formulation is the same except that the boundary conditions are:

$$\begin{array}{ll} \text{for } z = 0 & \Delta Q = - Q_{TU} \\ \text{for } z = L & \Delta Q = 0 \end{array}$$

This leads to the expression of the residual loads:

$$Q_R = Q_U - Q_{TU} \left( \frac{e^{\Omega z} e^{2\Omega(L-z)} - 1}{e^{2\Omega L} - 1} \right) \dots \dots \dots (21)$$

and to the expression of the residual stresses:

$$\tau_R = \tau_u + Q_{TU} \frac{\Omega}{P} e^{\Omega z} \left( \frac{e^{2\Omega(L-z)} + 1}{e^{2\Omega L} - 1} \right) \dots \dots \dots (22)$$

The example pile used for the compression test is used here for the tension test. The resulting residual loads and stresses are summarized in Table 6 and are shown in Fig. 23.

COMPRESSION TEST

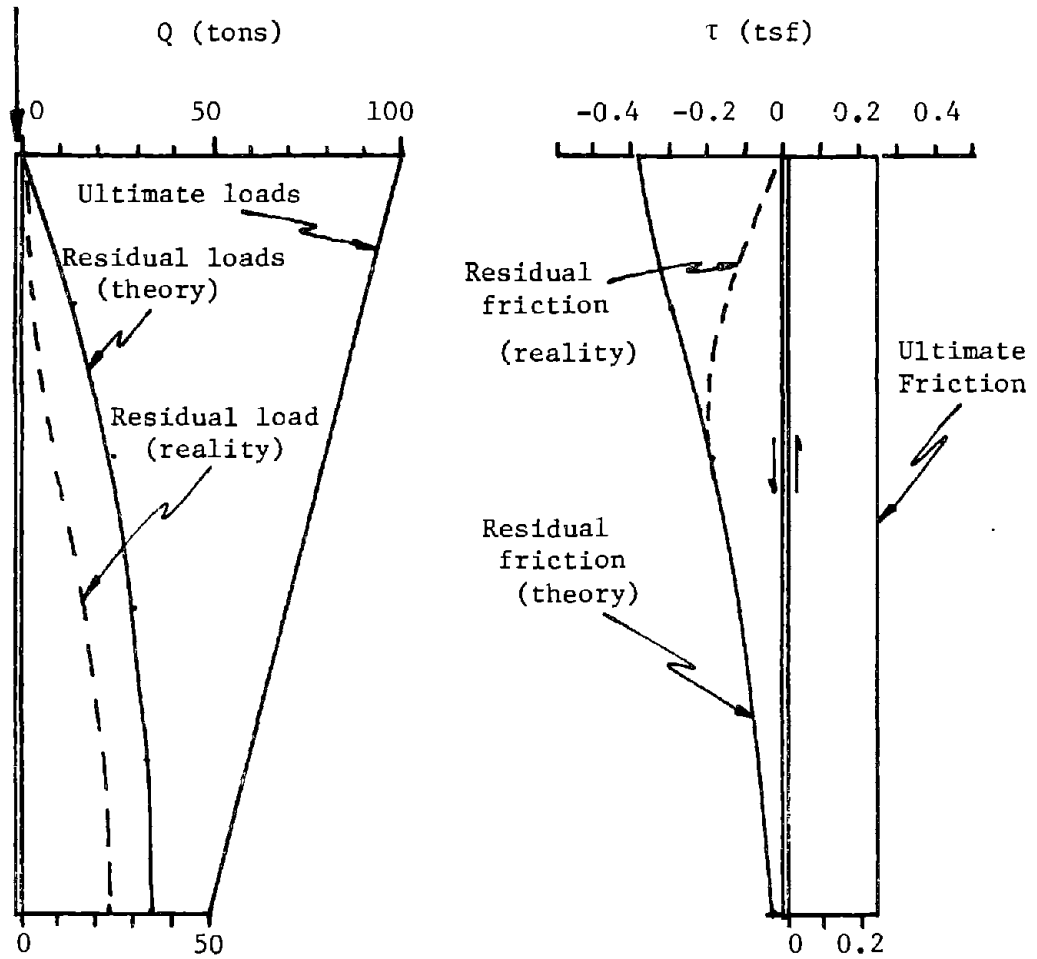


FIG. 22.- Example of Theoretical Residual Loads  
(1 ton = 8.9 kN; 1 tsf = 95.8 kPa)

TENSION TEST

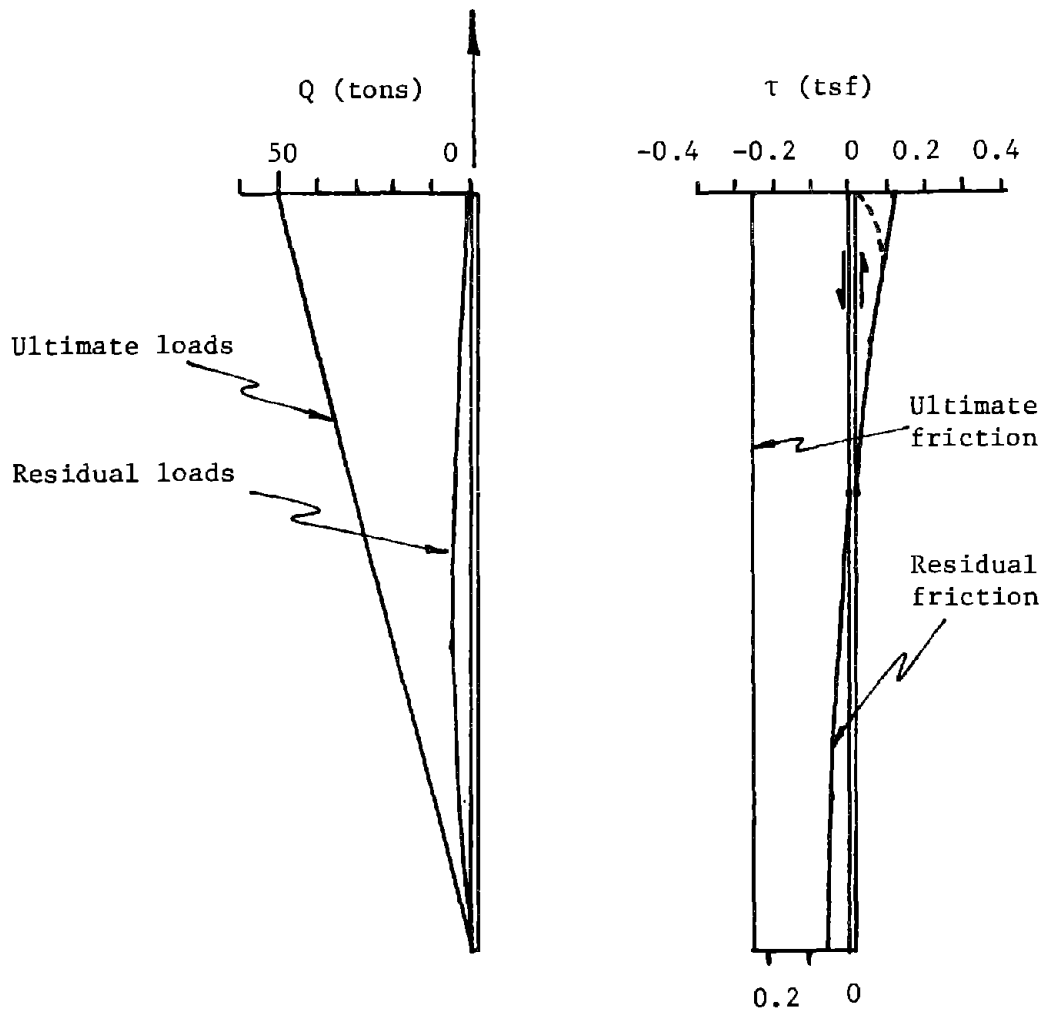


FIG. 23.- Example of Theoretical Residual Load After a Tension Test  
(1 ton = 8.9 kN; 1 tsf = 95.8 kPa)



TABLE 6.-Distribution of Residual Loads After Tension Test

Depth ft	Ultimate Load tons	Residual Load tons	Ultimate Friction tsf	Residual Friction tsf
0	- 50	0	- 0.25	+ 0.120
10	- 40	- 3.4	- 0.25	- 0.051
20	- 30	- 4.4	- 0.25	- 0.003
30	- 20	- 5.65	- 0.25	- 0.031
40	- 10	- 2.15	- 0.25	- 0.05
50	0	0	- 0.25	- 0.056

Note: 1 ft = 0.305 m; 1 ton = 8.9 kN; 1 tsf = 95.8 kN/m<sup>2</sup>

As can be seen, the residual loads are much smaller than for the compression test.

#### CONCLUSIONS

From this theoretical analysis, it can be concluded that:

1. The longer the pile, the larger the residual point load.
2. The more compressible the pile, the larger the residual point load.
3. The steeper the slope of the friction transfer curve, the larger the residual point load.
4. The shallower the slope of the point bearing transfer curve, the larger the residual point load.

It was also shown that the distribution of residual loads and residual stresses in a pile is directly related to the distribution of ultimate loads and ultimate stresses in that pile.

The engineering relevance of residual loads is that they are not considered in most pile load tests. Instead, the instrumentation is zeroed after the pile is driven. Therefore, the loads measured are the difference between the actual loads and the residual loads in the pile (Fig. 22). As a result, the measured point loads are too small and the friction values too high. Most current design procedures are based on load tests which ignore residual loads.

## CHAPTER V - OBTAINING RESIDUAL STRESSES FROM LOAD TESTS

### CONVENTIONAL LOAD TESTS

In a conventional load test on an instrumented pile, the following testing sequence is usually observed: first the pile is instrumented, second the pile is driven, third the instrumentation is zeroed, fourth the load test is performed. Zeroing the instrumentation after having driven the pile is equivalent to assuming that zero stresses exist in the pile after driving. Therefore, in a conventional load test residual stresses are not measured.

The difference in load distribution in the pile between the measured loads as described above and the true loads that exist in the pile is shown on Figs. 24 and 25 for a compression test and a tension test respectively. As can be seen, the interpretation of the results from a conventional compression test will lead to a point load which is lower than the true point load and to a friction load which is higher than the true friction load.

The interpretation of the results from a conventional tension test on the other hand, will lead to a point load which is larger than the true point load which is zero, and to a friction load which is smaller than the true friction load.

### EXISTENCE OF RESIDUAL STRESSES

The existence of residual stresses in hammer driven piles may be best exemplified by the following case (Fig. 26). At the Arkansas River site, two piles were installed, one was driven, the other one was vibrated into place. The conventional procedure of zeroing the instrumentation after placing the pile was applied before the two piles were loaded to failure in compression. After bringing the top load back to zero the load distributions in the piles indicated by the instrumentation showed drastic residual loads in the vibrated pile and very little, if any, residual loads in the driven pile.

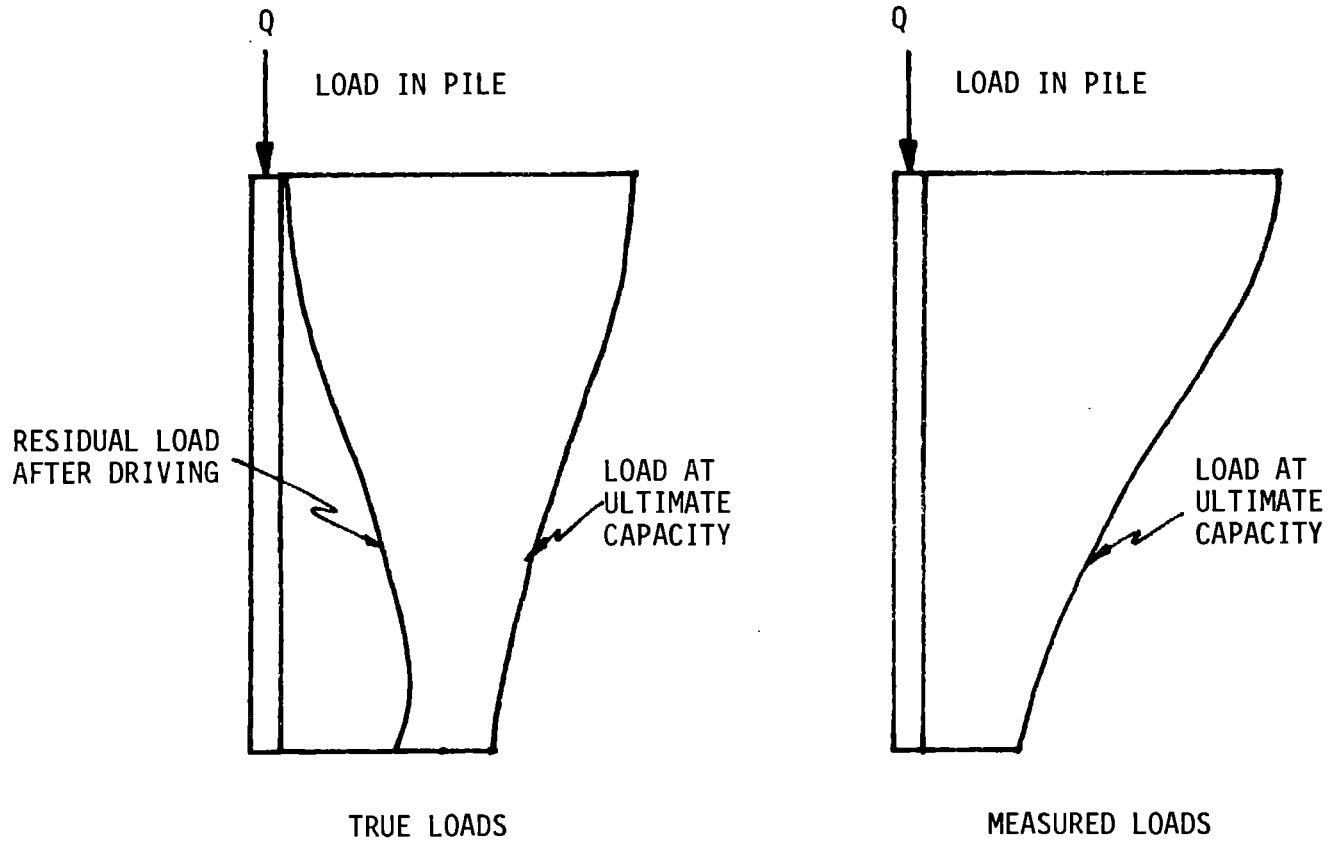


FIG. 24.- Load In Pile During Compression Test

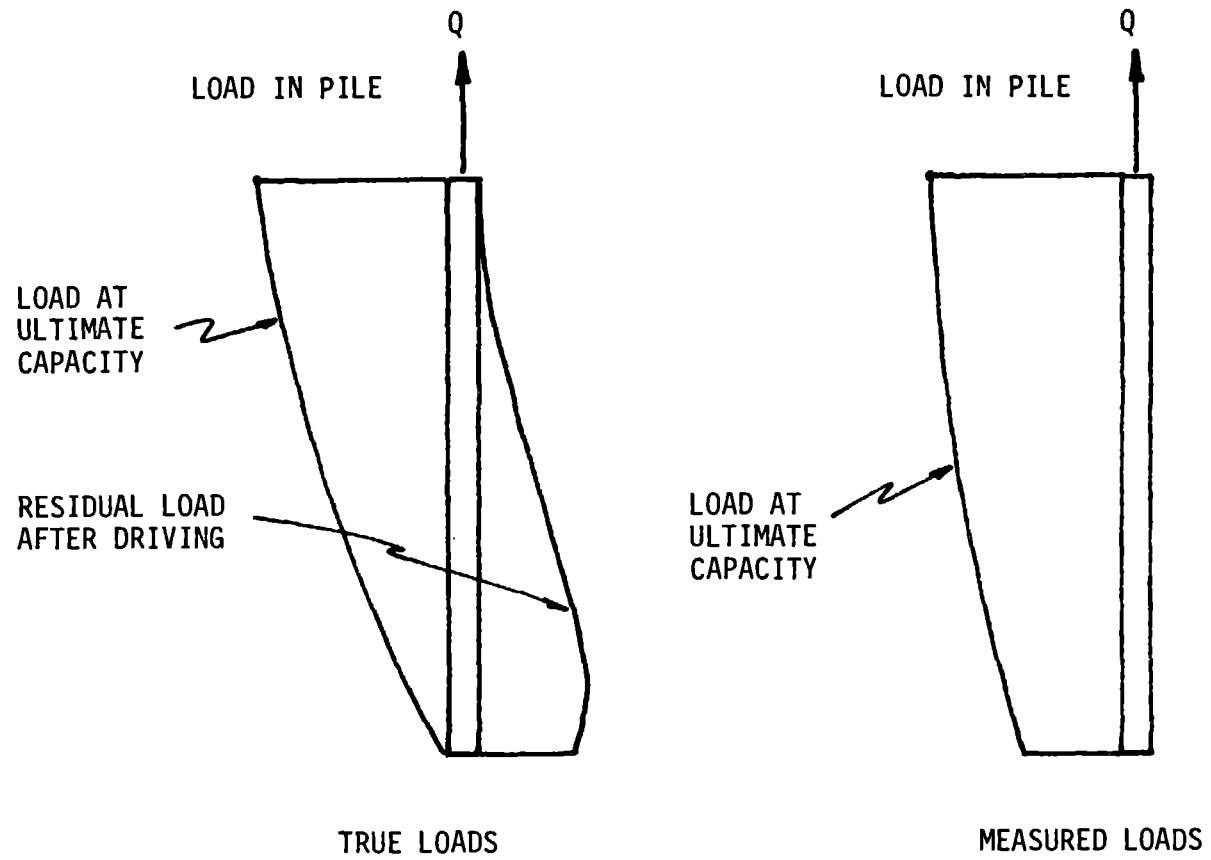


FIG. 25.- Load In Pile During Tension Test

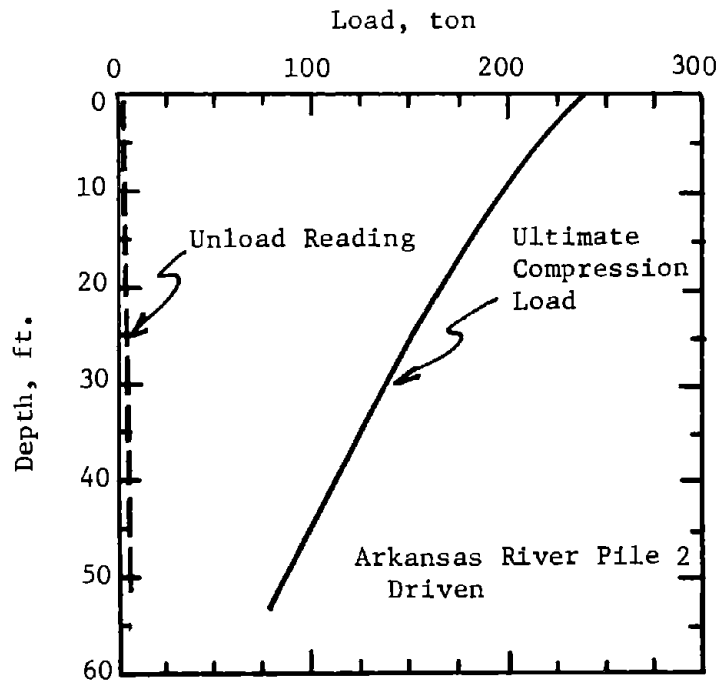
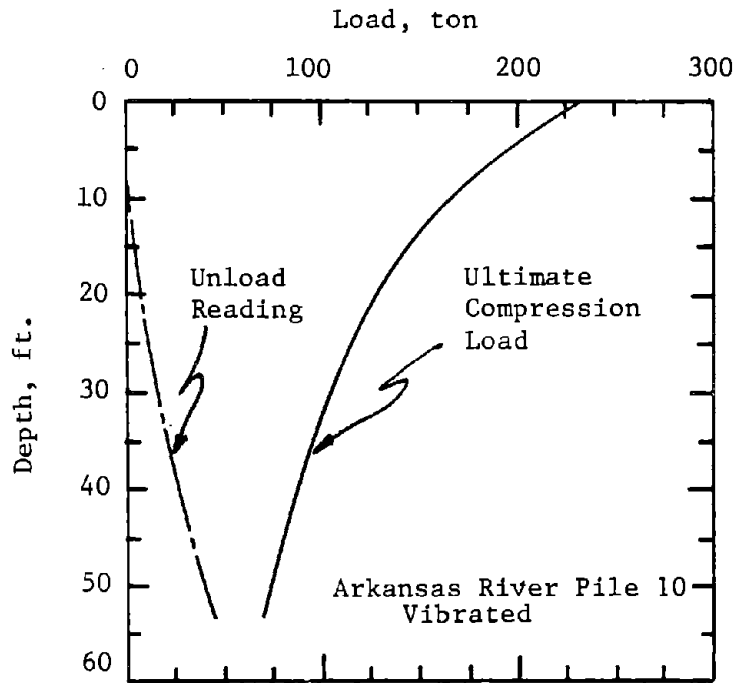


FIG. 26.- Comparison of Residual Loads in Vibrated and Driven Piles  
(1 ft = 0.305 m; 1 ton = 8.9 kN)

The above phenomenon is explained as follows. Vibrating a pile into the soil creates very little residual stresses and therefore, zeroing the instrumentation after vibrating a pile in the ground is a procedure which gives a close approximation of the true loads in the pile. The compression-decompression load test performed on the vibrated pile simulated a very slow hammer blow and residual loads appeared at the end of the unloading part of the test.

Driving a pile in the soil creates significant residual stresses and therefore zeroing the instrumentation after driving the pile is equivalent to having the residual load distribution as a zero reference. The compression-decompression load test which took place after the driving sequence could be considered as simulating another hammer blow. At the end of the unloading part of the test the load distribution came back to the residual load distribution. This load distribution appeared as zero load in the pile since the instrumentation had been zeroed under similar conditions after the driving process.

#### MEASURING RESIDUAL STRESSES

There are several methods that can be used to measure residual stresses. These methods are described in sequence in the following sections.

##### Method 1: Read Instrumentation Before and After Driving

The most direct method of measuring residual loads is to hang the pile in driving position under the hammer. While the pile is hanging under its own weight the instrumentation is zeroed. The pile is driven and the instrumentation is read immediately after final penetration is reached. The residual loads are then calculated directly.

The instrumentation in this case can be of the strain gage or strain rod type. In addition, pressure cells are sometimes placed under the pile tip for direct measurements of the residual point pressure. All other methods consist of zeroing the instrumentation after the pile is driven and of obtaining the residual load by using a combination of testing sequence and theoretical reasoning.

## Method 2: Hunter-Davisson Method

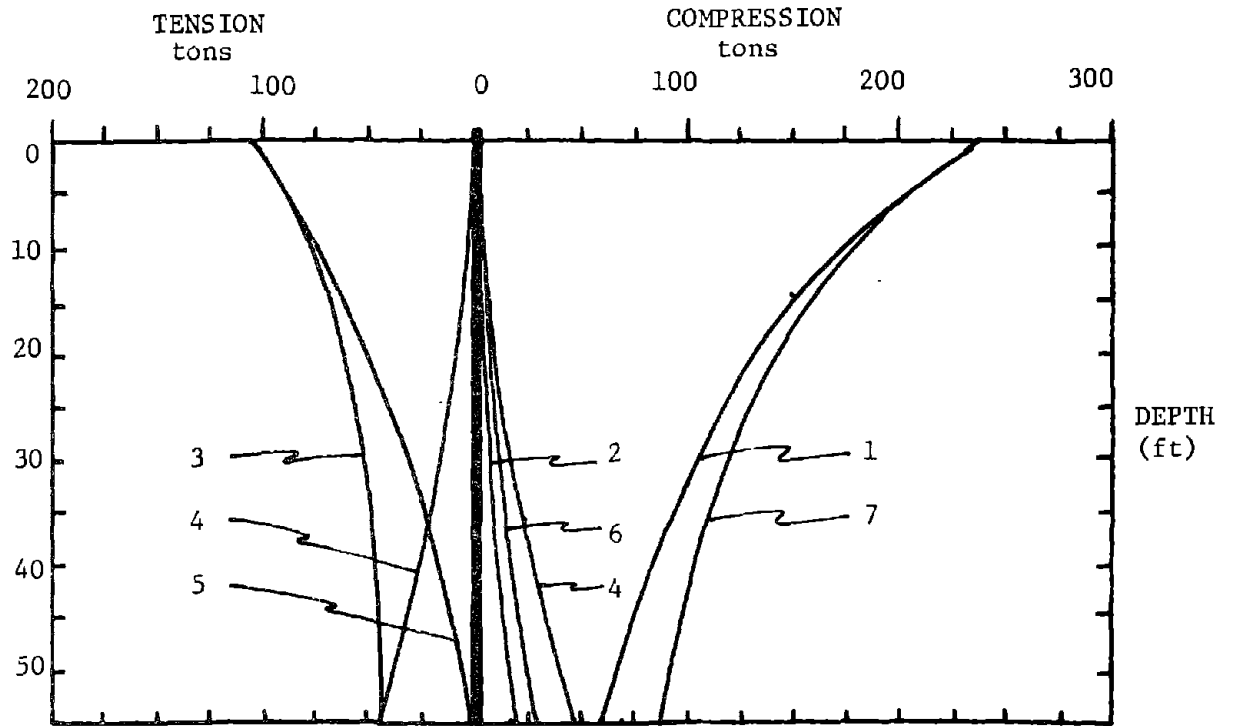
Hunter-Davisson (23) devised a method which involves a given testing sequence during the load test and then a special reasoning sequence during the data analysis.

The testing sequence consists of:

1. Drive the pile.
2. Zero the instrumentation.
3. Load the pile to failure in compression, read the instrumentation.
4. Unload the pile to zero top load, read the instrumentation.
5. Zero the instrumentation.
6. Load the pile to failure in tension, read the instrumentation.
7. Unload the pile to zero top load, read the instrumentation.

The reasoning and analysis sequence consists of (Fig. 27):

1. Curve 1 represents the measured ultimate compression load distribution, assuming no stresses in the pile at start of test.
2. Curve 2 represents the measured compression load distribution after complete release of the applied compressive load, assuming no stresses in the pile at start of test.
3. Curve 3 represents the measured ultimate tension load distribution assuming no stresses in the pile at start of test.
4. Curve 4 represents the measured tension load distribution after complete release of the applied tensile load, assuming no stresses in the pile at start of test.
5. It is assumed that no residual stresses exist at the end of the tension test. Therefore, curve 4 represents the residual compressive loads for the test and should be subtracted from curve 3 in order to give curve 5, the adjusted tension load distribution.
6. Curve 4 includes the original compressive residual loads in the pile due to driving before the compression test, plus the residual loads induced by the compression test. The subtraction of



- 1 - Ultimate Compression
- 2 - Unload Compression
- 3 - Ultimate Tension
- 4 - Unload Tension
- 5 - Corrected Tension
- 6 - Residual Load
- 7 - Corrected Compression.

FIG. 27.- Hunter-Davisson Method for Residual Load Correction  
 (from ref. 31) (1 ton = 8.9 kN; 1 ft = 0.305 m)



curve 2 from curve 4 gives curve 6, the original compressive residual loads in the pile.

7. Curve 6 is added to curve 1 to give curve 7, the adjusted compression load distribution.

This method is based on the assumption that no residual loads are induced by the tension test. As shown in the previous chapter, this assumption is incorrect. The error is zero at the top and bottom of the pile and peaks towards the middle of the pile where the residual tension load can be 25% of the ultimate tension load. This method will lead to accurate predictions of residual point load but somewhat erroneous residual friction stresses distribution.

#### Method 3: No Unloading Reading Method

Often, the testing sequence used for a load test does not follow rigorously the testing sequence required to apply the Hunter-Davisson method. Method 3 is used when no reading of the instrumentation is taken after unloading the pile, that is to say, when steps 4 and 6 for the testing sequence of Method 2 are not performed. Therefore, compared to Method 2, curves 2 and 4 are not available. In this case the tension load at the point is assumed to be the residual compressive load at the point after driving. This assumes that the change in residual loads created by the compression test is negligible. Fig. 26 shows the results of a load test for which this assumption is most appropriate (driven pile). Curve 4 for Method 3 is assumed to be a line joining the point load of curve 3 and zero load at the top.

#### Method 4: No Instrumentation Method

When the instrumentation of the pile is reduced to the measurement of top load and top movement, the distribution of load in the pile cannot be obtained. In Method 4 the ultimate tension load is assumed to be the ultimate friction load in compression. This friction load is subtracted from the ultimate compression load to give the ultimate point load. The validity of this assumption can be evaluated from the comparison of the measured ultimate friction load in tension and the measured ultimate friction load in compression for load tests which present enough detailed data.

## RESIDUAL STRESSES: LOAD TEST RESULTS

The results of the four methods are summarized in Table 7 for the load tests for which the analyses were possible. This table is based on the  $0.1xD$  failure criterion. A comparison of Methods 2 and 3 was possible for five piles at the Arkansas River site. The residual load given by Method 3 averaged 13 percent higher than that given by Method 2. This discrepancy is due to the fact that Method 3 assumes no additional residual loads were induced in the piles during the compression test. This is obviously not the case. A comparison of Method 4 with the results of Methods 1, 2 and 3 was possible for 14 piles. Methods 1, 2 and 3 yield a compressive side friction load, whereas Method 4 gives the tensile friction load. A comparison of the results shows that, on the average the friction in tension is only 70 percent of the friction in compression. This percentage varies from 40% to 110% and is lowest for short piles, H piles and tapered piles. Fig. 28 is a plot of the ratio of the friction load in tension divided by the friction load in compression versus the length of the pile. This figure shows that the ratio can be more than 1. Because of the difference between friction load in tension and friction load in compression, Method 4 was not used in further analyses in this study. The residual loads used in further analyses were those given by the method available for each pile; Method 1 being the most reliable method, Method 4 the least reliable.

TABLE 7.- Comparison of Methods of Obtaining Residual Loads from Load Test Data

SITE	PILE	METHOD 1: MEASURED			METHOD 2: HUNTER-DAVISSON			METHOD 3: NO UNLOAD READING			METHOD 4: COMPRESSION/TENSION	
		$Q_{res}$ tons	$Q_p$ tons	$Q_s$ tons	$Q_{res}$ tons	$Q_p$ tons	$Q_s$ tons	$Q_{res}$ tons	$Q_p$ tons	$Q_s$ tons	$Q_p$ tons	$Q_s$ tons
Arkansas River	1				37	87	85	32	82	90	77	95
	2				45	120	122	62	137	105	127	115
	3				48	163	109	64	179	93	152	120
	7 H				25	85	158	25	85	158	175	67
	10				10	83	159				134	108
	16				40	93	82	33	86	89	97	78
Low Sill	2							29	179	241	225	195
	4							37	125	315	215	225
	5							29	54	91	61	84
	6							51	186	244	245	185
Gregersen	A	3.3	6.5	20.5							17	10
	D/A	5.3	12.0	39.0							24	27
	C	1.3	4.5	29.5							18	12
	B/C	5.3	7.0	41.0							25	23
Sellgren	AI	7.0	66.0	11.5								
	AII	13.0	33.5	109.0								
Lock and Dam 26	3IP-III5 H				24.5							
Ogeechee River	H-15										248	173

Note: 1 ton = 8.9 kN

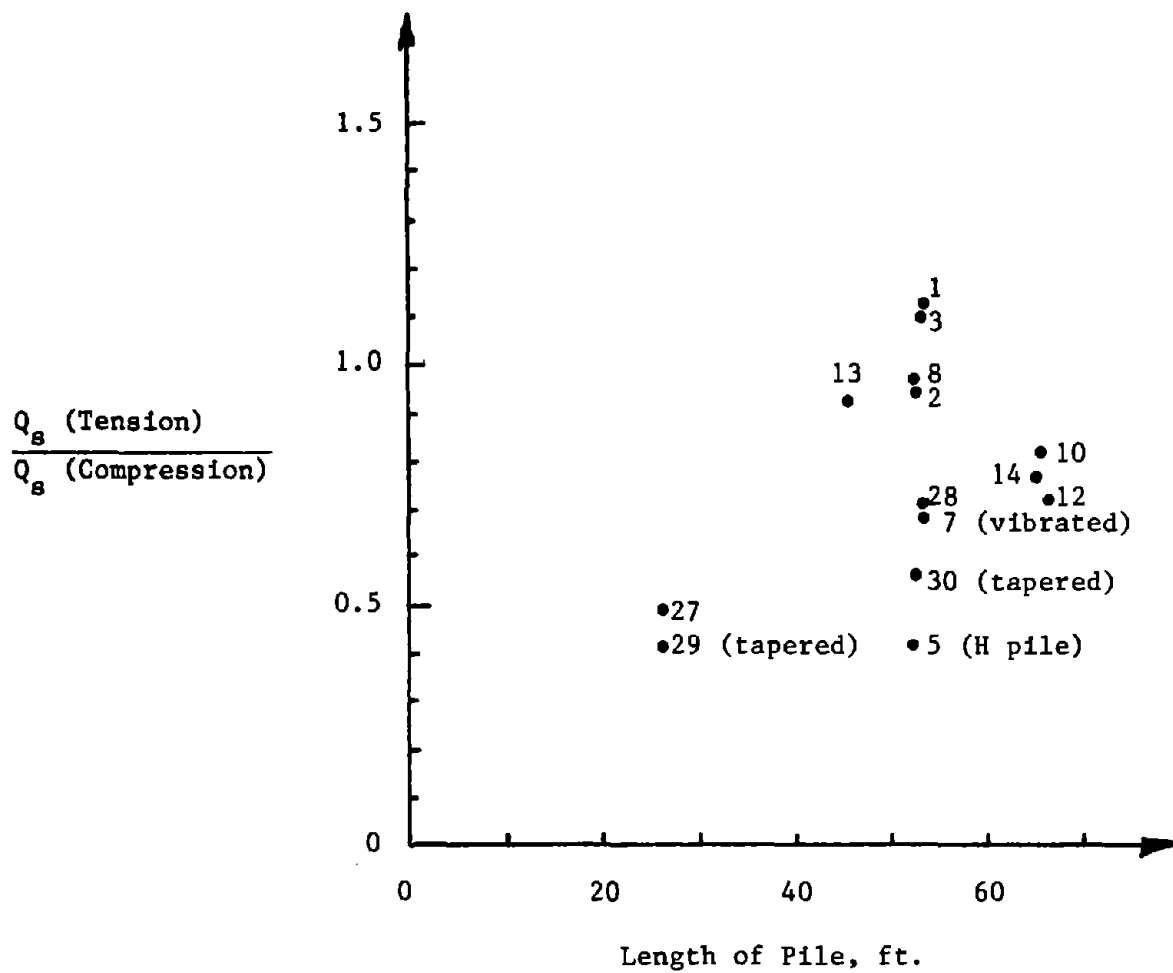


FIG. 28.- Comparison of the Friction Load in Tension and Compression  
(1 ft = 0.305 m)

## CHAPTER VI - OBTAINING RESIDUAL STRESSES WITH THE WAVE EQUATION

### GENERAL

There has been widespread interest in the use of the wave equation for pile driving analysis since the early 1960's. The main application has been in pile driveability studies and hammer selection. The wave equation has also been used to verify pile capacity during construction. In 1975 Holloway et al. (22) proposed the use of the wave equation for obtaining residual stresses in driven piles.

### THE MODEL

The pile is modeled as a system of concentrated weights connected by weightless springs. The soil is modeled as a spring and a dashpot (Fig. 29). The displacements and velocities of each of the pile segments and the forces between the segments are then computed using formulas developed by Smith (35).

The soil model used in this analysis is that proposed by Smith (36) and presented by Hirsch et al. (21). The model is a linear elastic-plastic model (Fig. 30). The movement necessary to initiate plastic deformation is called the quake and was taken as 0.1 in. (0.25 cm) for both side and point resistances. The values for side and point damping were taken as 0.05 sec/ft (0.16 sec/m) and 0.15 sec/ft (0.49 sec/m) respectively. The ratio between total soil resistance and point resistance was taken from the pile load test results and the side load was distributed uniformly along the pile.

### OBTAINING RESIDUAL STRESSES

Smith's equations are solved iteratively increasing the time step by small increments. When the energy and momentum of the system satisfy given criteria the solution is stopped. Any forces left in the pile at this time are residual forces. Locking these forces in the pile and "hitting" the pile again results in new solutions for the residual

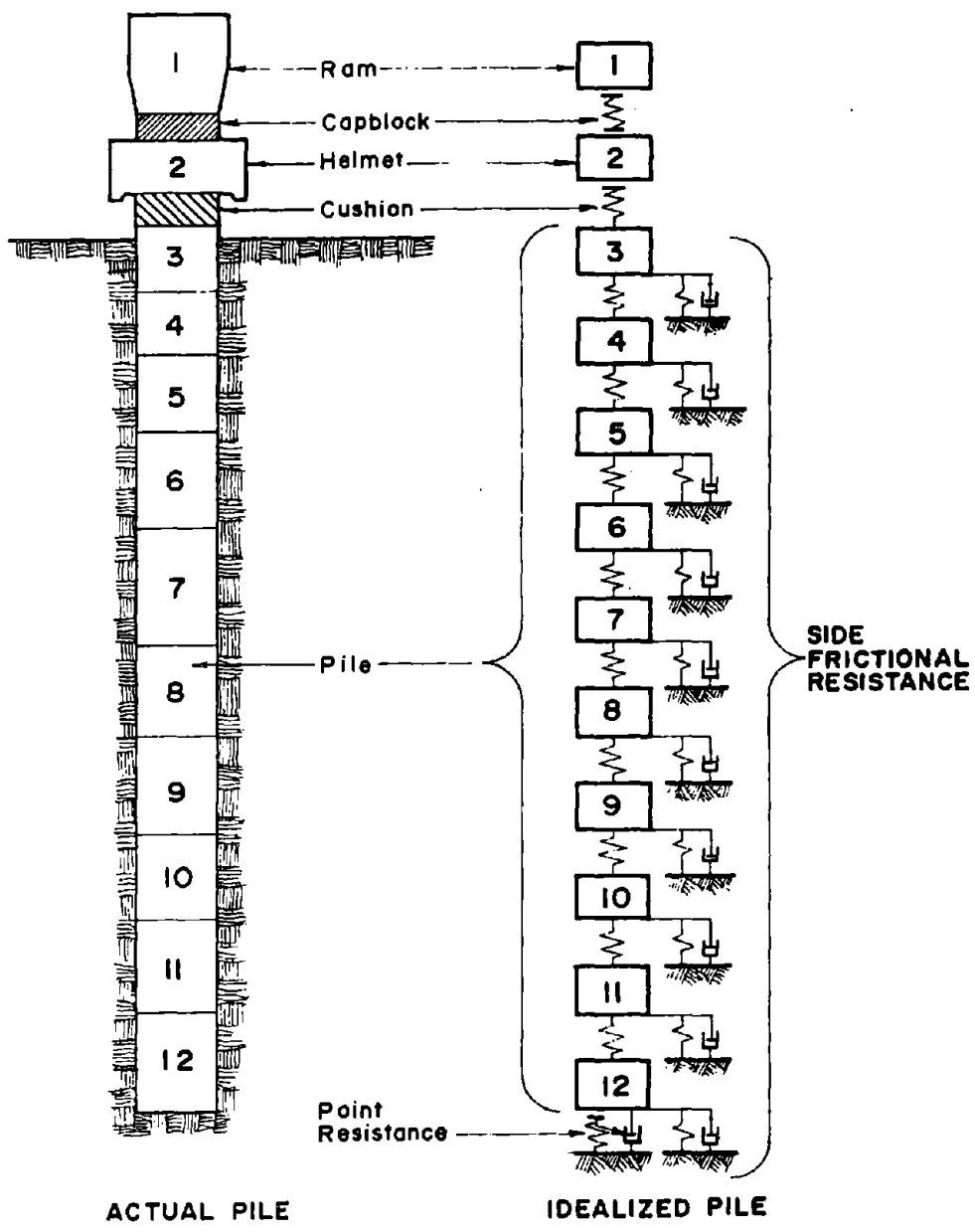


FIG. 29.- Pile and Soil Idealization for Use in the Wave Equation (after ref. 21)

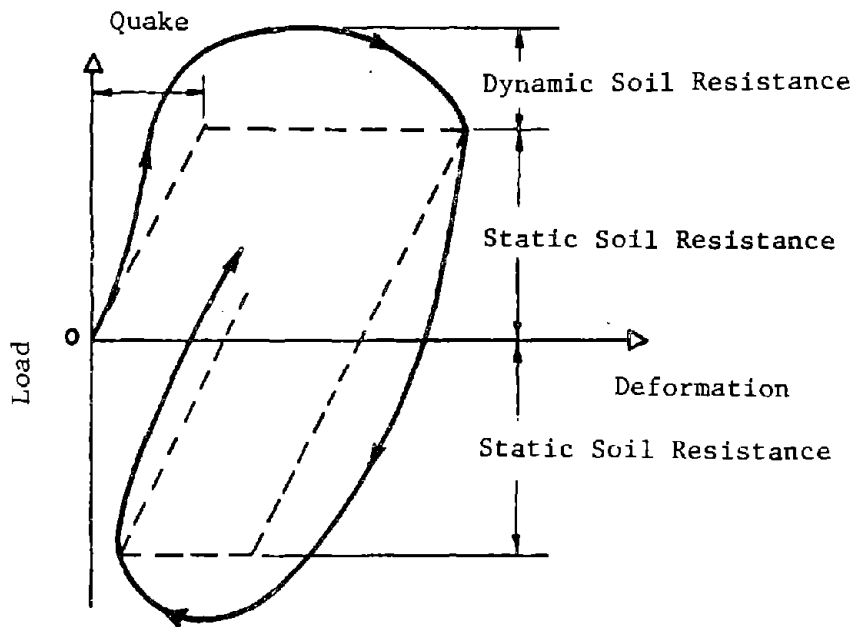


FIG. 30.- Smith's Soil Model  
 (after ref. 21)

forces. Fig. 31 shows a plot of the point load versus the time interval. The solution was performed for six blows, each of which ran 1000 iterations. After the third blow the solution repeated itself for each blow. In this study a series of five blows has always been found to be sufficient to obtain constant values for the residual stresses.

As seen in Fig. 31 the point load oscillates about, and converges towards a specific value. Thus the value of residual load may be obtained by plotting the point load versus number of time intervals and finding the value about which point load is oscillating. An example is shown in Fig. 32. The point load versus the time interval for the sixth blow on Lock and Dam 26 pile 5IP-I is shown. The load about which the point load is oscillating is marked with a dashed line.

The number of iterations or time intervals per blow required to determine the residual point load varied from pile to pile. The number also varied with the level of soil resistance: the lower the soil resistance, the larger the number of iterations required to determine the residual point load. The lower soil resistances also had a tendency to give more erratic results. In all cases studied, 1000 iterations per blow was sufficient to define the residual point load. This number may be decreased for higher soil resistance and may need to be increased for piles longer than 100 ft (30 m).

## RESULTS

A wave equation analysis was performed for all piles for which residual point loads were known and hammer data was available. A plot of the results for Arkansas pile 3 is shown in Fig. 33 in terms of the residual point load versus the blowcount on the pile. The residual point load predicted by this approach is plotted versus the measured residual point load in Fig. 34. An analysis of these results shows that the mean of the ratio of the predicted residual point load over the measured residual point load is 0.530 with a coefficient of variation of 0.669.

The results for this pile are also plotted in Fig. 35 in terms of



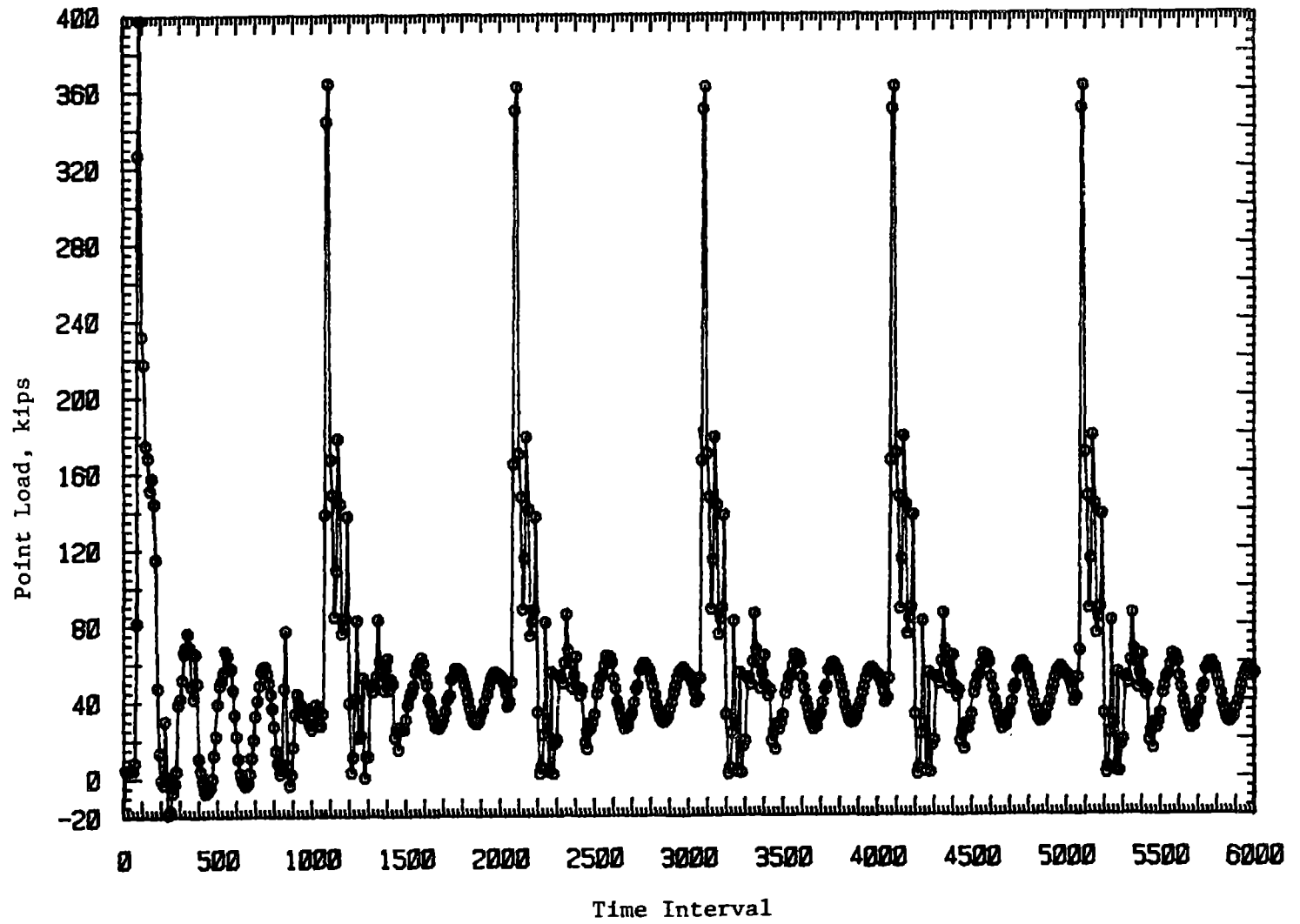


FIG. 31.- Variations of Point Load With Time for Six Hammer Blows  
(1 kip = 4.45 kN)

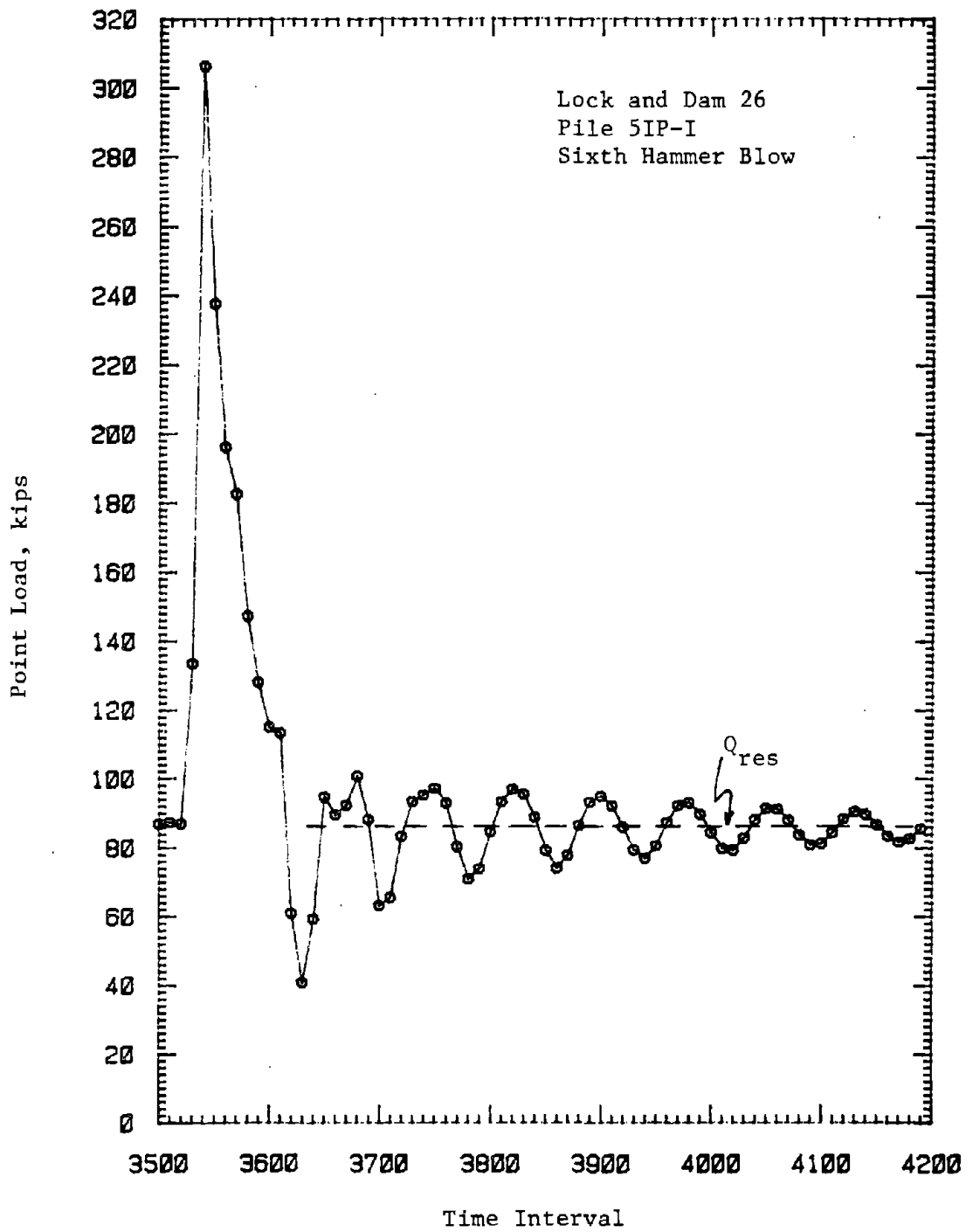


FIG. 32.- Obtaining Residual Point Load From Wave Equation Results  
(1 kip = 4.45 kN)

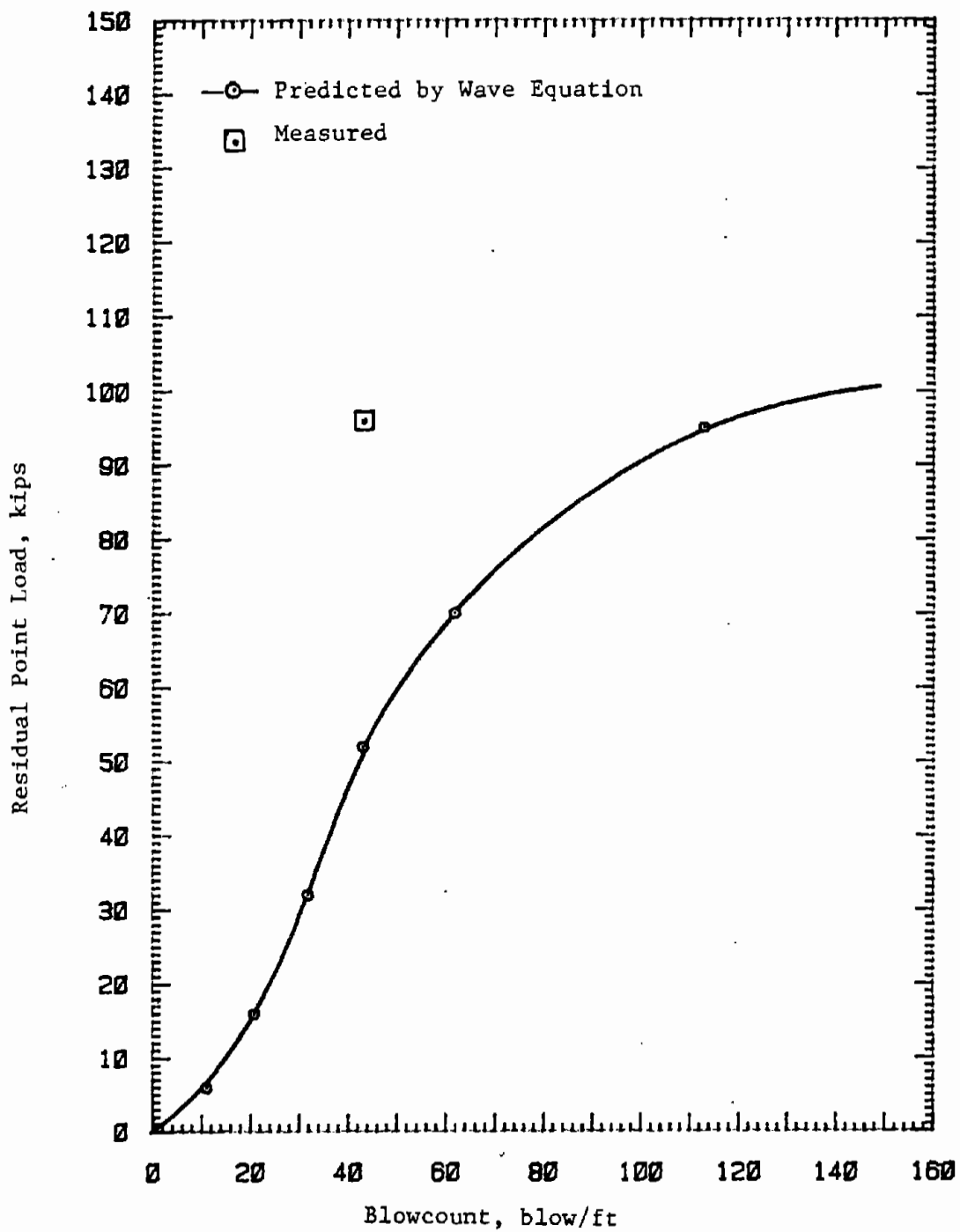


FIG. 33.- Residual Point Load Versus Blowcount  
 (1 kip = 4.45 kN; 1 blow/ft = 3.28 blow/m)

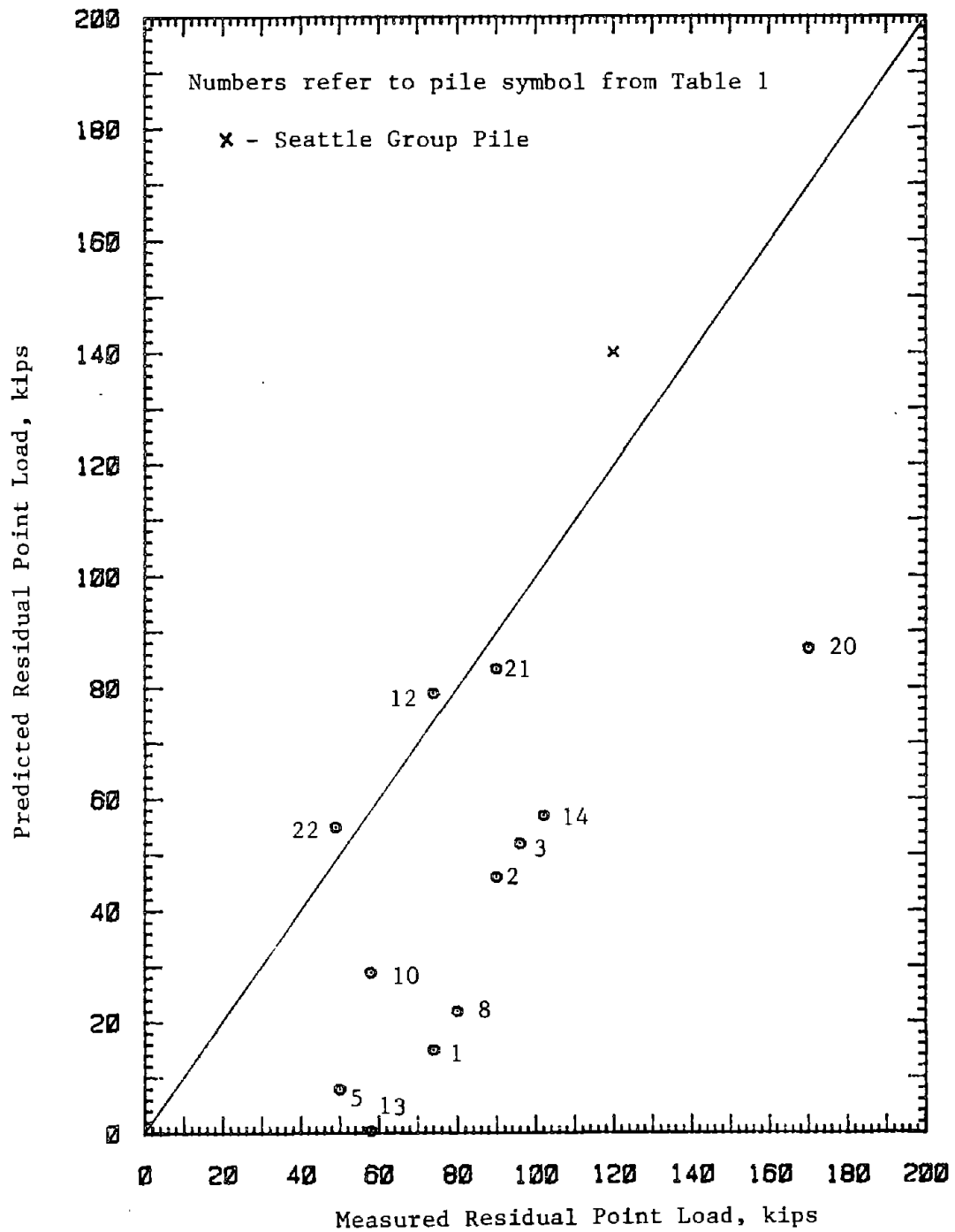


FIG. 34.- Comparison of Predicted Versus Measured Residual Point Load Using Blowcount Correlation (1 kip = 4.45 kN)

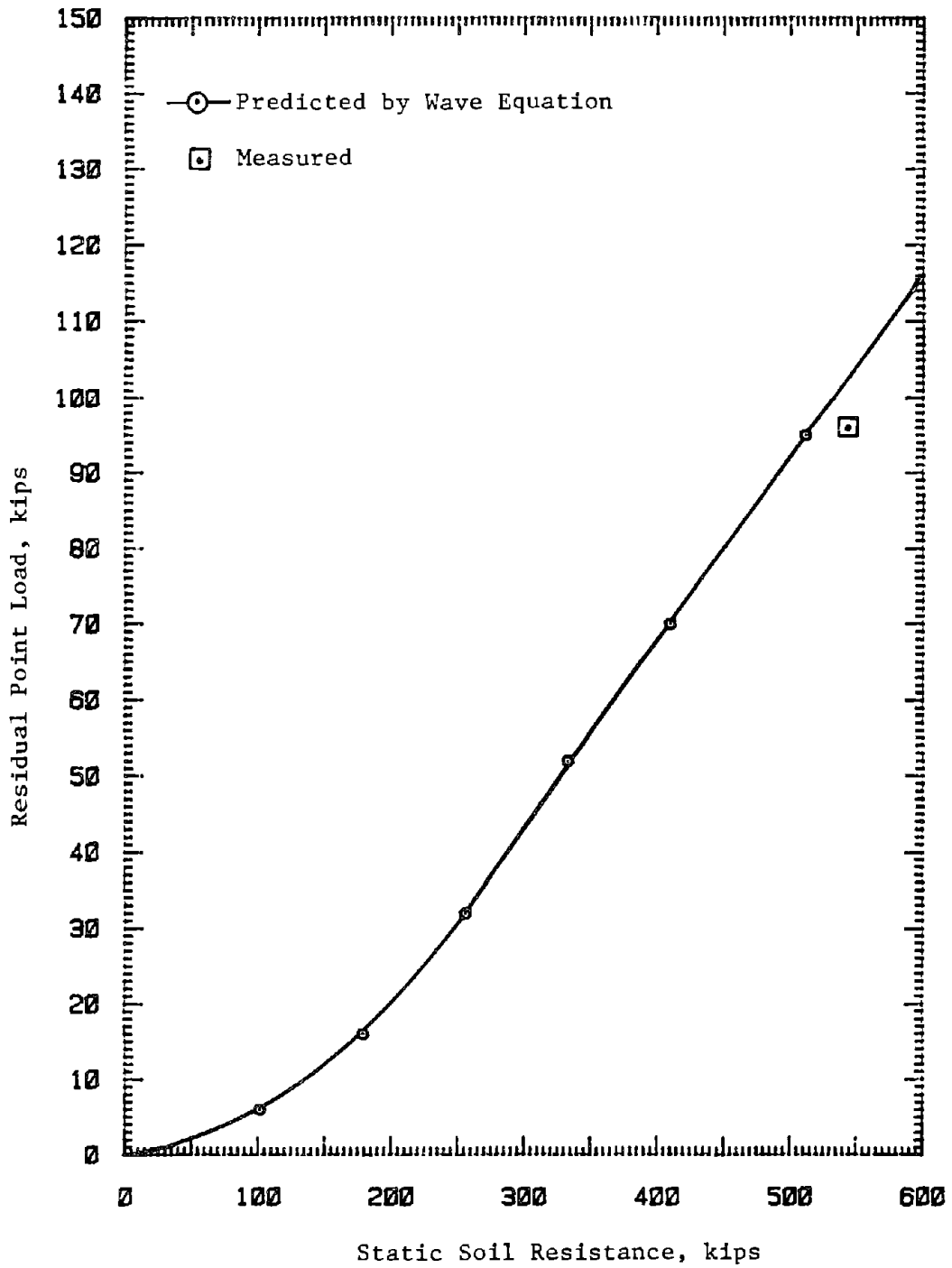


FIG. 35.- Arkansas River Pile 3: Residual Point Load Versus Static Soil Resistance (1 kip = 4.45 kN)

residual point load versus total static soil resistance at the time of driving. It was assumed that the static resistance at the time of driving was the same as the ultimate load from the compression load test ( $0.1 \times D$  failure criterion). This assumption is warranted, since the soil setup in sand is negligible. A plot of the residual point load predicted by this approach versus the measured residual point load is shown in Fig. 36. An analysis of the ratio of predicted residual point load over measured residual point load yields a mean of 1.116 with a coefficient of variation of 0.657. These results provide a better correlation than the previous results. The fact that the residual point load is related to the static total load at failure is consistent with the theoretical expression for the residual point load presented in Chapter IV (Eq. 19).

#### HYPERBOLIC SOIL MODEL

Holloway et al. (22) reported that the hyperbolic model for soil resistance yields more accurate results than does Smith's model. A limited study of the hyperbolic model used in the wave equation was performed. The results of this model are significantly different from those of the Smith model. Further case history comparisons and parameter studies are needed before definite conclusions can be made concerning this model for use in the wave equation.

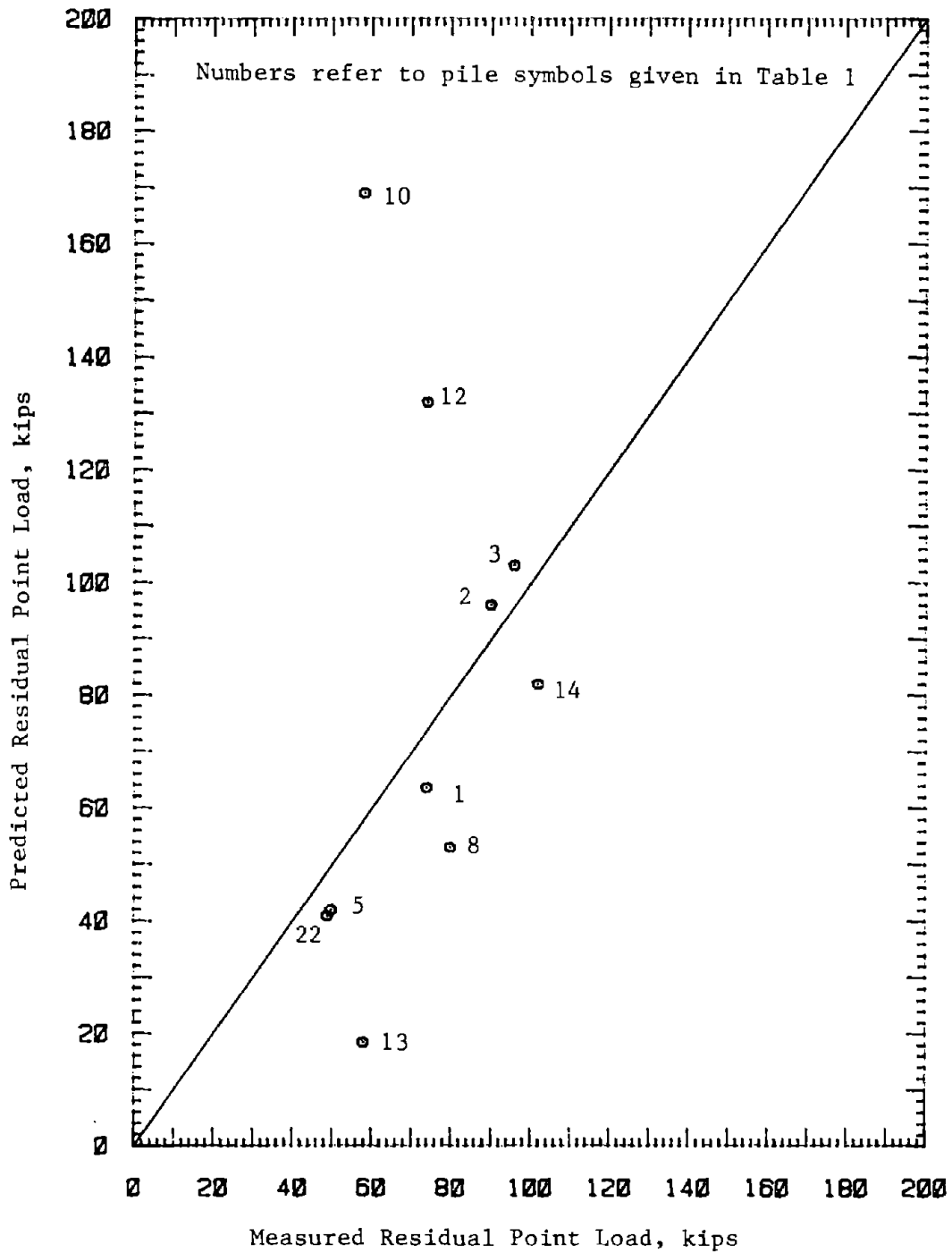


FIG. 36.- Comparison of Predicted Versus Measured Residual Point Load Using Ultimate Resistance Correlation (1 kip = 4.45 kN)

CHAPTER VII - LOAD TRANSFER ANALYSIS BY FINITE  
DIFFERENCE - PATTERN SEARCH APPROACH

INTRODUCTION

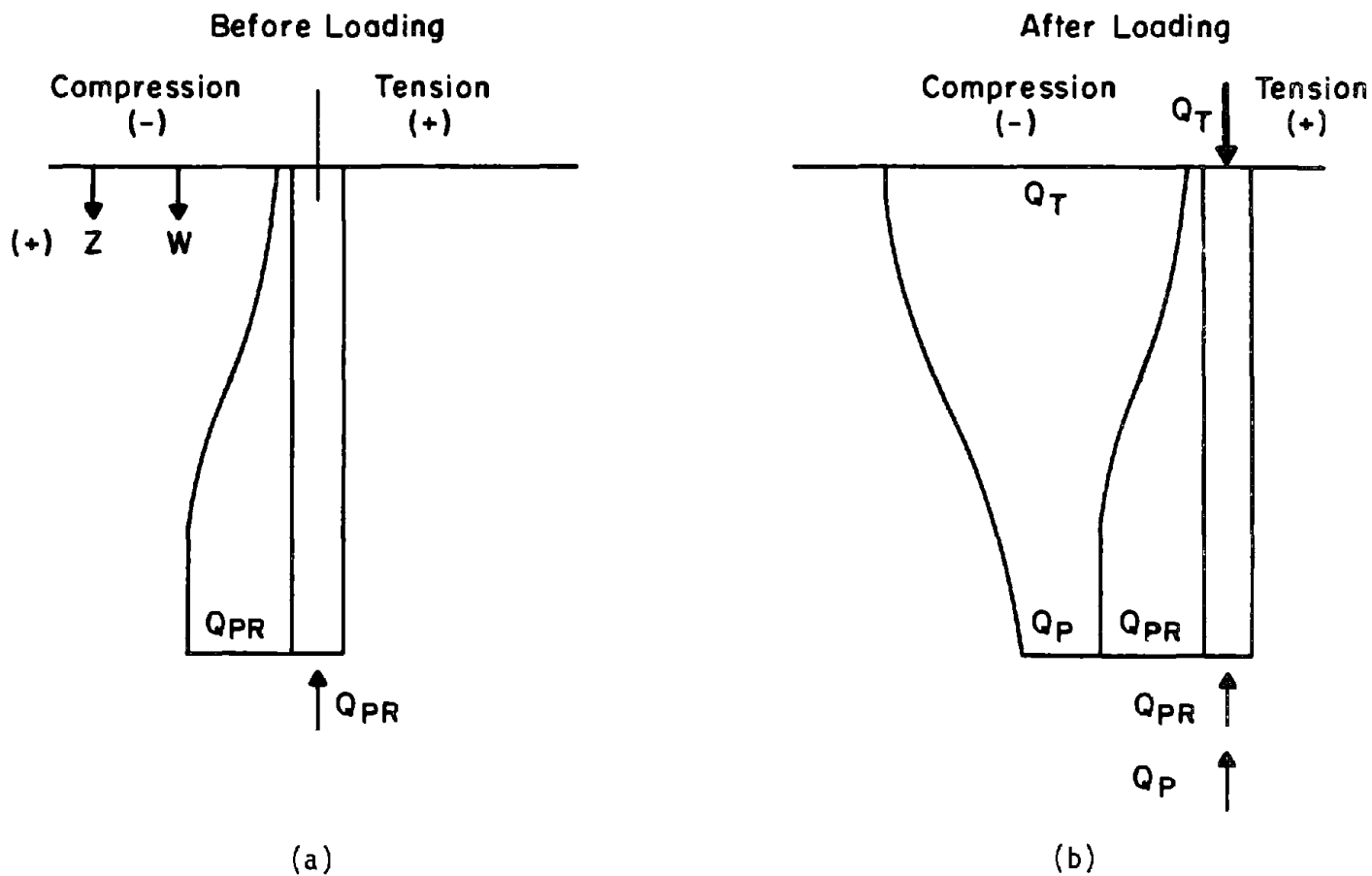
In Chapter IV, a description was given of the residual stresses that are found in piles after they are driven. Residual stresses are self-equilibrating because, with no load at the top of the pile, the sum of the shear forces along the side of the pile is equal to the residual compressive forces at the point of the pile. The internal stresses in the pile that are caused by these side shear and point compressive forces are compressive and are present in the pile when a load is applied to the top of the pile during a load test following the driving. This is illustrated in Fig. 37a. Because of this, they must be considered in determining the equilibrium of a pile-element under load as illustrated in Fig. 37b and in deriving the governing differential equation of the pile under load. The sign convention that is illustrated in Fig. 37 follows the structural convention of compression being negative and tension being positive. In addition, the positive z-coordinate direction is downward as is the positive direction for pile and soil displacement. The stresses acting on a tapered pile element are illustrated in Fig. 38.

NUMERICAL APPROXIMATION OF DIFFERENTIAL EQUATION

The differential equation that was developed in Chapter IV was extended to include a tapered pile element such as that shown in Fig. 38 and to account for the weight of the pile.

In order to closely represent reality it is necessary to approximate the differential equation numerically and to use a nonlinear constitutive equation for the soil-pile shear stress. The constitutive equation illustrated in Fig. 39 assumes that when a load is applied to the top of a pile, it first overcomes the residual shear stresses,  $\tau_r$ , with no vertical elastic compression of the pile, and then begins to





$Q_{PR}$  = point load in the pile due to residual stresses after driving

$Q_p$  = additional point load due to subsequent load application

$Q_T$  = load applied to the top of the pile.

FIG. 37. Loads in a Pile Before and After Loading

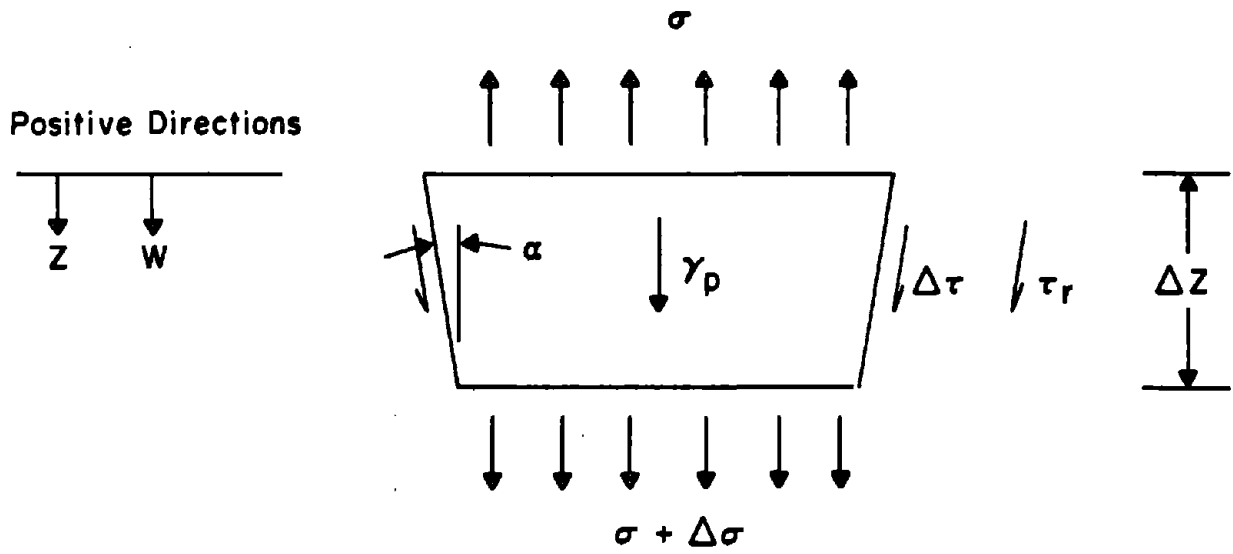
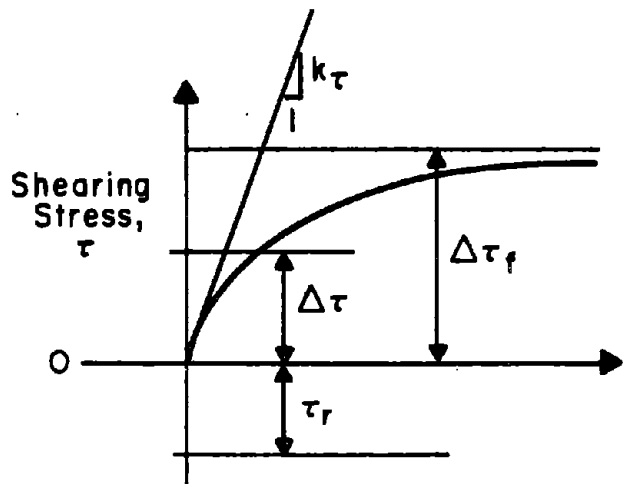
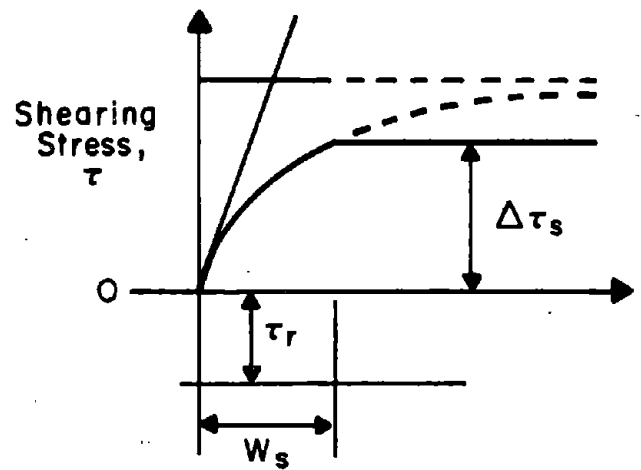


FIG. 38. Differential Element for a Pile



W, Vertical Displacement

Before Slip



W, Vertical Displacement

After Slip

FIG. 39. Illustration of Soil Constitutive Equation

build up additional shear stress,  $\Delta\tau$ , due to vertical displacement of the pile. The assumed constitutive equations for the residual shear stresses,  $\tau_r$ , and additional shear stresses,  $\Delta\tau$ , are as follows:

$$\tau_r = C e^{\gamma} \sin \phi z \dots \dots \dots (23)$$

$$\Delta\tau = \frac{w}{\frac{1}{k_\tau} + \frac{w}{\Delta\tau_f}} \dots \dots \dots (24)$$

where

$\Delta\tau_f$  = the asymptotic value of additional shear stress in the soil which  $\Delta\tau$  approaches as the vertical displacement increases

$k_\tau$  = the shear stiffness of the pile-soil interface

$C, \gamma, \phi$  = constants which describe the distribution of residual shear stresses after driving. These constants give patterns of residual stresses such as were illustrated in Fig. 19 in Chapter IV.

The parameters  $C$  and  $\phi$  were found to be dependent variables and thus a new constant,  $D$ , was defined for convenience in the pattern search as:

$$\phi = \frac{D}{C} \frac{A_p}{PL} \beta$$

There is a third phase in the assumed soil-pile shear stress constitutive equation when the additional shear stress reaches a limiting value,  $\Delta\tau_s$ , when a slip occurs between the soil and the pile. The slip occurs when the vertical displacement of the pile reaches a value of  $w_s$ .

It is further assumed that the shear stiffness,  $k_\tau$ , and ultimate shear strength,  $\Delta\tau_f$ , vary exponentially with depth, as follows:

$$k_\tau = A(z)^n \dots \dots \dots (25)$$

$$\Delta\tau_f = B(z)^m \dots \dots \dots (26)$$

The numerical approximation of the differential equation thus uses a total of nine constants, as follows:

- Soil shear stiffness,  $A, n$
- Maximum shear strength,  $B, m$
- Soil-pile point stiffness,  $k_p$
- Maximum pile point pressure,  $q_f$
- Residual soil shear stress,  $C, \gamma, \phi$

It is possible to determine all nine constants given above by a method of minimizing the sum of the squared errors between the observed and predicted side forces. This was done using an iterative pattern search computer program.

#### SUMMARY OF PILE ANALYSIS

The details of the pile length, diameter, cross sectional area, perimeter, and point area for each load test are given in Table 1 of this report. The following sections will report on the residual stress properties for each pile and then will give mean values and ranges of the soil properties derived from each pile analysis.

##### Residual Stress Properties

Table 8 shows the final values of  $C$ ,  $D$ , and  $\gamma$ . With three exceptions,  $C$  ranges between 0.10 and 1.0. The constant  $C$  may be viewed as a scale factor for residual shear stresses. It is proportional to the shear stiffness of the soil and the area of the point of the pile and is inversely proportional to the pile perimeter, its cross-sectional area, and its elastic modulus.

Low values of  $\gamma$  indicate that the loads in the pile due to residual stresses are not reduced with depth much below what would be expected with the simple elastic rebound formula given in Eq. 26. Conversely, high values of  $\gamma$  indicate that residual shear stresses are damped out very quickly with depth. The two largest values of  $\gamma$  come from short piles. In general, values of  $\gamma$  range between 0.04 and 1.0.

The value of  $D$  should be twice the constant that, when multiplied by  $L\beta$  gives the residual point pressure. The smaller values normally occur with longer piles.

TABLE 8.- Residual Stress Properties

SITE	PILE	PILE LENGTH ft	C	D	γ
Arkansas	1	55	0.0341	$0.822 \times 10^{-4}$	0.0868
	2	55	1.009	97.5	0.0452
	3	55	0.208	17.4	0.847
	6	42	0.494	29.0	$0.126 \times 10^{-4}$
	7	55	0.489	45.6	0.565
	9	55	0.347	31.3	0.707
	10	55	0.661	62.7	0.394
Low Sill	2	66.6	0.169	13.5	0.727
	5	46.5	0.245	21.1	0.075
	6	66.5	0.029	25.7	0.061
Ogeechee River	H-11	12.2	0.213	24.3	2.78
	H-12	22.3	0.369	33.6	$0.899 \times 10^{-5}$
	H-13	31.7	0.146	23.3	0.076
	H-14	41.7	0.355	23.1	$0.626 \times 10^{-5}$
	H-15	51.5	0.255	22.1	0.065
Tavenas	J-5	60.0	$0.335 \times 10^{-2}$	$0.709 \times 10^{-4}$	0.975
Gregerson	C*	26.24	0.338	30.4	$0.716 \times 10^{-5}$
	C+	26.24	0.338	30.4	$0.716 \times 10^{-5}$
West Seattle	A	100.0	0.441	40.9	0.202
	B	86.0	0.185	$0.822 \times 10^{-4}$	0.692
Lock & Dam 26	3IP-IIIS	54.0	0.154	21.0	0.268
Corpus Christi	Initial	38.0	0.381	24.3	$0.489 \times 10^{-2}$
	Final	38.0	0.123	$0.420 \times 10^{-2}$	2.43

\*strain gauges placed on steel  
+strain gauges placed on concrete  
Note: 1 ft = 0.3048 m)

### Soil Shear Stiffness and Strength Properties

Table 9 presents a summary of the calculated values of the soil shear stiffness values, including mean values and ranges of the constants A, n, B, m, and  $\Delta\tau_g$ . The soil shear stiffness at any depth, z, below the ground surface is given by

$$k_T = A(z)^n$$

and the asymptotic value of shear strength at any depth, z, is

$$\Delta\tau_f = B(z)^m$$

in which z is in inches,  $k_T$  is in lb/in.<sup>3</sup>, and  $\Delta\tau_f$  is in lb/in.<sup>2</sup>. Typical mean values of A range between 30 and 40 and of n are around 0.30 to 0.40. Typical mean values of B are between 1.0 and 6.0 and the means of the exponent m are around 0.30 to 0.50. The shear stress at which slip occurs varies with depth and with the material of which the pile is composed. However, the mean value of B, expressed in lb/in.<sup>2</sup>, is a good approximation of the shear stress at which slip occurs. There were four piles in which no slip occurred, i.e., the forces in the pile with depth were matched within very close tolerances, and the predicted displacement at the top of the pile was the same as was observed in the field for all load levels.

The amount of the variation of the constants around the mean differs between sites. The Arkansas site is characterized by high stiffness and high strength, with the exception of Piles No. 3 and 6. The mean stiffness constant, A, was remarkably uniform with the Ogeechee River test piles, where it appears that the mean strength coefficient, B, increased with the depth of the pile.

### Pile Point-Soil Stiffness and Strength Properties

An upper limit of 100,000 lb/in.<sup>3</sup> ( $2.71 \times 10^7$  kN/m<sup>3</sup>) was placed on the value of  $k_p$ , the soil stiffness constant at the pile point. In some cases, the pattern search routine sought the upper bound and

TABLE 9.- Soil Shear Stiffness and Strength Properties

SITE	PILE	PILE LENGTH, ft	A		n		B		m		$\Delta\tau_s$ RANGE, psi
			MEAN	RANGE	MEAN	RANGE	MEAN	RANGE	MEAN	RANGE	
Arkansas	1	55	48.9	40-61	0.12	0.08-0.17	7.95	7.0-9.1	0.50	0.40-0.61	9-10
	2	55	113.6	--	0.12	--	11.37	--	1.21	--	5
	3	55	35.8	31-40	0.36	0.31-0.39	2.46	2.1-2.8	0.35	0.32-0.38	3-10
	6	42	32.0	--	0.80	--	0.77	--	0.48	--	2-10
	7	55	91.9	--	1.08	--	0.68	--	0.40	--	2-7
	9	55	78.0	54-117	0.37	0.14-0.70	6.53	2.4-10.7	0.78	0.37-1.21	5-12
	10	55	59.3	31-109	0.34	0.30-0.38	6.14	3.9-10.6	0.70	0.46-1.17	6-11
Low Sill	2	66.6	32.9	29-36	0.35	0.32-0.36	2.38	2.1-2.6	0.34	0.32-0.36	NO SLIP
	5	46.5	31.7	25-43	0.54	0.53-0.66	2.23	1.8-3.0	0.38	0.32-0.41	3-11
	6	66.5	20.3	5-35	0.48	0.34-0.74	4.58	4.2-4.9	0.17	0.16-0.20	NO SLIP
Ogeechee River	H-11	12.2	34.2	5-66	0.72	0.39-1.05	0.76	0.36-1.06	0.45	0.23-0.67	1-7
	H-12	22.3	36.4	32-43	0.37	0.29-0.45	2.82	0.47-5.7	0.49	0.35-0.64	2-10
	H-13	31.7	27.6	20-35	0.10	0.05-0.20	5.74	5.3-6.7	0.27	0.18-0.37	4-8
	H-14	41.7	33.1	16-49	0.45	0.30-0.54	1.20	0.55-1.9	0.45	0.29-0.62	2-12
	H-15	51.5	39.3	39-40	0.00	--	7.00	--	0.40	--	4-10
Tavenas	J-5	60.0	27.4	5-39	0.48	0.33-0.76	0.88	0.30-2.6	0.32	0.28-0.36	1-2
Gregerson	C*	26.24	15.9	0.4-31	0.63	0.31-0.95	1.53	1.0-2.1	0.35	0.31-0.37	1-5
	C+	26.24	16.0	0.7-31	0.69	0.31-1.06	1.43	0.7-2.1	0.33	0.31-0.35	2-5
West Seattle	A	100.0	27.2	24-30	0.28	0.26-0.30	1.50	1.1-1.9	0.28	0.27-0.29	2-7
	B	86.0	32.7	25-40	0.21	0.03-0.40	3.00	0.9-5.1	0.35	0.30-0.40	NO SLIP
Lock & Dam 26	3IP-IIIS	54.0	22.0	--	0.27	--	3.06	--	0.41	--	NO SLIP
Corpus Christi	Initial	38.0	26.3	14-43	0.25	0.14-0.36	1.64	0.90-3.9	0.27	0.20-0.49	1-3
	Final	38.0	34.4	22-62	0.24	0.06-0.29	3.20	1.9-5.8	0.41	0.31-0.68	1-4

\*strain gauges on steel

+strain gauges on concrete

Note: 1 ft - 305 m; 1 psi = 6.89 kPa



remained there which accounts for the number of entries in Table 10 of the figure  $100,000 \text{ lb/in.}^3$  ( $2.71 \times 10^7 \text{ kN/m}^3$ ). The mean and the range of both the soil stiffness,  $k_p$ , and the soil strength,  $q_f$ , is given in that table.

The Ogeechee River test piles again exhibit an increase of stiffness and strength with the depth of pile. The variable nature of the soil at the Arkansas and Low Sill sites is shown with the large spread of the mean stiffness values and their ranges. An unusually low strength of soil was found at the Gregersen pile test site. Although the strength was reasonably constant between Piles A and B at the West Seattle test site, the stiffness at the point of the pile changed drastically as the pile depth changed from 86 feet (26.2 m) to 100 feet (30.5 m). The Corpus Christi site was very uniform in its soil stiffness and strength properties as the load increased by a factor of ten.

#### CONCLUSIONS

This chapter describes a method of analyzing the results of pile tests which is capable of incorporating very general constitutive relations for the soils around and beneath a pile, and of considering explicitly the presence of residual stresses in the pile and in the surrounding soil prior to the load test. The method is fairly inexpensive to use, requiring approximately five dollars of computer costs, including time and printing, to make a complete analysis of a load on a pile. Rapid convergence of the iterative procedure requires the input of initial guesses of the nine soil properties that are reasonably close (within a factor of 2 to 5) to the final values. The results of the calculations in this chapter and the formulas for starting values of the nine constants given in a previous section of this chapter should prove to be very helpful in this regard. After several trial runs with the pattern search method, it was decided that it is best to determine residual stress constants on the lower load level before there is much likelihood of slip and then keeping them constant for subsequent load levels.

TABLE 10 - Pile Point-Soil Stiffness and Strength Properties

SITE	PILE	PILE LENGTH ft	$k_p$ , (lb/in <sup>3</sup> )		$q_f$ , (lb/in <sup>2</sup> )	
			MEAN	RANGE	MEAN	RANGE
Arkansas	1	55	8400	4,900-15,500	1300	530-1750
	2	55	810	---	--	---
	3	55	100,000	---	760	720-780
	6	42	220	---	11	---
	7	55	940	---	--	---
	9	55	43,300	20,200-100,000	500	490-500
	10	55	38,300	17,200-100,000	2900	50-4300
Low Sill	2	66.6	66,700	29,500-100,000	650	590-690
	5	46.5	3900	1,170-49,500	760	200-990
	6	66.5	1600	810-52,400	1800	580-3100
Ogeechee River	H-11	12.2	4600	3,600-6,000	1000	990-1040
	H-12	22.3	3700	3,300-6,600	2000	920-2500
	H-13	31.7	14,000	8,900-52,000	2300	2100-2600
	H-14	41.7	20,400	15,200-45,500	3400	1700-6100
	H-15	51.5	51,000	34,300-104,000	2400	2300-2500
Tavenas	J-5	60.0	13,500	13,300-13,800	2700	2500-2800
Gregerson	C*	26.24	2600	---	67	65-69
	C+	26.24	4800	---	69	69-69
West Seattle	A	100.0	56,200	52,400-60,600	950	940-960
	B	86.0	3700	2,100-16,300	1100	900-1300
Lock & Dam 26	3IP-IIIS	54.0	100,000	---	620	---
Corpus Christi	Initial	38.0	11,100	3,400-20,400	3800	1700-4400
	Final	38.0	14,700	5,500-25,700	2900	2000-3100

\*strain gauges on steel  
+strain gauges on concrete  
Note: 1 lb/in<sup>2</sup> = 6.89 kPa

The results of the calculations appear to be reasonable and in many cases show a consistency that promises to improve markedly the ability to predict pile load-settlement and capacity predictions.

The constitutive equation for the soil in shear along the side of the pile was assumed to be rigid-elastic-plastic, in which residual stresses are overcome with no displacement under load and then a hyperbolic stress-displacement relation was assumed to exist until slip occurs. The versatility of the method described in this chapter is such that any other assumed constitutive relation could be inserted into the program with little effort. One such constitutive relation that would be desirable to investigate is one that imposes the same hyperbolic stress-displacement relation on the residual shear stresses as on the subsequently added shear stresses due to load. Such a constitutive equation has been formulated but limitations on time and budget on this project have required this further investigation to be deferred. If this constitutive equation is used, slight modification will be required in the part of the program that defines the sum of squared random errors that is to be minimized by the pattern search routine.

The soil constitutive equations and the method of characterizing the residual shear stresses that are described in this chapter should prove to be useful in predicting pile load-settlement and capacities, particularly if the constants that were derived can be shown to be correlated with the results of simple laboratory or in situ tests.

In summary, the method that has been developed and is described in this chapter is convenient to use for analysis of pile test data and promises to provide a sound basis for accurate predictions of pile displacement under load.

## CHAPTER VIII - A NEW DESIGN METHOD INCLUDING RESIDUAL STRESSES

### GENERAL

In order to identify the important parameters affecting pile behavior under load and formulate a design method which incorporates residual stresses, various correlations were performed. Due to a lack of other soil data at the sites only the SPT results were used in the correlations. Although several corrections for SPT N values have been proposed (9,38), uncorrected N values have been used throughout the correlations. This decision was made due to the fact that the corrections are not universally accepted. The engineer may apply whatever corrections he desires before using the proposed method, but none is recommended. The value of N used for correlation with the soil behavior at the pile point  $N_{pt}$ , is an average over a distance of four diameters either side of the pile point. The value of N used in correlations with the soil behavior along the side of the pile,  $N_{side}$ , is a weighted average along the length of the pile. The correlations were performed in three main categories: residual driving stresses, point pressure-point movement characteristics and side friction-pile movement characteristics.

All the correlations presented in this chapter were performed for displacement piles. Due to uncertainty regarding areas to use for the analysis of H-piles, they were not included in the correlations. Further discussion of H-piles is given in a later section of this chapter.

### THE REAL MEANING OF RESIDUAL STRESSES

As explained in Chapter IV the typical load test on an instrumented pile does not measure residual stresses in the pile. The measured top load and top movement are correct, but the measured distribution of load in the pile is incorrect. The measured point load is too low and the measured friction is too high. Due to this error in measurement,

all the predictive methods based on these load test results are in error. Therefore, for the purpose of developing a predictive method, residual stresses must be considered.

In an uninstrumented pile load test, residual stresses cannot be measured. This is usually not important however, since these load tests are normally performed to verify the capacity of the design pile. Since the measured top load and top movement are correct, there is no need to know the residual stresses. However, if the results of the pile load tests are extrapolated to a pile of a different length, the residual stresses must be considered. This is again due to the fact that the distribution of load is affected by residual stresses.

For piles entirely in sand, the shorter a pile is the more important the point capacity becomes. Since the point capacity is larger after considering residual stresses, short piles will become shorter. As the piles become longer the friction becomes more important. Since the friction is smaller after considering residual stresses, long piles will need to be longer to carry the same capacity.

It is rare to find a pile driven through 100 ft (30 m) or more of sand. The most common case for long piles is to be driven through clay with the tip seated in a sand layer. Measurements on piles in clay indicate residual driving stresses in the pile are less than five percent of the ultimate pile capacity, whereas in sand they may be more than 20 percent of the ultimate pile capacity. Thus, the current prediction methods for pile capacity in clay should not be affected significantly by residual stresses. Therefore, a pile driven through clay into sand should carry more load than predicted without considering residual stresses. The friction in the clay is not reduced by consideration of residual stresses, however the point bearing in the sand is increased due to consideration of residual stresses. Therefore, in most cases the consideration of residual stresses will result in greater pile capacity predictions.

## CORRELATIONS

### Residual Driving Stresses

The theoretical considerations of residual stresses presented in Chapter IV have pointed out various parameters governing the magnitude of the residual point pressure,  $q_{res}$ . The two main parameters are the pile length and the relative stiffness between the soil and the pile. The term in the solution to the governing differential equation which incorporates these items is  $L\beta$  where  $L$  is the pile length and  $\beta$  is defined as :

$$\beta = \sqrt{\frac{K_T P}{AE_p}} \quad \text{in which the units must be consistent,}$$

with

$K_T$  = initial slope of the friction transfer curve in loading,  
obtained as described later in this chapter.

$P$  = perimeter of the pile

$E_p$  = modulus of elasticity of the pile

$A$  = cross-section area of the pile

The term  $\beta$  is used instead of the term  $\Omega$  in Chapter IV since it uses the slope of the loading portion of the friction transfer curve. If the loading and unloading slopes are equal, then  $\Omega$  and  $\beta$  are equal.

A plot of  $q_{res}$  versus  $L\beta$  is shown in Fig. 40. A linear regression through the origin yields an expression for  $q_{res}$  of:

$$q_{res} = 5.57L\beta \quad \text{with } q_{res} \text{ in tsf} \dots \dots \dots (27)$$

The data point shown for the West Seattle pile was added after the correlation was made. This pile was instrumented with a load cell at the tip, and residual point load was measured after driving. No load test was made of the pile, so the value of  $K_T$  was predicted by

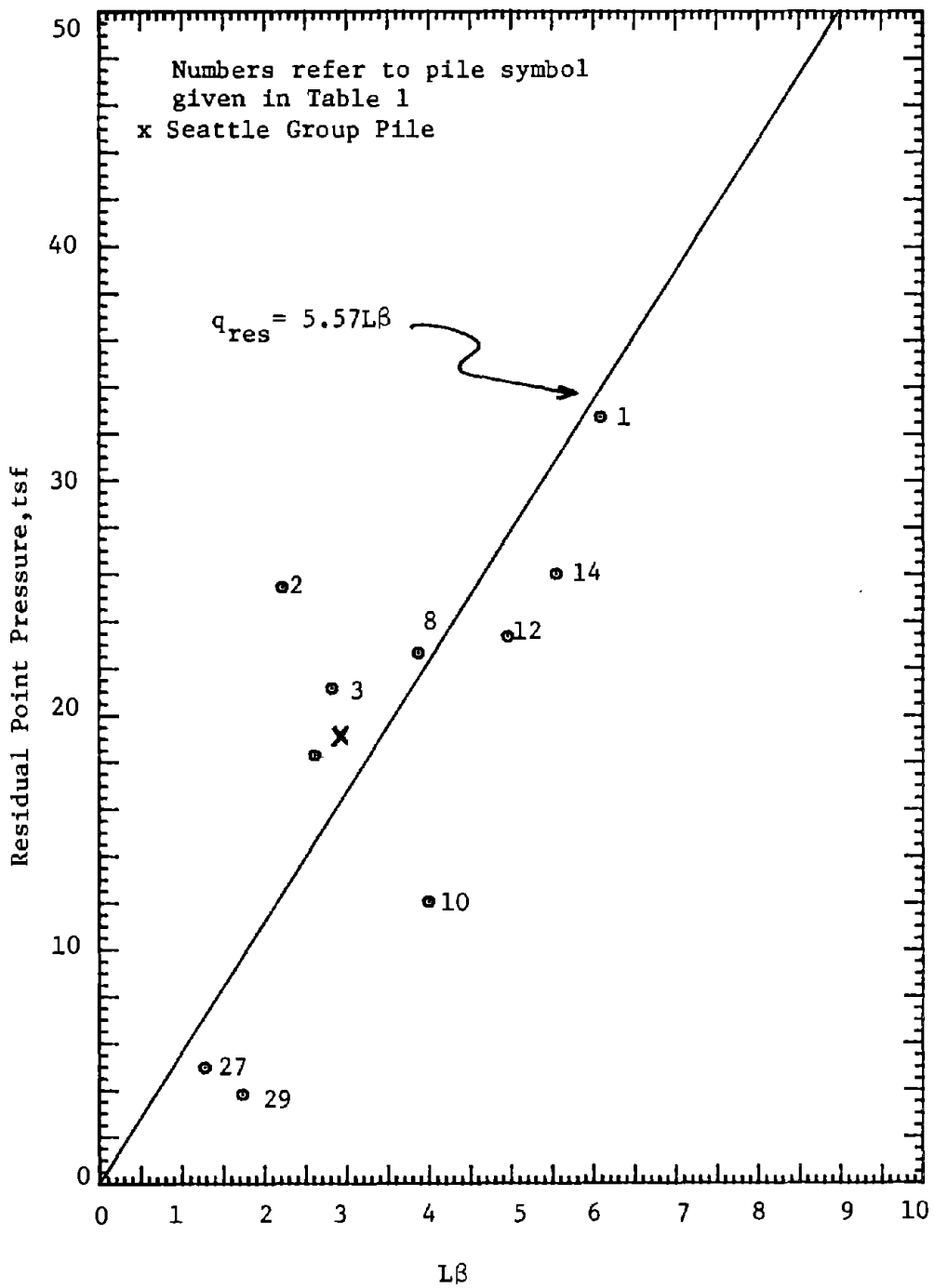


FIG. 40.- Residual Point Pressure Versus  $L\beta$   
(1 tsf = 95.8 kPa)

correlations presented later in this chapter. The results show very good agreement with the regression through the other data.

This correlation with  $L\beta$  showed much better agreement than a correlation between  $q_{res}$  and  $N_{pt}$ . This was expected since the  $N$  value only gives an indication of soil strength, whereas the term  $L\beta$  includes the soil-pile relative stiffness.

#### Point Load-Movement Characteristics

The majority of the load tests did not measure residual stresses in the pile. When they were not measured, the residual stresses were accounted for using the correlation presented in the previous section.

Using the hyperbolic model presented in Chapter III, two parameters are needed to describe the point load-point movement ( $q$ - $w$ ) curve. These parameters are the maximum asymptotic value,  $q_{max}$ , and the initial tangent modulus  $K_p$ .

Maximum Asymptotic Value.- Of primary importance in these correlations is whether or not the load tests actually reached a maximum point bearing capacity since a majority of the piles never reached a pile point movement equal to four percent of the pile diameter. The ratio of point load over  $N_{pt}$  for several point movements as a percent of the pile diameter are presented in Table 11 for 27 piles. Also presented are the asymptotic values from the hyperbolic regression in chapter III. In every case the asymptotic values are larger than the highest values from the load tests. Fig. 41 is a plot of the ratio of point load to  $N_{pt}$  versus point movement as percent of the point diameter for seven of the piles. From this plot it can be seen that some of the piles did not reach a maximum value of point pressure even after a movement equal to 25 percent of the pile diameter. For this reason the hyperbolic asymptote seems to be the best estimate of a maximum value and was used for all further correlations.

The best correlation that could be found between  $q_{max}$  and  $N_{pt}$  was a power law function with the equation:



TABLE 11.- Ratio of Point Pressure to  $\dot{N}_{pt}$  for Various Pile Movements

Pile	Movement Diameter						Asymptote
	2%	4%	8%	10%	15%	25%	
Arkansas							
1	0.98	1.25	1.52(7.0) <sup>a</sup>				2.02
2	0.80(1.4)						1.66
3	0.73	0.77(2.4)					0.95
6	0.29	0.37	0.41(4.9)				0.62
7	0.40	0.45(3.0)					0.57
9	0.11	0.15(3.4)					0.25
10	0.51(1.3)						1.35
16	0.38(1.1)						0.50
Low Sill							
1	0.68	0.70(2.2)					0.80
2	0.33	0.36(2.2)					0.46
3	0.42	0.54	0.65	0.70	0.83		0.94
4	0.42(0.9)						0.74
5	0.14	0.15	0.19	0.21	0.24	0.27(19.0)	0.33
6	0.48(1.7)						0.59
Ogeechee River							
H-11	1.67	2.5	3.08	3.42	3.96	5.07	6.67
H-12	5.41	5.86	6.77	7.05	7.13	7.30	7.57
H-13	5.91	7.01	8.53	8.87	9.21	9.88	10.09
H-14	3.16	3.56	4.27	4.27	4.21	4.13	4.24
H-15	2.27	2.79	3.72(7.6)				4.78
Corpus Christi							
Initial	1.40	1.77(3.6)					3.08
Final	1.54	1.85	1.87(4.2)				2.63
Seattle							
A	0.47	0.53(2.9)					0.64
B	0.70	0.76(2.3)					0.90
Tavenas							
J-5	2.22	2.73	2.89(4.4)				3.22
Lock & Dam 26							
M6	0.47	0.49	0.53	0.55	0.60	0.61(16)	0.64
3IP-III 5	0.69	0.74(2.5)					0.87
Gregersen							
A	3.55	5.28	6.04(4.9)				9.32

<sup>a</sup> - Numbers in parentheses are percent movements for highest load level in load test

Note: 1 tsf = 95.8 kN; 1 blow/ft = 3.28 blow/m

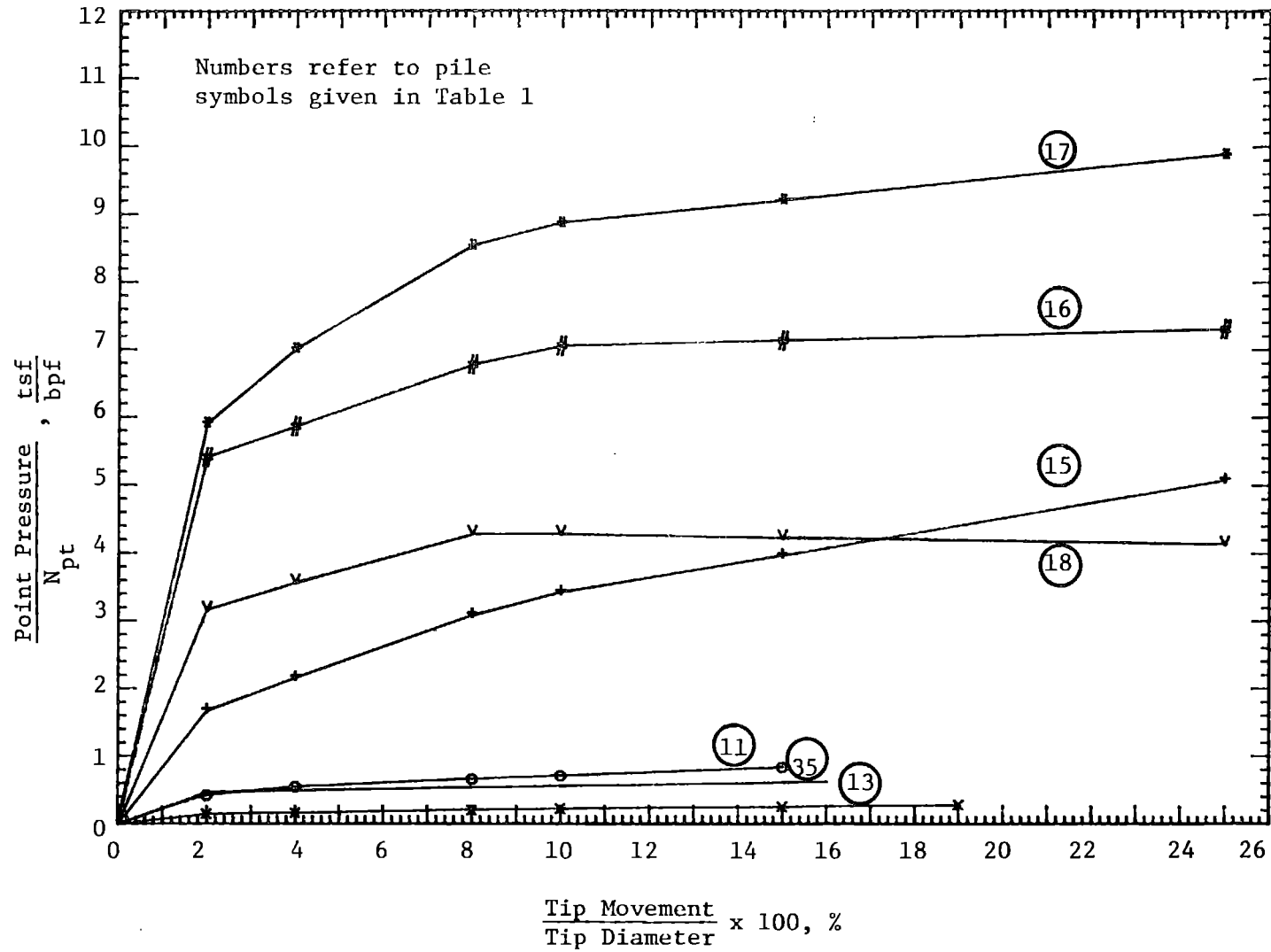


FIG. 41.-  $\frac{q}{N_{pt}}$  Versus  $(\frac{w}{D} \times 100)$  (1 tsf/bpf = 29.2 kPa/bpm)

$$q_{\max} = 19.75 (N_{pt})^{0.36} \quad \text{in tsf} \dots \dots \dots (28)$$

where  $N_{pt}$  is the average uncorrected blow count per foot of penetration within a zone equal to 4 pile diameters above, and 4 pile diameters below, the point of the pile.

A log-log plot of the data and regression are shown in Fig 42. No relationship could be observed between  $q_{\max}$  and the relative depth,  $L/D$ , for either varying  $N_{pt}$  values or silt content of the soil. This corresponds with findings by Olson and Dennis (30).

Initial Tangent Modulus.- The second parameter needed to describe the q-w curve is the initial tangent modulus,  $K_p$ . The best correlation for  $K_p$  with  $N_{pt}$  was power law function with the equation

$$K_p = 457.1(N_{pt})^{0.0065} \quad \text{in tsf/in.} \dots \dots \dots (29)$$

where  $N_{pt}$  is the uncorrected average N value as defined above. A log-log plot of this regression is shown in Fig. 43.

Side Friction-Pile Movement Characteristics

Maximum Asymptotic Value.- Correlations were performed for side friction parameters similarly to those for the point. No correlation could be found between  $f_{\max}$  and  $D/B$  with  $N_{side}$ . Again the best correlation was found using a power law function:

$$f_{\max} = 0.224 (N_{side})^{0.29} \quad \text{in tsf.} \dots \dots \dots (30)$$

where  $N_{side}$  is the weighted average of the uncorrected blow count per foot of penetration along the shaft of the pile. A log-log plot of the regression is shown in Fig. 44.

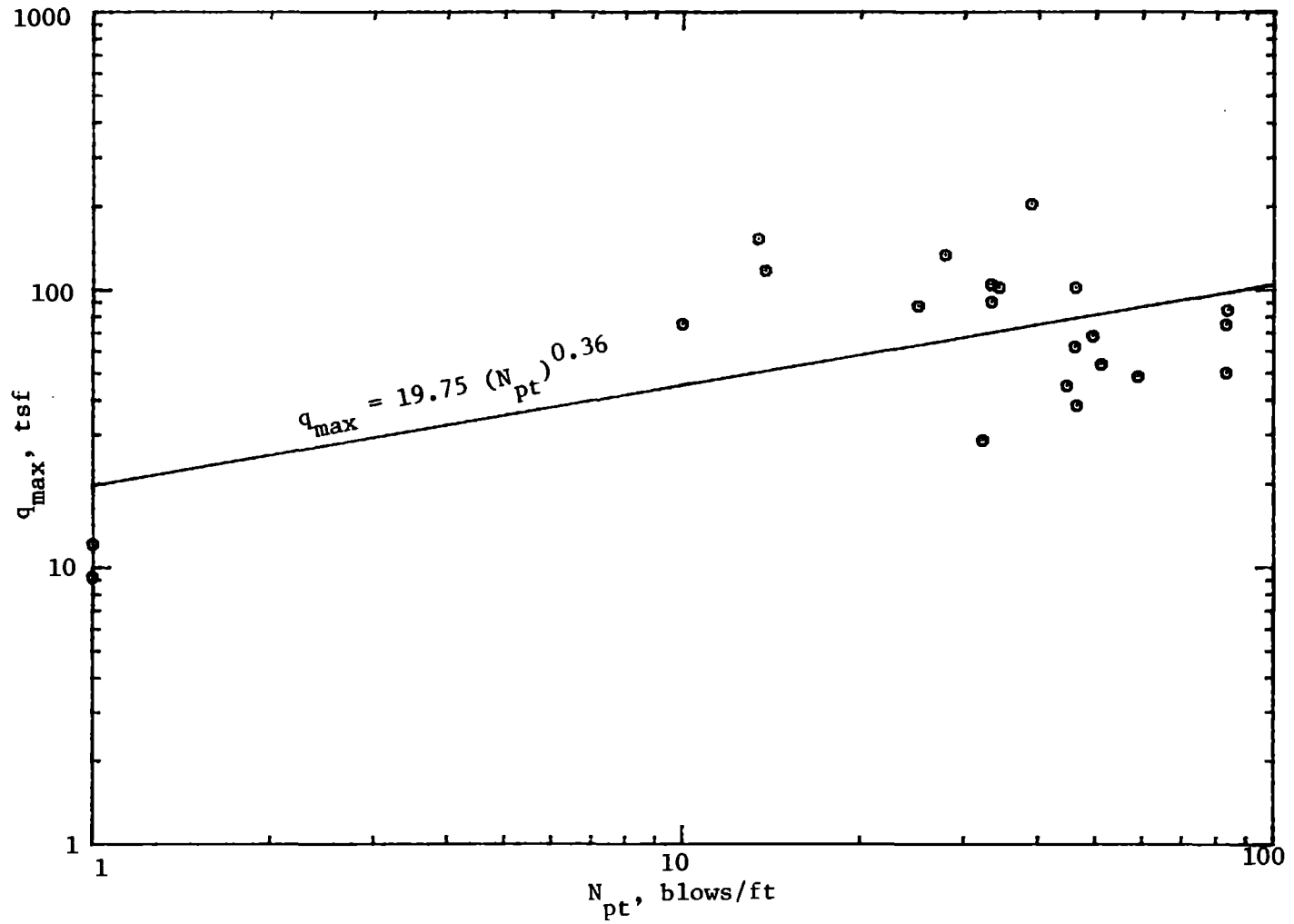


FIG. 42.- Log ( $q_{\max}$ ) Versus Log ( $N_{pt}$ ) (1 tsf = 95.8 kPa; 1 blow/ft = 3.28 blow/m)

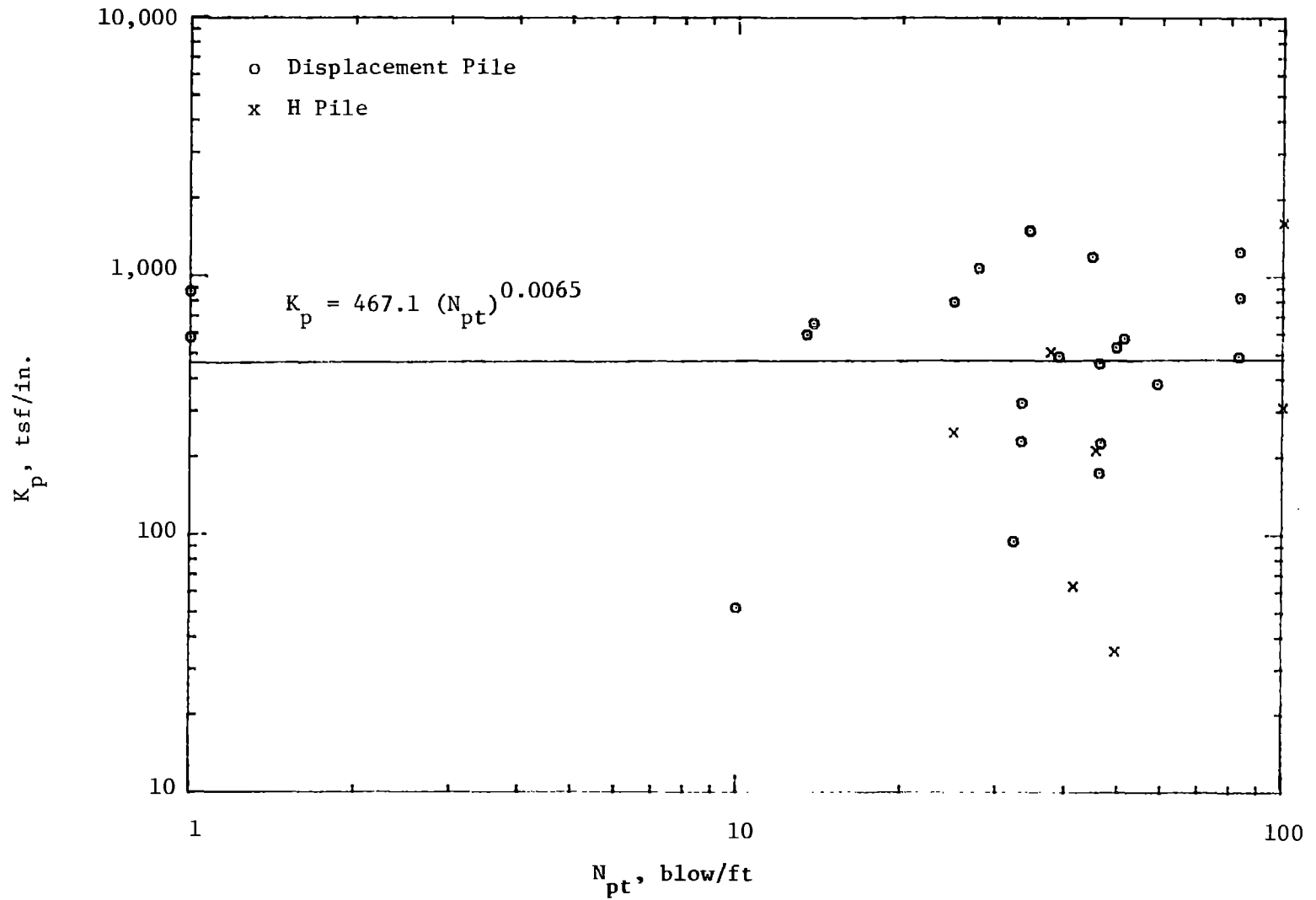


FIG. 43.- Log ( $K_p$ ) Versus Log ( $N_{pt}$ )  
(1 tsf/in = 37.7 kPa/cm; 1 blow/ft = 3.28 blow/m)

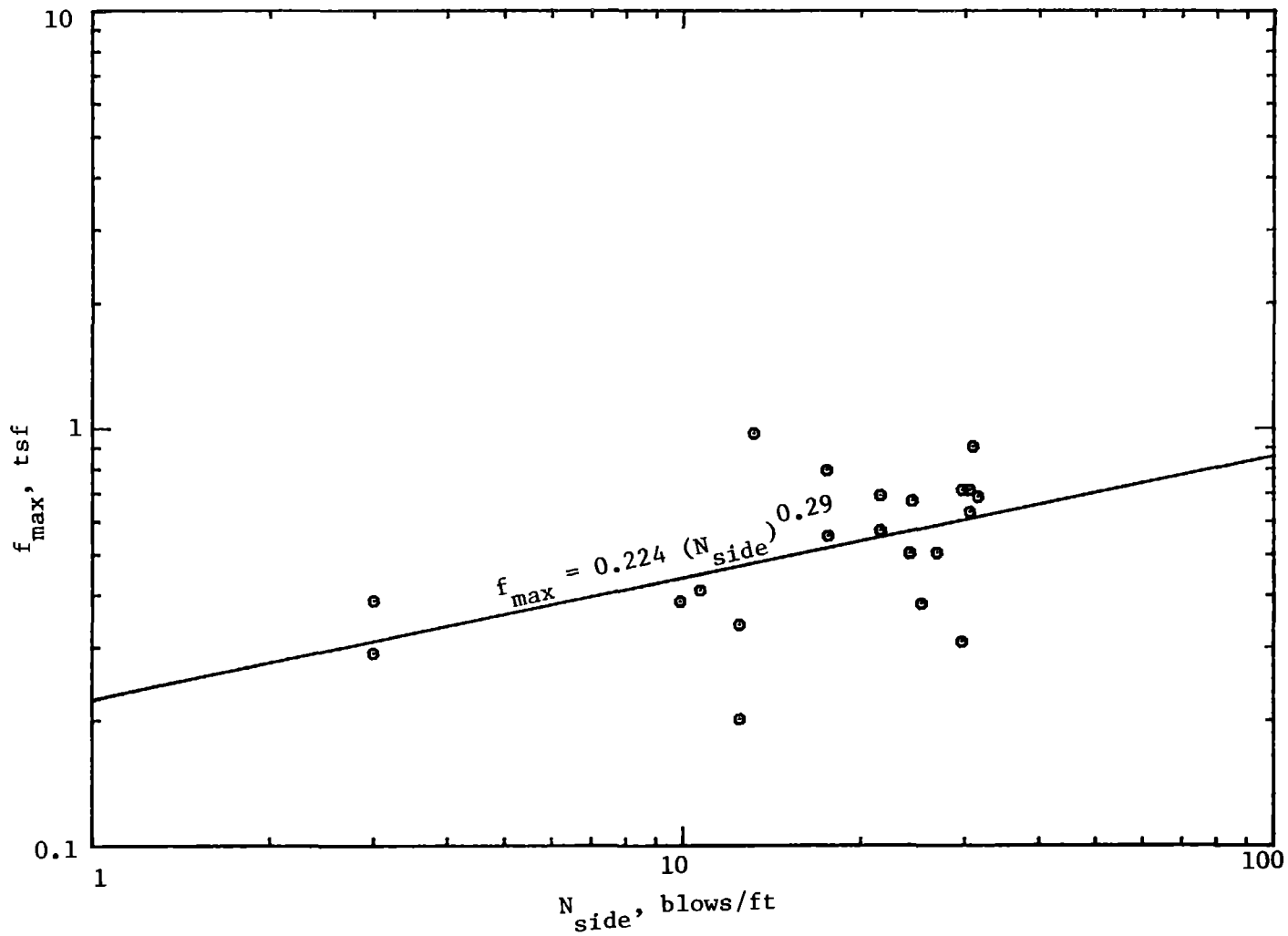


FIG. 44.- Log ( $f_{\max}$ ) Versus Log ( $N_{\text{side}}$ ) (1 tsf = 95.8 kPa; 1 blow/ft = 3.28 blow/m)

Initial Tangent Modulus.- A correlation for the initial tangent modulus for the f-w curves,  $K_T$ , yielded the expression

$$K_T = 5.01 (N_{side})^{0.27} \quad \text{in tsf/in.} \dots \dots \dots (31)$$

A log-log plot of this regression is presented in Fig. 45.

#### LOW DISPLACEMENT PILES (H-PILES)

All the previous correlations were performed on displacement piles. Due to their irregular shape, H-piles were not included in the correlations. There is uncertainty with H-piles as to what point area and perimeter the soil acts on. All analyses performed on the H-piles used the point area and perimeter of the rectangle enclosing the H section. The results of these analyses were plotted with the correlations for comparison. There is some agreement with the results of the displacement piles. However, more research must be done to determine the actual failure planes for this type of pile. For the present, a conservative design would be to use the smaller of the failure loads determined using the actual point area and perimeter of the pile and the area and perimeter of the rectangle enclosing the H section. The actual failure load will probably be between these.

#### A NEW DESIGN METHOD

Based on these correlations a new method of predicting pile behavior under axial load was developed, which considers residual stresses. The soil parameters required for input are the SPT uncorrected N values. The residual stresses are related to the pile length and the relative stiffness between the pile and the soil. The method predicts the entire load-settlement behavior of a pile under axial load.

#### Ultimate Capacity

The ultimate capacity is obtained using the correlations for the

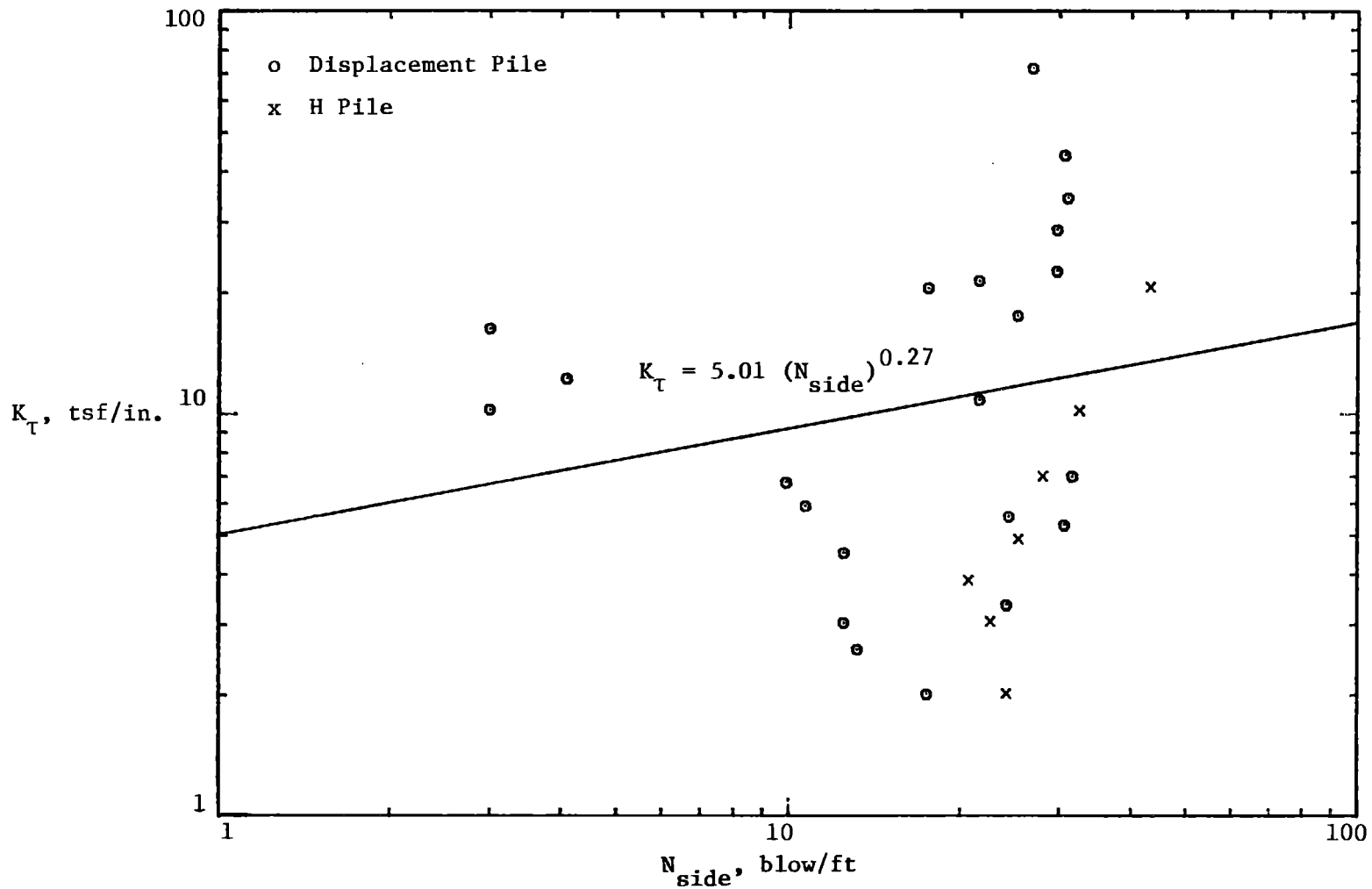


FIG. 45.- Log ( $K_T$ ) Versus ( $N_{side}$ )  
 (1 tsf/in = 37.7 kPa/cm; 1 blow/ft = 3.28 blow/m)



maximum point pressure and side friction. The equation for the point pressure was given in Eq. 28 as:

$$q_{\max} = 19.75 (N_{pt})^{0.36} \quad \text{in tsf}$$

where  $N_{pt}$  is the average of the uncorrected  $N$  values within four diameters either side of the pile point. The equation for the maximum side friction is

$$f_{\max} = 0.224 (N_{side})^{0.29} \quad \text{in tsf}$$

where  $N_{side}$  is the average of the uncorrected  $N$  values along the length of the pile.

The total pile capacity,  $Q_t$ , is then

$$Q_t = q_{\max} A_p + f_{\max} A_s \dots \dots \dots (35)$$

when  $A_p$  is the area of the pile point, and  $A_s$  is the surface area of the side of the pile.

Load Transfer Curves

In order to predict the load-settlement behavior of a pile, the q-w and f-w curves must be predicted. These curves are assumed to be hyperbolic and thus may be defined by an asymptotic value and an initial tangent modulus. The asymptotic values are given by the equations for  $q_{\max}$  and  $f_{\max}$  given in the previous section. The initial tangent modulus for the q-w curve,  $K_p$ , is given by Eq. 29 as:

$$K_p = 457.1(N_{pt})^{0.0065} \quad \text{in tsf/in.}$$

The initial tangent modulus for the f-w curve,  $K_T$ , is given by Eq. 31 as:

$$K_T = 5.01(N_{side})^{0.27} \quad \text{in tsf/in.}$$

Due to the presence of residual stresses in the pile, the transfer curves do not begin at the origin. The q-w curve is raised by the residual point pressure,  $q_{res}$ , and the f-w curve is lowered by the residual friction,  $f_{res}$ , as shown in Fig. 46. These two terms may be found from Eq. 27 as:

$$q_{res} = 5.57 L\beta \text{ in tsf}$$

where:

L = the pile length

$$\beta = \sqrt{\frac{K_T P}{AE_p}}$$

and

$$f_{res} = q_{res} \frac{A_p}{A_s}$$

Using these parameters the entire q-w and f-w curves may be predicted. The equations are:

$$q = \frac{w}{\frac{1}{K_p} + \frac{w}{q_{max} - q_{res}}} + q_{res} \dots \dots \dots (36)$$

and

$$f = \frac{w}{\frac{1}{K_T} + \frac{w}{f_{max} + f_{res}}} - f_{res} \dots \dots \dots (37)$$

It is important to note that the curves are only valid for driven piles. Piles installed with a vibratory hammer or jettted, may not develop the residual point pressure indicated by these predictions.

#### AXIALLY LOADED PILE PROGRAM

In order to predict the load-settlement curve for a pile, an axially

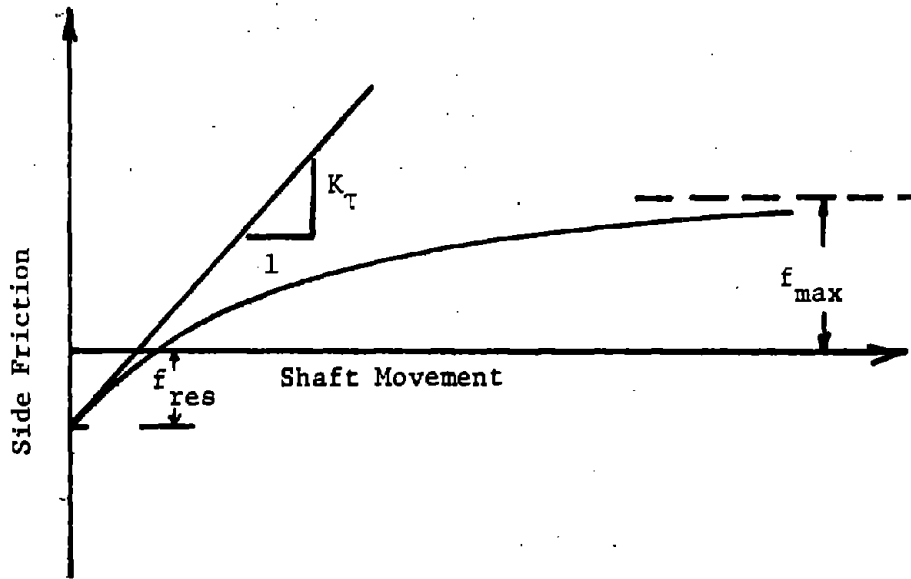
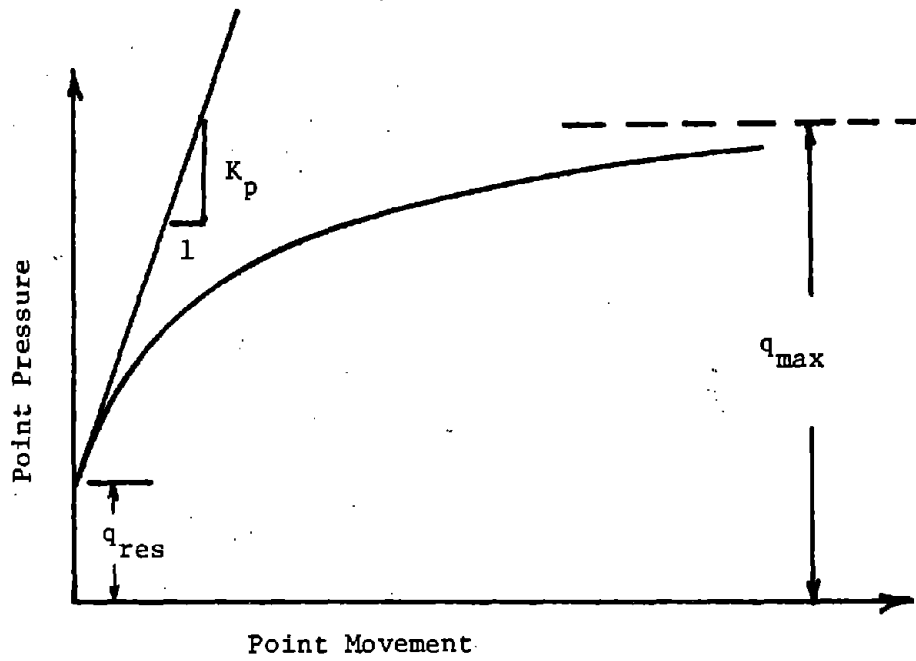
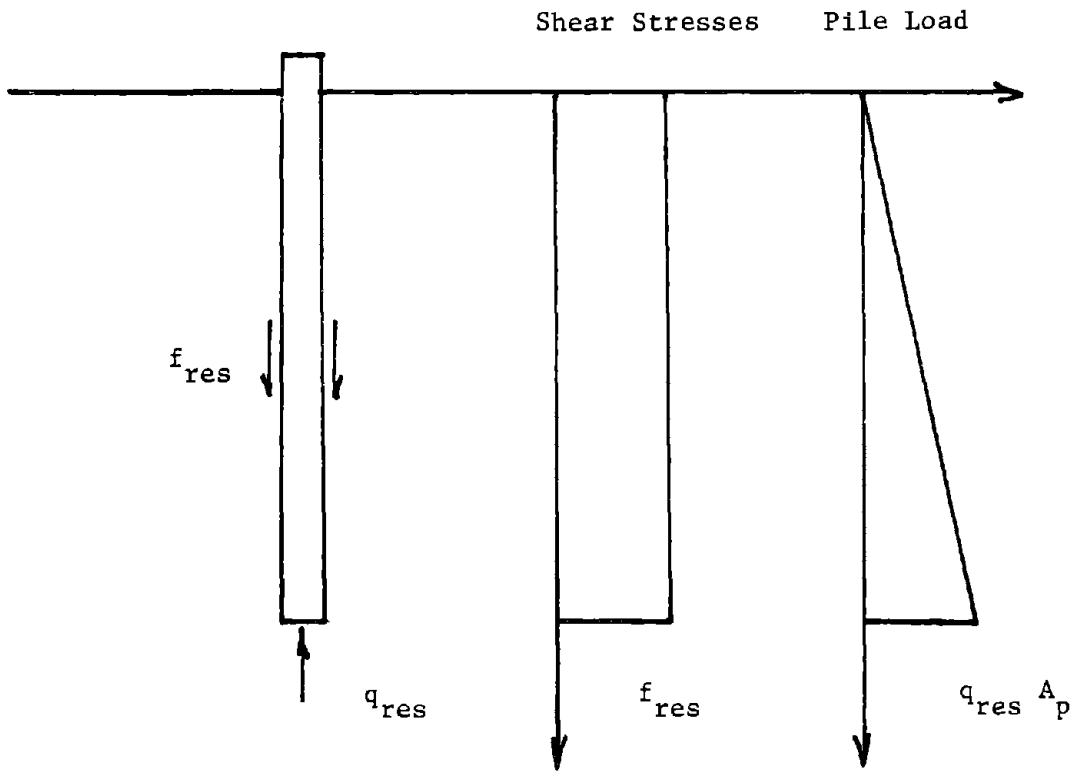


FIG. 46 .- Examples of Hyperbolic Load Transfer Curves

loaded pile computer program may be used. This type of program has been described in detail by Coyle and Reese (13). Minor modifications must be made to incorporate residual stresses in this type of program. At zero movement the pile is under a compressive loading due to the residual stresses. The elastic compression of the pile under this compressive residual load must be subtracted from all settlements computed by the program. If this modification is not made, the program will overpredict pile settlements. This elastic compression of the pile is calculated by using the state of stress shown on Fig. 47.

This new method was used with an axially loaded pile program modified as above to predict the load-settlement curves for the piles considered in this study. The curves are presented with the measured load-settlement curves in Chapter IX with a statistical analysis of the results.



$$q_{res} = 5.57 L\beta \quad (\text{in tsf})$$

FIG. 47.- Elastic Compression of Pile Under Residual State of Stress

CHAPTER IX - PREDICTIONS BY CONVENTIONAL METHODS

PREDICTIONS OF ULTIMATE CAPACITY

The conventional static formula method is always used initially to determine the pile size (cross-sectional area and depth of penetration) required to carry a design load. Use of the static formula method requires a knowledge of soil shear strength which is determined from either laboratory or in situ tests. The familiar static bearing capacity equation is generally written as follows:

$$Q_{ultimate} = Q_{side} + Q_{point} \dots \dots \dots (38)$$

where

$$Q_{side} = f_s A_s \dots \dots \dots (39)$$

and

$$Q_{point} = q_o A_p \dots \dots \dots (40)$$

The terms  $A_s$  and  $A_p$  represent the side and point areas of the pile, respectively. The term  $f_s$  is the unit side (frictional) resistance, and the term  $q_o$  is the unit point bearing resistance. Both  $f_s$  and  $q_o$  are related to soil shear strength, usually through the use of adjustment factors or coefficients.

The unit frictional resistance for piles in sand is generally determined from the following equation:

$$f_s = Kp \tan \delta \dots \dots \dots (41)$$

The term (K) is the lateral earth pressure coefficient; the term (p) is the effective vertical pressure at the depth of interest; and the term ( $\delta$ ) is the friction angle between the pile material and the sand.

The unit point bearing resistance for piles in sand is generally determined from the following equation:

$$q_0 = p_0 N_q \dots \dots \dots (42)$$

The term ( $p_0$ ) in this equation is the vertical effective pressure at the pile point; and the term ( $N_q$ ) is the bearing capacity factor for sand.

API Method - The American Petroleum Institute (API) method is used in the design of pile foundations for offshore structures (1). The equations used to predict  $f_s$  and  $q_0$  are the same as equations 41 and 42. The recommended design factors used in this method are presented in Table 12. These factors are considered applicable for medium-dense to dense sands. In addition, the recommended value for K is 0.5 to 1.0 for axial compressive loads.

TABLE 12.- API Design Factors

Soil Type	$\phi'$	$\delta$	$\frac{N}{q}$
Clean Sand	35°	30°	40
Silty Sand	30°	25°	20
Sandy Silt	25°	20°	12
Silt	20°	15°	8

These design factors, with  $K = 0.7$ , were used to predict bearing capacity for the test piles included in this study. Where no soil unit weights were reported, the SPT N values were used with the correlation presented by Bowles (6) to obtain an estimate. These values for unit weight were used to calculate the effective vertical pressure. The results of these bearing capacity predictions are given in Table 13.

Meyerhof Method - The Meyerhof method (27) used in this study is the method which includes the use of a Standard Penetration Test N-value for sand. Meyerhof's recommended equations are as follows:

$$f_s = \frac{\bar{N}}{50} \dots \dots \dots (43)$$

and  $q_0 = 0.4 \frac{NL}{D} \leq 4N \dots \dots \dots (44)$

TABLE 13.- API Code Predictions

Site	Pile	Q <sub>p</sub> (tons)	Q <sub>s</sub> (tons)	Q <sub>t</sub> (tons)
Arkansas	1	71.1	102.7	173.8
	2	108.0	124.2	232.2
	3	141.6	144.1	285.7
	6	a	a	a
	7	a	a	a
	9	a	a	a
	10	108.0	124.9	232.9
	16	100.1	121.1	221.2
Low Sill	1	a	a	a
	2	187.1	165.7	352.8
	3	a	a	a
	4	125.7	141.4	267.1
	5	32.5	48.5	81.0
	6	152.7	150.2	302.9
Vesic	H-11	16.6	3.6	20.2
	H-12	39.1	17.0	56.1
	H-13	56.7	35.9	92.6
	H-14	66.3	77.6	143.9
	H-15	99.1	106.4	205.5
Seattle	A	393.7	629.4	1023.1
	B	307.2	420.9	728.1
Tavenas	H-5	a	a	a
	J-5	60.9	113.4	174.3
Gregersen	A	15.5	14.4	29.9
	D/A	26.6	49.6	76.2
	C	8.0	12.4	20.4
	B/C	13.7	46.1	59.8
Corpus Christi	Initial	66.3	46.2	112.5
	Final	66.3	46.2	112.5
Sellgren	AI	b	b	b
	AII	b	b	b
LD26 ELLIS	M6	27.3	37.2	64.5
LD26 REPL	31P-IIIS	a	a	a

a - H Piles

b - No SPT N-Values

Note: 1 ton = 8.9 kN



The term ( $\bar{N}$ ) is the average standard penetration resistance, in blows per foot, within the embedded length of the pile. The term ( $N$ ) is the average standard penetration resistance, in blows per foot, near the pile point. These equations yield  $f_s$  and  $q_0$  in tons per square foot.

Eqs. 43 and 44 were used to predict bearing capacity for the test piles included in this study and the results are given in Table 14. A reduction factor was not applied to Eq. 43 for H-piles in accordance with a verbal recommendation from Meyerhof. However, a correction factor was applied to Eq. 44 to account for the influence of overburden pressure on the N-value in sand (28).

Coyle-Castello Method - The Coyle and Castello method (12) does not require the use of Eqs. 41 and 42. Correlations were developed by Coyle and Castello for the unit resistances,  $f_s$  and  $q_0$ . These unit resistances are correlated with relative depth (depth of penetration to diameter ratio -  $L/D$ ) and friction angle ( $\phi'$ ) of sand. For piles with non-circular cross-sections,  $D$  is the diameter of a circle with the same cross-sectional area. The correlation for unit side (frictional) resistance is presented in Fig. 48. Relative depth for this correlation is determined using the midpoint depth of the appropriate pile segment. The correlation for unit point resistance is presented in Fig. 49. Relative depth for this correlation is determined using the depth at the pile point. Eqs. 38, 39, and 40 are used with these correlations to predict bearing capacity. If the standard penetration test N-value is used to obtain the friction angle ( $\phi'$ ), a corrected N-value ( $N'$ ) should be used for fine silty-sand below the water table (6). The equation used to get the corrected N-value ( $N'$ ) is as follows:

$$N' = 15 + \frac{1}{2} (N-15) \dots \dots \dots (45)$$

Since the corrected N-value ( $N'$ ) was used to get ( $\phi'$ ) in the development of the correlations, it should be used when making bearing

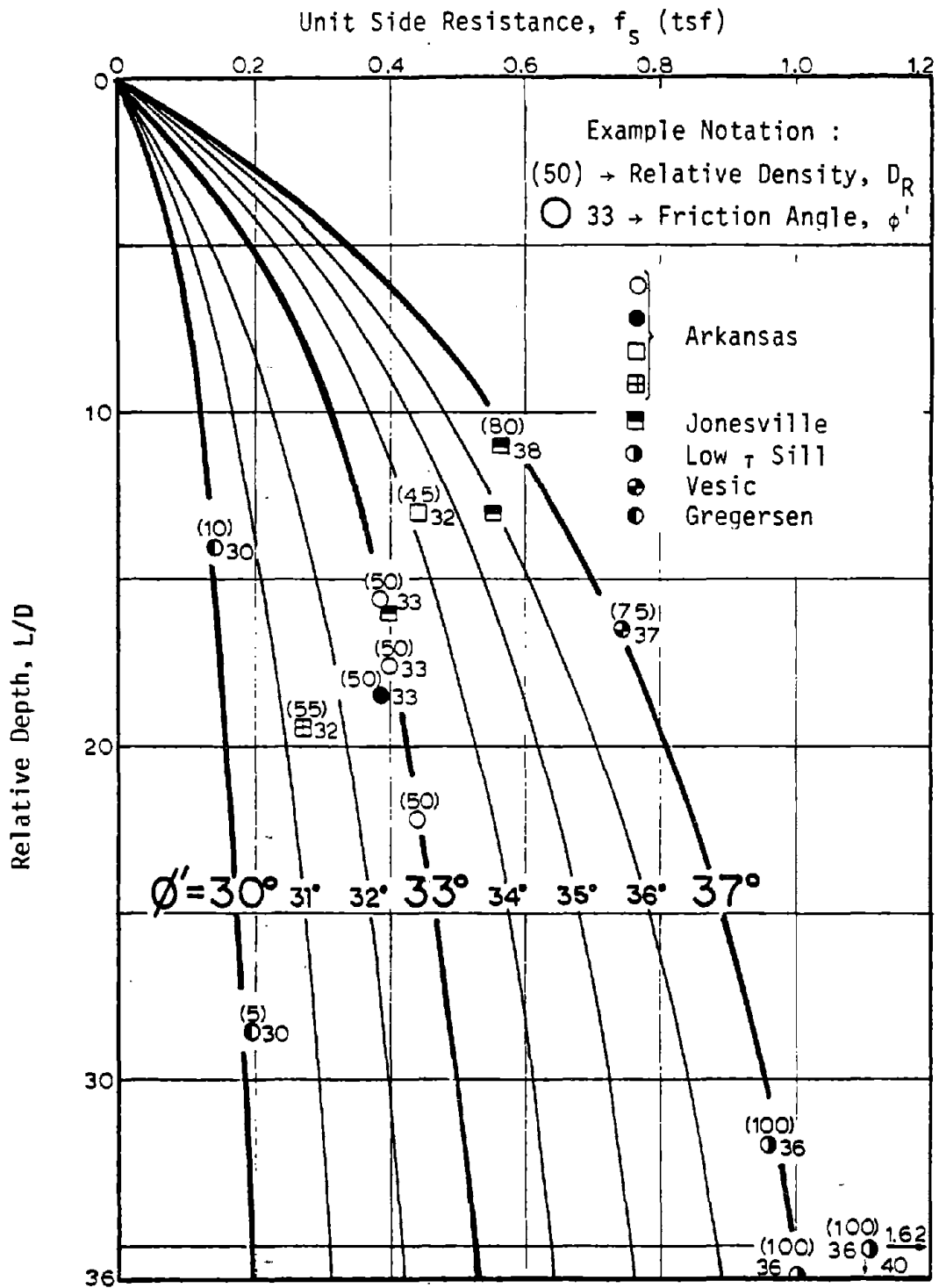


FIG. 48.-  $f_s$  From Coyle-Castello Method  
 (1 tsf = 95.8 kPa)

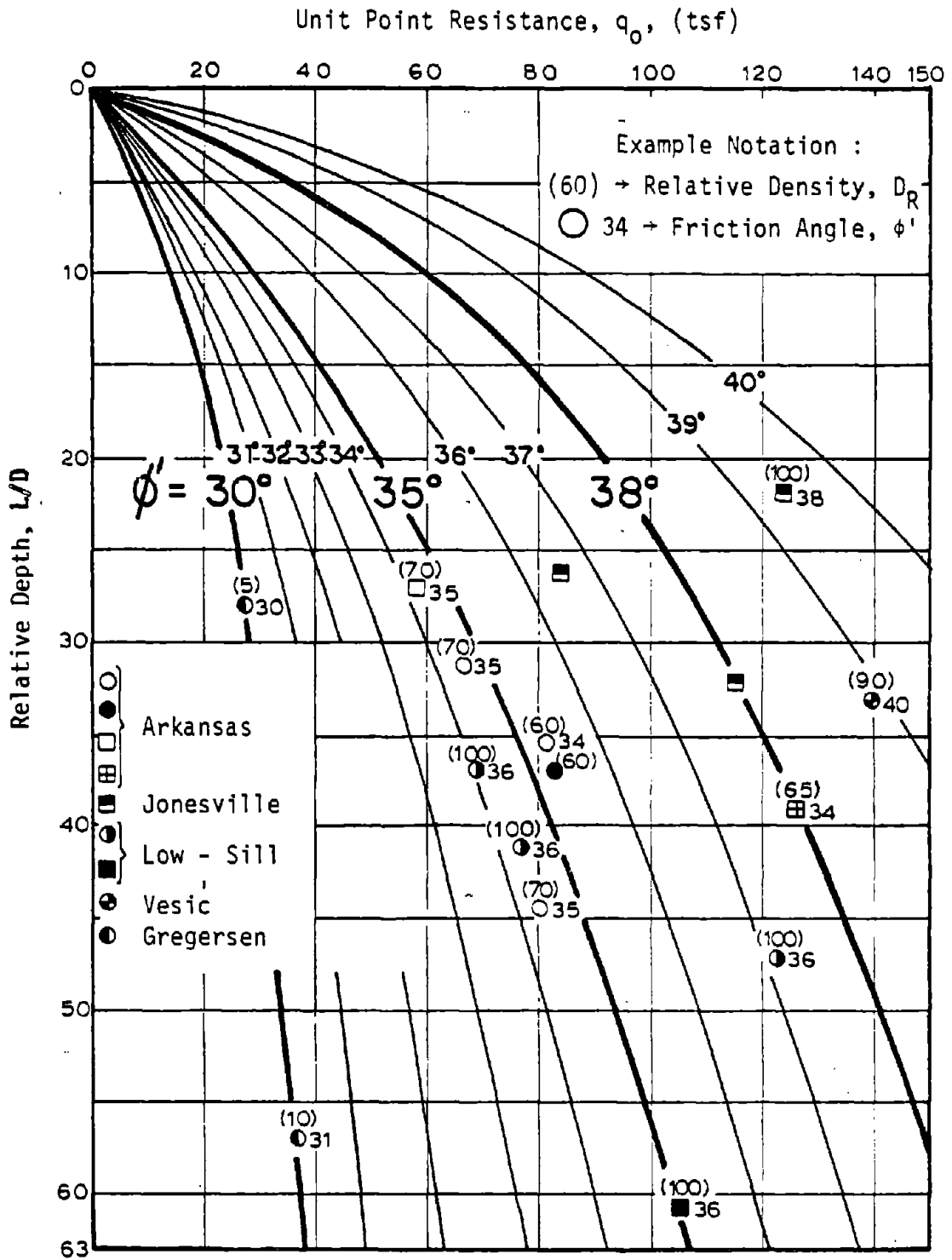


FIG. 49.-  $q_0$  From Coyle-Castello Method  
 (1 tsf = 95.8 kPa)

TABLE 14 - Meyerhof Predictions

Site	Pile	Q <sub>p</sub> (tons)	Q <sub>s</sub> (tons)	Q <sub>t</sub> (tons)
Arkansas	1	140.2	107.7	247.9
	2	296.9	107.5	404.4
	3	408.6	143.2	551.8
	6 <sup>a</sup>	228.8	85.0	313.8
	7 <sup>a</sup>	226.1	101.4	327.5
	9 <sup>a</sup>	248.1	127.0	375.1
	10	296.9	108.1	405.0
	16	253.6	139.6	393.0
Low Sill	1 <sup>a</sup>	413.5	326.8	740.3
	2	683.1	212.6	895.7
	3 <sup>a</sup>	468.7	215.6	684.3
	4	449.8	183.4	633.2
	5	147.3	70.8	218.1
	6	556.8	198.1	754.9
Vesic	H-11	70.7	3.8	74.5
	H-12	120.2	18.8	139.0
	H-13	106.0	29.3	135.3
	H-14	197.9	48.9	246.8
	H-15	261.5	81.3	342.8
Seattle	A	483.8	410.5	894.3
	B	473.9	340.7	814.6
Tavenas	H-5 <sup>a</sup>	94.7	117.8	212.5
	J-5	79.7	95.8	175.5
Gregersen	A	2.7	4.6	7.3
	D/A	5.3	6.4	11.7
	C	1.4	3.9	5.3
	B/C	2.7	5.9	8.6
Corpus Christi	Initial	248.9	38.0	286.9
	Final	248.92	38.0	286.9
Sellgren	AI	b	b	b
	AII	b	b	b
LD26 ELLIS	M6	122.3	54.0	176.3
LD26 REPL	31P-III5 <sup>a</sup>	187.5	142.6	330.1

a - H-Piles (Side area and point area determined using outside perimeter).

b - No SPT N-Values

Note: 1 ton = 8.9 kN

capacity predictions.

The results of the bearing capacity predictions using this method are given in Table 15. It is important to note that the Coyle and Castello predictions should be compared with results from field load tests where the failure (ultimate) load is determined by the  $0.1 \times D$  criterion (42). This definition of failure (ultimate) is the load which induces a total settlement equal to 10% of the pile point diameter for driven piles.

Comparison of Ultimate Capacity Predictions.- A comparison of the three conventional methods of predicting bearing capacity (API, Meyerhof, and Coyle-Castello) for the test piles included in this study is presented in Table 16. In addition, the ultimate loads are given in this table, based on the failure criteria presented in Chapter II. For comparison purposes, the maximum applied load for each pile is also given in Table 16.

A study of Table 16 reveals several general trends. The API method is generally conservative (underpredicts) and Meyerhof's method is generally unconservative (overpredicts). In order to better quantify the results, frequency distributions of predicted over measured total loads are shown in Figs. 50 through 53 for the three methods, plus the new method presented in the previous chapter. The  $0.1 \times D$  failure criteria was used for the comparison since that is the criterion used by Coyle and Castello to develop their methods. The failure criterion used by the API and Meyerhof methods is not stated in their publications. The new method, called the Briaud-Tucker method on Fig. 53, yields the entire load-settlement curve. Thus, the load corresponding to a pile settlement of  $0.1 \times D$  could be obtained. A summary of the mean, Standard deviation, coefficient of variation and the percent of the mean corresponding to 90% confidence level is given in Table 17. These results verify that the API method is conservative and Meyerhof's method is unconservative. These methods also have a large coefficient of variation. The Coyle and Castello and the Briaud and Tucker methods show a mean value very close to 1.0. The coefficient of variation for the Coyle and Castello method is larger than that for the Briaud and

TABLE 15.- Coyle and Castello Predictions

Site	Pile	$Q_p$ (tons)	$Q_s$ (tons)	$Q_t$ (tons)
Arkansas	1	133.4	96.1	229.5
	2	150.2	102.0	252.2
	3	227.0	107.6	334.6
	6	a	a	a
	7	a	a	a
	9	a	a	a
	10	150.2	102.6	252.8
	16	118.2	117.3	235.5
Low Sill	1	a	a	a
	2	264.6	186.1	450.7
	3	a	a	a
	4	236.4	162.3	398.7
	5	110.3	60.2	170.5
	6	295.3	168.6	463.9
Vesic	H-11	26.5	4.7	31.2
	H-12	44.2	11.4	55.6
	H-13	79.5	39.8	119.3
	H-14	141.4	51.9	193.3
	H-15	247.4	92.9	340.3
Seattle	A	430.8	318.2	749.0
	B	357.9	183.7	541.6
Tavenas	H-5	a	a	a
	J-5	164.3	189.4	353.7
Gregersen	A	19.8	11.3	31.1
	D/A	24.4	28.7	53.1
	C	10.6	9.7	20.3
	B/C	13.6	25.3	38.9
Corpus Christi	Initial	115.6	27.4	143.0
	Final	115.6	27.4	143.0
Sellgren	AI	b	b	b
	AII	b	b	b
LD26 ELLIS	M6	62.5	44.2	106.7
LD26 REPL	31P-III5	a	a	a

a - H-Piles

b - No SPT N-Values

Note: 1 ton = 8.9 kN

TABLE 16.- Comparison of Ultimate Loads

SITE	PILE	Prediction Method (tons)			Failure Criteria (tons)			Maximum Applied Load (tons)
		API	Meyerhof	Coyle-Castello	Asymptote	Davisson	0.1xD	
Arkansas River	1	174	248	230	216	161	172 a	172
	2	232	404	252	322	207	242	250
	3	286	552	335	264	230	272 a	259
	6		314		257	132	183 a	183
	7		328		297	189	243	255
	9		375		268	222	250 a	250
	10	234	405	253	283	200	242 a	230
	16	221	393	235	146	154	175 a	167
Low Sill	1		740		346	358	390 a	358
	2	353	896	451	377	338	420 a	372
	3		684		255	185	240	240
	4	267	633	399	402	400 a	440 a	341
	5	81	218	171	158	135	145	145
	6	303	755	464	378	365 a	430 a	345
Vesic	H-11	20	75	31	134	35	76	105
	H-12	56	139	56	24.5	172.5	232	237.5
	H-13	93	135	119	328	205	297	315
	H-14	144	247	193	418	290	347	400
	H-15	206	343	340	545	350	421	430
Seattle	A	1023	894	749	608	525	525	535
	B	728	815	542	532	450	450	450
Tavenas	H-5		213		171	120	162.5	162.5
	J-5	174	176	354	177	109	150	150
Gregersen	A	30	7	31	28.4	24.3	27	30
	D/A	76	12	53	c	44.5	51	52
	C	20	5	20	29.5	26.4	30	31
	B/C	60	9	39	c	42.7	48	52
Corpus Christi	Initial	113	287	143	217	108.2	150 a	134
	Final	113	287	143	213	134.6	168 a	157
Sellgren	AI				107	58.3	77.5	90
	AII				189	129.2	142.5	158
Lock and Dam 26	M6	65	176	107	119	75	95	110
	3IP-IIIS		330		173	150 a	*	150

a - Load-Settlement Curve extrapolated to obtain value.  
 b - Load-Settlement Curve could not be extrapolated with confidence  
 c - Not enough Load Transfer Data.  
 Note: 1 ton = 8.9 kN

API CODE

110

$\frac{\text{NUMBER OF LOAD TESTS}}{\text{TOTAL LOAD TESTS}}$

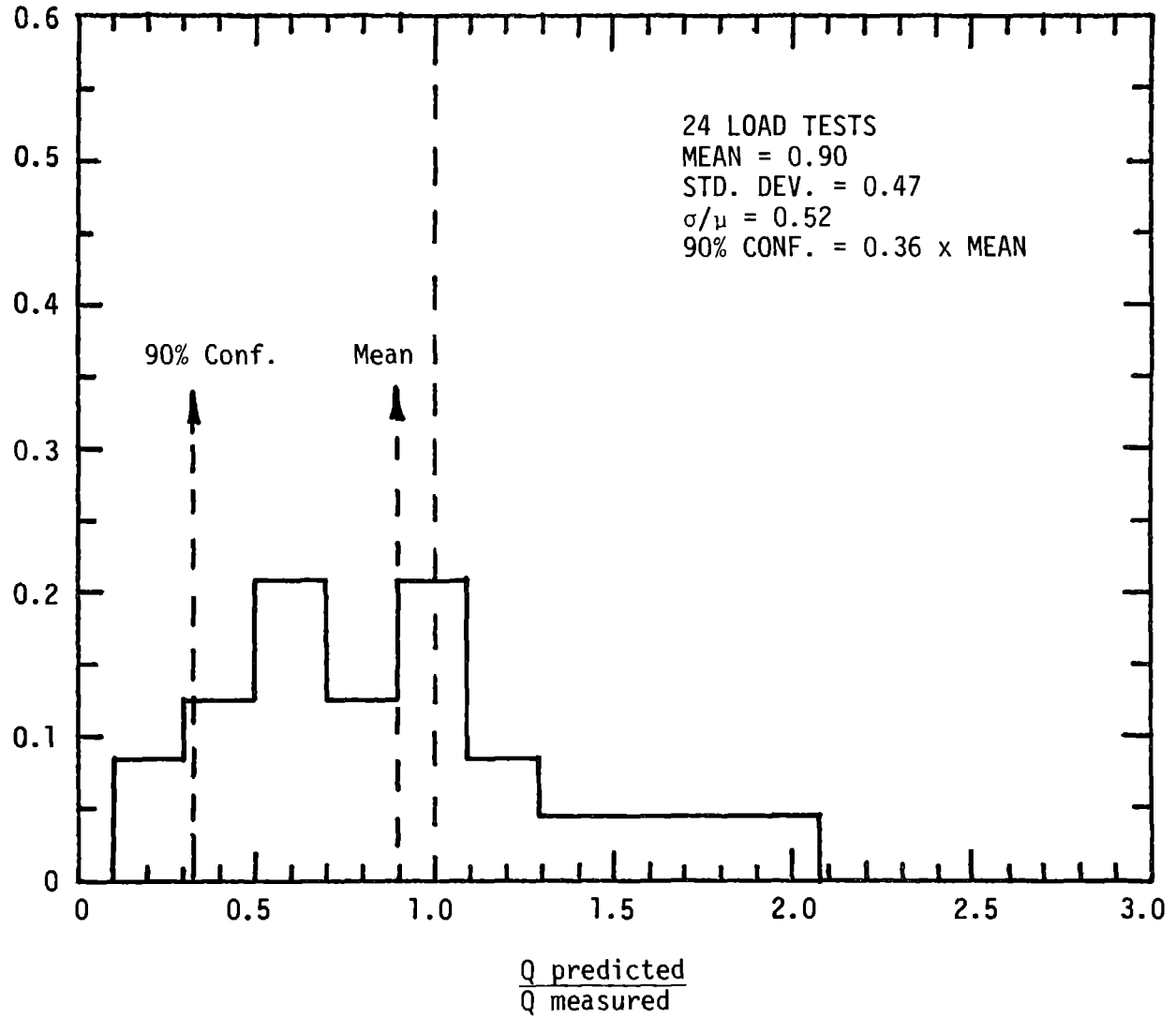


FIG. 50 - Frequency Distribution. API Code. Total Load



SPT: MEYERHOF

$\frac{\text{NUMBER OF LOAD TESTS}}{\text{TOTAL LOAD TESTS}}$

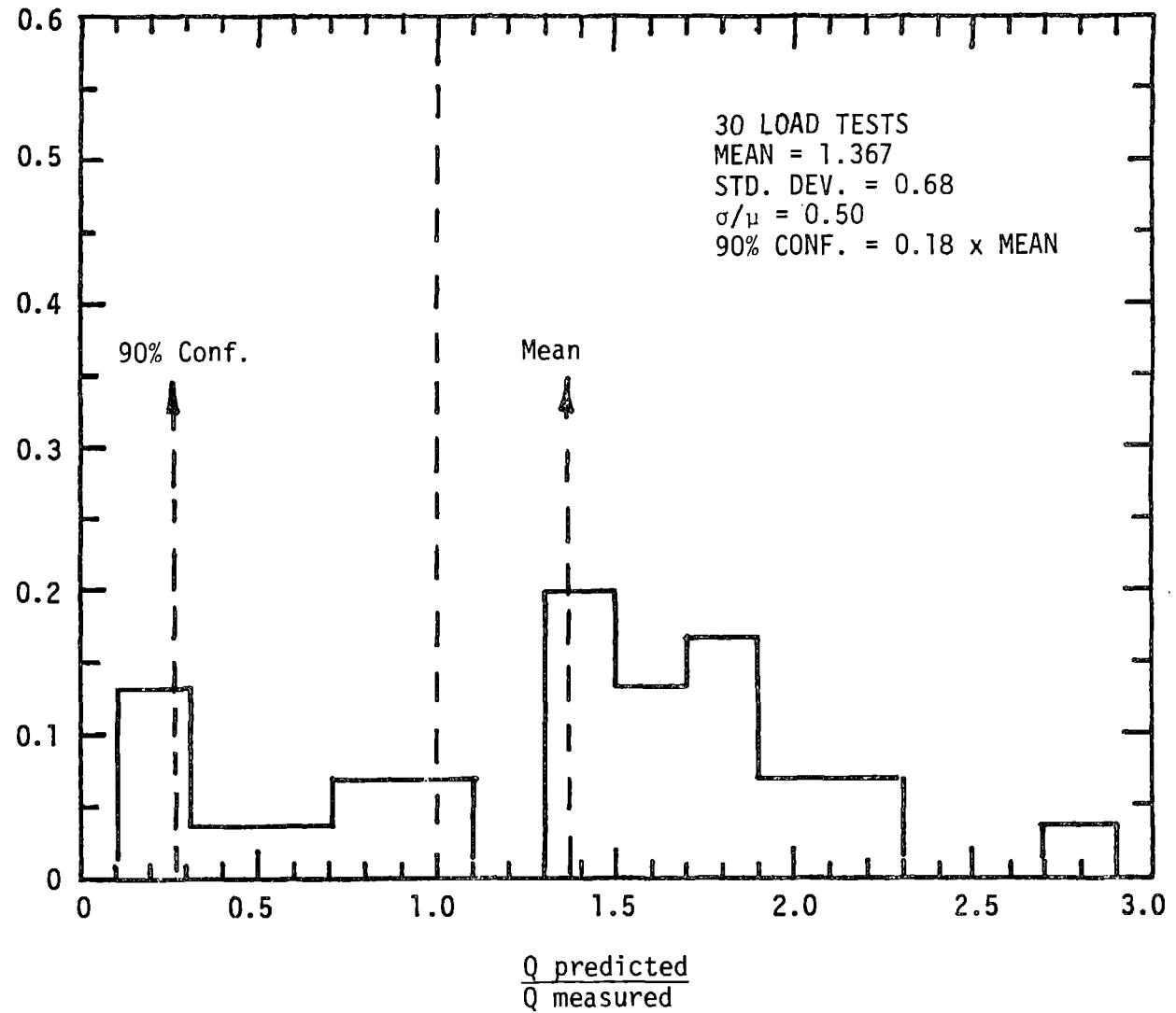


FIG. 51 - Frequency Distribution. Meyerhof Method. Total Load

COYLE-CASTELLO METHOD

$\frac{\text{NUMBER OF LOAD TESTS}}{\text{TOTAL LOAD TESTS}}$

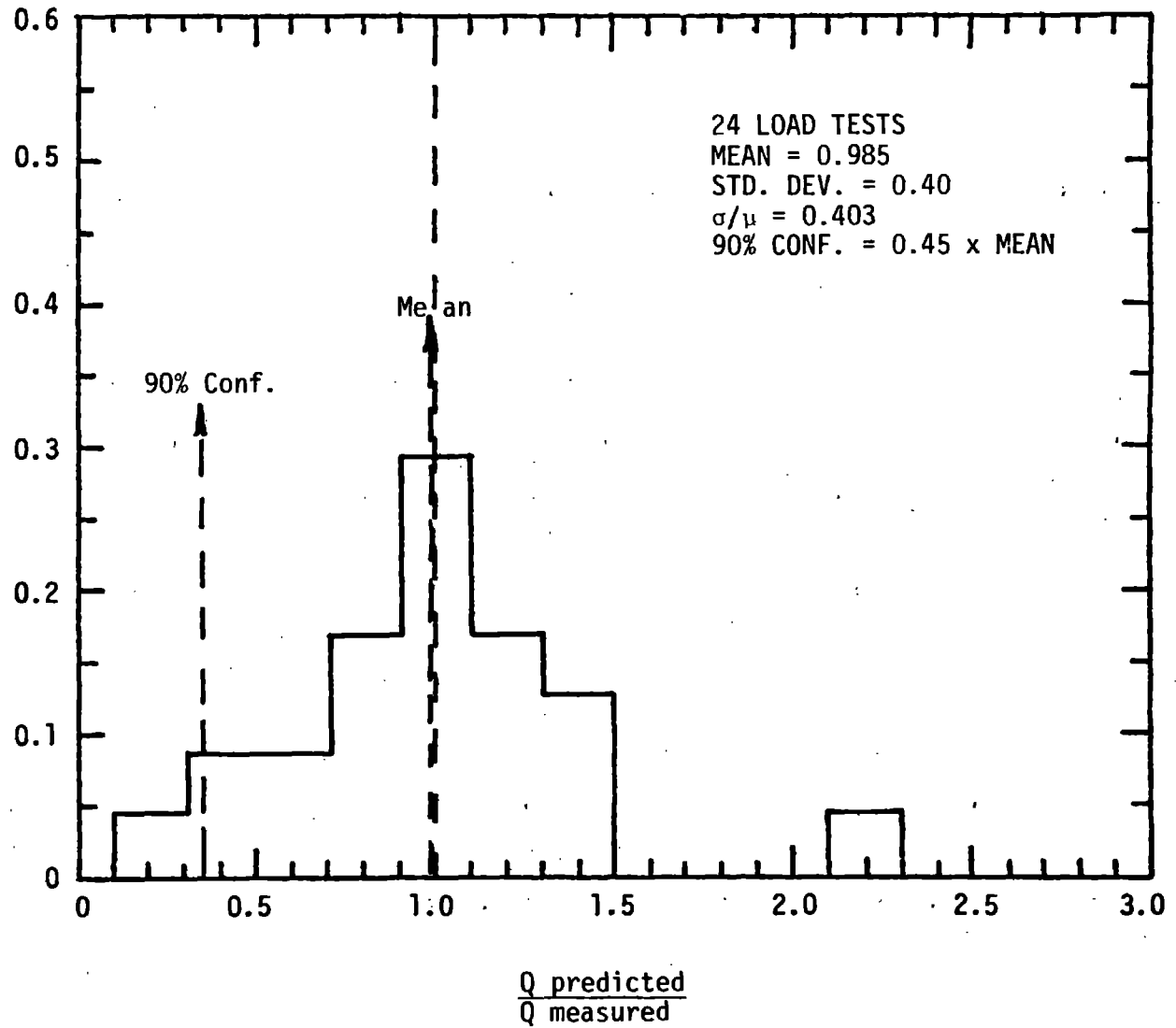


FIG. 52 .- Frequency Distribution. Coyle-Castello Method. Total Load

SPT: BRLAUD-TUCKER METHOD

$\frac{\text{NUMBER OF LOAD TESTS}}{\text{TOTAL LOAD TESTS}}$

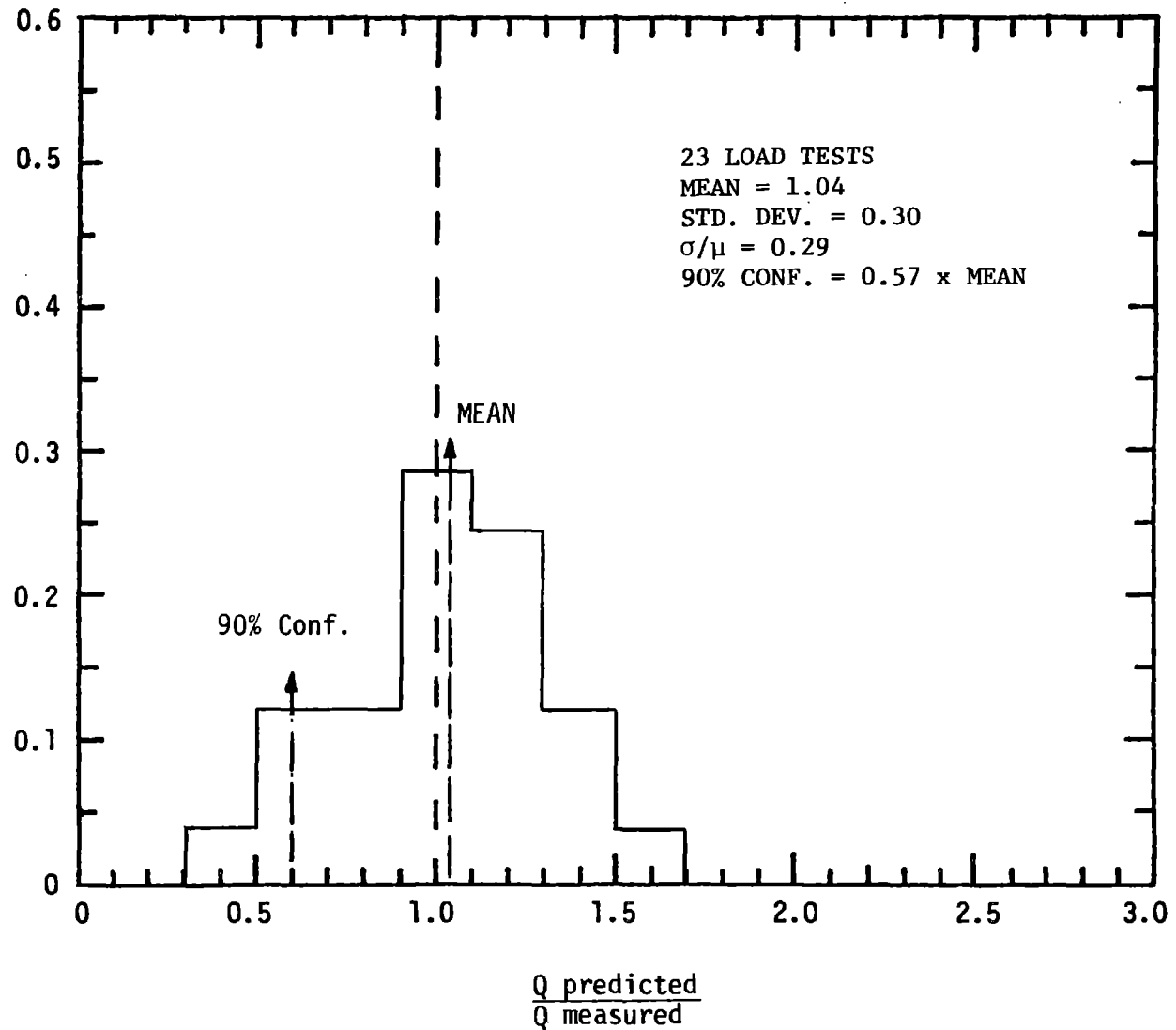


FIG. 53.- Frequency Distribution. Briaud-Tucker Method. Total Load

TABLE 17.- Summary of Frequency Distribution Results

<u>Method</u>	<u>Mean</u>	<u>Standard Deviation</u>	<u>Coefficient of Variation</u>	<u>Coefficient K for 90% Confidence 90% Conf. -</u>	<u>Comment on Data Base</u>
API	0.90	0.47	0.52	0.36	Somewhat different
Meyerhof	1.367	0.68	0.50	0.18	Somewhat different
Coyle & Castello	0.985	0.40	0.403	0.45	Somewhat different
Briaud & Tucker	1.04	0.30	0.29	0.57	Same

Tucker method, indicating a larger amount of scatter in the results. Thus, overall the new design method gives the best results. It should be kept in mind however, that the data base analyzed here is somewhat different from that used to develop the first three methods, whereas it is the same as that used to develop the new method.

The overprediction of the Meyerhof method is due mainly to the prediction of point capacity. From the data presented in the previous chapter, a value of  $4 \times N$  for the point capacity would be valid only up to a  $N$  value of about 20 blow/ft. Therefore the method may yield better results using a maximum value of point resistance of 80 tsf to 100 tsf (0.8 kPa to 1.0 kPa).

#### PREDICTIONS OF LOAD-SETTLEMENT BEHAVIOR

The static formula methods are used to predict ultimate bearing capacity, but they do not predict pile settlement. The best way to obtain pile settlement is to conduct a pile load test. In many cases, the design of foundation piles is based on allowable settlement. A method has been proposed to predict pile settlement, i.e., predict a load-settlement curve. This method is based on a computer program which utilizes non-linear soil resistance properties (13). The method requires a knowledge of unit skin friction versus movements and unit point bearing versus movement relationships.

Two procedures for nonlinear resistance versus movement relationships were used in this study to predict load-settlement curves. Both procedures were developed at Texas A&M University and were developed using the results of instrumented pile load tests in sand. Instrumented pile load test data was analyzed to develop plots of friction versus movement and point bearing versus movement curves. These curves were then used to develop the empirical input needed for the computer program which gives the predicted load-settlement curve.

##### Coyle t-z Curve Method

The first procedure was developed during the past five years as

additional instrumented pile load tests were reported in the literature (14). The resistance-movement curves which were developed during this time are presented in Tables 18 and 19. The curve from Table 18 is in terms of unit skin friction resistance expressed in percentage of the ultimate frictional resistance. For example, at a movement of 0.075 in. (0.19 cm) 50 percent of the ultimate frictional resistance is developed. The curve from Table 19 is in terms of ultimate point load rather than unit point bearing resistance. For example, at a movement of 0.10 in. (0.25 cm) 60 percent of the ultimate point load is developed.

TABLE 18.- Friction Movement Curve

Percent Friction Developed Ratio	Movement in.
0	0
0.50	0.075
0.75	0.125
0.90	0.200
1.00	0.300
1.00	0.500

Notes: Uses  $f_{(ult)}$  from Coyle-Castello  
 1 in. = 2.54 cm

TABLE 19.- Point Bearing - Movement Curve

Point Load lb.	Movement in.
0	0
0.60 $Q_p(ult)$	0.10
1.00 $Q_p(ult)$	0.30
1.25 $Q_p(ult)$	0.75

Notes: Uses  $Q_p(ult) = q_o A_p$  ( $q_o$   
 from Coyle-Castello)

1 lb = 4.45 N; 1 in. = 2.54 cm

### Briaud-Tucker Method

The second procedure was developed as a part of this study and was detailed in the previous chapter. Hyperbolic resistance-movement curves were developed in terms of unit frictional resistance ( $f_g$ ) and unit point bearing resistance ( $q_0$ ) versus movement ( $w$ ). These relationships have already been presented in Chapter VIII, but are repeated to show the application with respect to predicted load-settlement curves. Eq. 36 and 37 from Chapter VIII are used to express the relationships:

$$f = \frac{w}{\frac{1}{K_\tau} + \frac{w}{(f_{\max} + f_{\text{res}})}} - f_{\text{res}} \quad \text{in tsf}$$

$$q = \frac{w}{\frac{1}{K_p} + \frac{w}{(q_{\max} - q_{\text{res}})}} + q_{\text{res}} \quad \text{in tsf}$$

where

$$K_\tau = 5.01 (N_{\text{side}})^{0.27} \quad \text{in tsf/in.}$$

$$f_{\max} = 0.224 (N_{\text{side}})^{0.29} \quad \text{in tsf}$$

$$K_p = 457.1 (N_{\text{pt}})^{0.0065} \quad \text{in tsf/in.}$$

$$q_{\max} = 19.75 (N_{\text{pt}})^{0.36} \quad \text{in tsf/in.}$$

$$q_{\text{res}} = 5.57 L\beta \quad \text{in tsf} \quad \text{in tsf}$$

$$f_{\text{res}} = \frac{A_p}{A_s}$$

N = Standard Penetration Test N-Value

L = pile length

$$\beta = \sqrt{\frac{K_T P}{AE_p}}$$

P = pile perimeter

A = pile cross-sectional area

E<sub>p</sub> = pile modulus of elasticity

### Comparison of the Results

The predicted load-settlement curves which were developed for the test piles included in this study are presented in Figs. 54 through 76. For each test pile the measured load-settlement curve is presented along with the predicted curve using both the Coyle and Briaud-Tucker procedures. In addition, a single point is plotted to indicate the ultimate bearing capacity for the API and Meyerhof's static analysis. Coyle and Castello correlations were used to obtain ultimate frictional and point resistances with the Coyle procedure. Eqs. 36 and 37 were used to obtain maximum unit frictional and point bearing resistances with the Briaud-Tucker procedure. A careful examination of Figs. 54 to 76 shows that both procedures give reasonably accurate predicted load-settlement curves for most test piles. In general, the Briaud-Tucker procedure gives the best results.



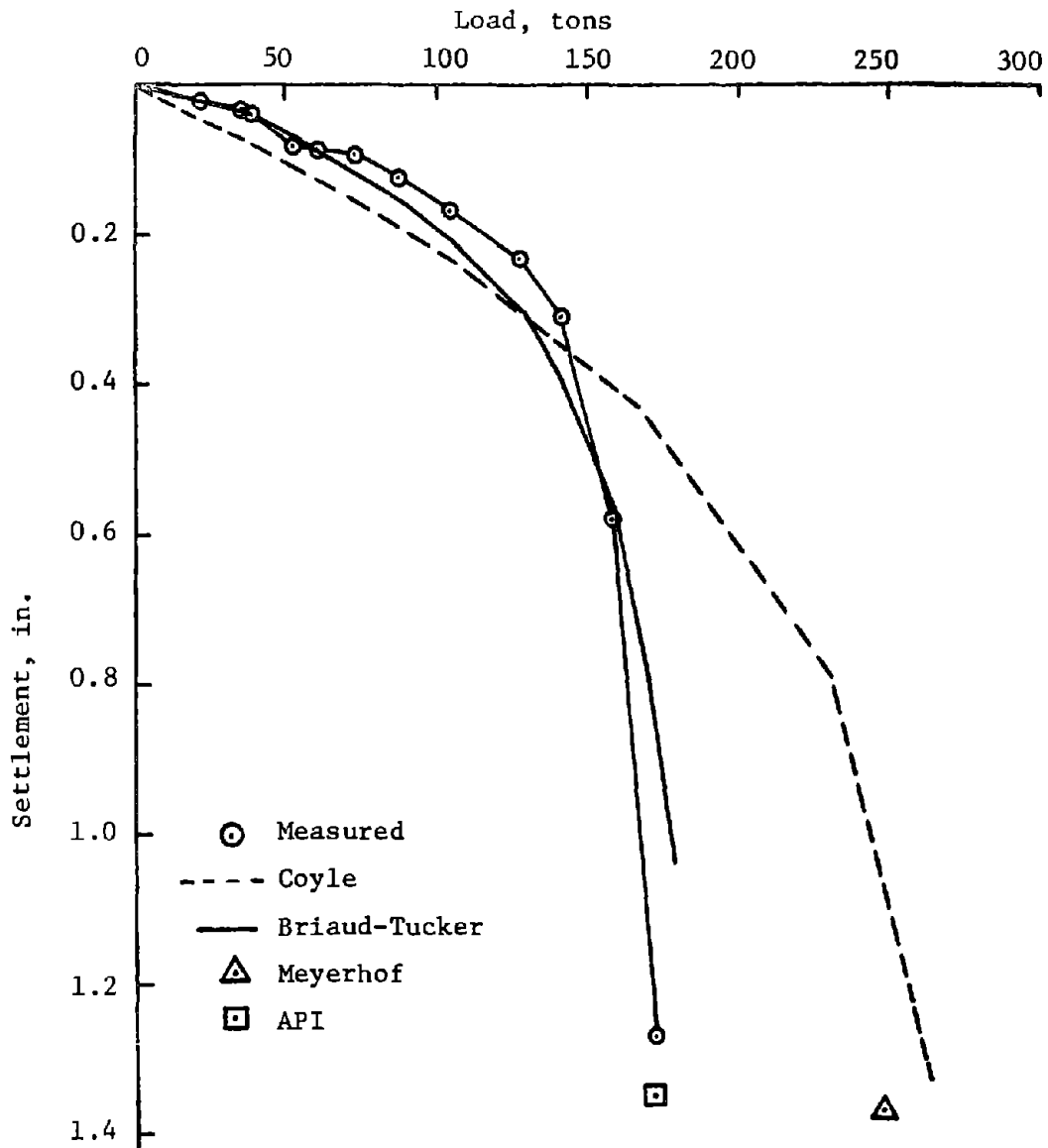


FIG. 54.- Arkansas River Pile 1: Load-Settlement Predictions by Coyle and Briaud-Tucker Methods  
(1 ton = 8.9 kN; 1 in. = 2.54 cm)

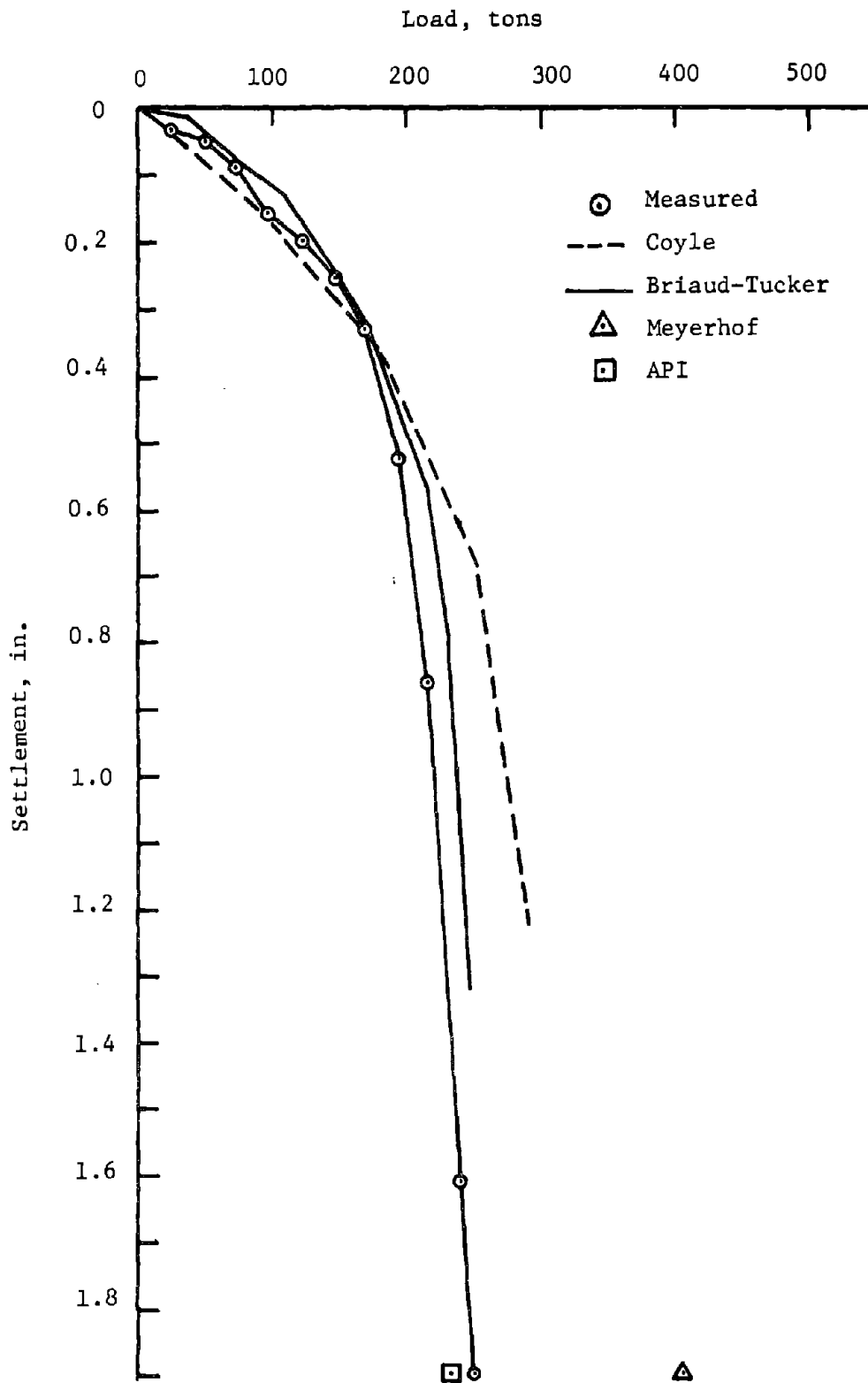


FIG. 55.- Arkansas River Pile 2: Load-Settlement Predictions by Coyle and Briaud-Tucker Methods (1 ton = 8.9 kN; 1 in. = 2.54 cm)

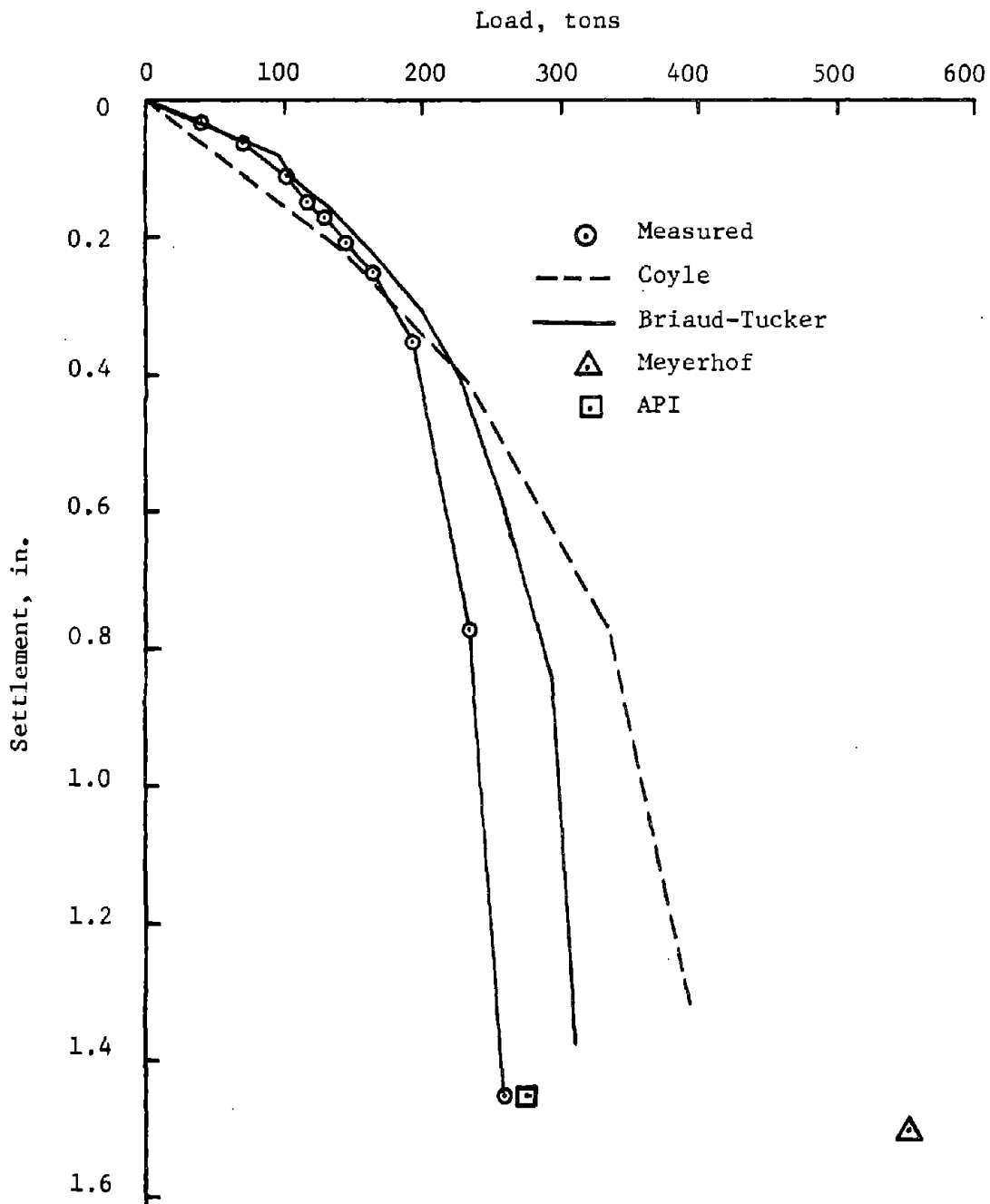


FIG. 56.-- Arkansas River Pile 3: Load Settlement Predictions by Coyle and Briaud-Tucker Methods (1 ton = 8.9 kN; 1 in. = 2.54 cm)

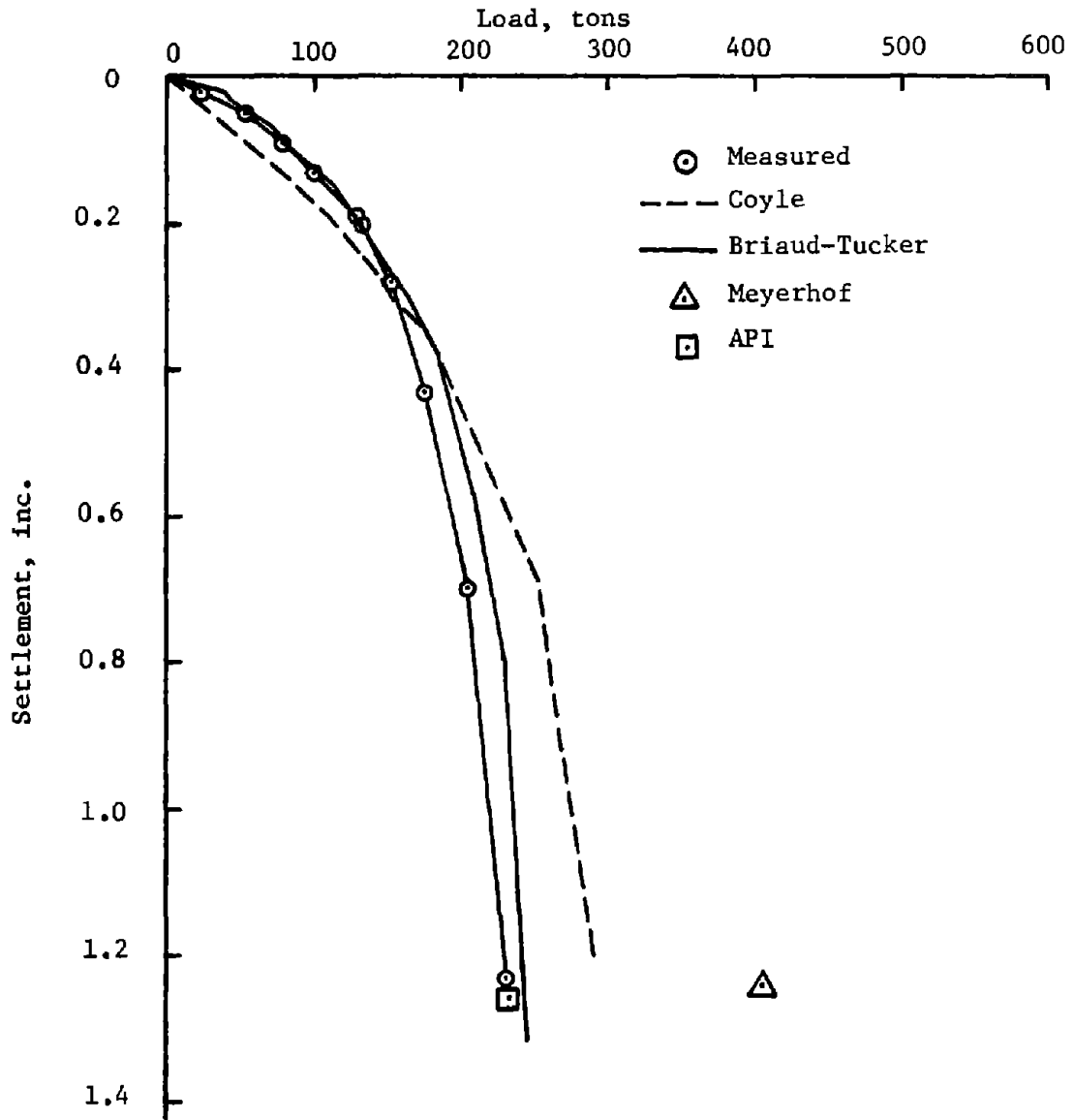


FIG. 57.- Arkansas River Pile 10: Load-Settlement Predictions by Coyle and Briaud-Tucker Methods (1 ton = 8.9 kN; 1 in. = 2.54 cm)

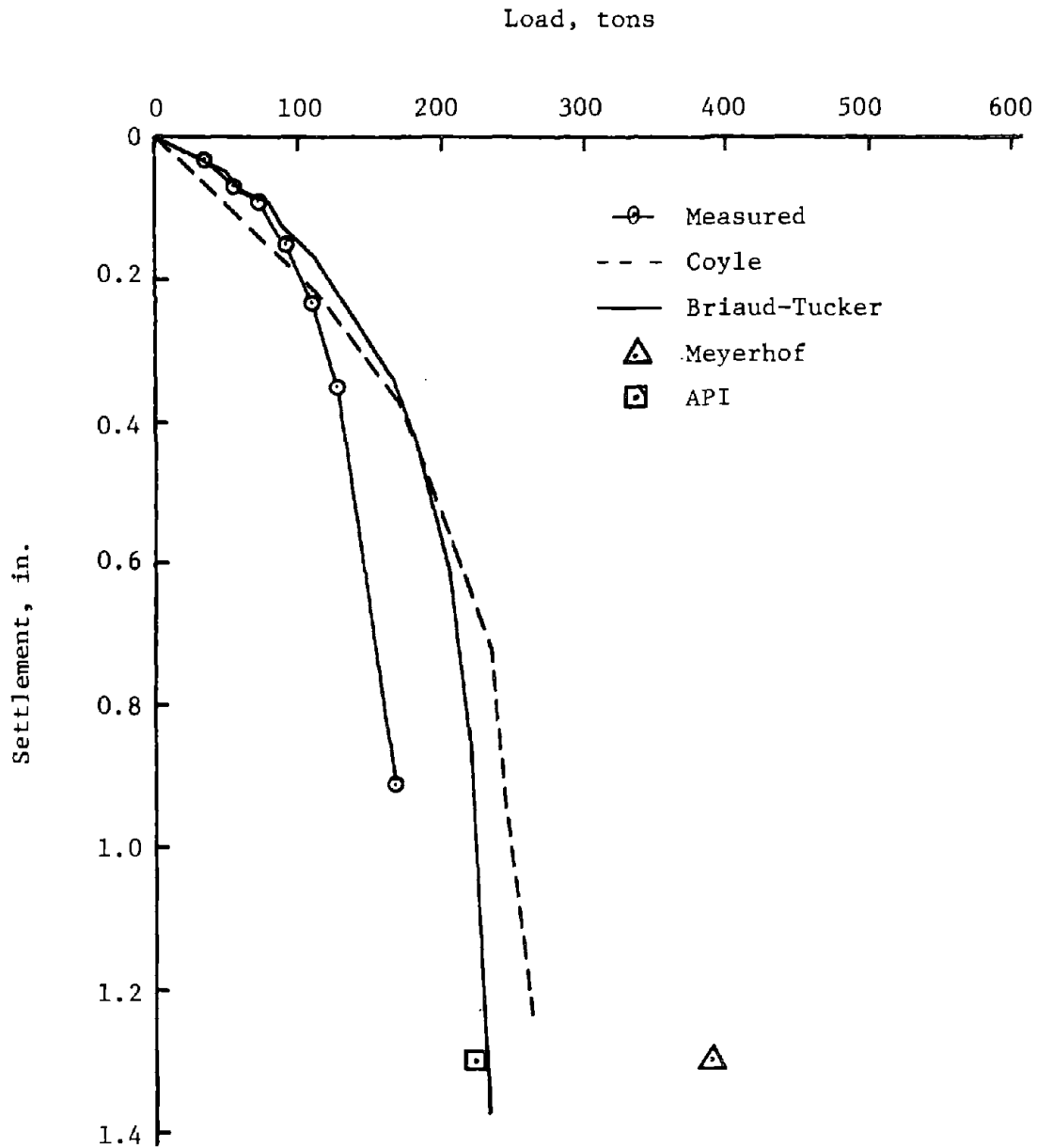


FIG. 58 - Arkansas River Pile 16: Load-Settlement Predictions by Coyle and Briaud-Tucker Methods (1 ton = 8.9 kN; 1 in. = 2.54 cm)

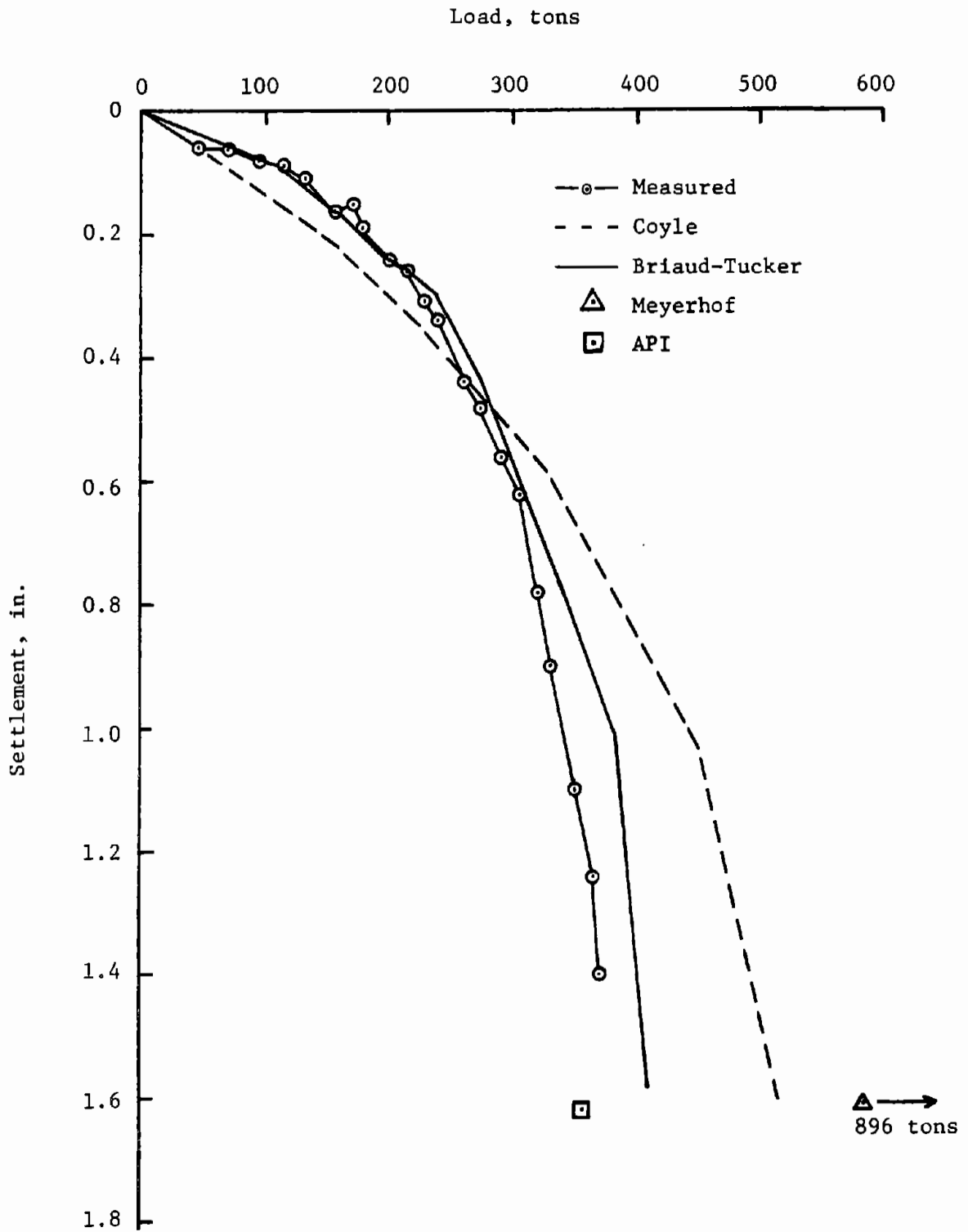


FIG. 59. - Low Sill Structure Pile 2: Load-Settlement Predictions by Coyle and Briaud-Tucker Methods (1 ton = 8.9 kN; 1 in. = 2.54 cm)

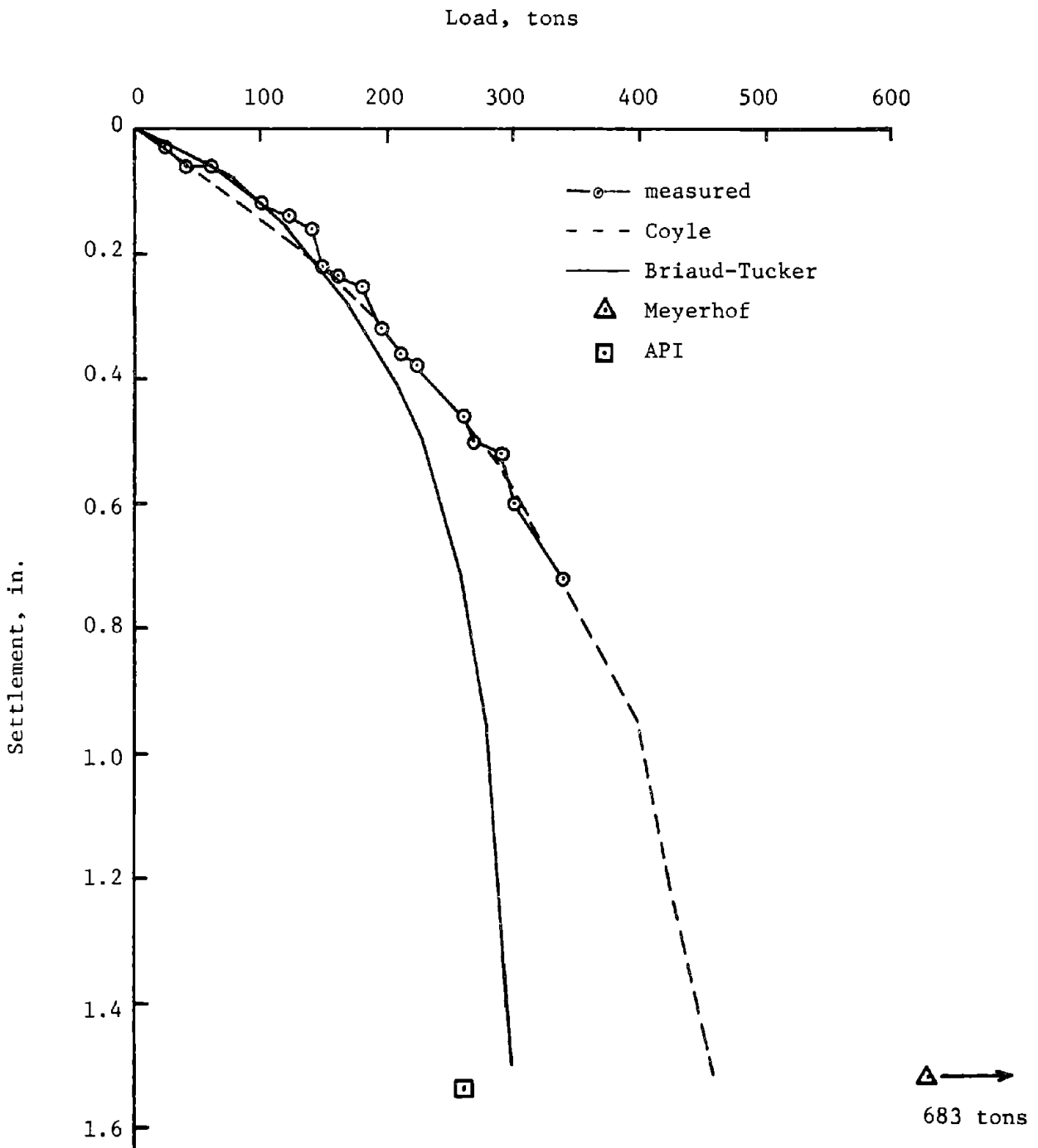


FIG. 60.- Low Sill Structure Pile 4: Load-Settlement Predictions by Coyle and Briaud-Tucker Methods (1 ton = 8.9 kN; 1 in. = 2.54 cm)

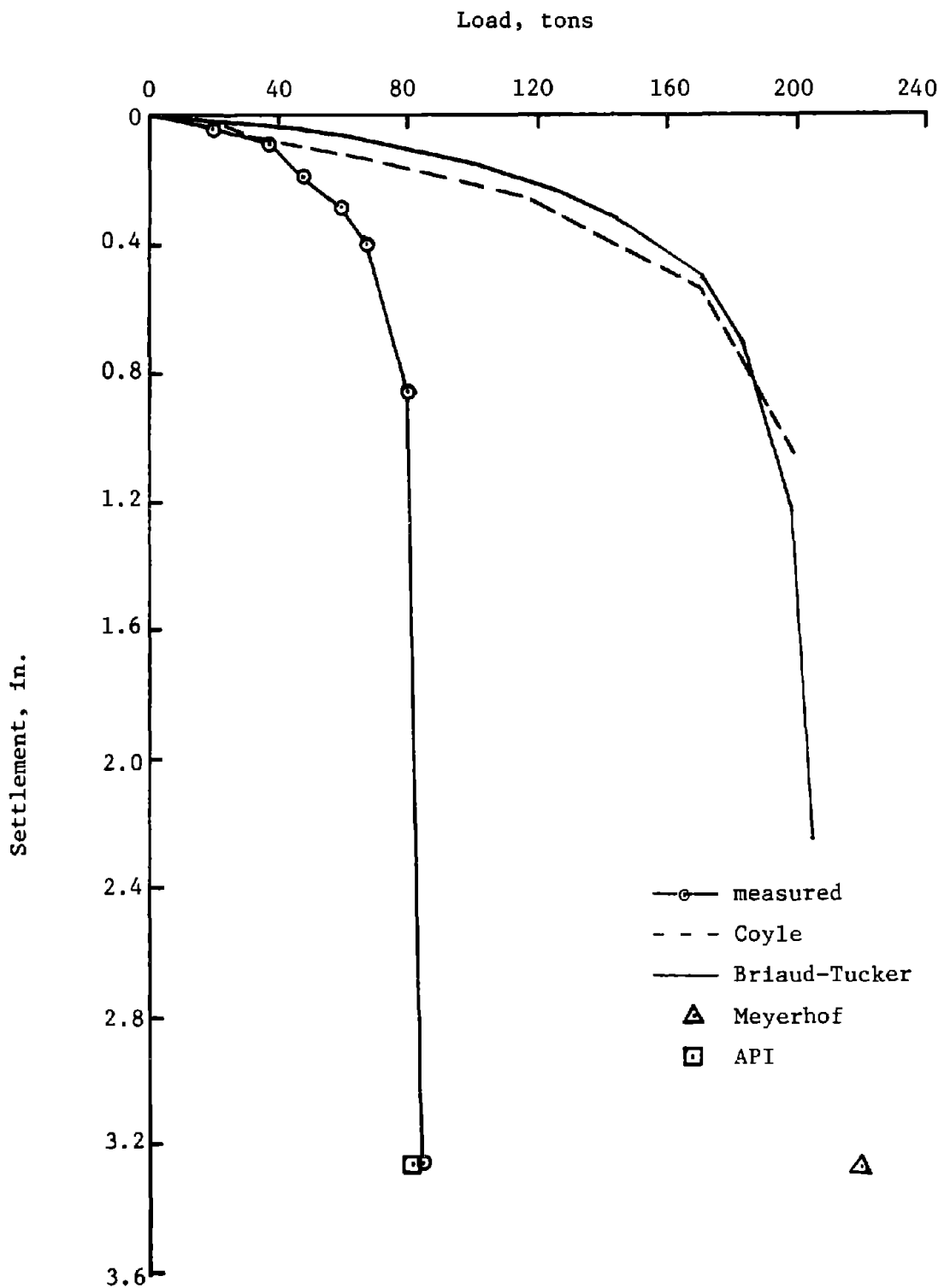


FIG. 61.- Low Sill Structure Pile 5:  
 Load-Settlement Predictions by  
 Coyle and Briaud-Tucker Methods  
 (1 ton = 8.9 kN; 1 in. = 2.54 cm)



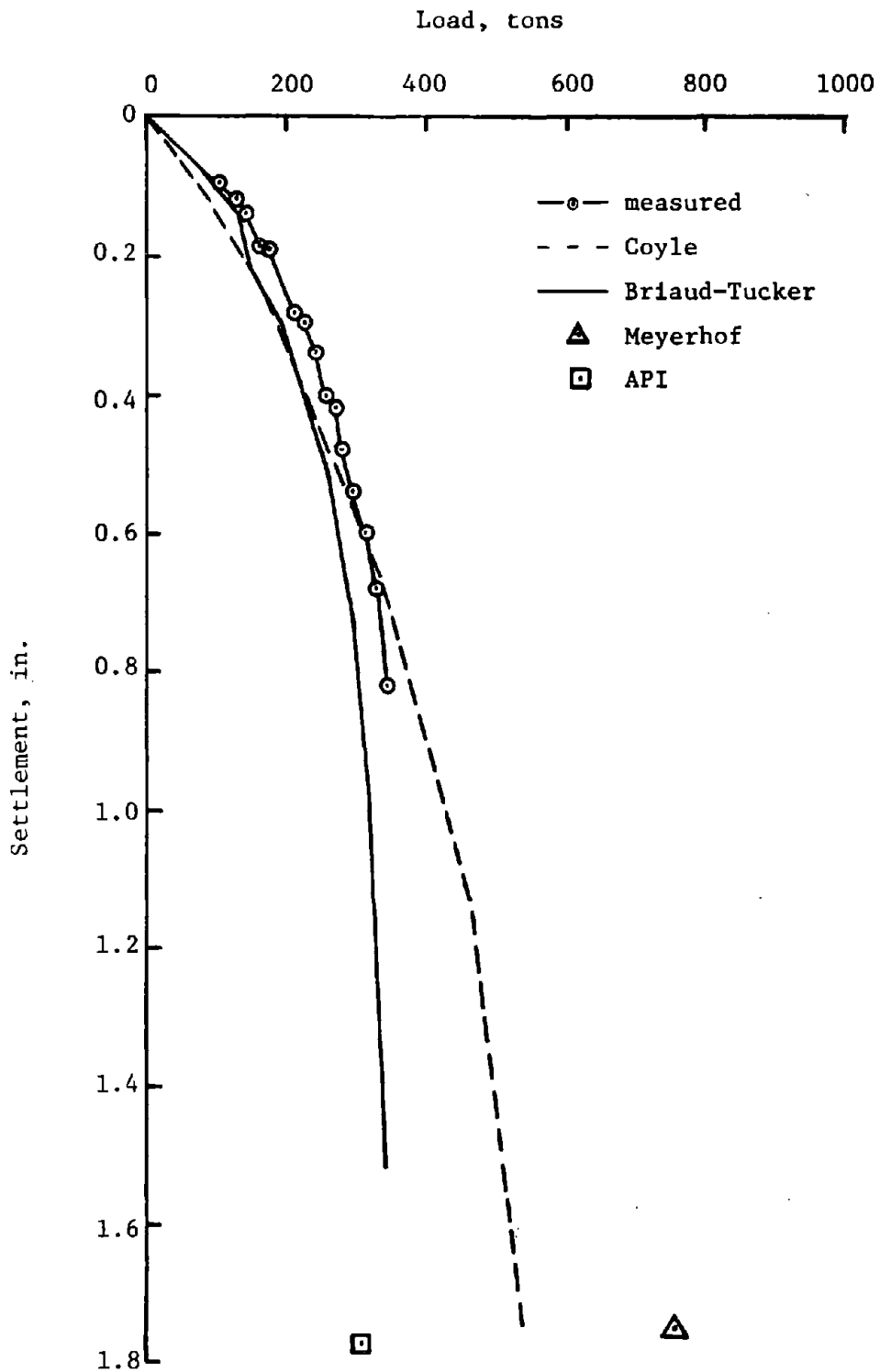


FIG.62.- Low Sill Structure Pile 6:  
 Load-Settlement Predictions by  
 Coyle and Briaud-Tucker Methods  
 (1 ton = 8.9 kN; 1 in. = 2.54 cm)

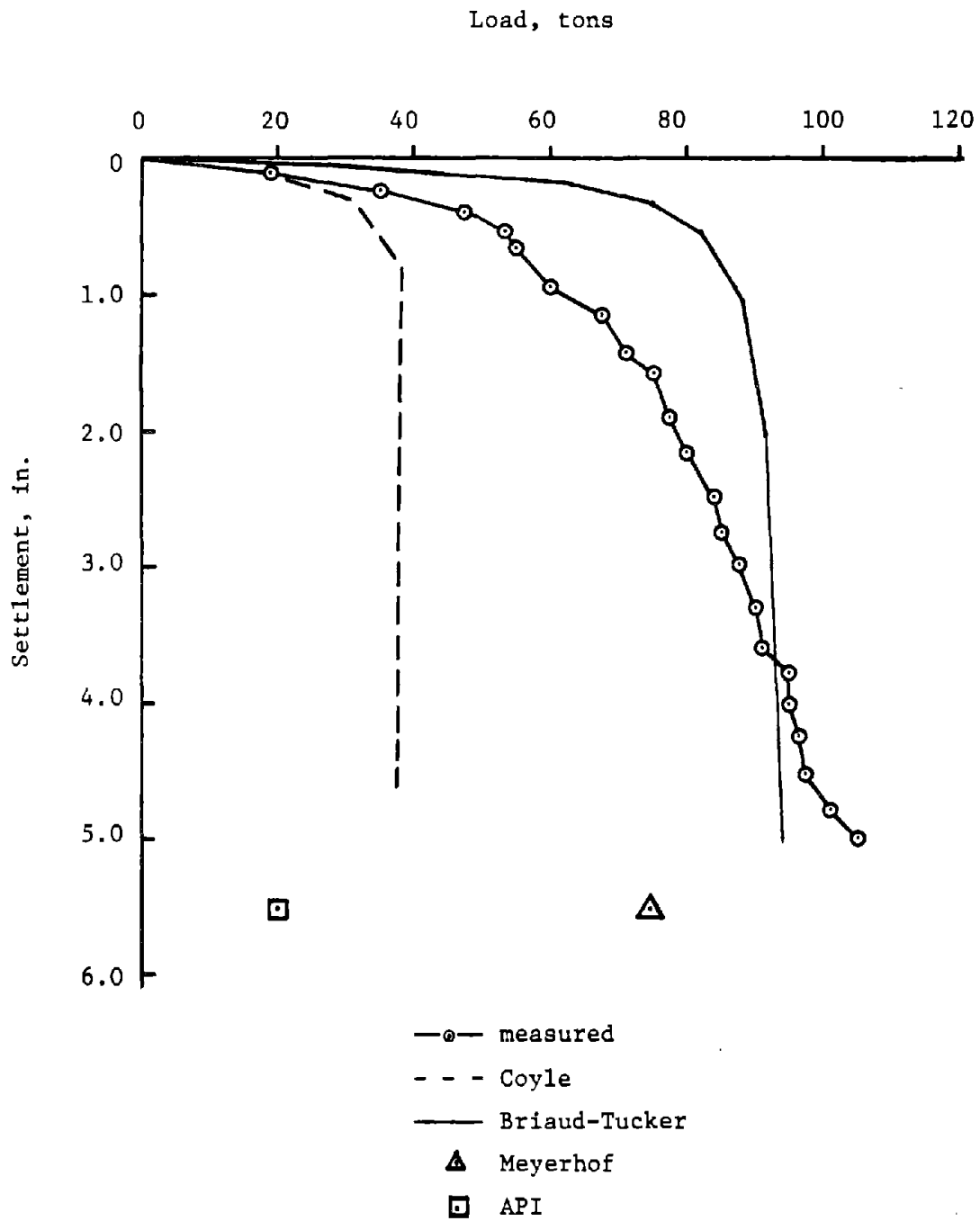


FIG. 63. - Ogeechee River Pile H-11:  
 Load-Settlement Predictions by  
 Coyle and Briaud-Tucker Methods  
 (1 ton = 8.9 kN; 1 in. = 2.54 cm)

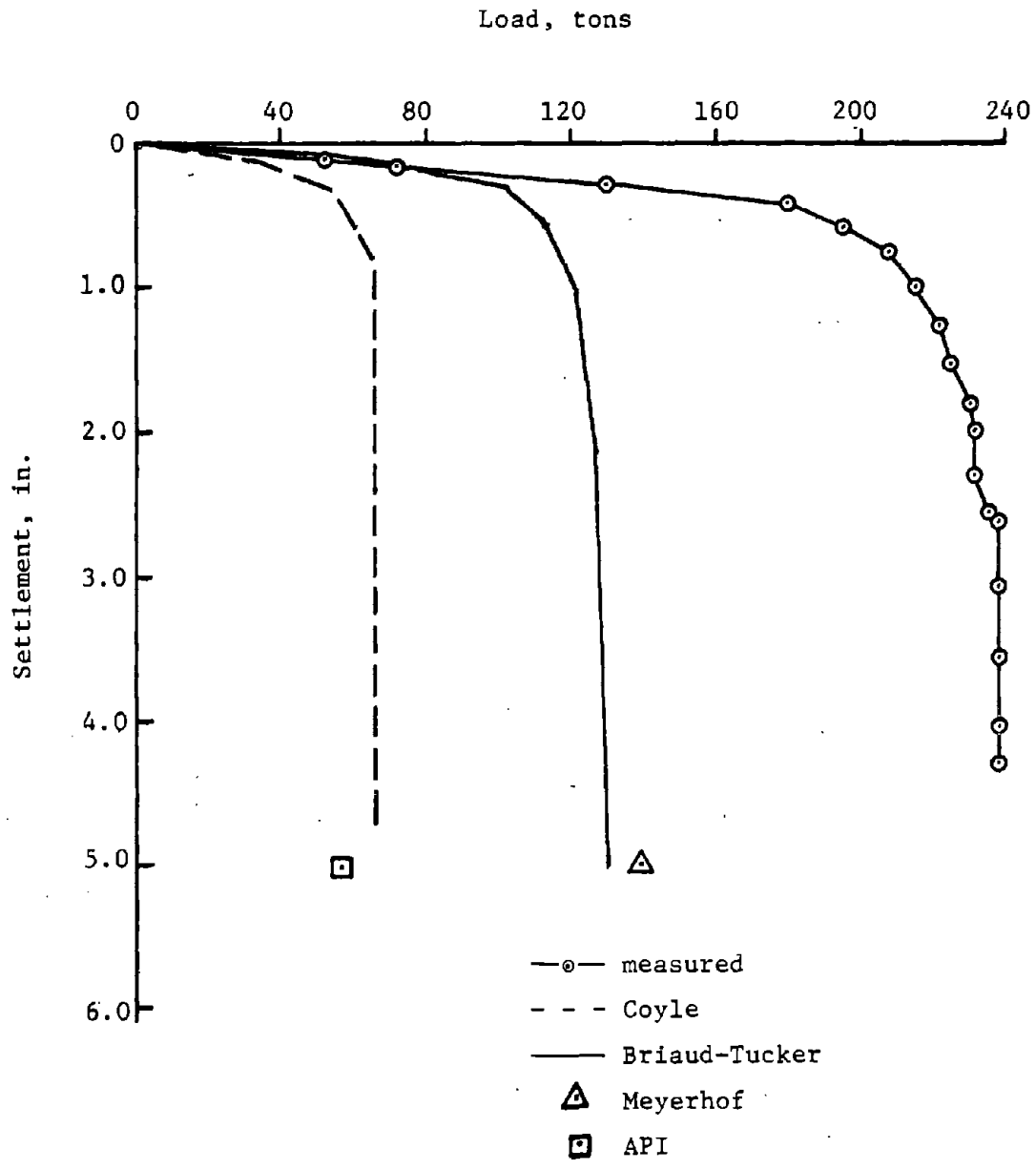


FIG. 64.- Ogeechee River Pile H-12:  
 Load-Settlement Predictions by  
 Coyle and Briaud-Tucker Methods  
 (1 ton = 8.9 kN, 1 in. = 2.54 cm)

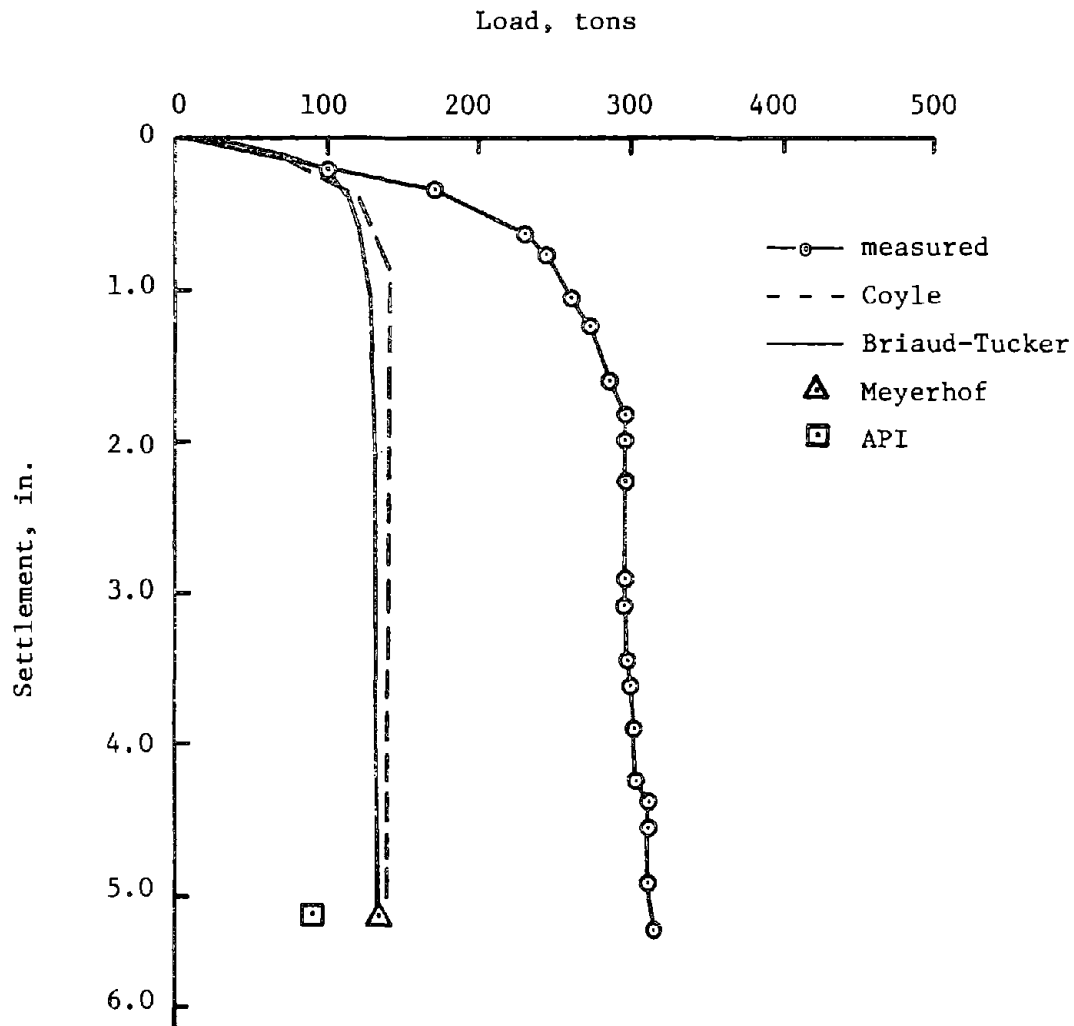


FIG. 65.- Ogeechee River Pile H-13:  
 Load-Settlement Predictions by  
 Coyle and Briaud-Tucker Methods  
 (1 ton = 8.9 kN; 1 in. = 2.54 cm)

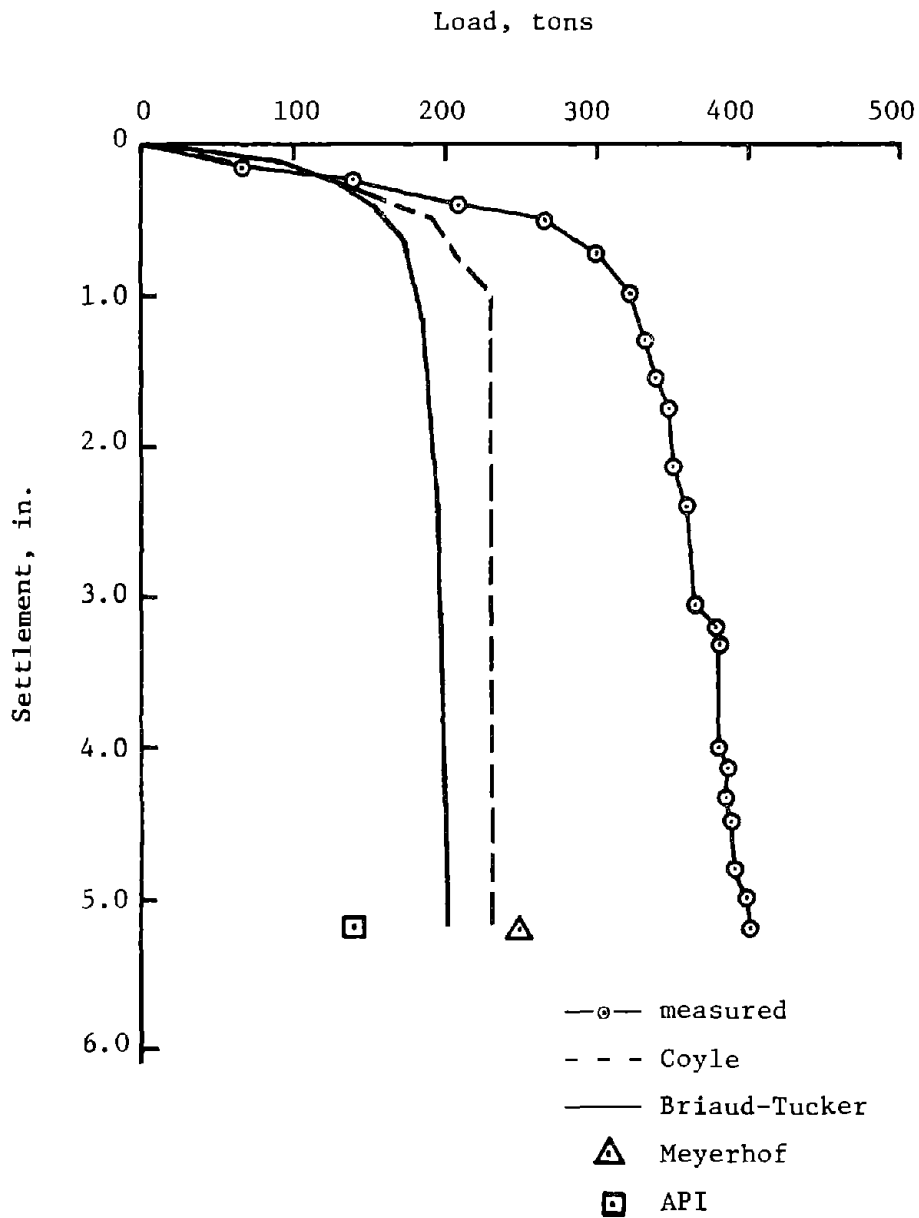


FIG. 66.- Ogeechee River Pile H-14:  
 Load-Settlement Predictions by  
 Coyle and Briaud-Tucker Methods  
 (1 ton = 8.9 kN; 1 in. = 2.54 cm)

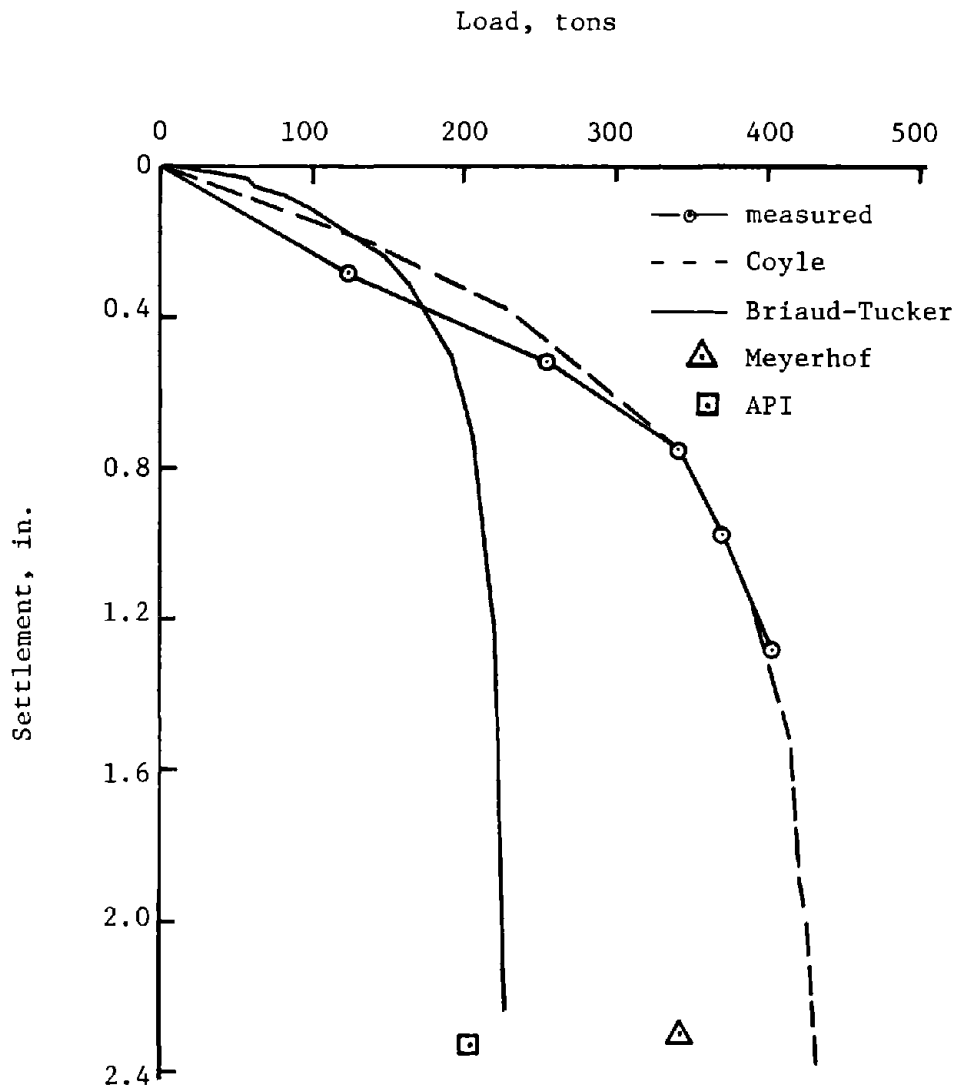


FIG. 67.- Ogeechee River Pile H-15:  
 Load-Settlement Predictions by  
 Coyle and Briaud-Tucker Methods  
 (1 ton = 8.9 kN; 1 in. = 2.54 cm)

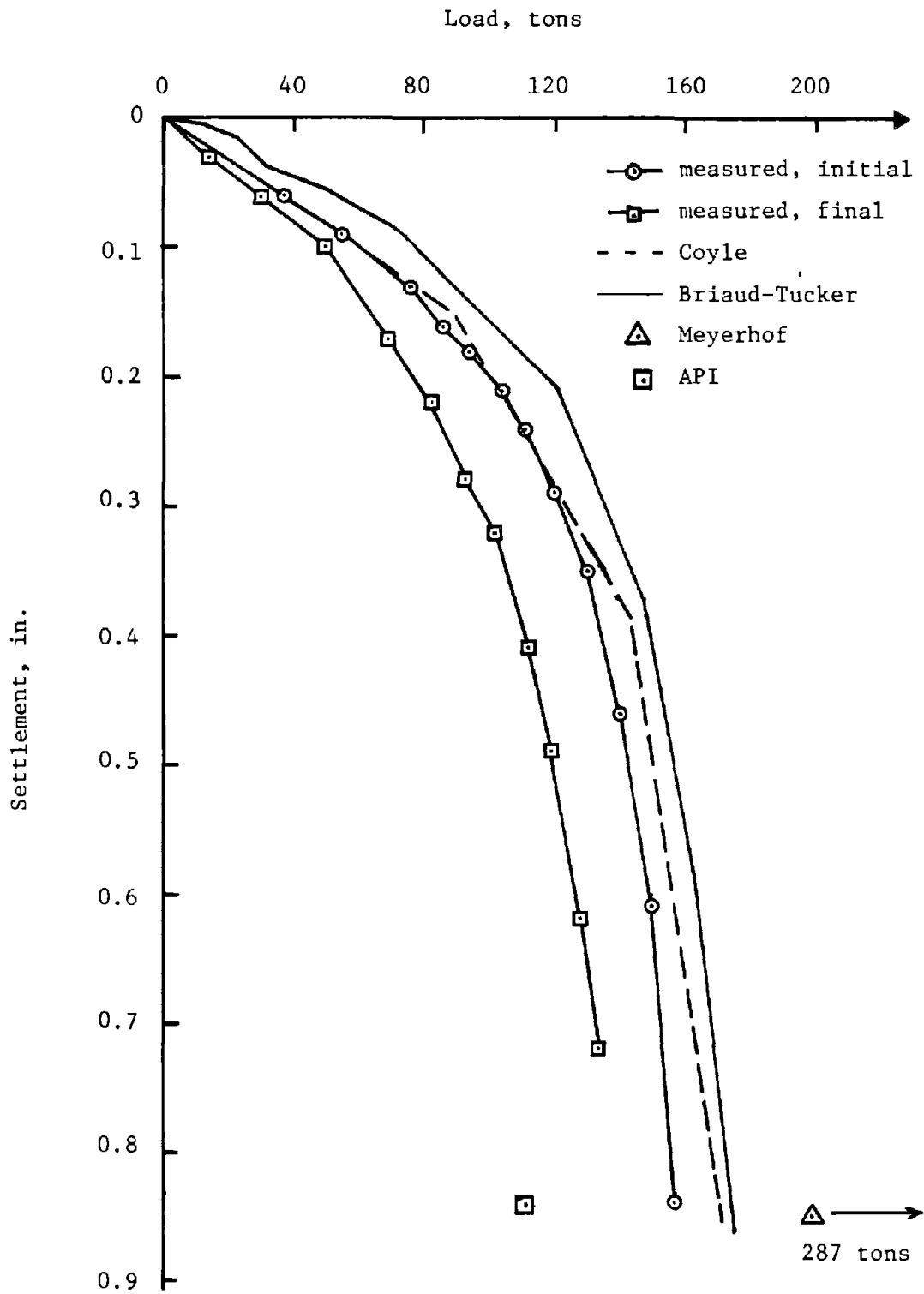


FIG. 68. - Corpus Christi Pile: Load-Settlement Predictions by Coyle and Briaud-Tucker Methods (1 ton = 8.9 kN; 1 in. = 2.54 cm)

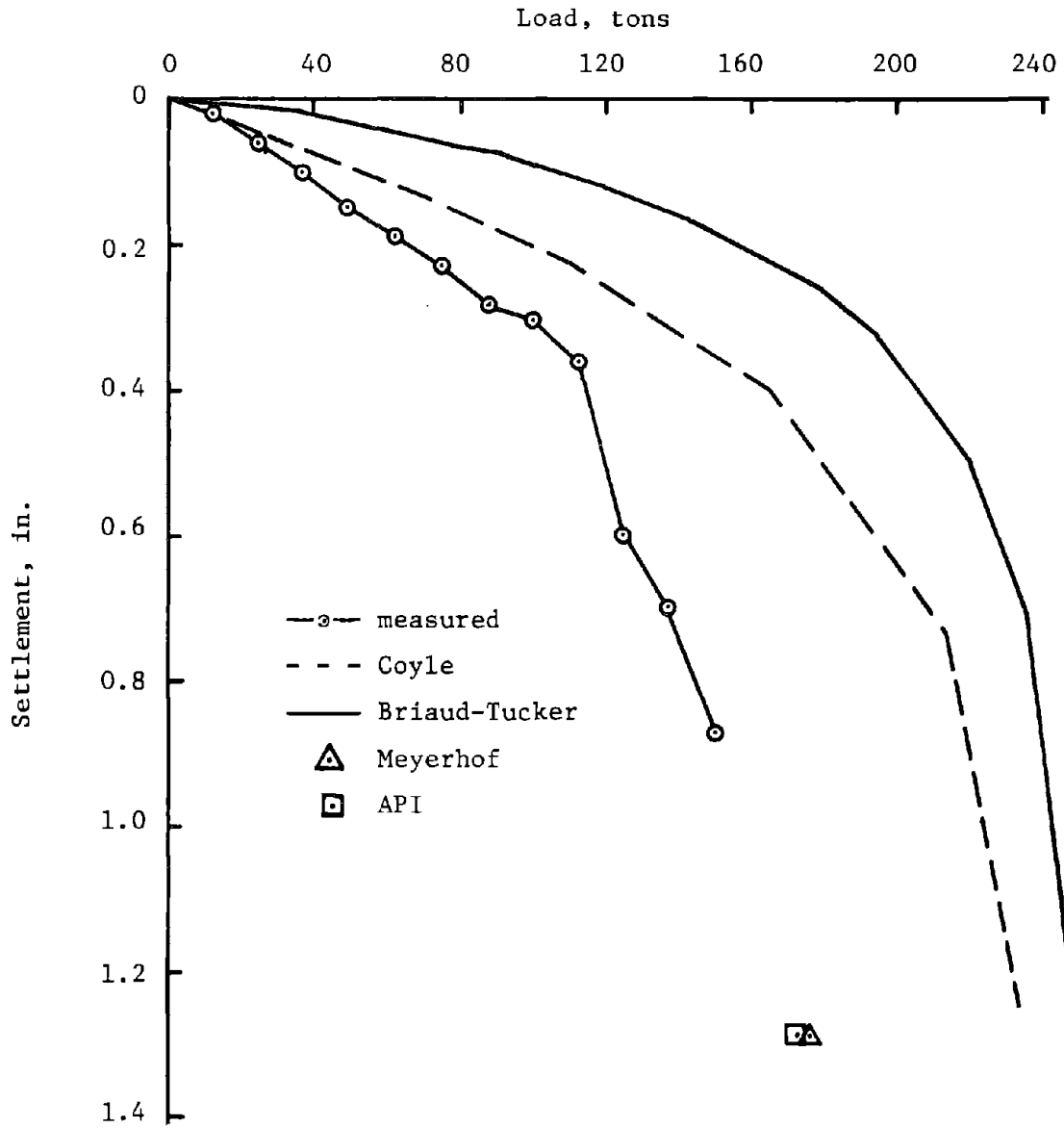


FIG. 69.- Tavenas Pile J-5: Load-Settlement Predictions by Coyle and Briaud-Tucker Methods (1 ton = 8.9 kN; 1 in. = 2.54 cm)



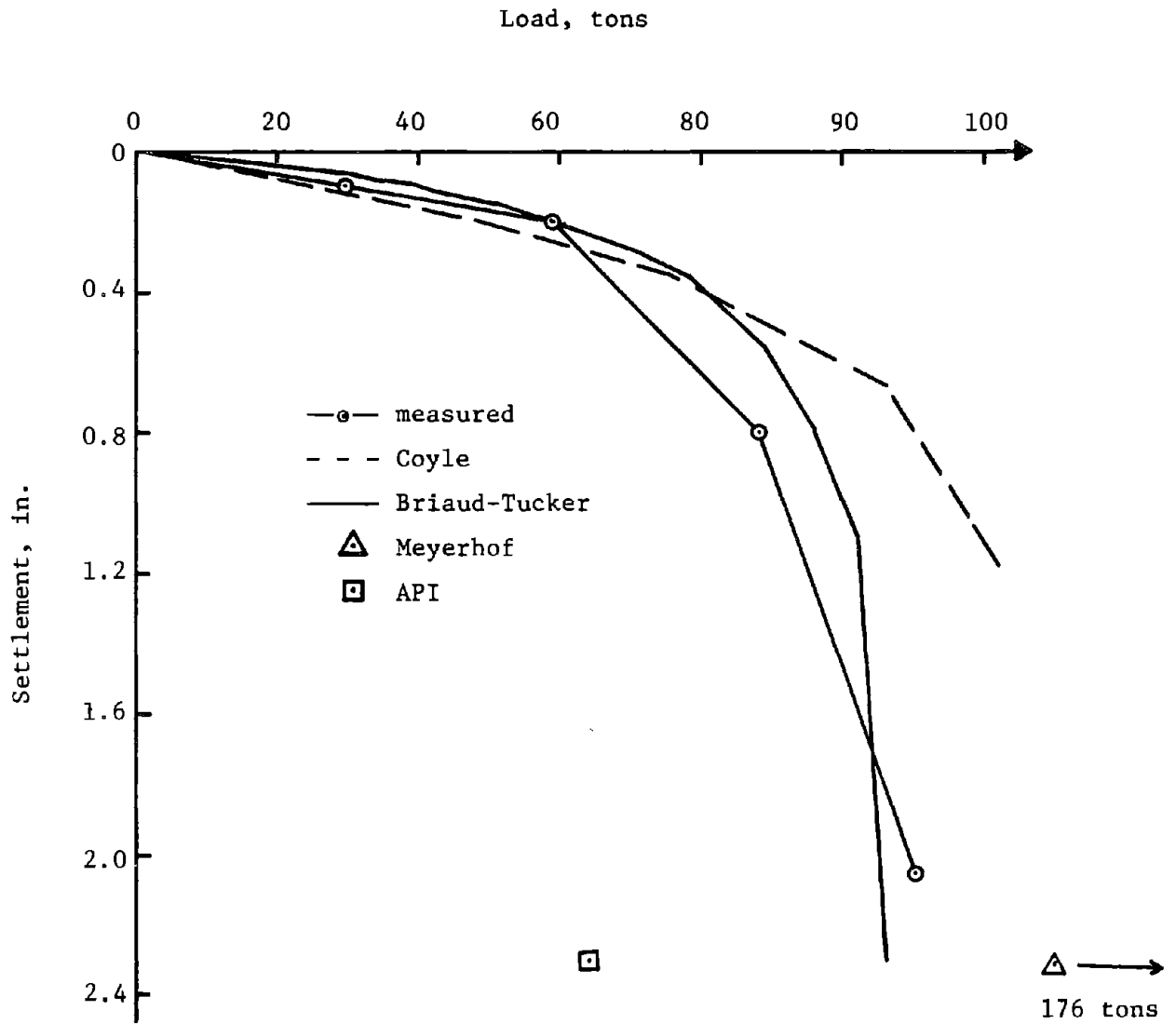


FIG. 70.- Lock and Dam 26 Ellis Island Site M6: Load-Settlement Predictions by Coyle and Briaud-Tucker Methods (1 ton = 8.9 kN; 1 in. = 2.54 cm)

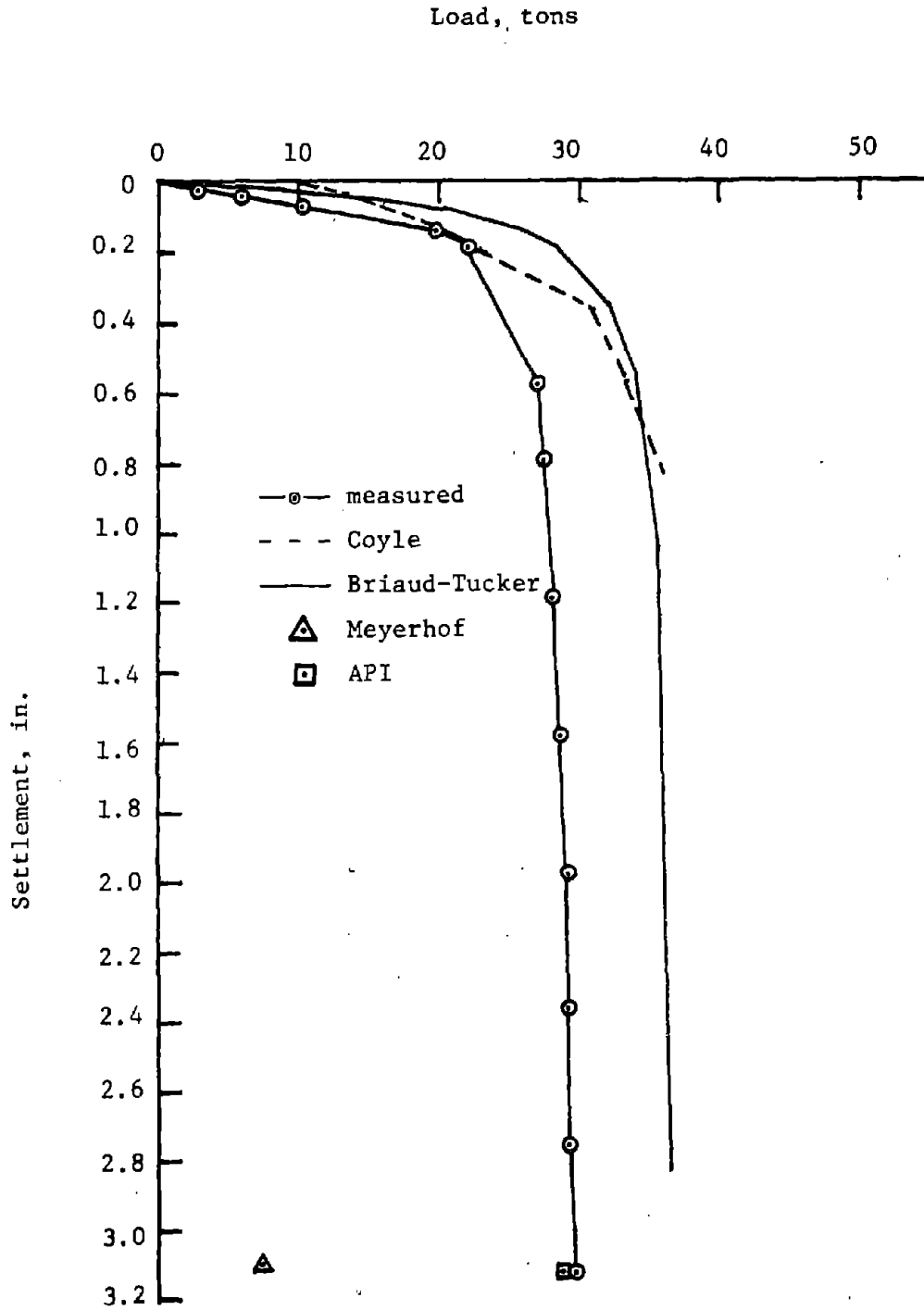


FIG. 71.- Gregersen Pile A: Load-Settlement Predictions by Coyle and Briaud-Tucker Methods (1 ton = 8.9 kN; 1 in. = 2.54 cm)

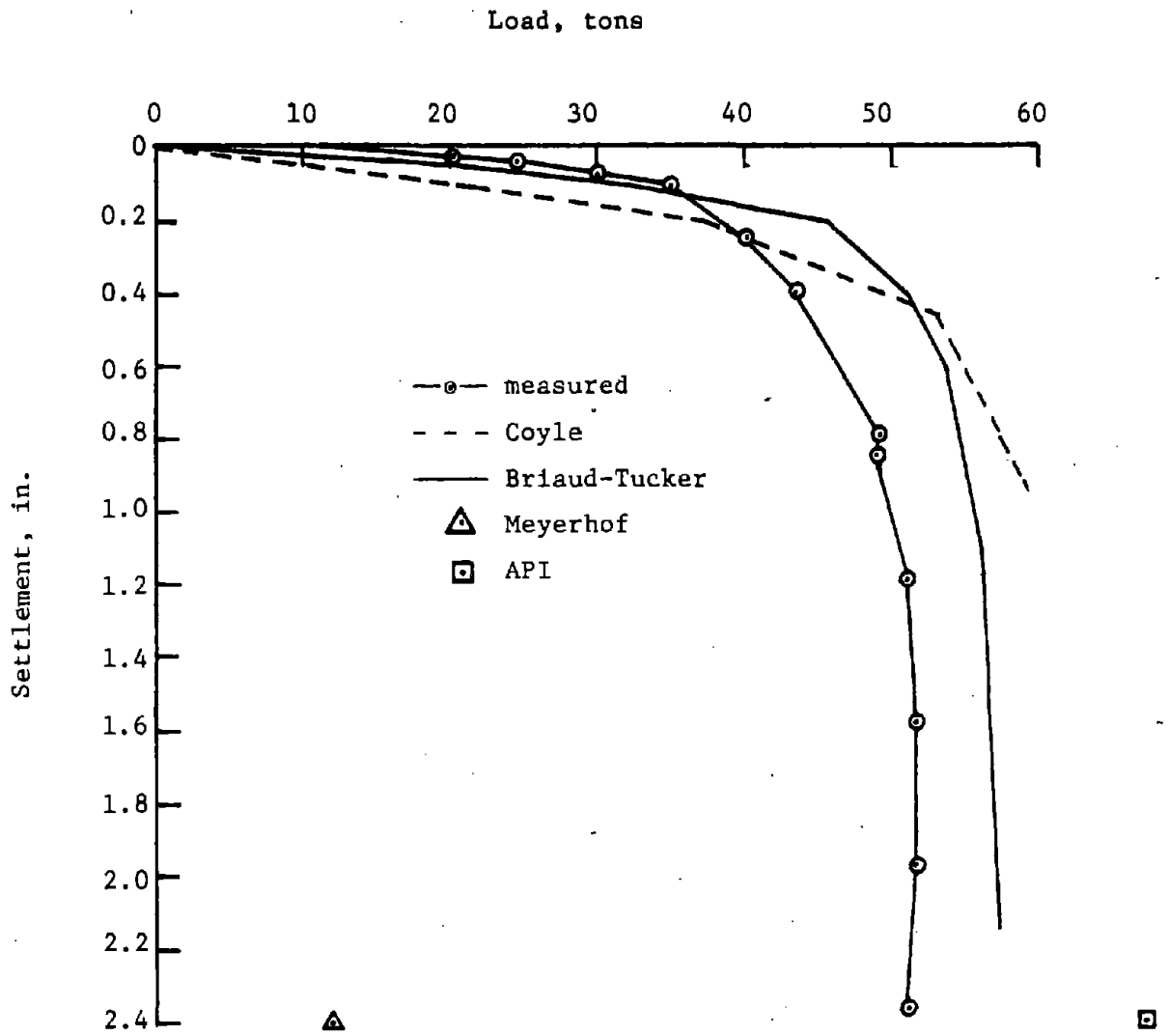


FIG. 72.- Gregersen Pile D/A = Load-Settlement Predictions by Coyle and Briaud-Tucker Methods (1 ton = 8.9 kN; 1 in. = 2.54 cm)

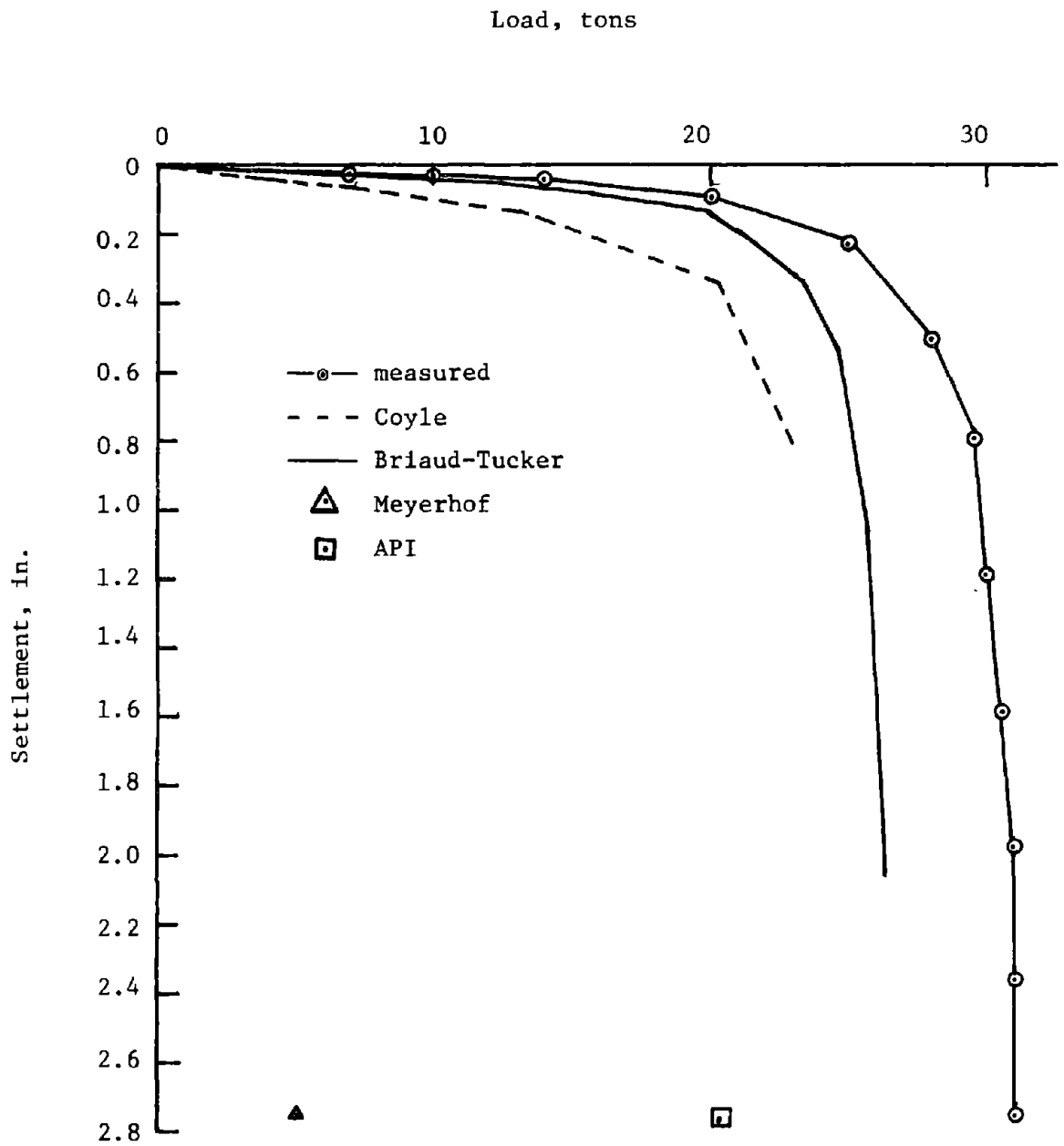


FIG. 73. - Gregersen Pile C: Load-Settlement Predictions by Coyle and Briaud-Tucker Methods (1 ton = 8.9 kN; 1 in. = 2.54 cm)

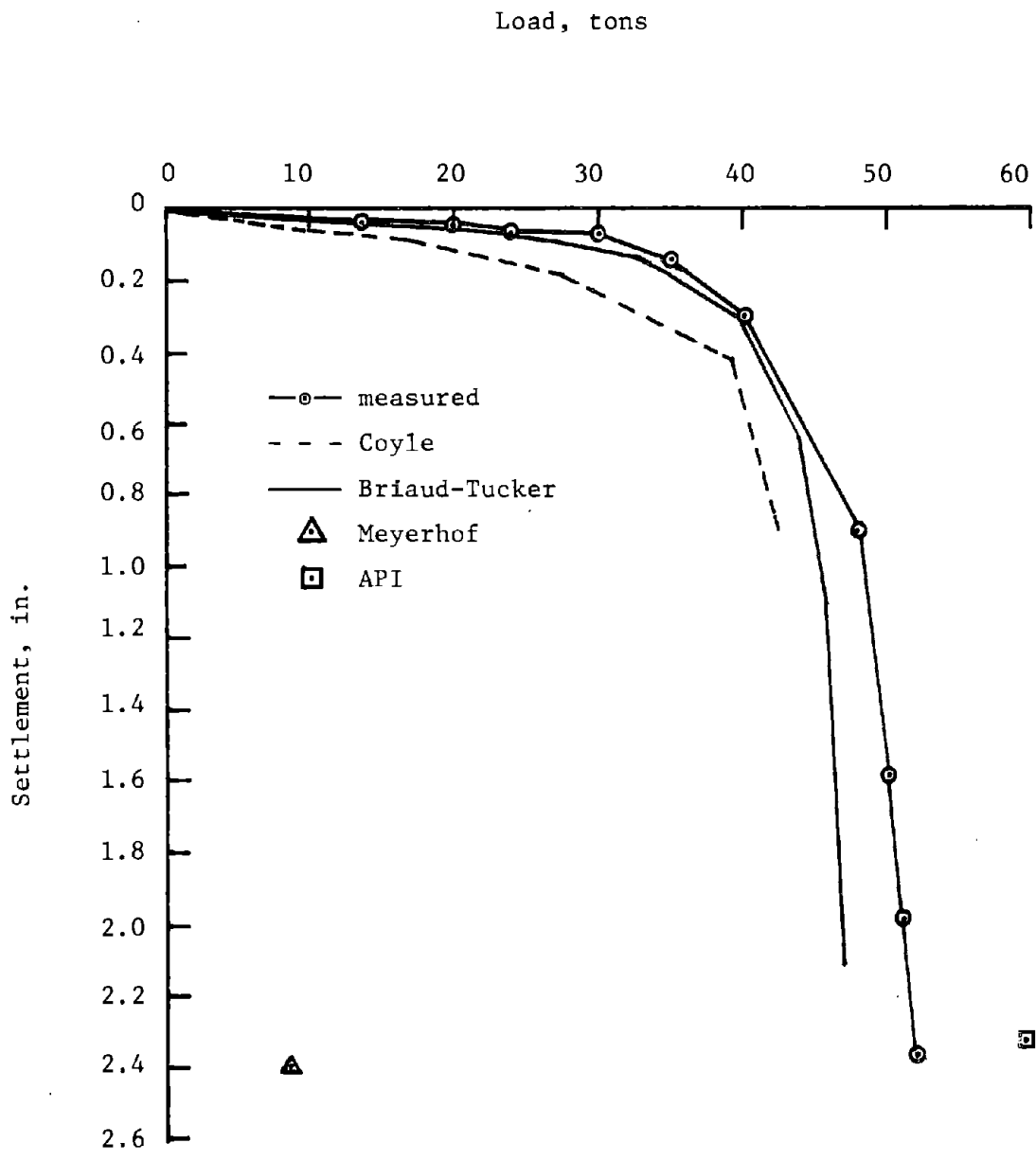


FIG. 74.- Gregersen Pile B/C: Load-Settlement Predictions by Coyle and Briaud-Tucker Methods (1 ton = 8.9 kN; 1 in. = 2.54 cm)

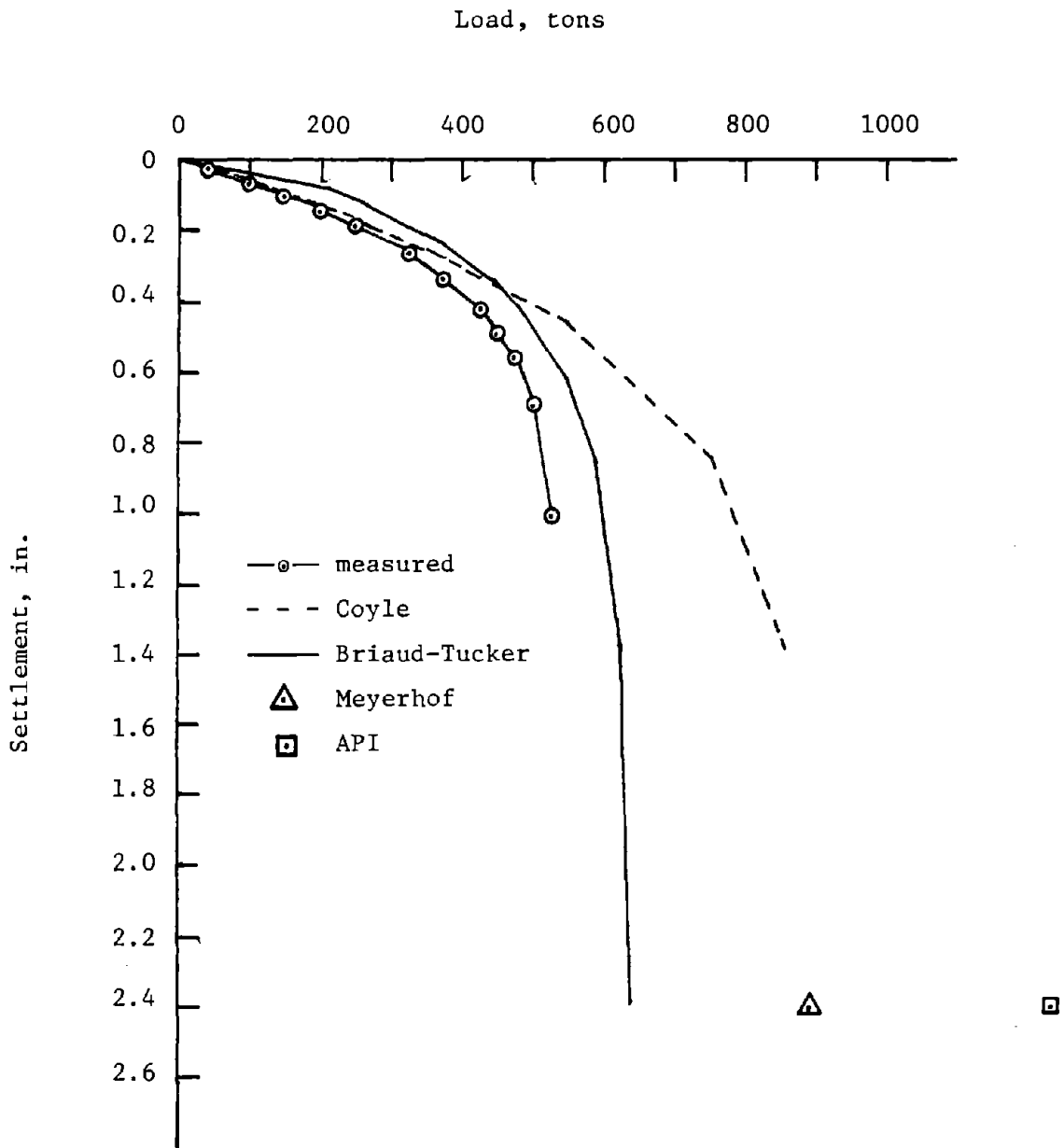


FIG. 75. - West Seattle Freeway Pile A:  
 Load-Settlement Predictions by  
 Coyle and Briaud-Tucker Methods  
 (1 ton = 8.9 kN; 1 in. = 2.54 cm)

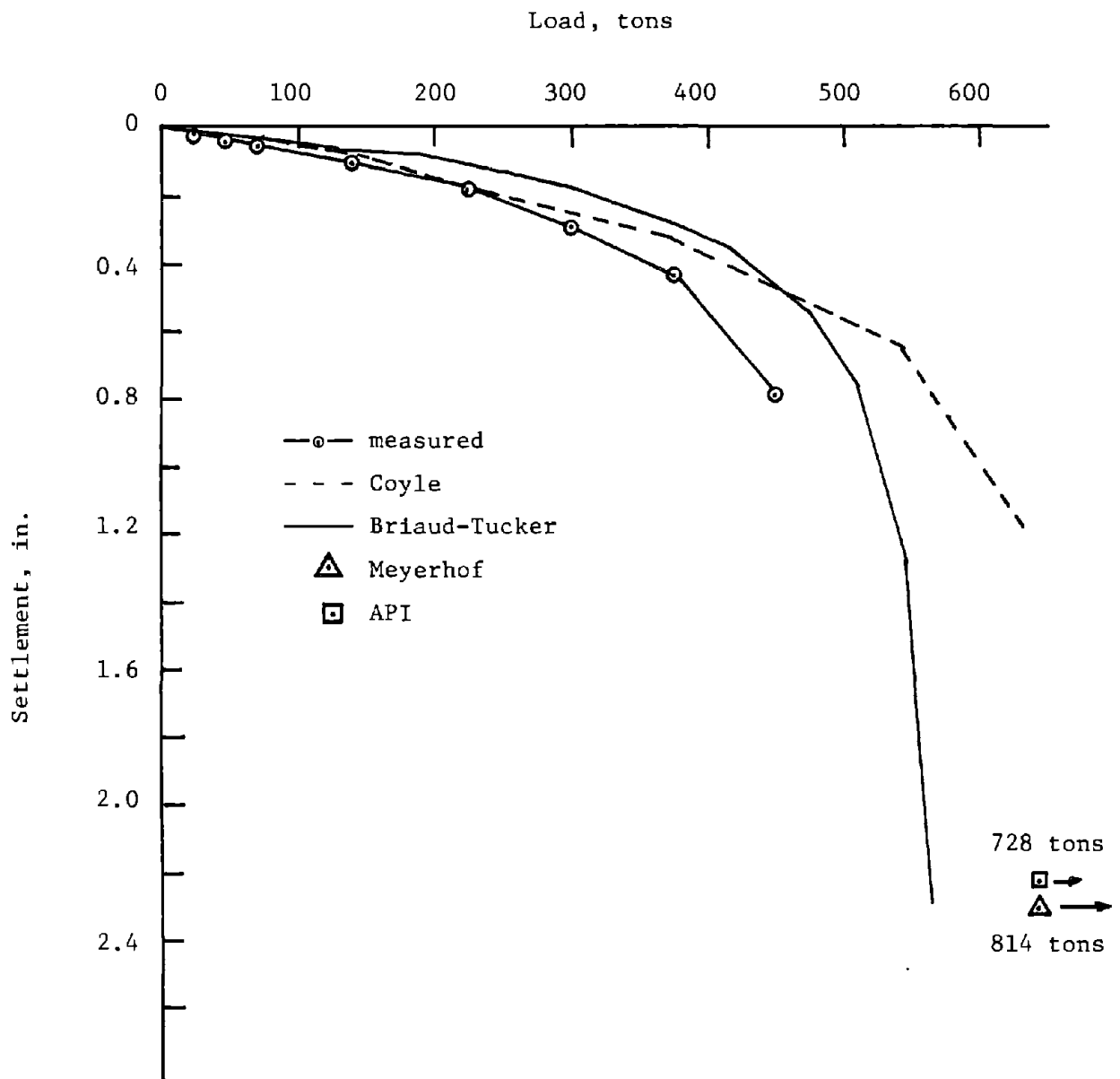


FIG. 76.- West Seattle Freeway Pile B:  
 Load-Settlement Predictions by  
 Coyle and Briaud-Tucker Methods  
 (1 ton = 8.9 kN; 1 in. = 2.54 cm)

CHAPTER X - PREDICTIONS BY THE CONE PENETROMETER  
AND PRESSUREMETER METHODS

PRESSUREMETER METHODS

Ultimate Capacity

The basic formula for estimating the ultimate vertical capacity of a pile,  $Q_{ult}$ , may be expressed by the sum of point resistance,  $Q_p$ , and skin resistance,  $Q_s$ , or

$$Q_{ult} = Q_p + Q_s = q_p A_p + f_s A_s \dots \dots \dots (46)$$

in which  $q_p$  = the unit bearing capacity of the pile point of area  $A_p$  and  $f_s$  = unit skin friction on the shaft of area  $A_s$ . No matter what type of test data is used, this relationship does not change.

The unit bearing capacity of the pile point,  $q_p$ , has been defined in terms of pressuremeter test results as:

$$q_p = k(p_{1e}^*) - q_{ov} \dots \dots \dots (47)$$

in which  $k$  = pressuremeter bearing capacity factor,  $p_{1e}^*$  = the equivalent net limit pressure near the pile point and  $q_{ov}$  = the total overburden pressure at the pile point. The equivalent net limit pressure  $p_{1e}^*$  is obtained using the relationship:

$$p_{1e}^* = \sqrt[n]{p_{11}^* \times p_{12}^* \dots p_{1n}^*} \dots \dots \dots (48)$$

where  $p_{11}^*$ ,  $\dots$ ,  $p_{1n}^*$  are the net limit pressures obtained from tests performed within  $\pm 1.5 D$  of the pile point where  $D$  is the diameter of the pile. The pressuremeter bearing capacity factor,  $k$ , is a function of the type of soil, the strength of the soil, and the shape and embedment depth of the pile. Three design methods were used to



determine  $k$  and  $f_s$ . These methods have been proposed by Menard (26), Baguelin, Jezequel and Shields (4), and Bustamante and Gianceselli (12). In the method proposed by Menard (26), Method A, the pressuremeter bearing capacity factor,  $k$ , used in predicting the axial capacity of piles can be obtained from Fig. 77 after first calculating the penetration depth to radius ratio of the pile  $h_e/R$ , and after determining the soil category near the pile point (Table 20). The penetration depth to radius ratio,  $h_e/R$  is obtained from:

$$\frac{h_e}{R} = \frac{1}{R} \sum_{i=1}^n \frac{\Delta z_i P_{li}^*}{p_{le}^*} \dots \dots \dots (49)$$

where  $R$  = pile radius,  $p_{li}^*$  = the net limit pressures obtained from tests between the ground surface and the tip of the pile and  $\Delta z_i$  = the thicknesses of the elementary layers corresponding to the pressuremeter tests. For the unit skin friction,  $f_s$ , Menard recommends using Fig. 78 which gives values of skin friction as a function of the limit pressure. For traditional bored or driven piles, curves A and B are to be used. Curve B is used within three diameters of the point because of increased skin friction in this region caused by loading the pile. For steel piles or piles with a permanent lining, Menard advises to reduce the values given by curves (A) and (B) by 20% in cohesive soils and by 30% in sands or submerged sands and gravels. Menard states that: since skin friction decreases as the pile diameter increases, the values given in Fig. 78 are applicable to a pile diameter of 24 in. (60 cm) and should be reduced by 10% for a diameter of 32 in. (80 cm) and by 30% for a diameter of 48 in.(120 cm).

The second design method, Method B, was proposed by Baguelin, Jezequel and Shields (4). The pressuremeter bearing capacity factor  $k$  is obtained from Figs 79a through 79d for bored piles and from Figs 80a through 80d for driven piles. Each graph, a through d, represents a different soil type and  $k$  can be found from these graphs once the net limit pressure and the penetration depth to width ratio are known. The unit side friction,  $f_s$ , is obtained from Fig. 81 for a given value of  $p_l$ . A distinction is made between relatively rough, porous

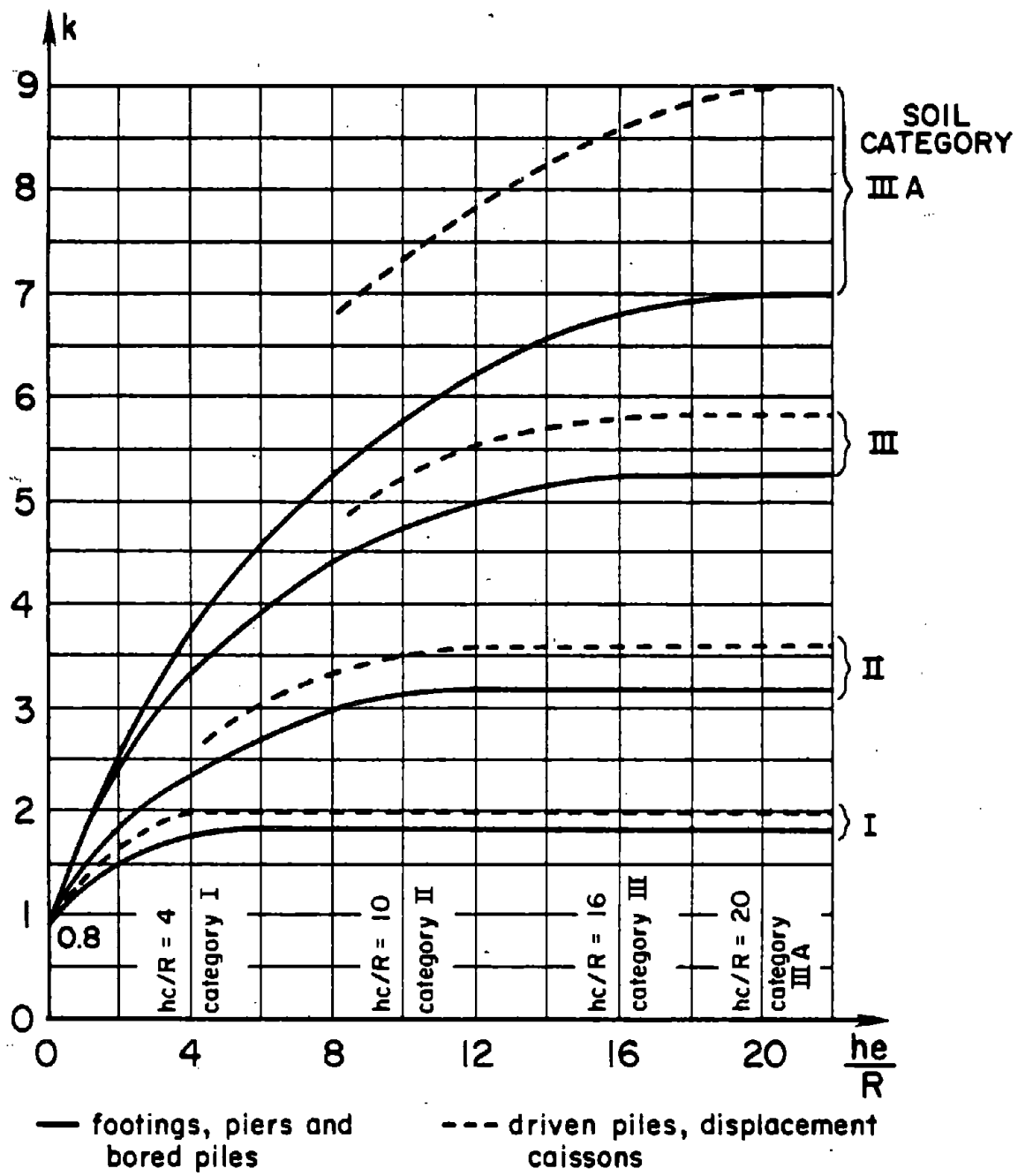


FIG. 77.- Bearing Capacity Factor Chart for Piles;  
for Use With Method A (from ref. 26)

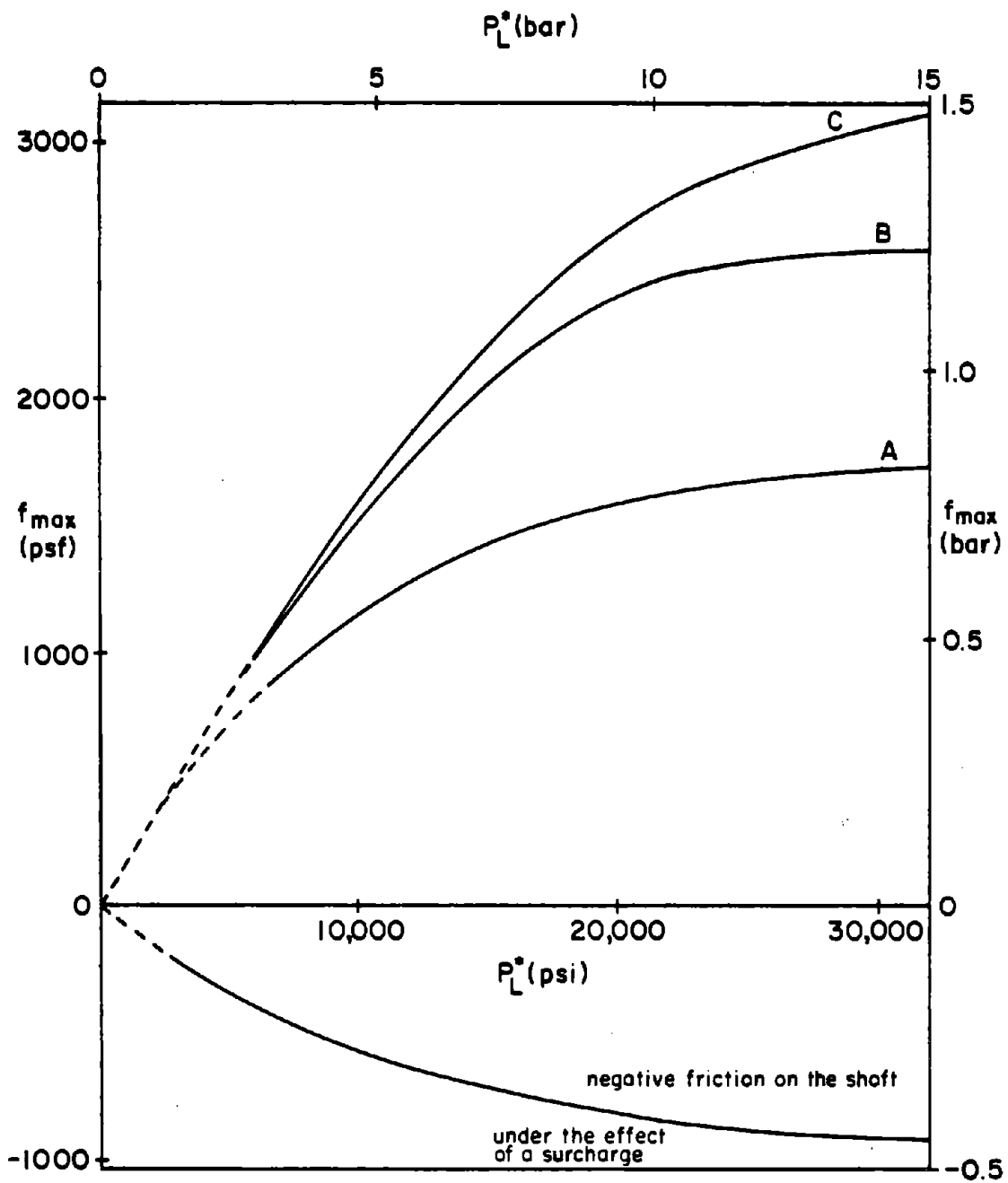
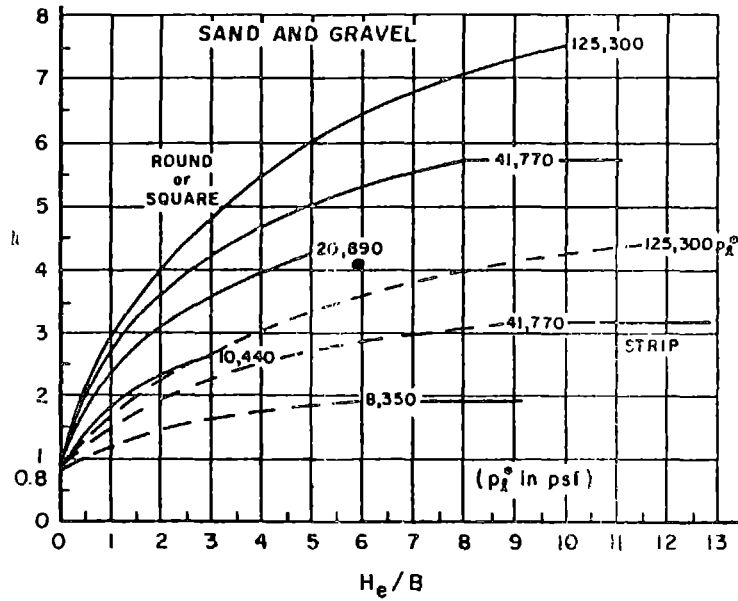


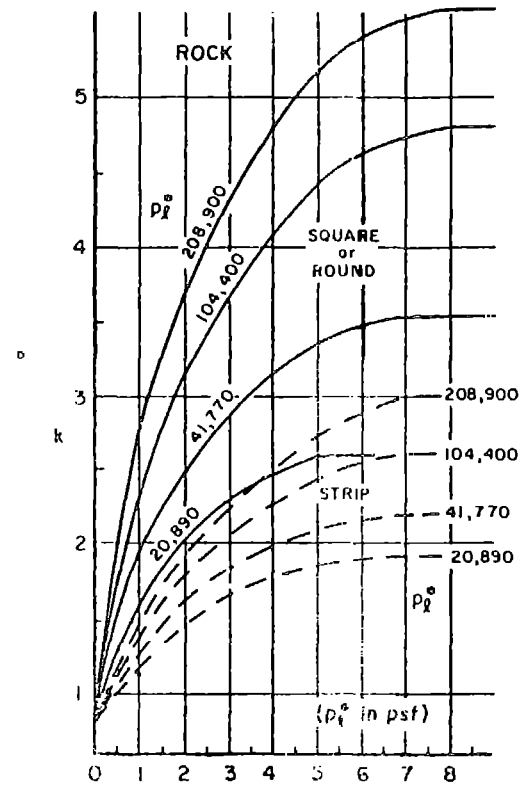
FIG. 78.- Skin Friction Design Chart for Use With Method A (from ref. 26)

TABLE 20.- Soil Categories - Menard Method

Ranges of Pressures Limit $p_L$	Nature of Soil	Soil Categories
0 - 25062 psf (0 - 12 bars)	Clay	Category I
0 - 14620 psf (0 - 7 bars)	Silt	
37593 - 83540 psf (18 - 40 bars)	Firm Clay or Marl	Category II
14620 - 62655 psf (12 - 30 bars)	Compact Silt	
8354 - 16708 psf (4 - 8 bars)	Compressible Sand	
20885 - 62655 psf (10 - 30 bars)	Soft or Weathered Rock	
20885 - 41770 psf (10 - 20 bars)	Sand and Gravel	Category III
83540 - 208850 psf (40 - 100 bars)	Rock	
62655 - 125310 psf (30 - 60 bars)	Very Compact Sand and Gravel	Category IIIA

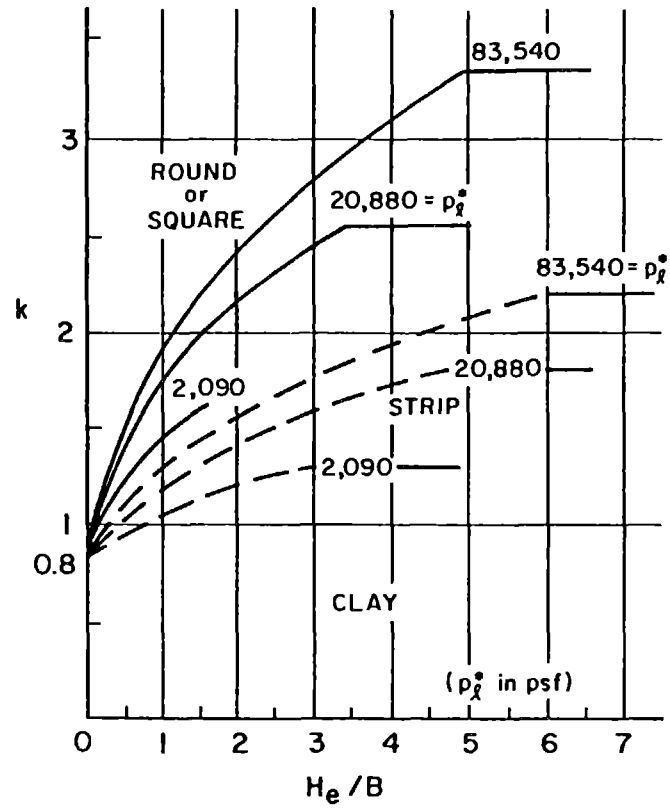


(a)

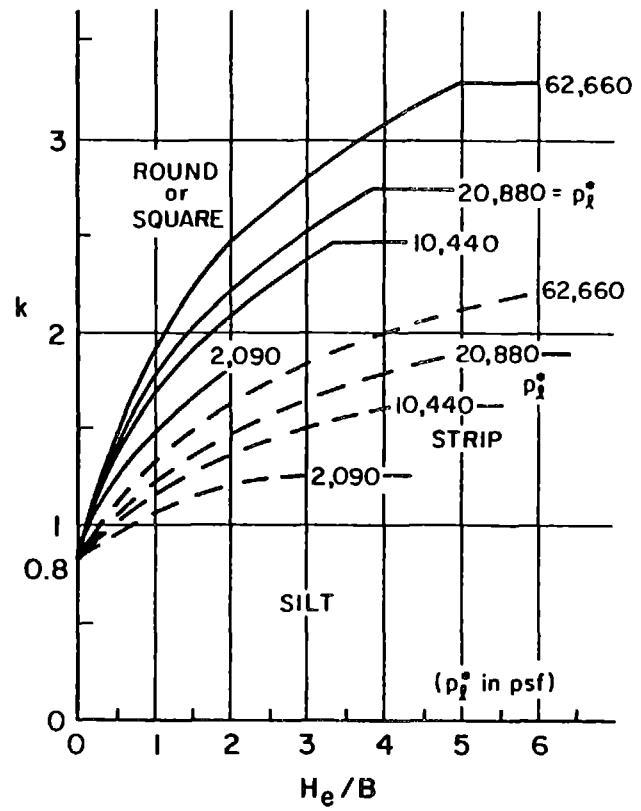


(b)

FIG. 79.- Bearing Capacity Factor Charts for Bored Piles; for Use With Method B (from ref. 4)

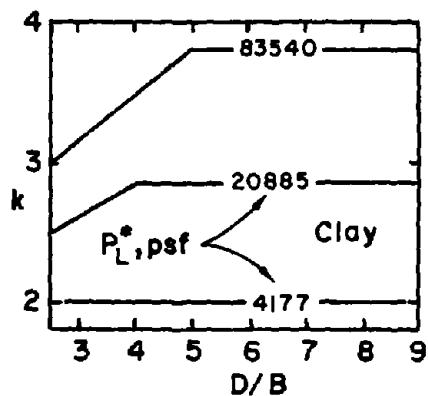


(c)

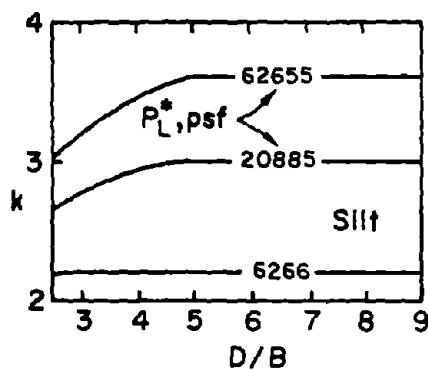


(d)

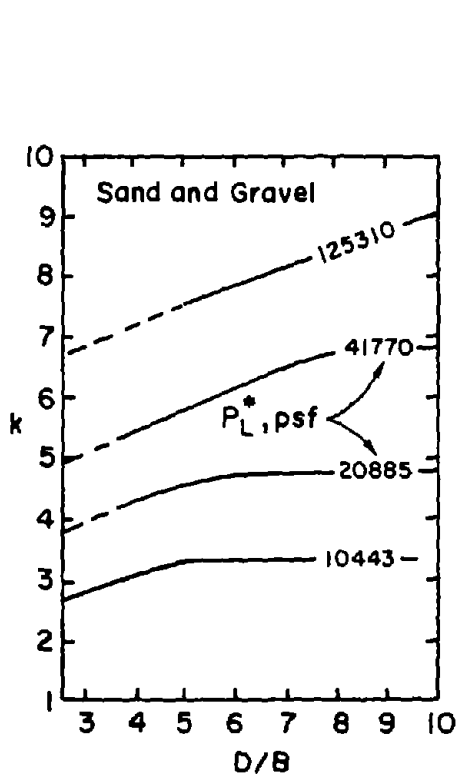
FIG. 79.- Continued



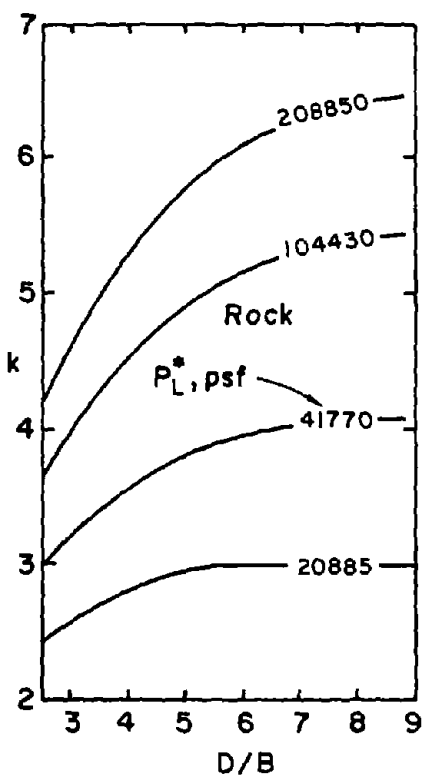
(a)



(b)

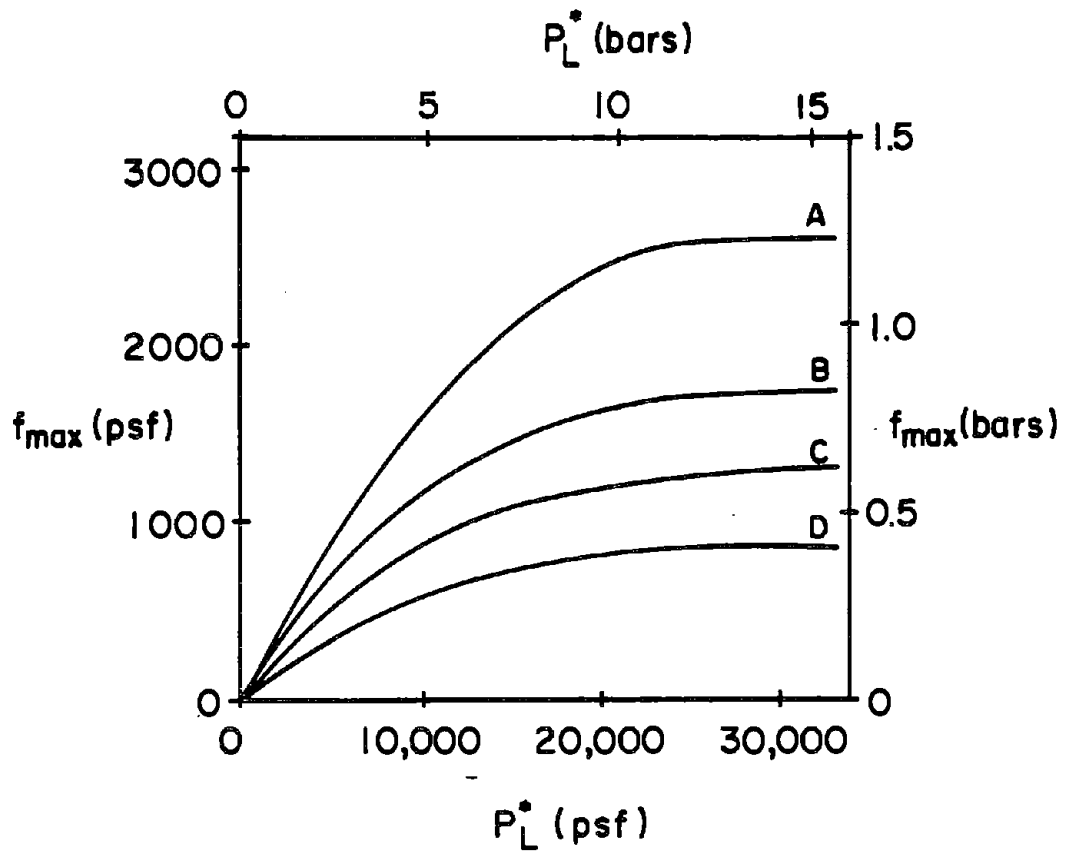


(c)



(d)

FIG. 80.- Bearing Capacity Charts for Driven Piles; for Use With Method B (from ref. 4)



- A - Displacement/Concrete/Granular
- B - No Displacement/Concrete/Any Soil or Displacement/Steel/Granular or Displacement/Concrete/Cohesive
- C - Displacement/Steel/Cohesive
- D - No Displacement/Steel/Any Soil

FIG. 81.- Skin Friction Design Chart for Use With Method B (from ref. 4)



pile material such as concrete or wood, and smooth, impervious material such as steel. Baguelin, Jezequel and Shields also make a distinction between displacement and non-displacement piles.

The third method, Method C, was proposed by Bustamante and Gianceselli (9). Like the method proposed by Menard (26), the soil is broken down into categories (Table 21) and the penetration depth to radius ratio  $h_e/R$  is used to obtain the pressuremeter bearing for capacity,  $k$  bored piles or driven piles (Fig. 82). The unit skin friction,  $f_s$  can be obtained from the appropriate curve shown in Fig. 83 (A, A<sub>bis</sub>, B, C, D, E, F) after determining the soil and foundation type from Table 22.

### Load-Settlement Curve

To predict the load-settlement curve at the top of the pile, the load transfer curves at the point and along the shaft of the pile,  $q-w$  and  $f-w$  respectively, are first obtained. The  $q-w$  curve represents the variation of the pressure exerted by the pile point on the soil,  $q$ , versus the movement of the pile point,  $w$ . Similarly, the  $f-w$  curve represents the variation of the friction developed between the soil and the pile,  $f$ , versus the movement of the pile shaft,  $w$ . Three methods exist to determine these curves using pressuremeter test results. These methods were proposed by Menard and Gambin (19), Baguelin, Frank and Jezequel (2) and Bustamante and Gianceselli/Frank and Zhao (9,16).

In the method proposed by Menard and Gambin (19) both the  $q-w$  and the  $f-w$  curves are represented by elastic-plastic models as can be seen in Fig. 84. The ultimate values of  $q$  and  $f$ , called  $q_{max}$  and  $f_{max}$  respectively, are found by using Menard's method for ultimate capacity which was described earlier. The slopes  $q/w$  and  $f/w$  of the elastic portion of the curves are given by:

$$\frac{q}{w} = \frac{2E_R}{\lambda R} \quad \text{for } R \leq 2.5 \text{ ft (0.76 m)} \quad \dots \dots \dots (50)$$

and 
$$\frac{f}{w} = \frac{E_o}{CR} \quad \text{for } R \leq 1.0 \text{ ft (0.3 m)} \quad \dots \dots \dots (51)$$

TABLE 21. Soil Categories - Bustamante and Ganeselli Method

Limit Pressure PL	Soil Type	Category
0 - 14620 psf (0 - 7 bars)	Soft Clay	
0 - 16708 psf (0 - 8 bars)	Silt and Soft Chalk	1
0 - 14620 psf (0 - 7 bars)	Loose Clayey, Silty or Muddy Sand	
20885 - 41770 psf (10 - 20 bars)	Medium Dense Sand and Gravel	
25062 - 62655 psf (12 - 30 bars)	Clay and Compact Silt	
31328 - 83540 psf (15 - 40 bars)	Marl and Limestone-Marl	
20885 - 52213 psf (10 - 25 bars)	Weathered Chalk	2
52213 - 83540 psf (25 - 40 bars)	Weathered Rock	
> 62655 psf (> 30 bars)	Fragmented Chalk	
> 93983 psf (> 45 bars)	Very Compact Marl	
> 52213 psf (> 25 bars)	Dense to Very Dense Sand and Gravel	3
> 93983 psf (> 45 bars)	Fragmented Rock	

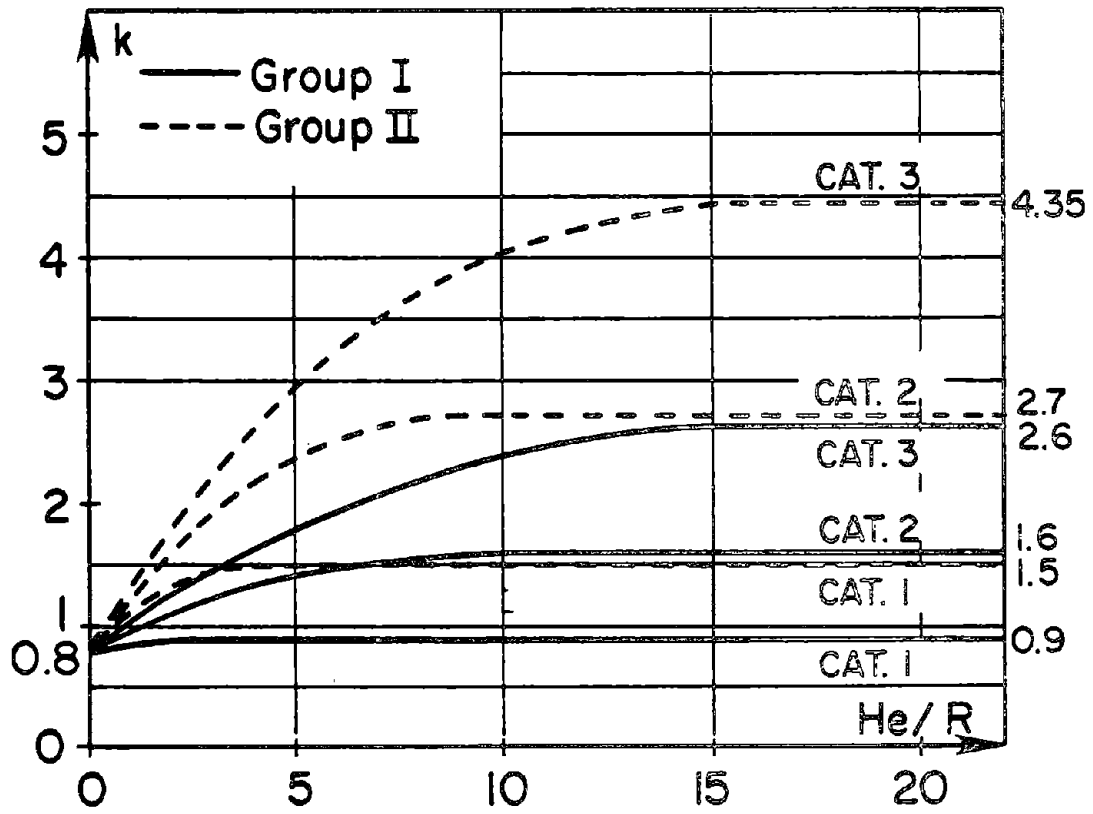


FIG. 82 .- Bearing Capacity Factor Chart for Use With Method C  
(from ref. 12)

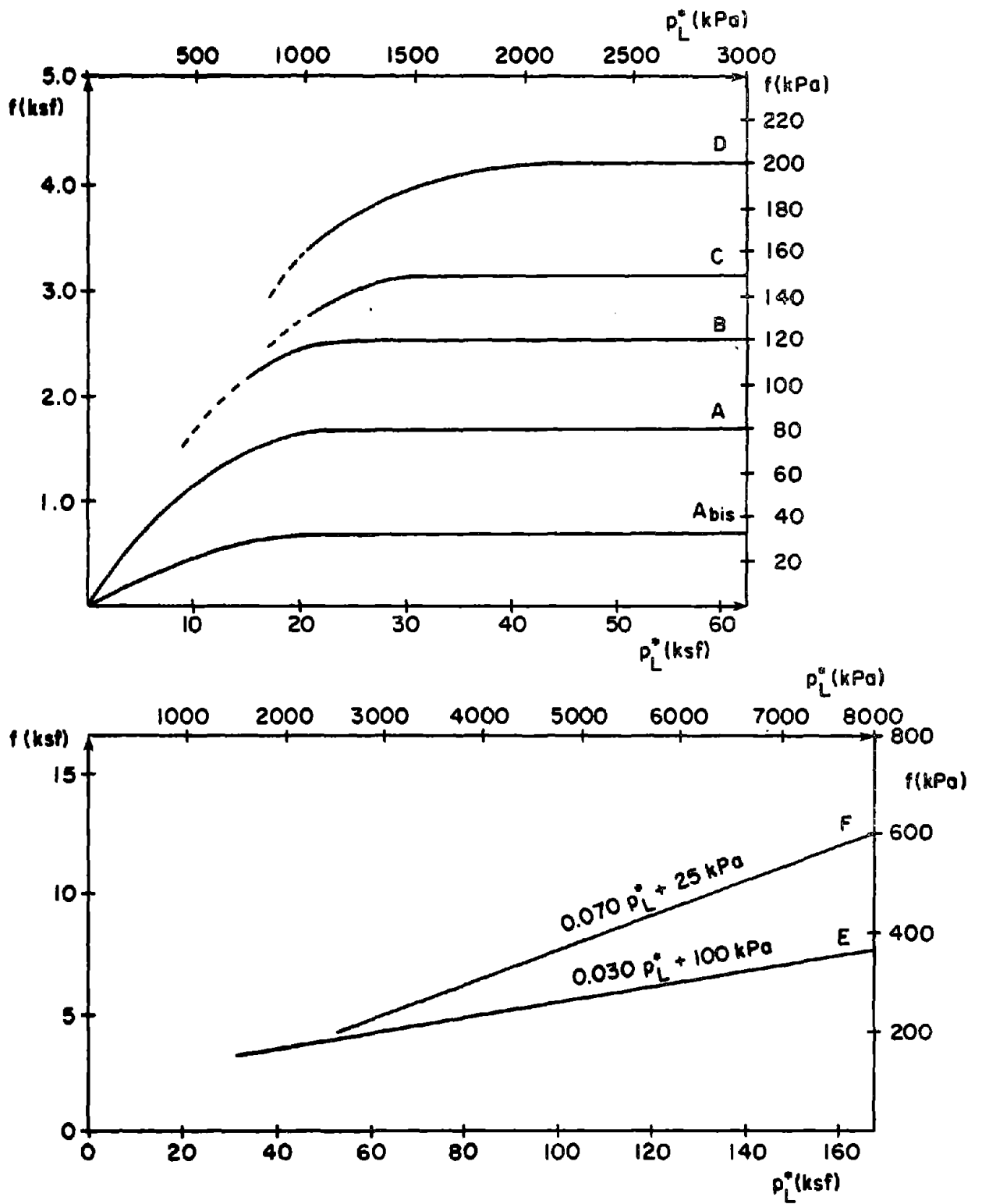


FIG. 83.- Skin Friction Design Chart For Use With Method C (from ref. 12)

TABLE 22.- Choosing the Skin Friction Design Curve for Bustamante and Gianselli Method

SOIL TYPE	LIMIT PRESSURE $P_L (10^5 \text{ Pa})$	INSTALLATION PROCEDURE AND PILE MATERIAL.						
		DRILLED	DRILLED WITH CASING		DRIVEN	INJECTED		
			CONCRETE	CONCRETE		STEEL	CONCRETE	STEEL
Clayey, Silty or Muddy Sand	< 7	A bis	A bis	A bis	A bis	A bis	A	-
Soft Chalk	< 7	A bis	A bis	A bis	A bis	A bis	A	-
Soft to Stiff Clay	$\leq 30$	(A) <sup>1</sup> A bis	(A) <sup>1</sup> A bis	A bis	(A) <sup>1</sup> A bis	A bis	A	D <sup>2</sup>
Silt and Compact Silt	$\leq 30$	(A) <sup>1</sup> A bis	(A) <sup>1</sup> A bis	A bis	(A) <sup>1</sup> A bis	A bis	A	D <sup>2</sup>
Medium Dense Sand and Gravel	10 to 20	(B) <sup>1</sup> A	(A) <sup>1</sup> A bis	A bis	(A) <sup>1</sup> A	A	B	$\geq D$
Dense to Very Dense Sand and Gravel	> 25	(C) <sup>1</sup> B	(B) <sup>1</sup> A	A	(C) <sup>1</sup> B	B	B	$\geq D$
Weathered to Fragmented Chalk	> 10	(C) <sup>1</sup> B	(B) <sup>1</sup> A	A	(C) <sup>1</sup> B	B	C	$\geq D$
Marl and Limestone Marl	15 to 40	(E) <sup>1</sup> C	(C) <sup>1</sup> B	B	E <sup>3</sup>	E <sup>3</sup>	E	F
Very Compact Marl	> 45	E	-	-	-	-	F	> F
Weathered Rock	25 to 40	F	F	-	F <sup>3</sup>	F <sup>3</sup>	$\geq F$	> F
Fragmented Rock	> 45	F	-	-	-	-	$\geq$	> F

1. Use the letter in bracket for a careful execution of the drilled shaft with a low disturbance drilling technique or for a soil which will set up or densify around the driven pile.
2. For soils with  $P_L \geq 15 \times 10^5 \text{ Pa}$ .
3. Only if driving is possible.

### Method A (Menard Gambin)

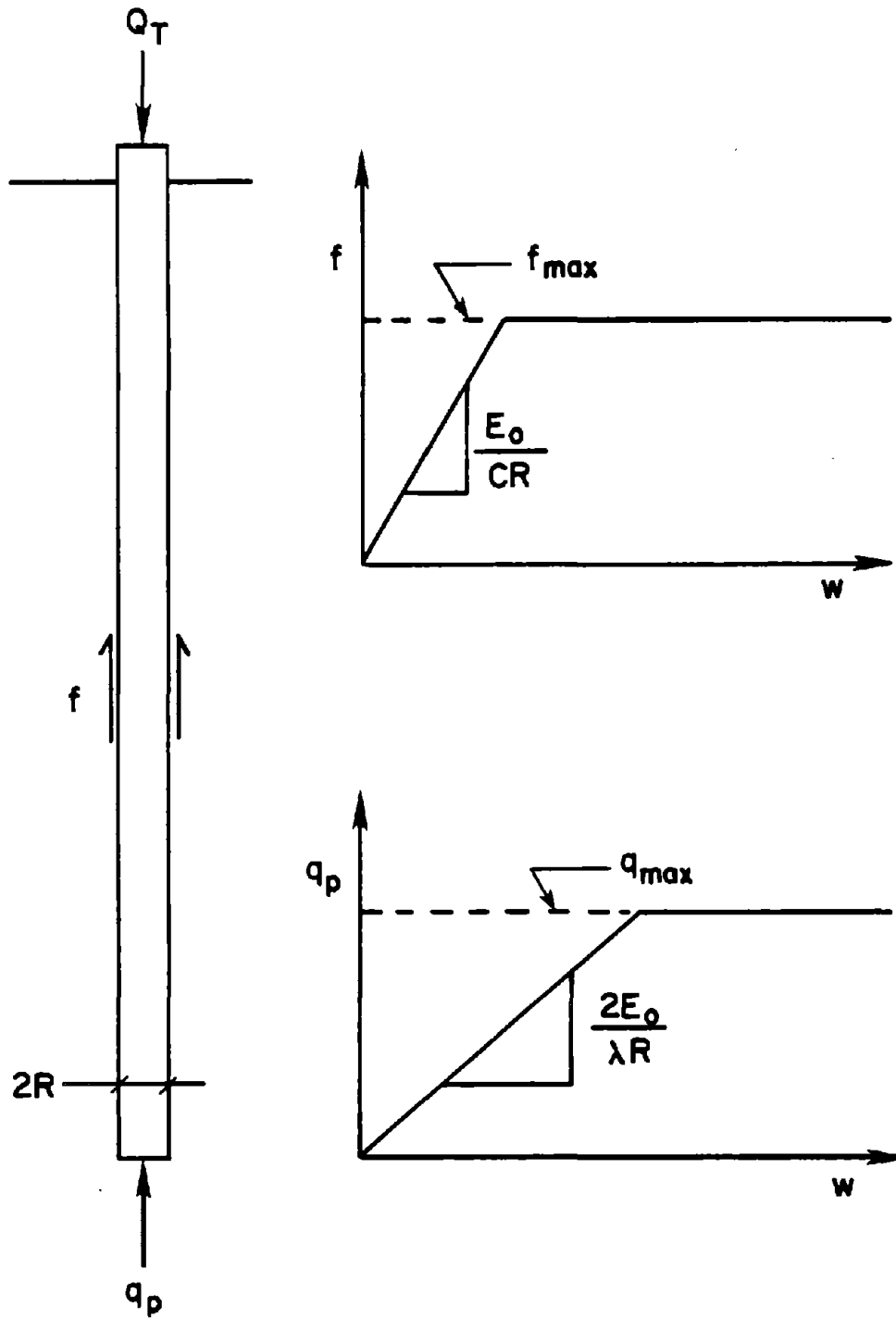


FIG. 84.-  $q$ - $w$  and  $f$ - $w$  Curves For Use With Method A.

or 
$$\frac{f}{w} = \frac{E_o}{CR_o \left(\frac{R}{R_o}\right)^\alpha} \quad \text{for } R > 1.0 \text{ ft (0.3m) . . . . . (52)}$$

where  $E_R$  = pressuremeter reload modulus as defined in Reference 10.

$R$  = pile radius,

$E_o$  = pressuremeter first load modulus as defined in Reference 10.

$R_o$  = 1.0 with  $R$  in ft or 0.30 with  $R$  in meters  
= coefficient given in Table 23

$C$  = coefficient of friction mobilization (Table 24)

$\lambda$  = a shape factor

= 1.00 for circular cross-sections

1.12 for square cross-sections

1.53 for length/width = 2

2.65 for length/width = 10

Baguelin, Frank and Jezequel (1) developed a procedure for determining load transfer curves using results from a selfboring pressuremeter. This procedure was used to predict the load transfer curves of piles using preboring pressuremeter test results instead of selfboring pressuremeter test results. For this reason this method is called pseudo Baguelin, Frank and Jezequel method. The referenced procedure (2) calls for the use of the small strain selfboring pressuremeter modulus. Because the reload preboring pressuremeter modulus  $E_R$  correlates favorably with that selfboring pressuremeter modulus,  $E_R$  was used in the calculations. The  $q$ - $w$  and  $f$ - $w$  curves using the pseudo Baguelin, Frank and Jezequel method are shown on Fig. 85. The ultimate values of  $q$  and  $f$  are obtained using the ultimate capacity method proposed by Baguelin, Jezequel and Shields (4) method. This method was presented earlier. The slopes of the elastic portion of the model are given by

$$\frac{q}{w} = \frac{2E_R}{\pi(1-\nu^2)R} \dots \dots \dots (53)$$

$$\frac{f}{w} = \frac{E_R}{2(1+\nu)(1+\ln(\frac{L}{2R}))R} \dots \dots \dots (54)$$

TABLE 23.- Values of the Parameter  $\alpha$

Soil Type	Peat		Clay		Silt		Sand		Sand and Gravel	
	$E_m/p_1^*$	$\alpha$	$E_m/p_1^*$	$\alpha$	$E_m/p_1^*$	$\alpha$	$E_m/p_1^*$	$\alpha$	$E_m/p_1^*$	$\alpha$
<b>Over-consolidated</b>			>16	1	>14	2/3	>12	1/2	>10	1/3
<b>Normally consolidated</b>		1	9-16	2/3	8-14	1/2	7-12	1/3	6-10	1/4
<b>Weathered and/or remoulded</b>			7-9	1/2		1/2		1/3		1/4
<b>Rock</b>	Extremely fractured			Other			Slightly fractured or extremely weathered			
	$\alpha = 1/3$			$\alpha = 1/2$			$\alpha = 2/3$			

TABLE 24.- Coefficient of Friction Mobilization C - Gambin Method

Type of Pile	Friction Pile		End Bearing Pile
	h/R = 10	h/R = 20	
Drilled Pile	4.5 - 5.0	5.2 - 5.6	2.8 - 3.2
Driven Pile	1.8 - 2.0	2.1 - 2.3	1.1 - 1.3



Method B (Pseudo-Baguelin)

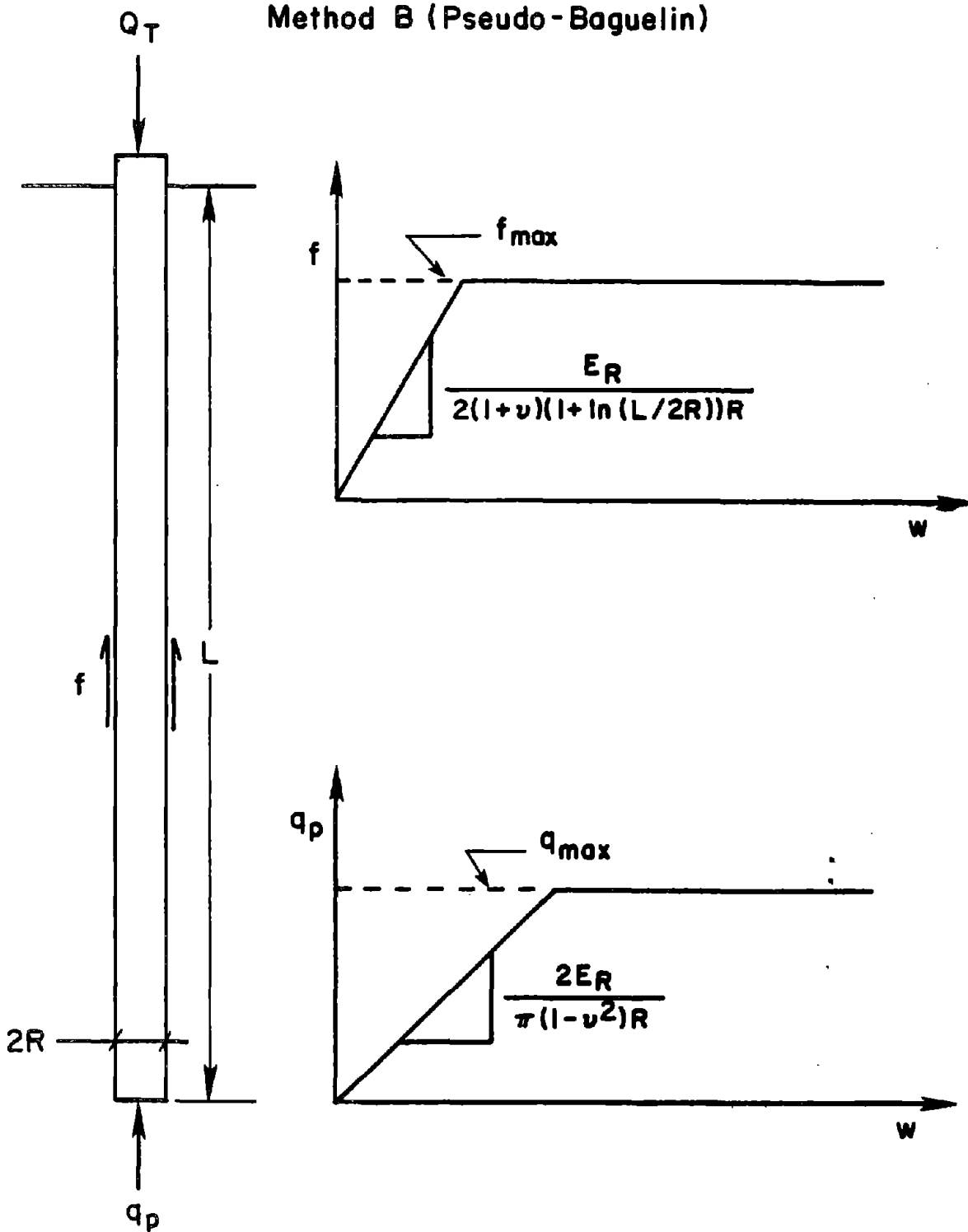


FIG. 85.- q-w and f-w Curves for Use With Method B.

where  $E_R$  is the pressuremeter reload modulus,  $\nu$  is Poisson's ratio,  $R$  is the pile radius and  $L$  is the pile length.

The third method used to predict load transfer curves of piles using pressuremeter test results was developed by Frank and Zhao (16). These curves, as shown in Fig. 86, are bilinear elastic-plastic models. The ultimate values of  $q$  and  $f$  are obtained by using Bustamante and Gianceselli's ultimate capacity method as previously described. The first slope in the elastic range of the models is given by:

$$\frac{q}{w} = \frac{5.5E_o}{R} \dots \dots \dots (55)$$

$$\frac{f}{w} = \frac{\alpha E_o}{R} \dots \dots \dots (56)$$

where  $E_o$  is the initial pressuremeter modulus,  $R$  is the pile radius and  $\alpha$  is a coefficient equal to 0.76  $R$  (with  $R$  in feet) or 2.5  $R$  (with  $R$  in meters). The second slope in the elastic range is 5 times softer than the first slope and the change in slope occurs at one half the value of  $q_{max}$  or  $f_{max}$ .

CONE PENETROMETER METHODS

Ultimate Capacity

Four methods were used to calculate the ultimate unit bearing capacity,  $q_p$ , and unit skin friction,  $f_s$ , using cone penetrometer test results. These are the methods proposed by DeRuiter and Beringen (15), Bustamante and Gianceselli (8), Schmertmann (31) and a method which makes direct use of the cone penetrometer results.

The first method was proposed by DeRuiter and Beringen (15). They found, based on load test-CPT correlations, that the pile end bearing is governed by the cone point resistant  $q_c$  over a zone extending from 0.7 to 4 pile diameters below the pile tip and up to 8 pile diameters

### Method C (Frank Bustamante)

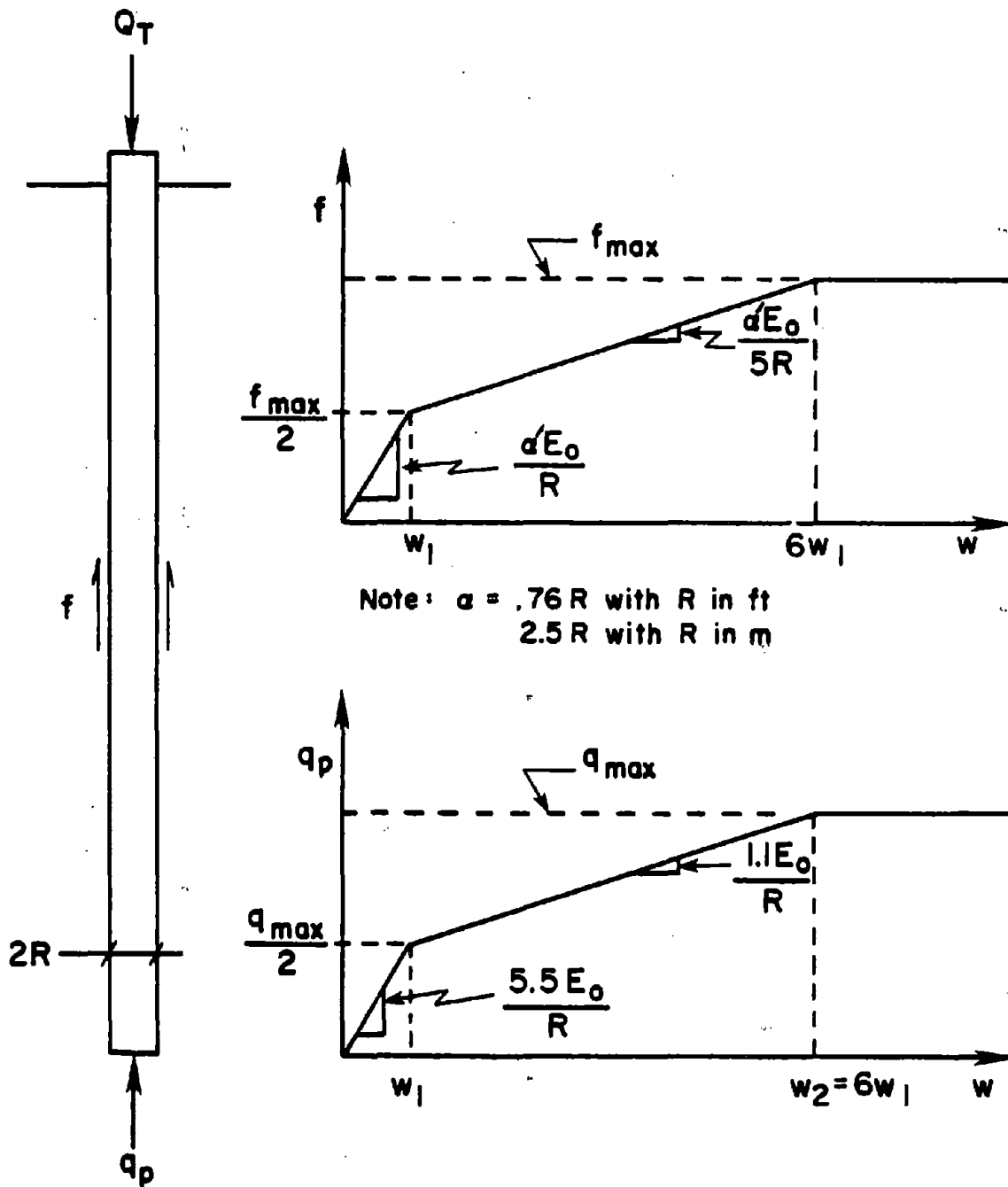


FIG. 86 -- q-w and f-w Curves for Use With Method C.

above the pile tip. Fig. 87 illustrates these zones and shows the formula to obtain the ultimate unit bearing capacity ( $q_p$ ). For overconsolidated cohesionless soils, a limit value for  $q_p$  is imposed (Fig. 88) to account for a reduction in strength during the driving of the pile. The unit skin friction,  $f_s$ , according to DeRuiter and Beringen is the minimum of

- 1) 1.25 tsf
- 2) average CPT sleeve friction
- 3)  $q_c$  (average)/300 (compression) or  $q_c$  (average)/400 (tension).

Bustamante and Gianeselli (15) proposed a method by which the ultimate unit bearing capacity,  $q_p$  is obtained from the relationship:

$$q_p = k_c q_c \text{ (near the point) } \dots \dots \dots (57)$$

and the ultimate unit skin friction from the relationship:

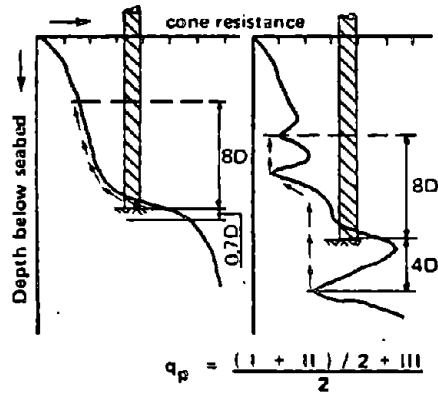
$$f_s = \frac{q_{c(\text{average})}}{\alpha} \leq f_{\text{max}} \dots \dots \dots (58)$$

The coefficients,  $k_c$ ,  $\alpha$  and  $f_{\text{max}}$  are obtained from Table 25. They are a function of the soil type, pile type and the method of installation of the pile.

Schmertmann (31) suggests using the value of  $q_p$  obtained from DeRuiter and Beringen (15) for piles in sand and in clay. For side frictional resistance however, he suggests using the following relationship:

$$Q_s = k \left[ \sum_{d=0}^{8B} \frac{d}{8B} f_s A_s + \sum_{d=8B}^L f_s A_s \dots \dots \dots (59) \right]$$

- where  $Q_s$  = total ultimate side friction resistance  
 $k$  = ratio of unit pile friction to CPT sleeve friction  
 (see Fig. 89)  
 $d$  = depth to the middle of the depth interval being considered  
 $B$  = pile width or diameter



**Key**

- D** : Diameter of the pile
- I** : Average cone resistance below the tip of the pile over a depth which may vary between 0.7D and 4D
- II** : Minimum cone resistance recorded below the pile tip over the same depth of 0.7D to 4D
- III** : Average of the envelope of minimum cone resistances recorded above the pile tip over a height which may vary between 6D and 8D. In determining this envelope, values above the minimum value selected under II are to be disregarded
- q<sub>p</sub>** : Ultimate unit point resistance of the pile

FIG. 87.- Point Bearing of Pile in Sand  
(from ref. 20)

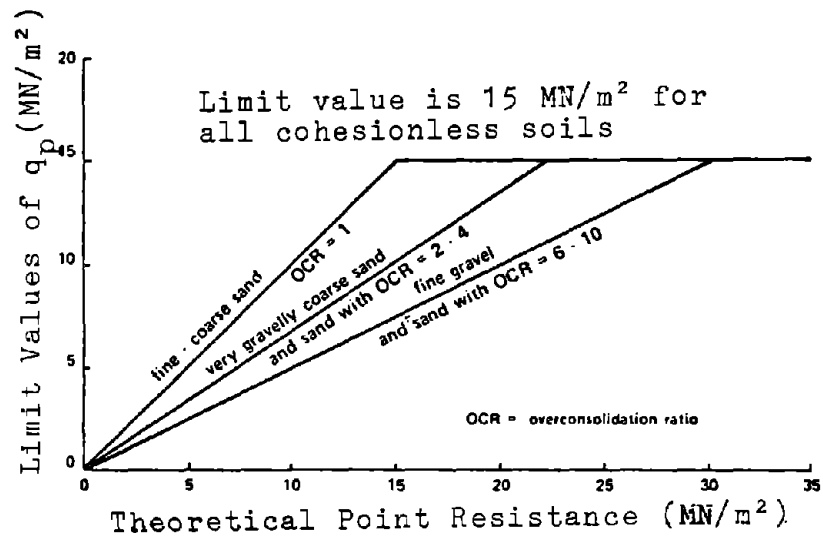


FIG. 88.- Limit Values for Point Bearing of Piles in Sand (from ref. 20)

TABLE 25.- CPT/Pile Capacity Factor - Bustamante and Gianeselli Method

Soil Type	$q_p$ ( $10^2$ kPa)	Bearing Factor $k_c$		Coefficient				Maximum Value of $f_s$ (kPa '1)					
		Bored Pile	Driven Pile	Bored Pile		Driven Pile		Bored Pile		Driven Pile		Injected Low Pressure	Pile High Pressure
				w/o Casing	with Casing	Concrete	Steel	w/o Casing	with Casing	Concrete	Steel		
Mud and Soft Clay	< 10	0.4	0.5	30	30	30	30	15	15	15	34	35	-
Medium Stiff Clay	10-50	0.35	0.35	40	80	40	80	(80) 35	(80) 35	(80) 35	35	80	$\geq$ 120
Loose Sand and Silt	$\leq$ 50	0.4	0.5	60	150	60	120	35	35	35	35	80	-
Stiff to Hard Clay & Silt	> 50	0.45	0.55	60	120	60	120	(80) 35	(80) 35	(80) 35	35	80	$\geq$ 200
Soft Chalk	$\leq$ 50	0.2	0.3	100	120	100	120	35	35	35	35	80	-
Medium Dense Sand and Gravel	50-120	0.4	0.5	100	200	100	200	(120) 80	(80) 35	(120) 80	80	120	$\geq$ 200
Weathered and Fissured Chalk	> 50	0.2	0.4	60	80	60	80	(150) 120	(120) 80	(150) 120	120	150	$\geq$ 200
Dense to very Dense Sand and Gravel	> 120	0.3	0.4	150	300	150	200	(150) 120	(120) 80	(150) 120	120	150	$\geq$ 200

- (1) The numbers between parentheses can be used if the method of pile installation is particularly favorable to pile capacity: careful drilling and low disturbance for bored piles, densification of the soil around the pile for driven piles.

$$q_p (\text{pile}) = k_c q_p (\text{CPT}); \quad f_R (\text{pile}) = \frac{q_p (\text{CPT})}{\alpha}$$

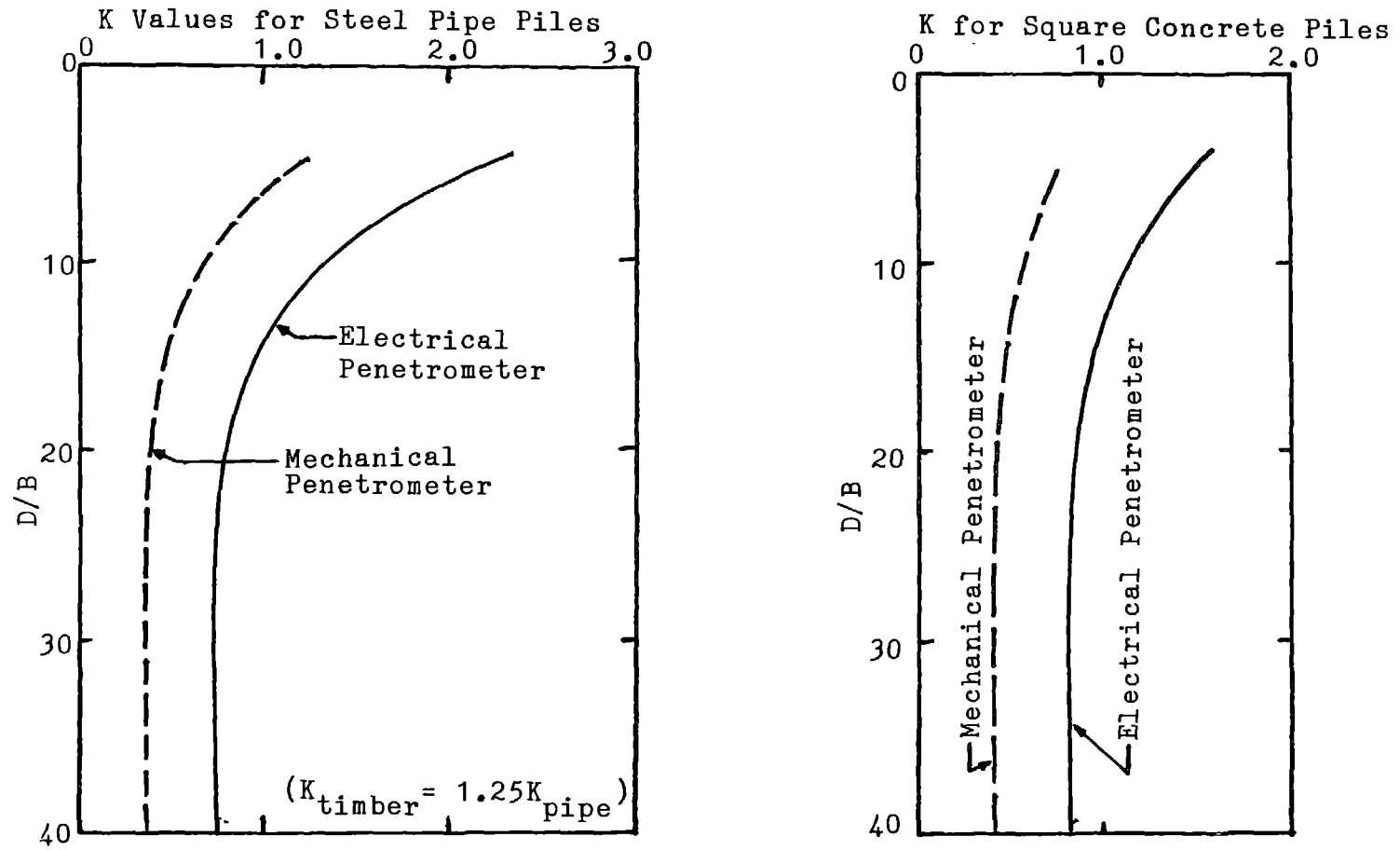


FIG. 89.- Penetrometer Design Curves for Pile Side Friction in Sand  
(from ref. 31)



$f_s$  = unit CPT sleeve friction resistance for depth interval considered.

$A_s$  = pile shaft area for depth interval considered.

When  $f_s$  does not vary significantly with depth, this can be simplified to:

$$Q_s = k \left[ 1/2 (f_s A_s)_{0-8B} + (f_s A_s)_{8B-L} \right] \dots \dots \dots (60)$$

where no  $f_s$  data are available Schmertmann suggests

$$Q_s = 0.10\mu \quad q_c \quad A_s \quad \text{for electrical penetrometer results.}$$

or  $Q_s = 0.067\mu \quad q_c \quad A_s$  for mechanical penetrometer results.

where  $q_c$  = average cone resistance and

$\mu$  = Bjerrums field vane shear strength correction factor obtained from Fig. 90.

The CPT method consisted of the average cone point resistance,  $q_c$ , within the depth of influence of the pile point as the unit bearing capacity,  $q_p$ , and of using the average sleeve friction from the cone penetrometer test as the unit skin friction for the pile  $f_s$ .

Load-Settlement Curve

Verbrugge (38) proposed an elastic plastic model for the q-w and f-w curves. The slope of the elastic portion is given by:

$$q/w = \frac{3.125E}{D} \dots \dots \dots (61)$$

$$f/w = \frac{0.22E}{D} \dots \dots \dots (62)$$

where  $D$  = diameter of a circular pile or 1.2 x width for a square pile,

$E = 36 + 2.2 \quad q_c$  (tsf) for bored piles,

and  $E = 108 + 6.6 \quad q_c$  (tsf) for driven piles

The maximum value of  $f$  in cohesionless soils can be obtained by one of the following relationships:

$$(s_u)_{\text{field}} = \mu (s_u)_{\text{vane}}$$

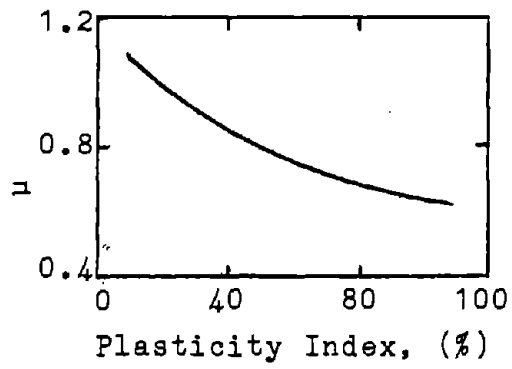


FIG. 90.- Bjerrum's Field Vane Shear Strength Correction Curve (from ref. 5)

$f_{\max} = 0.011 q_c$  Driven concrete piles

$f_{\max} = 0.009 q_c$  Driven steel piles

$f_{\max} = 0.005 q_c$  Drilled concrete piles

$f_{\max} = 0.003 q_c$  Drilled steel piles

where  $f_{\max} \leq 0.8$  tsf for Drilled piles and

$f_{\max} \leq 1.2$  tsf for Driven piles.

Verbrugge does not make any recommendation for  $q_{\max}$  for the pile.

Here,  $q_{\max}$  was obtained by using Bustamante and Gianeselli's method (8).

#### COMPARISON OF RESULTS

Pressuremeter test results were available at two sites and cone penetrometer test results were obtained at five sites. One site, Lock and Dam 26 Ellis Island Site, had both pressuremeter and cone penetrometer test results. Predictions of pile capacity were performed using the methods presented previously. The results of the ultimate load predictions are summarized in Table 26. The load-settlement predictions are presented in Figs. 91 through 104. The results of those methods which predict only ultimate load are shown as single points on the load-settlement plots.

In general, the predictions agree well with the measured results. The predictions using the cone penetrometer methods were compared to the ultimate load given by the asymptotic values of the hyperbolic regression presented in Chapter IV. The ratios of the predicted loads over the measured loads were computed and the mean, standard deviation and coefficient of variation of these values for each method are given in Table 27. Overall, the Bustamante and Gianeselli method and the Verbrugge method gave the best results. The mean of the ratios of predicted over-measured total loads was 1.06 and 0.94 for these methods respectively. These methods also predicted the distribution of the load between point bearing and side friction very well. The other three methods predicted total loads reasonably well but overpredicted the point load by 100% to 200%, and underpredicted the friction load.

TABLE 26.- Pile Capacity Predictions by CPT and PMT Methods  
(1 ton = 8.9 kN)

SITE	PILE	Cone Penetrometer Methods												Pressuremeter Methods											
		DeRuiter-Beringen			Bustamante-Gianeselli			Schmertmann			Cone			Verbrugge		Menard-Gambin			Pseudo-Baguelin			Bustamante-Gianeselli			
		Q <sub>p</sub>	Q <sub>s</sub>	Q <sub>T</sub>	Q <sub>p</sub>	Q <sub>s</sub>	Q <sub>T</sub>	Q <sub>p</sub>	Q <sub>s</sub>	Q <sub>T</sub>	Q <sub>p</sub>	Q <sub>s</sub>	Q <sub>T</sub>	Q <sub>s</sub>	Q <sub>T</sub>	Q <sub>p</sub>	Q <sub>s</sub>	Q <sub>T</sub>	Q <sub>p</sub>	Q <sub>s</sub>	Q <sub>T</sub>	Q <sub>p</sub>	Q <sub>s</sub>	Q <sub>T</sub>	
tons	tons	tons	tons	tons	tons	tons	tons	tons	tons	tons	tons	tons	tons	tons	tons	tons	tons	tons	tons	tons	tons	tons	tons	tons	
Ogeechee River	H-11	91	5	.96	62	23	85	91	4	95	141	9	150	9	71										
	H-12	214	23	237	92	70	162	214	10	224	230	26	256	68	158										
	H-13	230	42	272	106	139	245	230	15	245	265	42	307	114	204										
	H-14	182	54	237	106	189	295	183	17	200	265	54	319	165	260										
	H-15	251	69	320	106	259	365	251	23	274	265	69	334	228	334										
Tavenas West	J-5	70	60	130	39	226	265	70	*	*	78	*	*	203	242										
Seattle Freeway	A	272	176	448	249	528	777	272	621	893	497	792	1289	528	776										
	B	172	161	333	124	485	609	172	729	901	249	728	977	456	580										
Gregersen	A	16	7	23	8	36	44	16	*	*	15	*	*	24	33										
	D/A	27	16	43	15	79	94	27	*	*	28	*	*	50	64										
	C	8	6	14	4	31	35	8	*	*	9	*	*	21	25										
	B/C	13	14	27	8	73	81	13	*	*	15	*	*	46	53										
LD26 Ellis	M6	99	45	144	76	112	188	99	*	*	190	*	*	106	182	209	84	293	239	125	364	131	89	220	
Sellgren	AI															70	97	167	70	90	160	33	70	103	

\* No friction values, f<sub>B</sub>, available

170

TABLE 27.- Ratio of Predicted Load Over Measured Load: CPT Methods

	DeRuiter-Beringen		Bustamante-Gianeselli			Schmertmann			Cone			Verbrugge		
	Q <sub>p</sub>	Q <sub>s</sub>	Q <sub>T</sub>	Q <sub>p</sub>	Q <sub>s</sub>	Q <sub>T</sub>	Q <sub>p</sub>	Q <sub>s</sub>	Q <sub>T</sub>	Q <sub>p</sub>	Q <sub>s</sub>	Q <sub>T</sub>	Q <sub>s</sub>	Q <sub>T</sub>
Mean,	1.99	0.37	0.75	1.23	1.32	1.06	1.99	0.57	0.93	2.72	0.80	1.20	1.07	0.94
Standard Deviation,	1.68	0.10	0.21	1.14	0.32	0.39	1.68	0.73	0.47	2.64	0.68	0.56	0.34	0.36
Coefficient of Variation	0.85	0.28	0.27	0.92	0.24	0.36	0.85	1.29	0.51	0.97	0.85	0.47	0.32	0.38

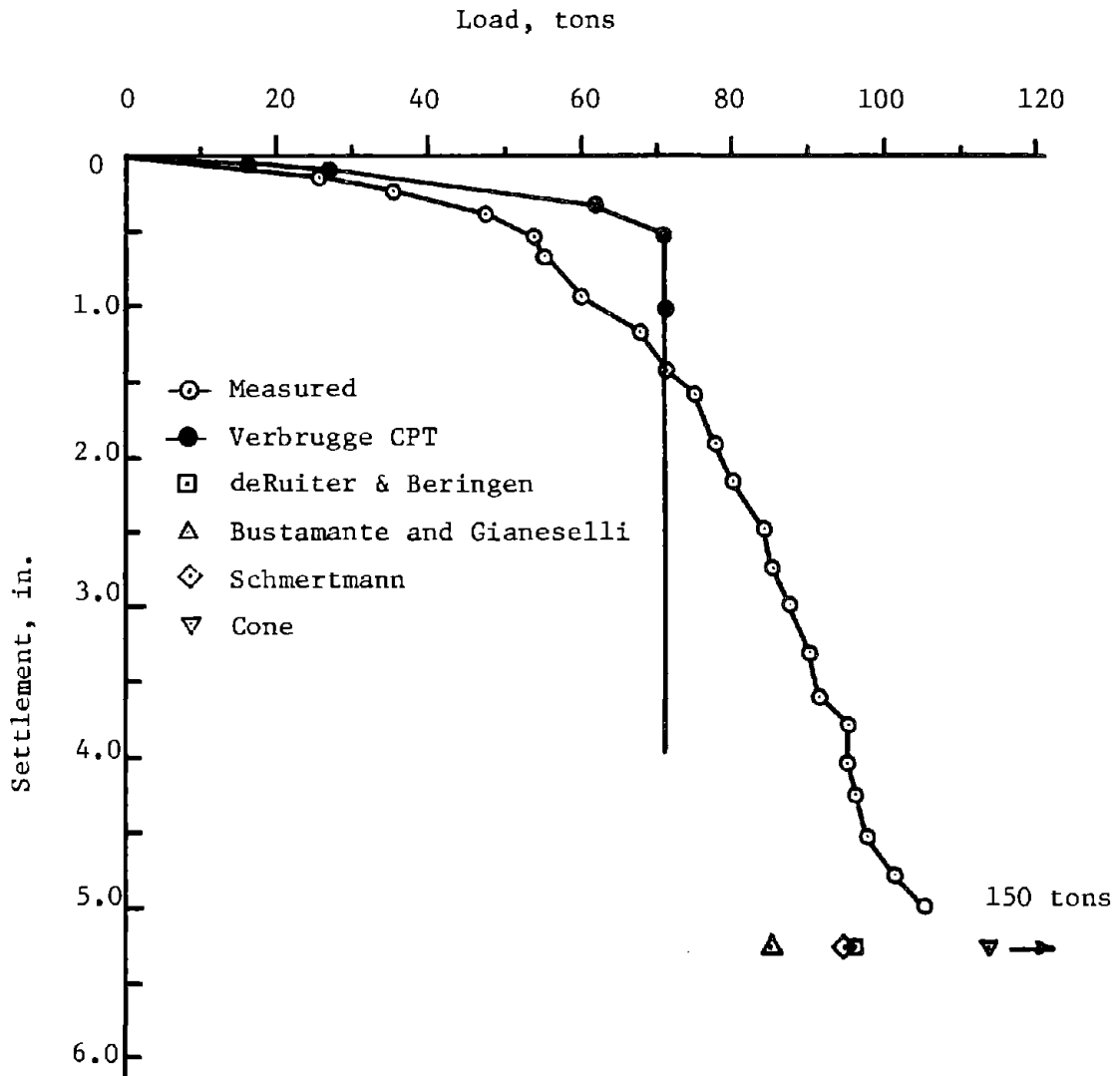


FIG. 91.- Ogeechee River Pile H-11: Load-Settlement Prediction by CPT Method  
 (1 ton = 8.9 kN; 1 in. = 2.54 cm)

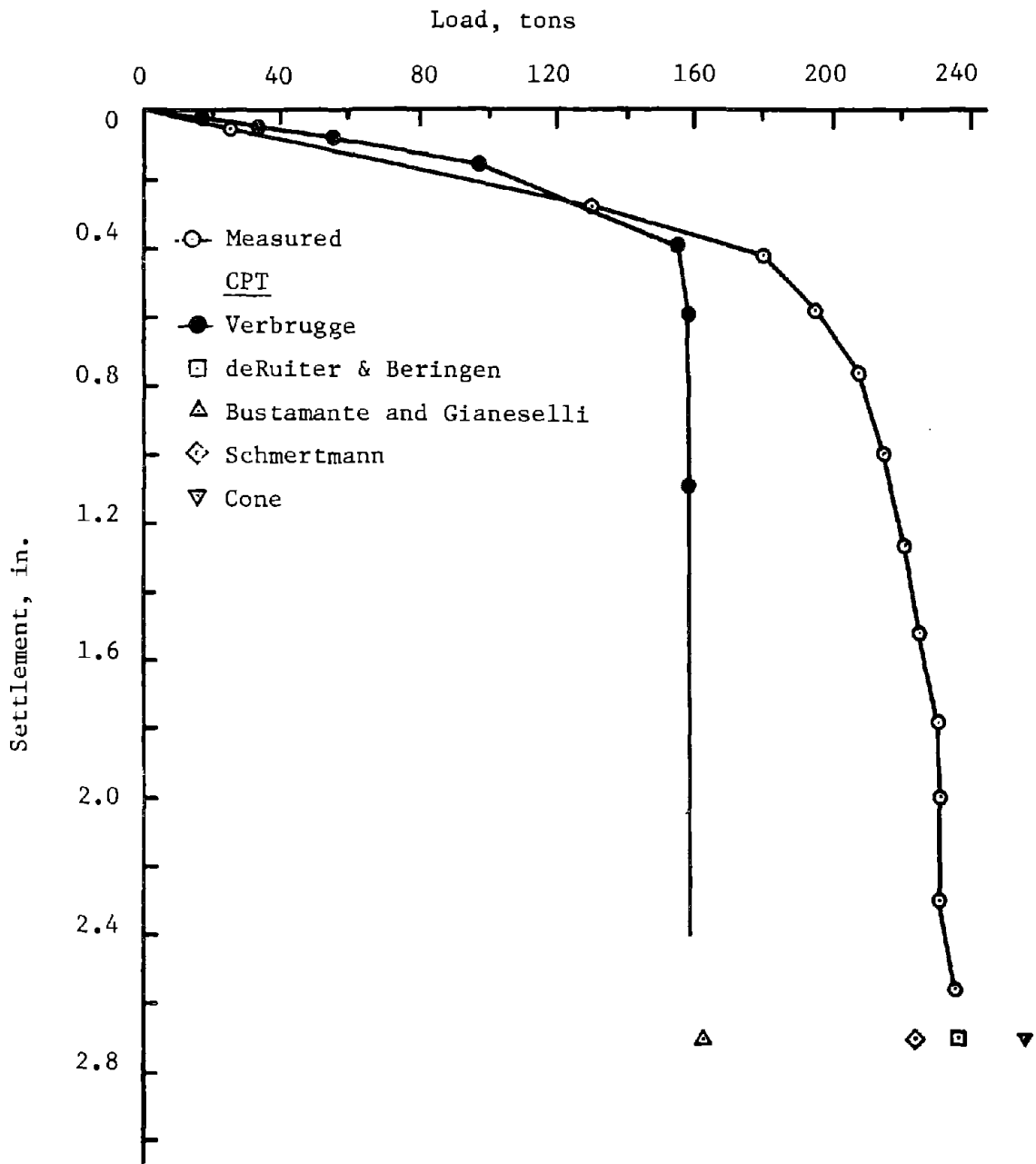


FIG. 92.- Ogeechee River Pile H-12: Load-Settlement Prediction by CPT Method (1 ton = 8.9 kN; 1 in. = 2.54 cm)

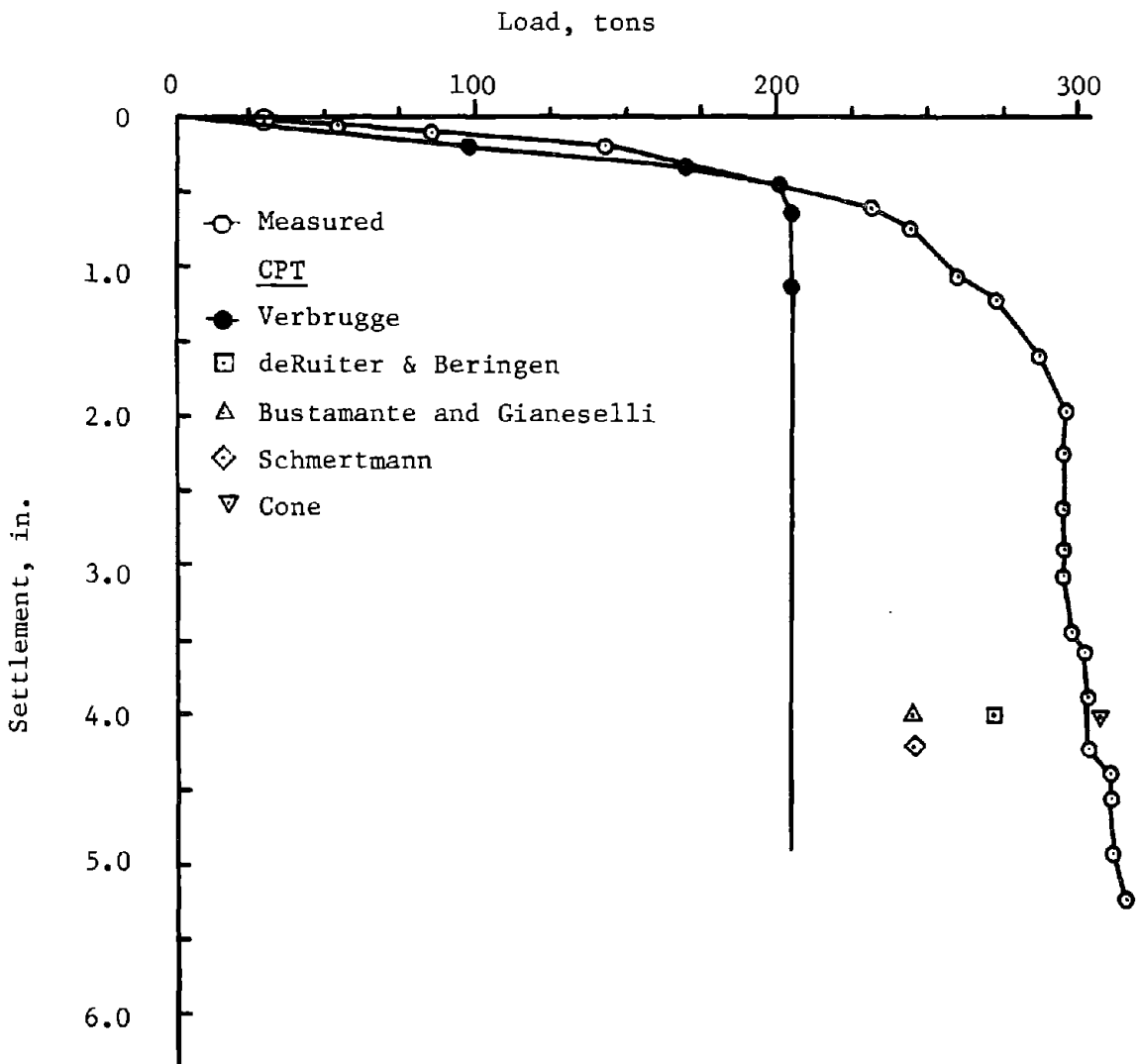


FIG. 93.- Ogeechee River Pile H-13: Load-Settlement Prediction by CPT Method (1 ton = 8.9 kN; 1 in. = 2.54 cm)

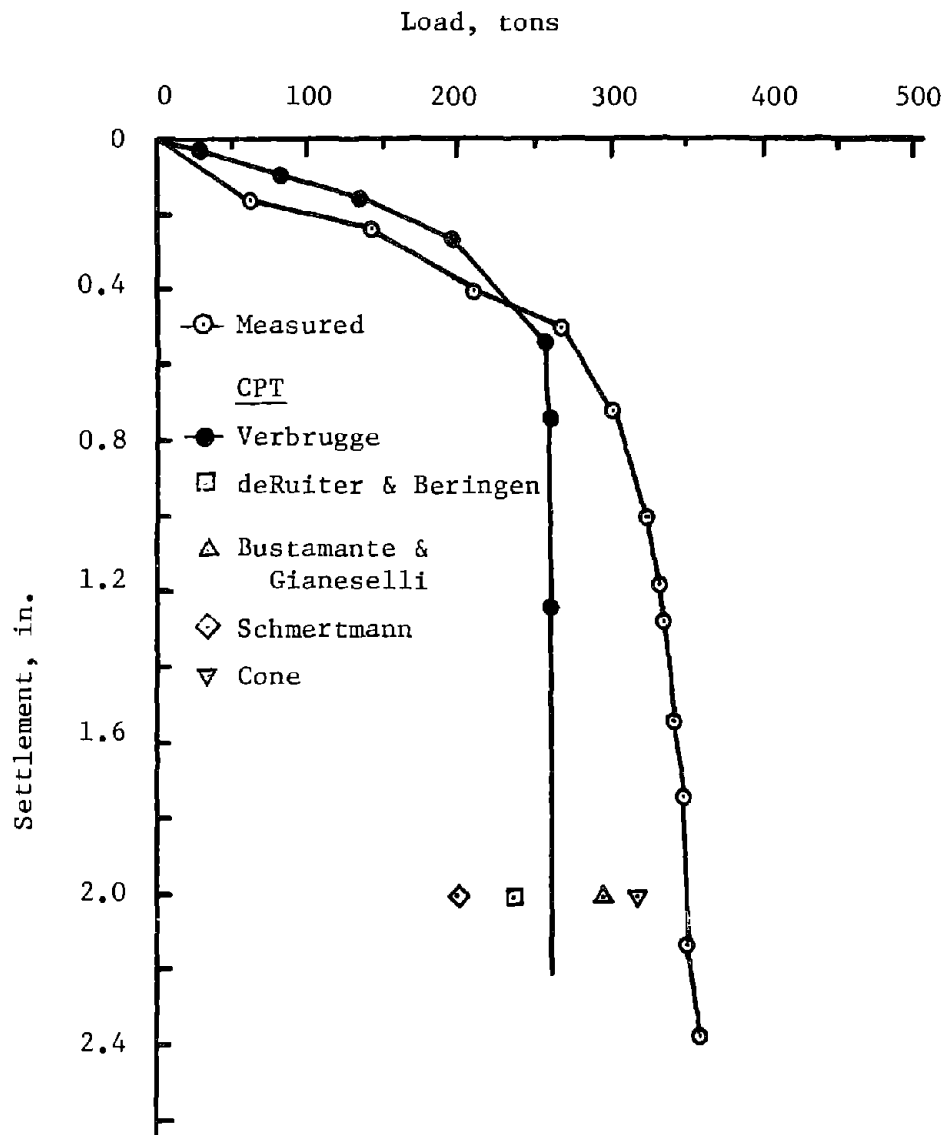


FIG. 94.- Ogeechee River Pile H-14: Load-Settlement Prediction by CPT Method  
 (1 ton = 8.9 kN; 1 in. = 2.54 cm)



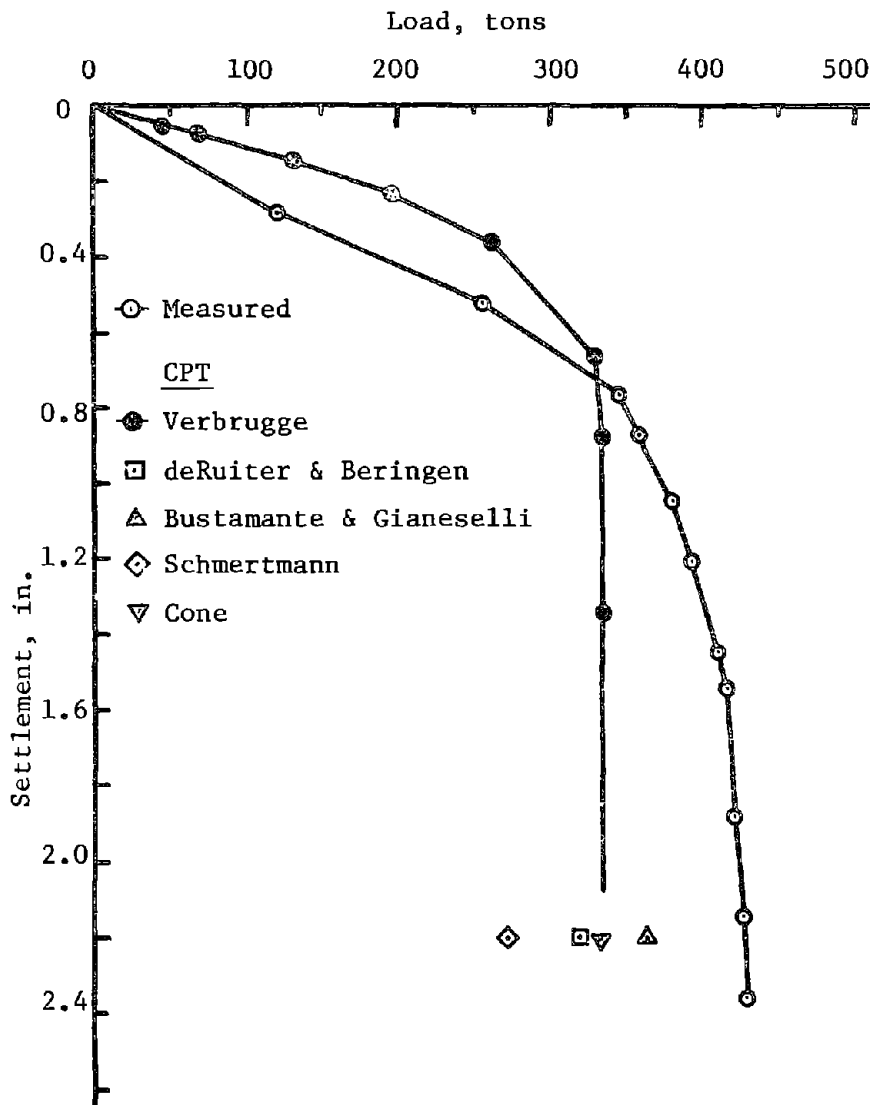


FIG. 95.- Ogeechee River Pile H-15: Load-Settlement Prediction by CPT Method  
(1 ton = 8.9 kN; 1 in. = 2.54 cm)

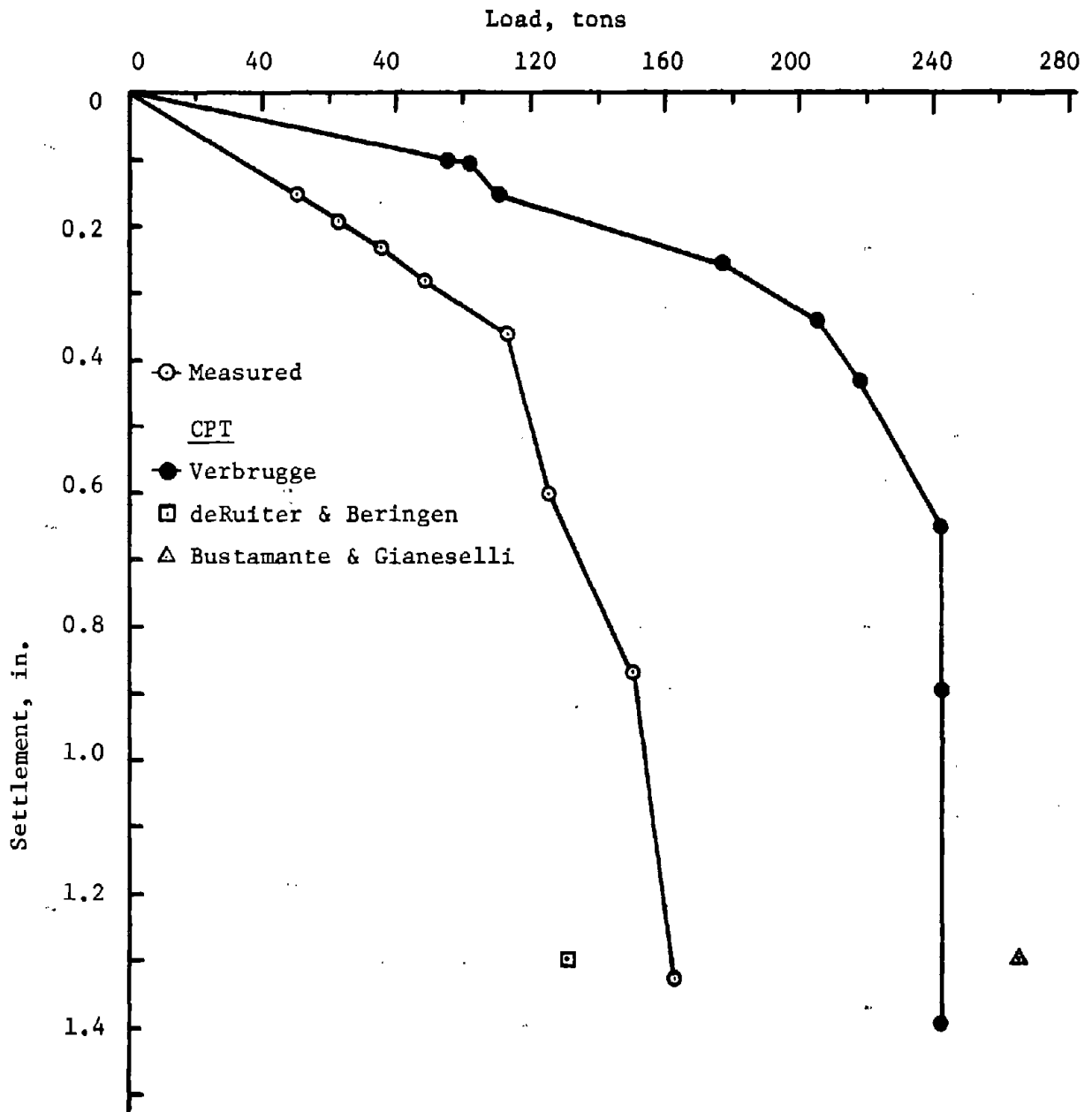


FIG. 96.- Tavenas Pile J-5: Load-Settlement Predictions by CPT Method (1 ton = 8.9 kN; 1 in. = 2.54 cm)

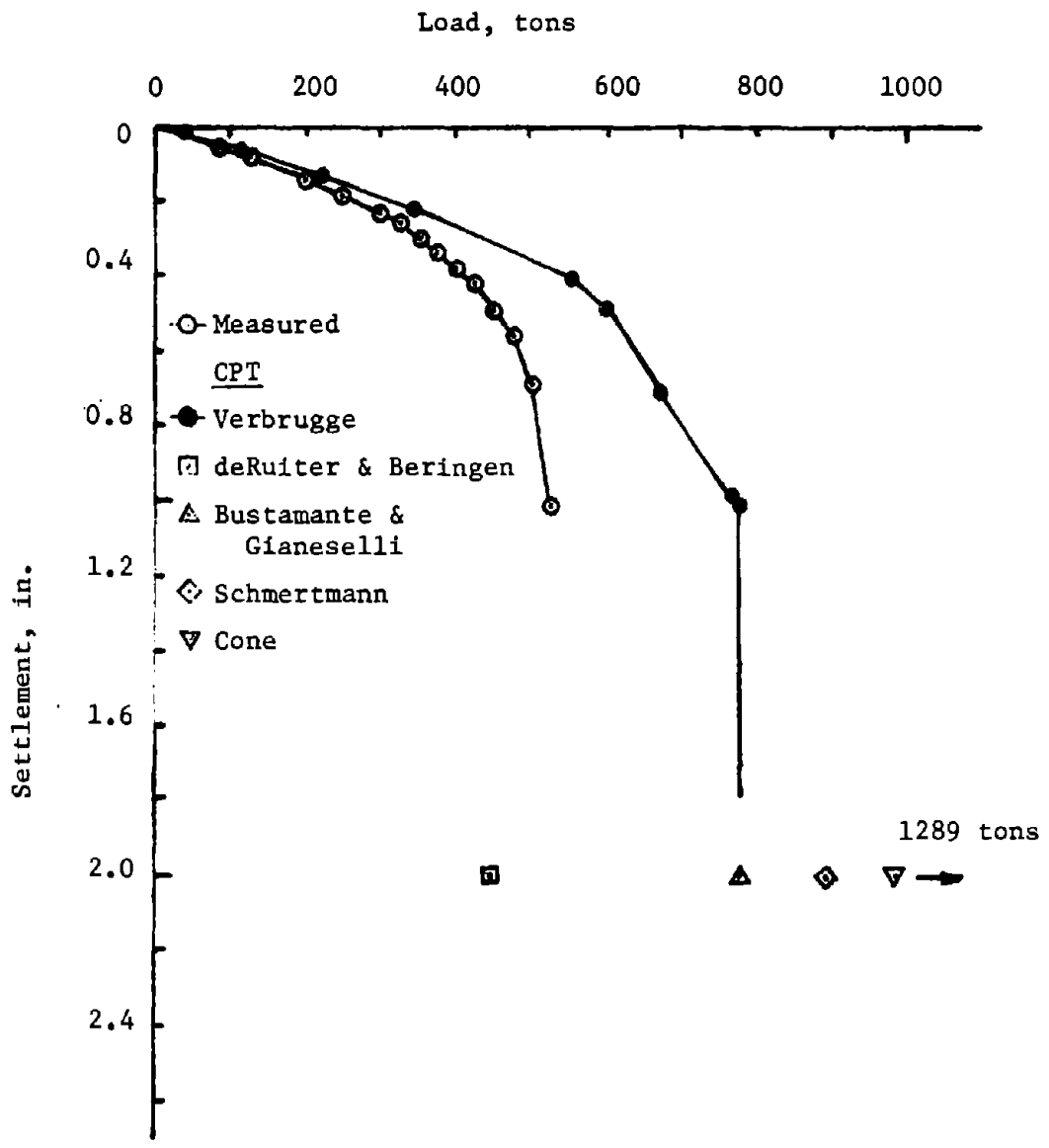


FIG. 97.- West Seattle Freeway Pile A: Load-Settlement Predictions by CPT Method (1 ton = 8.9 kN; 1 in. = 2.54 cm)

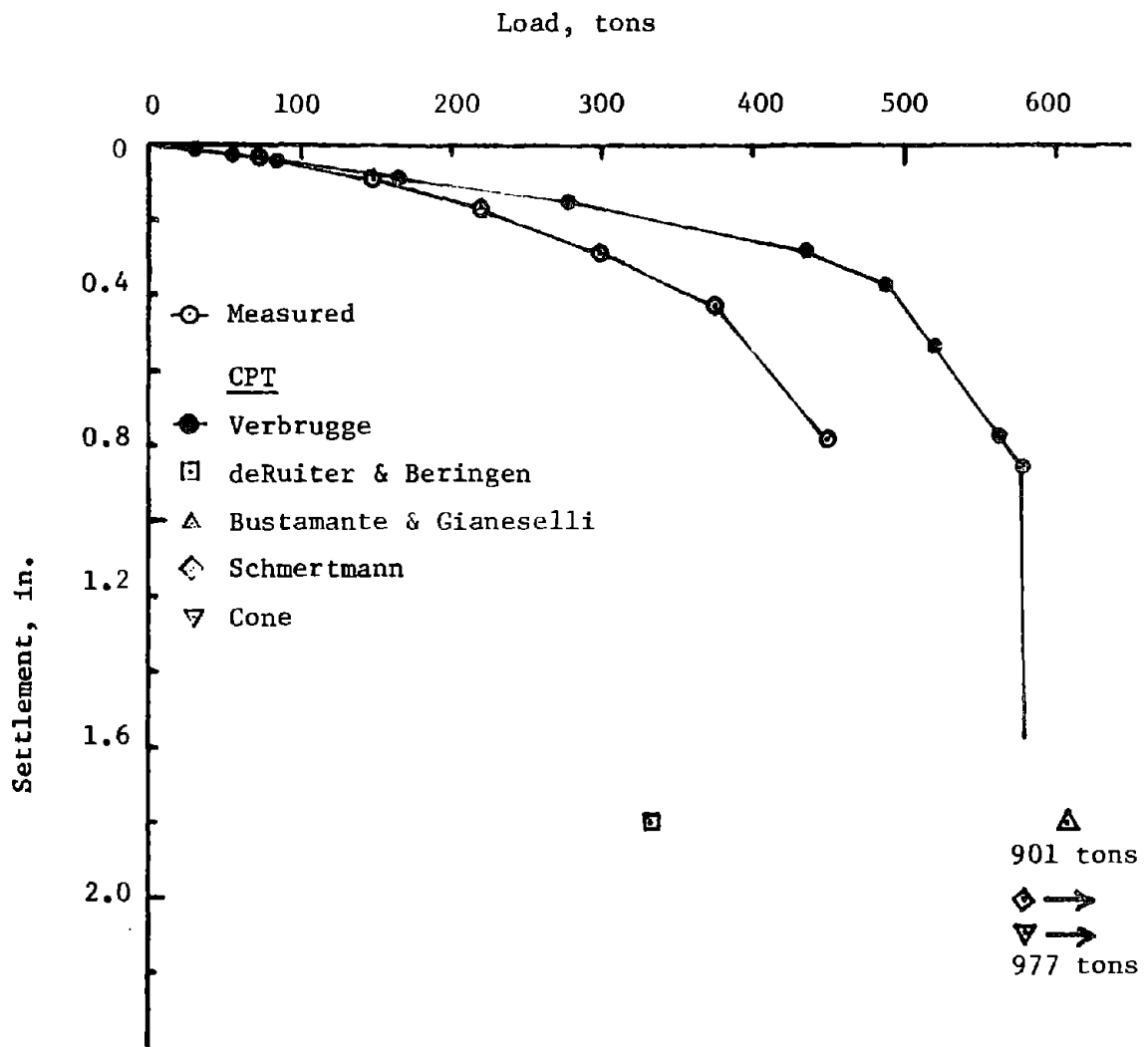


FIG. 98.- West Seattle Freeway Pile B: Load-Settlement Predictions by CPT Method  
(1 ton = 8.9 kN; 1 in. = 2.54 cm)

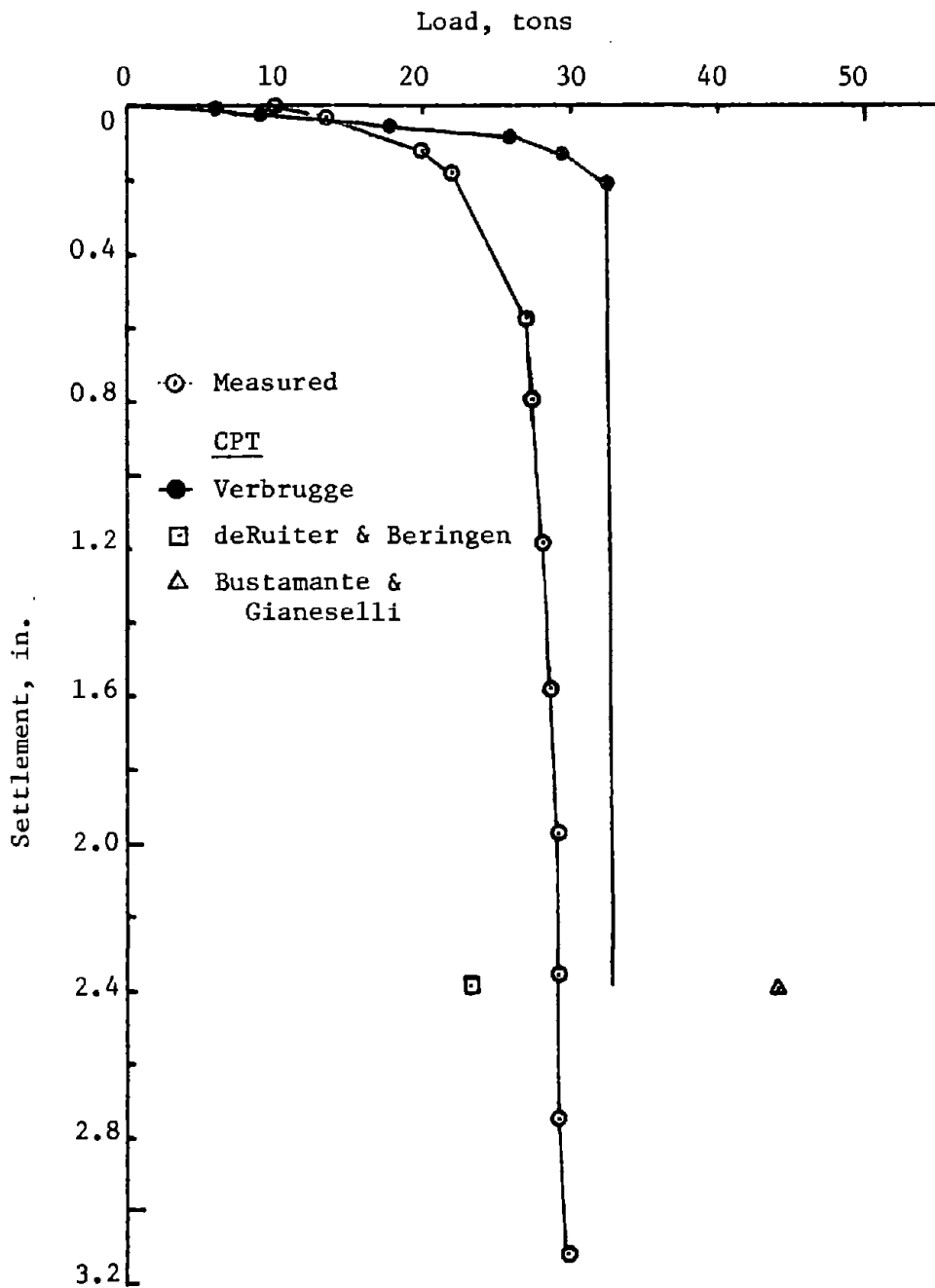


FIG. 99.- Gregersen Pila A: Load-Settlement Predictions by CPT Method (1 ton = 8.9 kN; 1 in. = 2.54 cm)

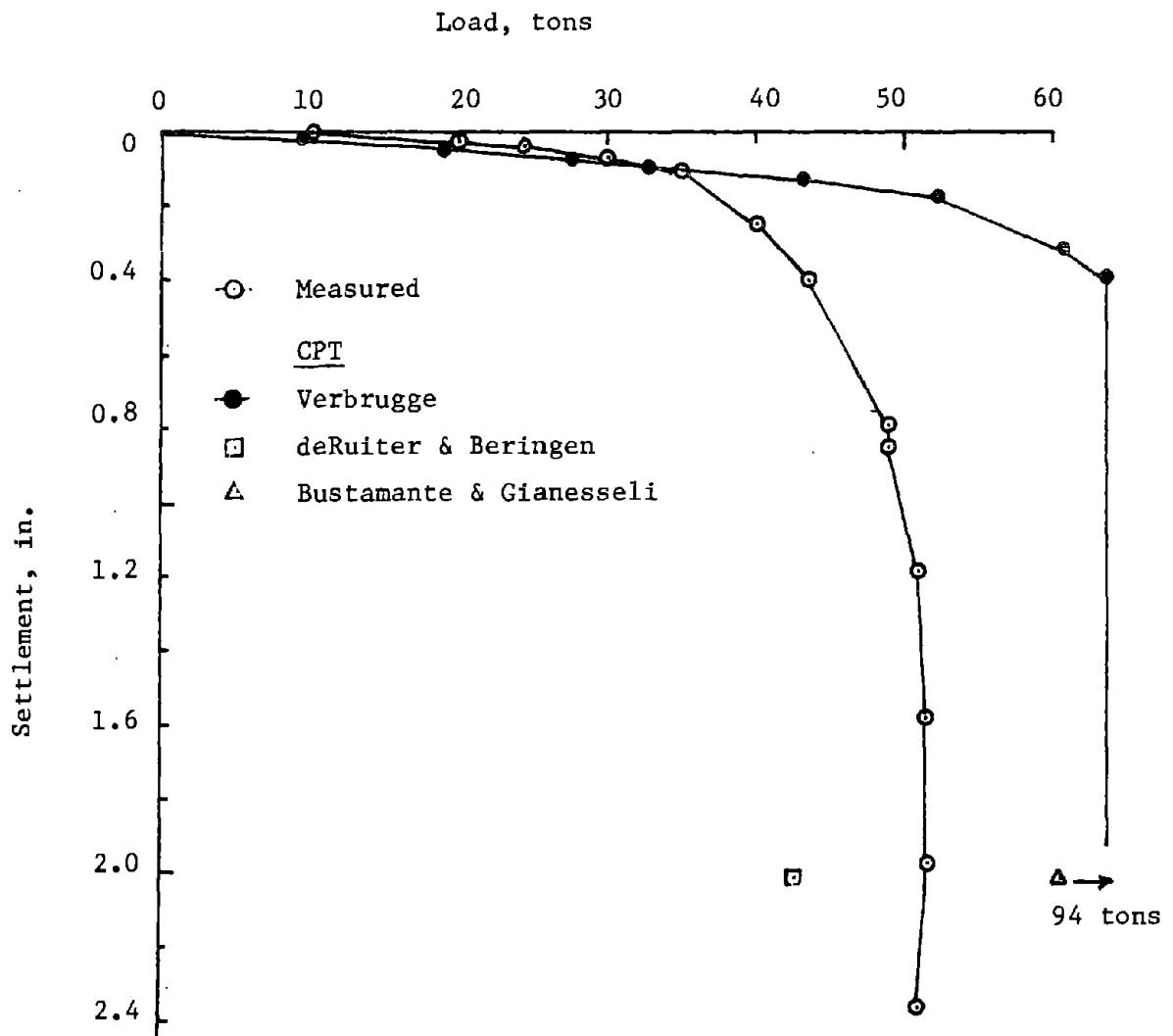


FIG. 100.- Gregersen Pile D/A: Load-Settlement Predictions by CPT Method (1 ton = 8.9 kN; 1 in. = 2.54 cm)

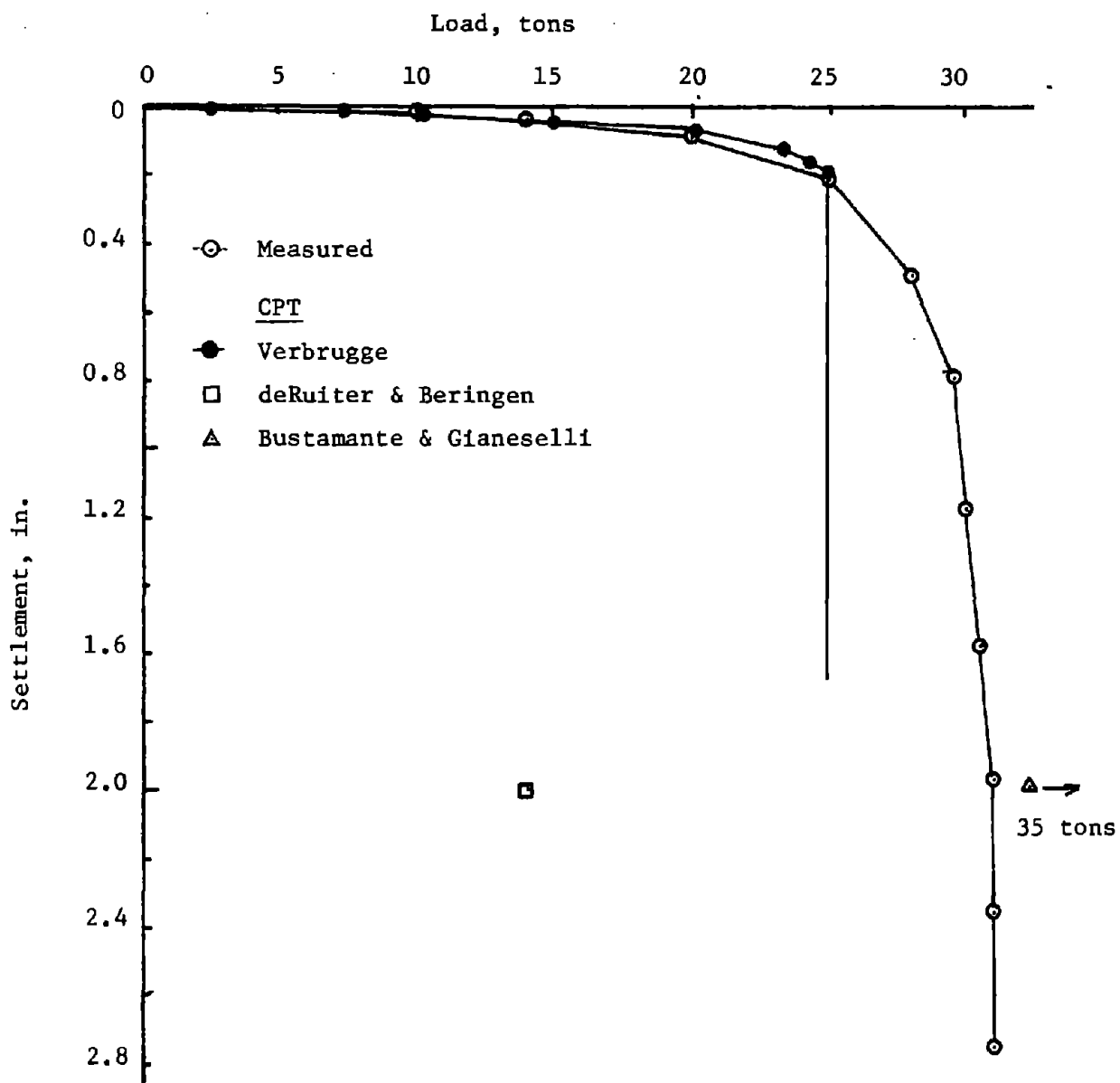


FIG. 101.- Gregersen Pile C: Load-Settlement Prediction by CPT Method (1 ton = 8.9 kN; 1 in. = 2.54 cm)

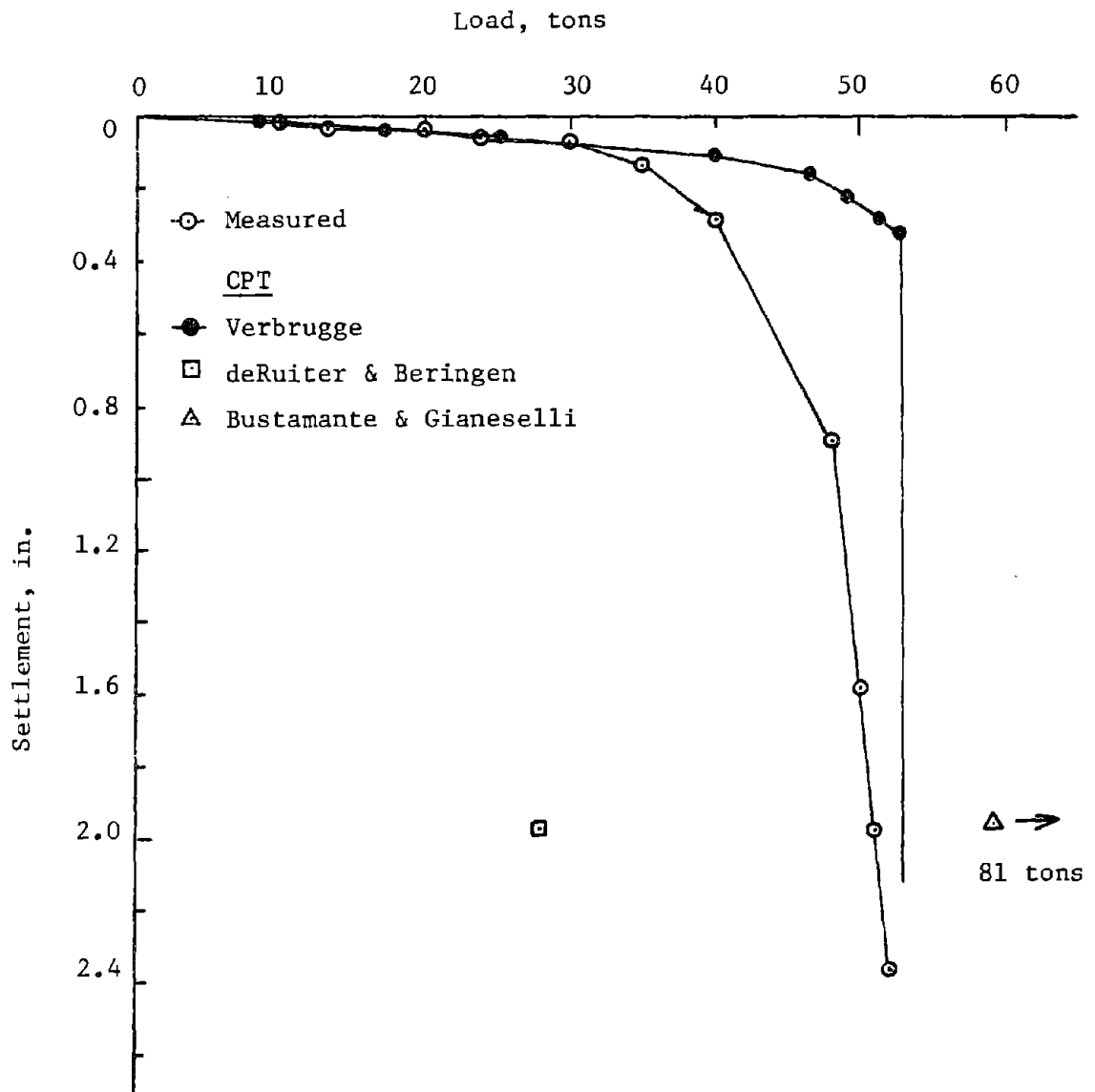


FIG. 102.- Gregersen Pile B/C: Load-Settlement Prediction by CPT Method (1 ton = 8.9 kN; 1 in. = 2.54 cm)



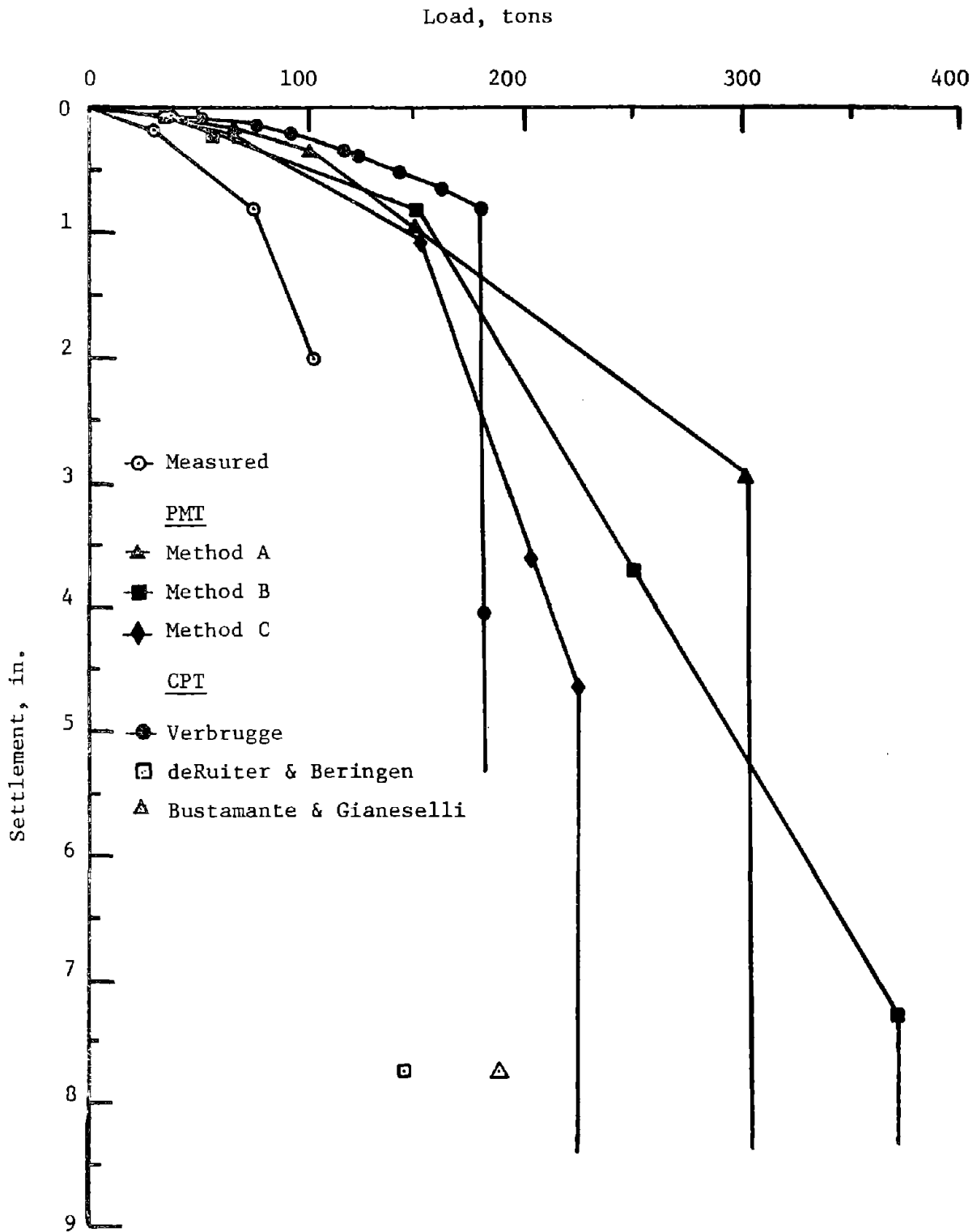


FIG. 103.- Lock and Dam 26 Ellis Island Site Pile M6: Load-Settlement Predictions by PMT and CPT Methods (1 ton = 8.9 kN; 1 in. = 2.54 cm)

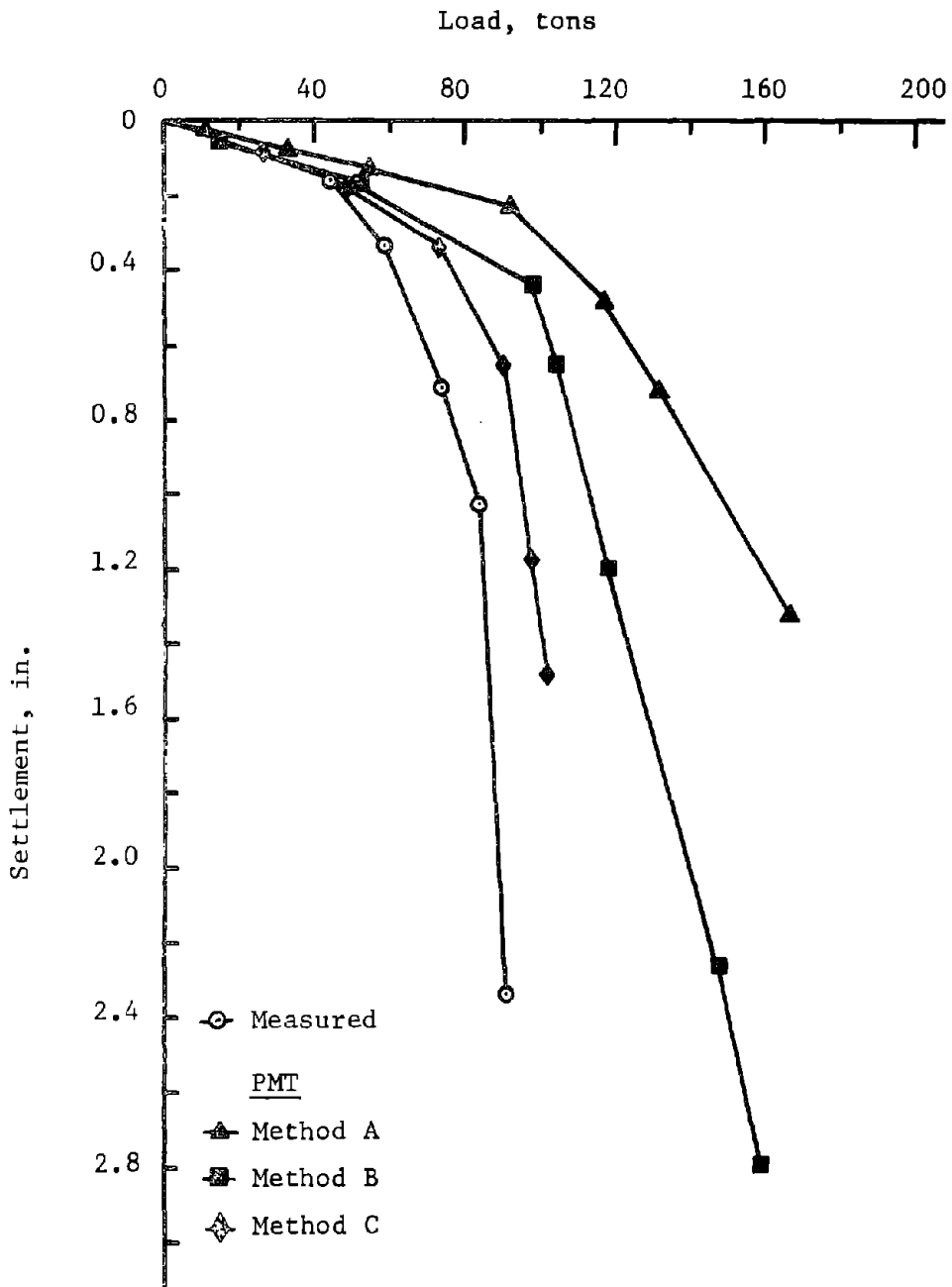
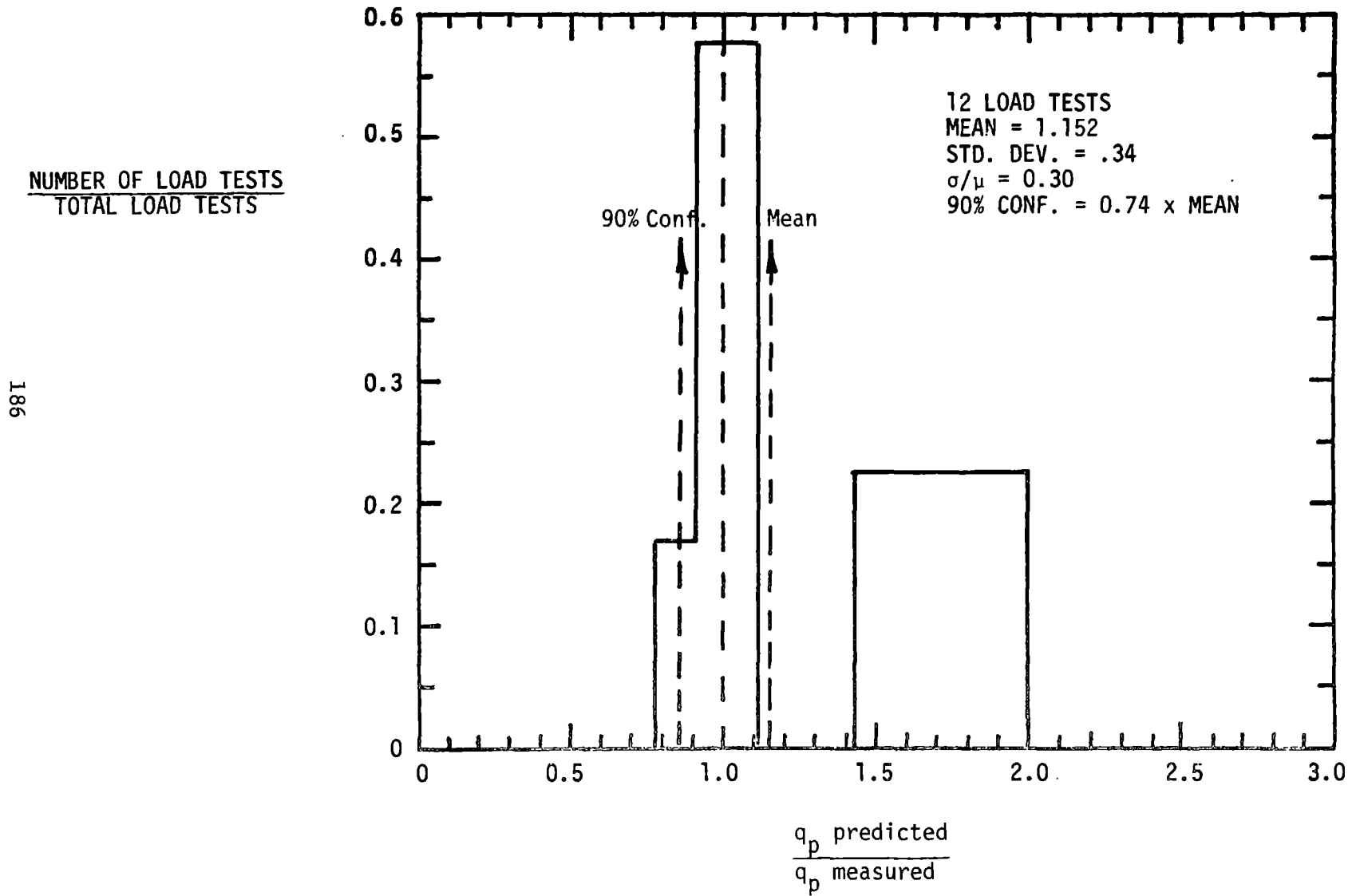


FIG. 104.- Sellgren Pile AI: Load-Settlement Predictions by PMT Methods (1 ton = 8.9 kN; 1 in. = 2.54 cm)

Although the Verbrugge method predicted the ultimate loads quite well, this method underpredicted settlement. At low load levels the prediction generally agrees with the measured results. As the load increases, however, the actual settlement becomes greater than the predicted. This indicates that the elastic modulus of the soil is nonlinear. Future research in this area should consider correlations with CPT data to obtain a nonlinear soil model.

Due to the limited amount of data, no general conclusions can be made regarding the pressuremeter methods. The overprediction for the pile at Lock and Dam 26 may be explained by the loading history of the pile. It was subjected to repeated cyclic lateral loading before the axial load test. This loading makes the results of the axial load test questionable in terms of the capacity of pile loaded only axially. There were not enough cases for a meaningful frequency distribution to be prepared for these methods. However, the data base collected by Bustamante and Gianceselli (8) to propose their PMT and CPT methods was used to prepare frequency distributions. Figs. 105 through 110 present the results for that data base which includes piles in all soil types. The results are summarized in Table 28. The two methods both slightly overpredict pile capacity with the cone penetrometer yielding the best results. The coefficient of variation is much lower than those obtained from the conventional methods. Using a data base not limited to instrumented piles, Olson and Dennis (30) found that the CPT methods provide slightly better accuracy than the SPT methods; the pressuremeter methods were not included in their study. Based on these results, the CPT and PMT are quite promising tools for use in predicting pile capacity.

CONE PENETROMETER METHOD



181

FIG. 105.- Frequency Distribution. Cone Penetrometet Method. Point Load

CONE PENETROMETER METHOD

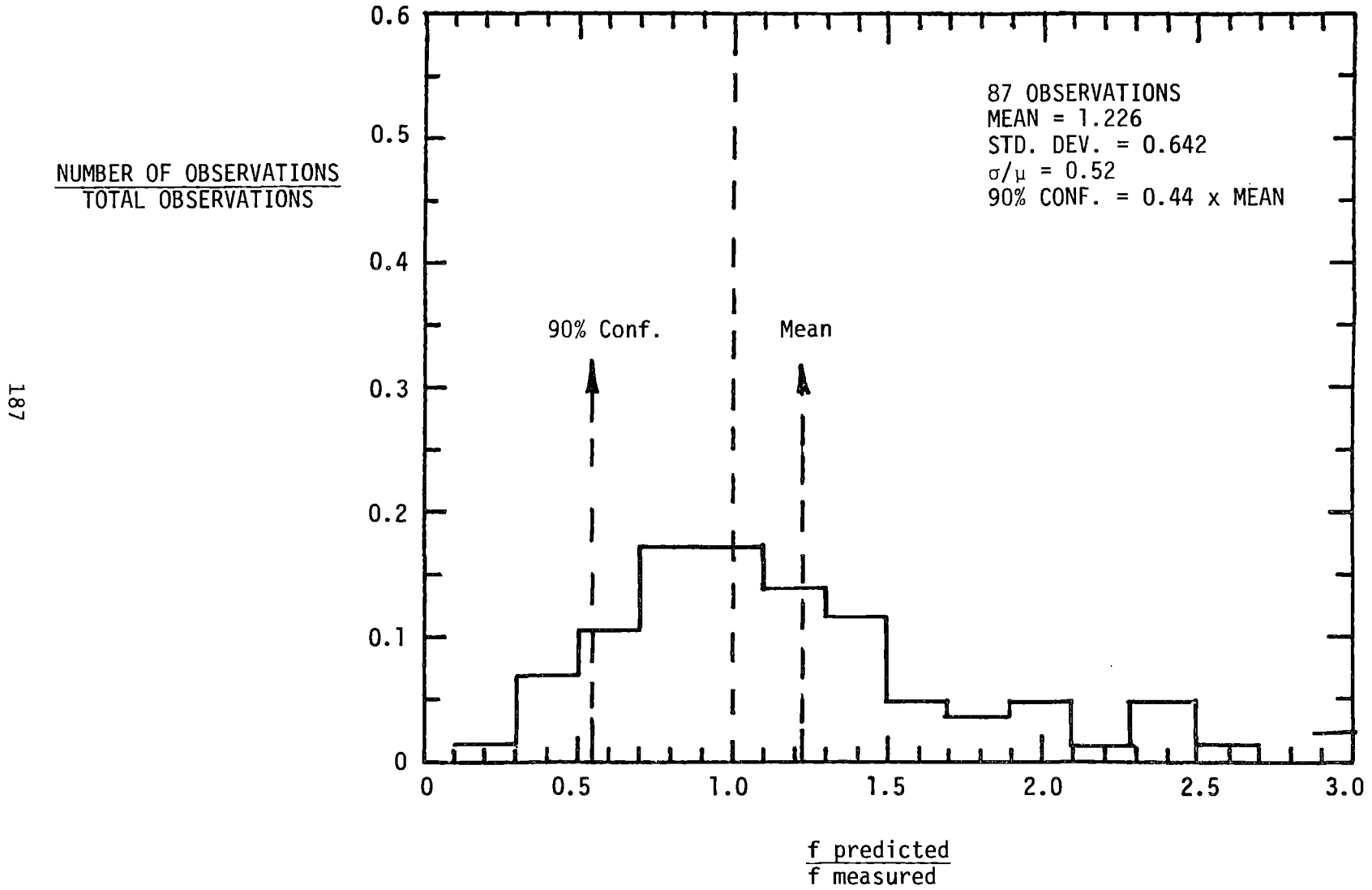


FIG.106. - Frequency Distribution. Cone Penetrometer Method. Side Load

CONE PENETROMETER METHOD

$\frac{\text{NUMBER OF LOAD TESTS}}{\text{TOTAL LOAD TESTS}}$

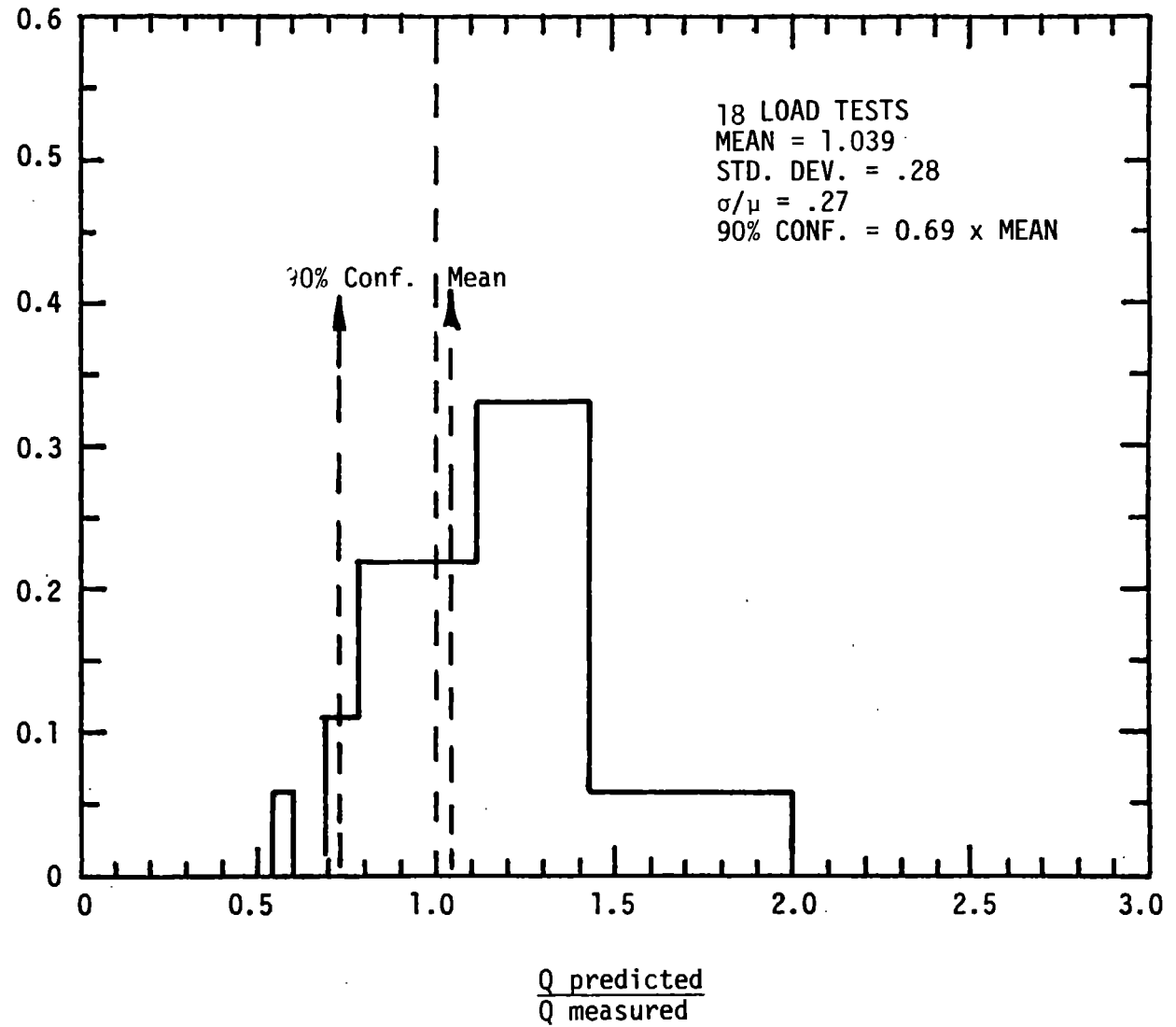


FIG. 107.- Frequency Distribution. Cone Penetrometer Method. Total Load

PRESSUREMETER METHOD

NUMBER OF LOAD TESTS  
TOTAL LOAD TESTS

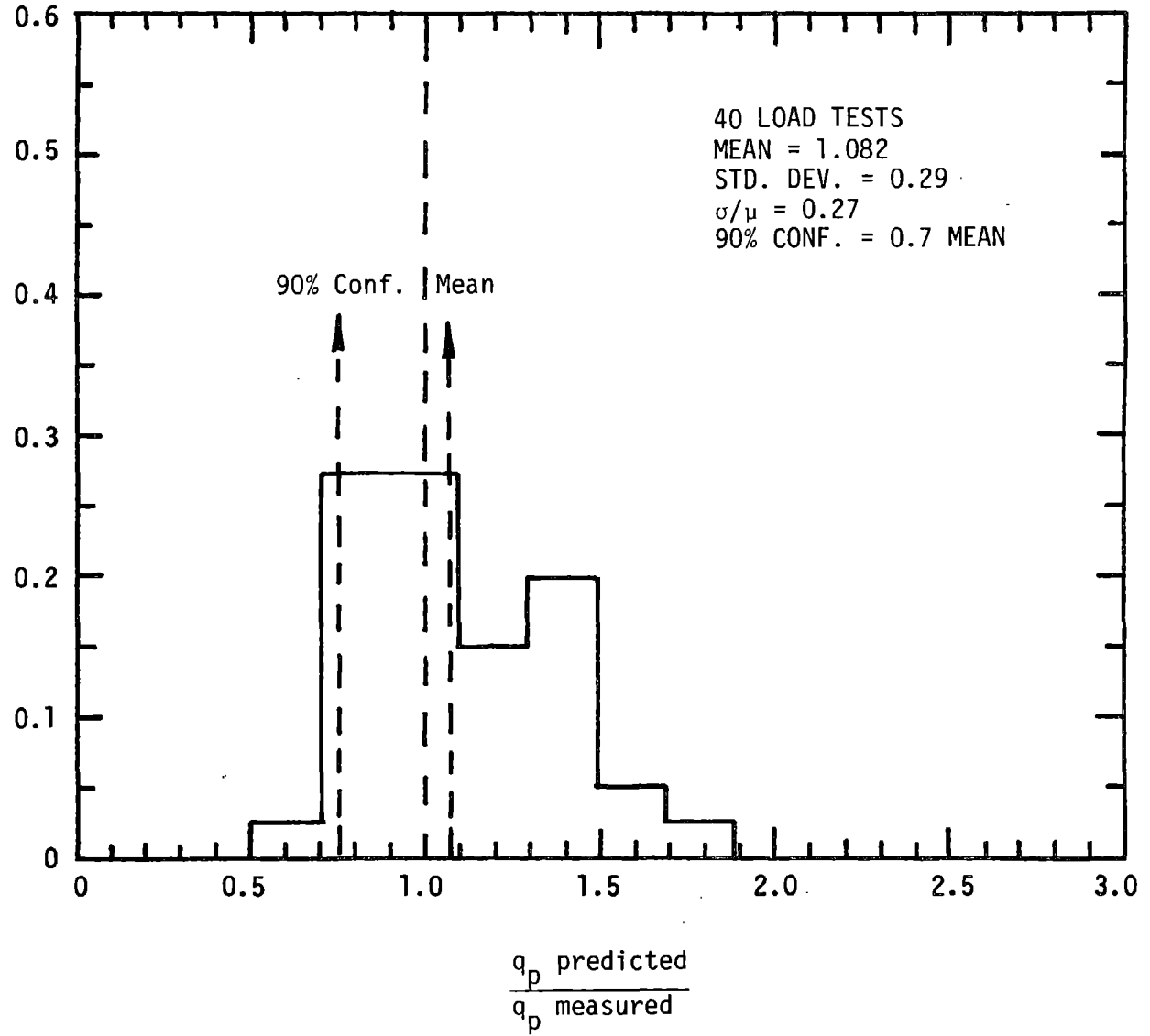


FIG. 108.- Frequency Distribution • Pressuremeter Method. Point Load

PRESSUREMETER METHOD

190

$\frac{\text{NUMBER OF LOAD TESTS}}{\text{TOTAL LOAD TESTS}}$

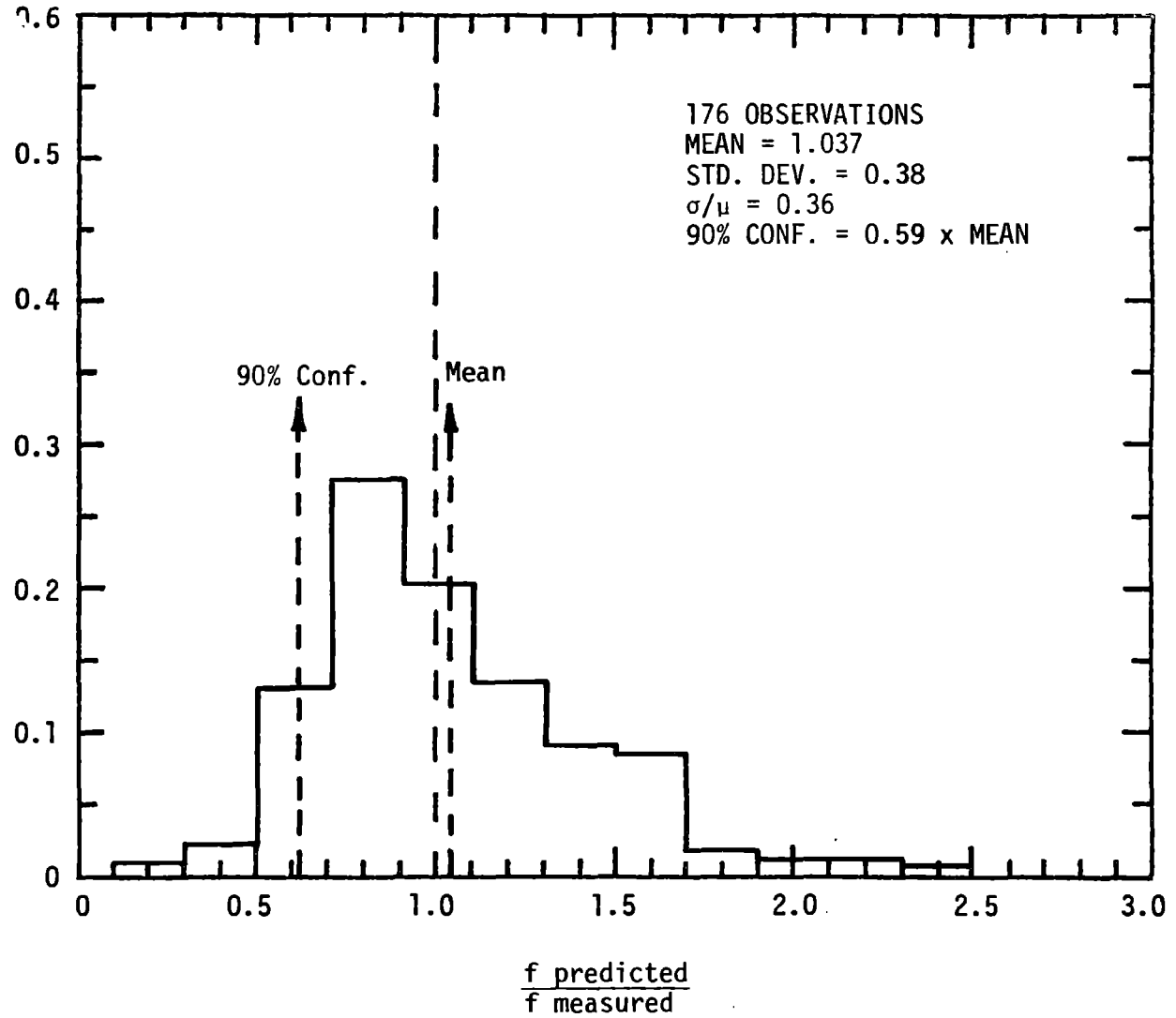


FIG. 109. - Frequency Distribution. Pressuremeter Method. Side Load



PRESSUREMETER METHOD

$\frac{\text{NUMBER OF LOAD TESTS}}{\text{TOTAL LOAD TESTS}}$

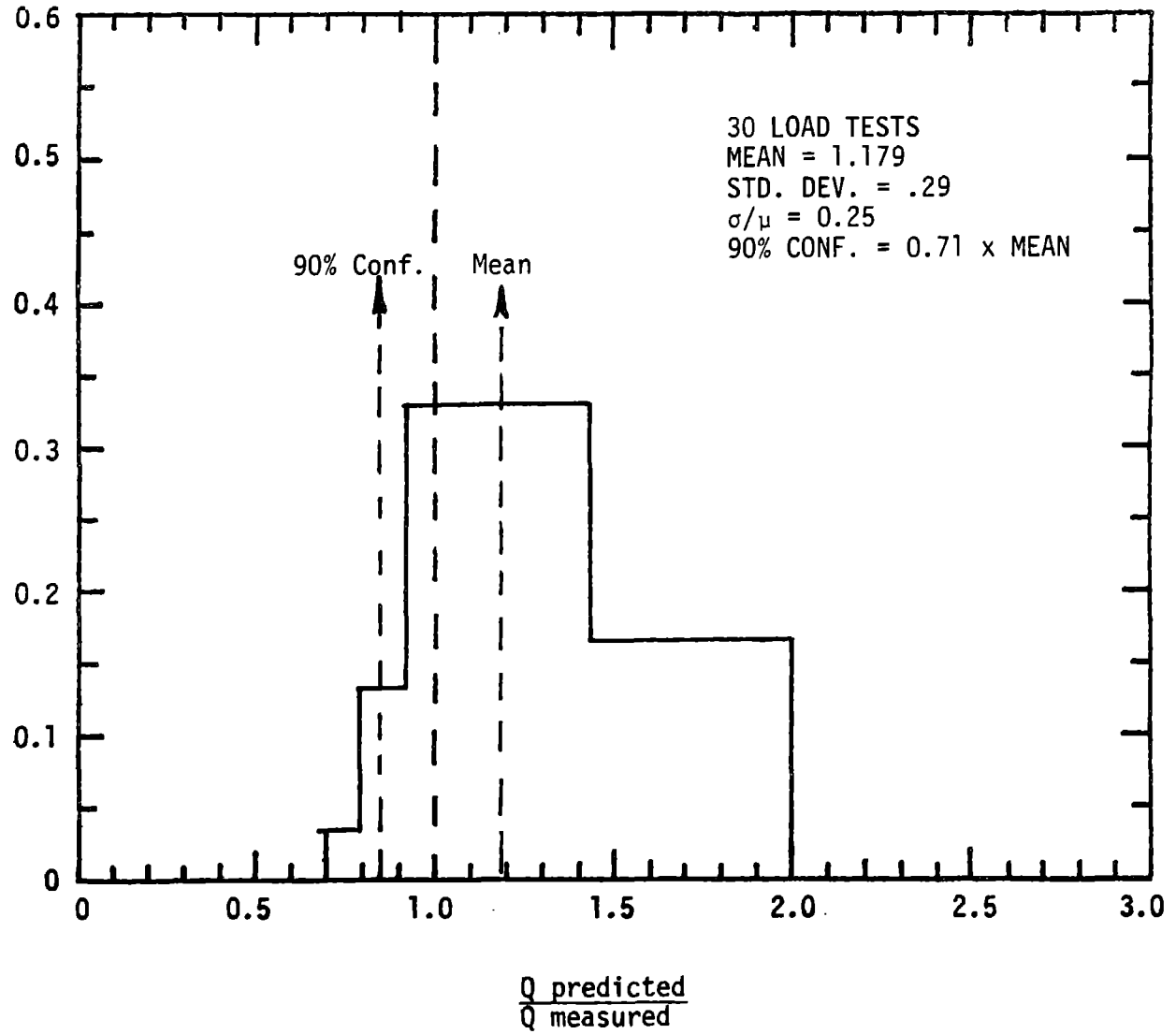


FIG. 110. - Frequency Distribution. Pressuremeter Method. Total Load

**TABLE 28.- Summary of Frequency Distribution Results  
for PMT and CPT Methods**

<u>Method</u>		<u>Mean</u>	<u>Standard Deviation</u>	<u>Coefficient of Variation</u>	<u>Coefficient K for 90% Confidence 90% Conf. -</u>	<u>Comment on Data Base</u>
Cone Penetrometer	Total	1.039	0.28	0.27	0.69	Same
	Friction	1.226	0.642	0.52	0.44	
	Point	1.152	0.34	0.3	0.74	
Pressuremeter	Total	1.179	0.29	0.25	0.71	Same
	Friction	1.037	0.38	0.36	0.59	
	Point	1.082	0.29	0.27	0.70	

## CHAPTER XI - IMPROVING THE STATE OF THE PRACTICE

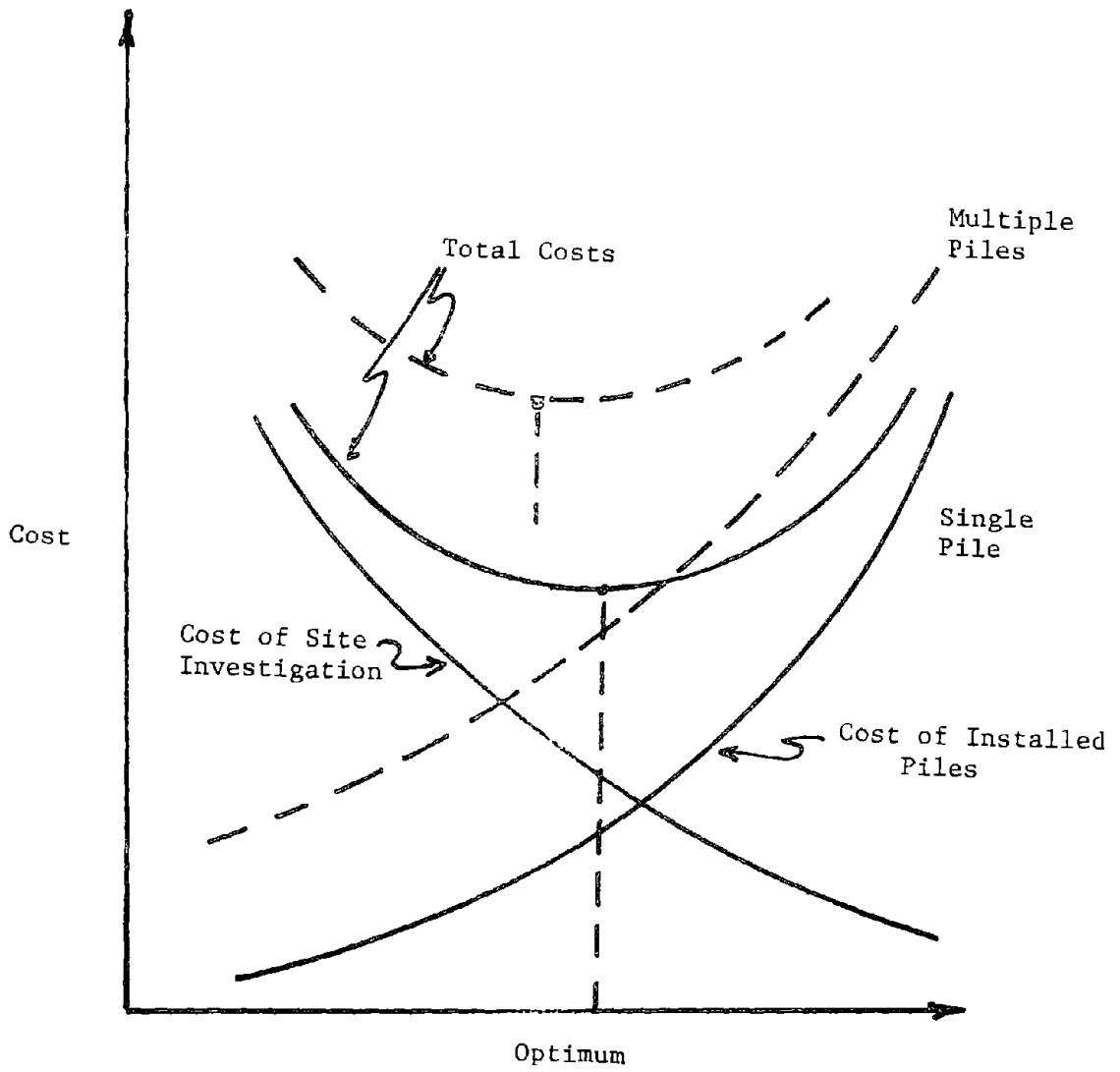
### RESULTS OF INTERVIEW

Within the context of the topic "Behavior of Piles and Pile groups in Cohesionless Soils," the following series of questions were asked to Mr. R. A. Hawkins of Raymond Kaiser Engineers:

1. What geotechnical practices need to be improved to obtain better soil characterization?
2. Is a cost analysis such as the one shown on Figure 111 feasible?
3. Is it cost beneficial to obtain 95 percent or better confidence in given parameters if construction activity negate benefits of improved site characterization?

In response to the first question, Mr. Hawkins pointed out several areas where improvement is needed. The reporting of the site investigation is often incomplete, omitting ground elevations and water table information, and not clearly written. "Considerable license" is taken in applying the unified soil classification system for visual classification. The standardized procedure for the Standard Penetration Test (SPT) is not always followed and problems associated with caving of the borehole are not always recognized. All of these factors could be greatly improved by placing better trained technicians or engineers in the field for the site investigation. Mr. Hawkins also pointed out that improved or new equipment such as the SPT energy measuring device, the cone penetrometer, the pressuremeter and the dilatometer "promise to advance the state of the art".

In answer to the second question, Mr. Hawkins commented that "the cost evaluation of site investigations is not so clear-cut" as Fig. 111 indicates. It is very easy to look back at a successful project and decide that less site investigation is necessary. However, the uncertainties in the mind of the designer due to an incomplete site investigation bear directly on his conservatism in design and hence, cost to the owner. There are many other items affecting the cost of the foundation much more than the site investigation, such as the job location, size of job, foundation specifications, time schedule, pile



Coefficient of Variation of Design Data

FIG. 111.- Cost of Site Investigation Versus Cost of Installed Piles

type and conditions of the site. In general, the site investigation is more important than its relative cost. On most projects the cost of the site investigation varies from less than 1 percent to around 5 percent of the final foundation cost. Another area where savings is possible is with driving criteria for piles. Use of wave equation analyses can turn each pile log into a valuable penetration record.

According to Mr. Hawkins, the 95% confidence level is clouded by other factors. The definition of 95% confidence level necessarily includes the engineers prior knowledge and experience in the area. Some effects of construction activity are beneficial, such as compaction, and some are negative, such as inadvertent batter and the jetting of piles. However, Mr. Hawkins concludes that "in spite of the sometimes dramatic changes construction activity can have on site parameters, the engineer and contractor must have a clear idea of what was there to start with". Mr. J.B. Hilton of Raymond Builders added that the extent of the site investigation is influenced by several factors including size of the project, settlement criteria, nature of subsurface strata, and variability of the site. As a result it is difficult to make "blanket generalizations which are accurate for all cases".

In a more general interview, Dr. M. W. O'Neill of the University of Houston commented that residual stresses in piles were probably a function of the mean effective stress (or depth) and soil compressibility or rigidity. He added that the pressuremeter would be useful to measure the soil rigidity. Related to the questions mentioned previously, Dr. O'Neill stated that "there is probably limited benefit to be gained on a production project by doing highly detailed borings". However, he added that more flexible contracts which allow design changes based on feedback from the pile driving records would be an area of great cost savings. He felt that a cost evaluation such as presented in Fig. 111 may be of some benefit to perform for a specific case, but would be impossible to generalize.

## PRECISION ON THE SOIL PARAMETERS

A statistical analysis of the soil data at the Lock and Dam 26 Ellis Island site showed that the coefficient of variation is about the same for the SPT, the CPT and PMT. If it is concluded from the previous chapter that the CPT and PMT methods lead to a better precision of ultimate capacity prediction, the difference may be attributed to two factors: 1. The CPT and PMT are more repeatable from one site to another than the SPT, 2. The parameters measured during the CPT and PMT are more related to the ultimate capacity of a pile than the blow count.

It was shown in Chapter VIII that the relation between the blow count  $N$  and the ultimate point pressure for the pile  $q_{\max}$  is not linear. This may be explained as follows.

In very loose sand the SPT blow count is very low, the SPT does not apply a sufficiently large number of blows to densify the sand and the blow count is representative of the sand in its undisturbed state. In very loose sands however, the pile will apply a large number of blows to the sand, densify it and  $q_{\max}$  will be much larger than the  $q_{\max}$  for the undisturbed loose sand. In very dense sand the number of blows for both the SPT and the pile are large and a similar soil condition is created around the split spoon and the pile. These two observations may explain why the ratio of  $q_{\max}/N$  is high at low SPT blow counts and low at high SPT blow counts.

The CPT and the PMT on the other hand, measure a soil response under the same conditions whether the soil is loose or dense. The cone penetrometer provides directly measured values of friction and point resistance. It seems however, that the friction sleeve is too close to the point to give unquestionable results. A sleeve friction located 18 in. (46 cm) behind the tip (10 diameters) would probably give more reliable results. Unlike the SPT, the CPT and PMT do not create a soil condition similar to the one that exists around the pile after driving except in the case of the PMT slotted tube technique.

The shear wave velocity test did give a lower coefficient of variation than all other tests. This test gives a very low strain shear modulus which may be useful for the initial tangent modulus of the hyperbolic model.

#### COST SAVING ASPECTS

##### Considering residual stresses

In the past, residual stresses have been ignored in design methods. As will be shown in the following example, using a design method that does consider residual stresses can lead to significant savings.

Problem 1: Find the length of pile required to sustain a 75 tons (667.5 kN) working load. The pile is a square 16 in. x 16 in. (40.6 cm x 40.6 cm) concrete pile.

Solution : SPT profile is constant with  $N = 25$  blows/ft (82 blows/m)

##### 1. Not considering residual stresses

Not considering residual stresses, the equations for  $q_{\max}$  and  $f_{\max}$  are:

$$q_{\max} = 12.59 N^{0.41} \quad (\text{tsf})$$

and

$$f_{\max} = 0.288 N^{0.25} \quad (\text{tsf})$$

Thus

$$Q_p = 12.59 (25)^{0.41} \times 1.78 = 83.9 \text{ tons (746 kN)}$$

$$Q_s = 0.288 (25)^{0.25} \times 1.33 \times 4 \times L = 3.43 L$$

$$Q_T = 75 \text{ tons} \times \text{Factor of Safety} = 75 \times 3 = 225 \text{ tons (2002.5kN)}$$

Then the equation for pile length is:

$$83.9 + 3.43L = 225 \quad \text{which gives } L = 41 \text{ ft (12.5 m)}$$

2. Considering residual stresses

To consider residual stresses, use Eqs. 28 and 30 from Chapter VIII which are as follows:

$$q_{\max} = 19.75 N^{0.36} \quad (\text{tsf})$$

$$f_{\max} = 0.224 N^{0.29} \quad (\text{tsf})$$

These equations give:

$$Q_p = 19.75 (25)^{0.36} \times 1.78 = 112 \text{ tons (997 kN)}$$

$$Q_s = 0.224 (25)^{0.26} \times 1.33 \times 4 \times L = 3.03 L$$

$$Q_T = 225 \text{ tons (2002.5 kN)}$$

This yields an equation for the pile length of:

$$112 + 3.03 L = 225 \quad \text{which gives } L = 37.3 \text{ ft (11.4 m)}$$

This represents a savings of 9%.

Problem 2: Same as Problem 1 but the working load is now 150 tons (4005 kN)

1. Considering no residual stresses

The equation for pile length is:

$$83.9 + 3.43 L = 450 \quad \text{which gives } L = 106.7 \text{ ft (32.5 m)}$$



## 2. Considering residual stresses

The equation for pile length is:

$$112 + 3.03 L = 450 \quad \text{which gives } L = 111.6 \text{ ft (34.0 m)}$$

The pile must be lengthened about 4%.

The above example points out the potential cost saving of considering residual stresses in design. The consideration of residual stresses in the interpretation of compression load tests on piles driven through sand into sand leads to higher point loads and lower friction loads. Very long piles rely essentially on friction to develop the resistance to load; as a result very long piles driven through sand into sand will be underdesigned if use is made of design methods that ignore residual stresses. Very long piles driven through clay into sand however, will be overdesigned as far as the point load is concerned, if use is made of design methods that ignore residual stresses; this is based on the assumption that residual stresses play a minor role in the interpretation of pile load tests in clay. Short piles on the other hand, rely more on point bearing to develop the resistance to load than do very long piles; as a result, short piles driven through sand or clay into sand will generally be overdesigned if use is made of design methods that ignore residual stresses.

The point at which the reduction in friction load equals the increase in point load is a function of the pile size and the soil strength. The larger the pile, the deeper the breakeven point will be. Also, the stronger the soil, the deeper the breakeven point will be.

### Developing an optimum method of design

The errors involved in the prediction of the capacity of a pile foundation are due to the following factors:

- soil heterogeneity.
- precision of soil test.
- adequacy of soil test.
- precision of design method.
- construction activity.

These factors are discussed one by one in the following paragraphs.

Minimizing the error due to soil heterogeneity while optimizing costs is related to the minimum number of borings necessary to obtain a satisfactory level of confidence on the soil variability at a site. At Lock and Dam No. 26 there was very little to be gained from performing more than 6 borings for the selected 400 ft x 200 ft area. Beyond this number of borings a pile load test would be more beneficial than added borings.

The SPT is not a precise soil test. This situation can be improved by the use of free fall hammers and/or of energy measuring devices at the top of the rods. The PMT can be a precise soil test if the borehole is performed by drillers who have gathered long experience with PMT borehole preparation. The PMT can be performed in almost all soils. The CPT cannot be performed in all soils, but has the definite advantage of being a very precise soil test.

The SPT is a test which simulates the driving of the pile (except in very loose to loose sand as discussed earlier). The CPT is a test which simulates the loading of the pile. The PMT is a test which gives information on deformation characteristics. It is suggested that a combination of those three tests would give an optimum in soil testing adequacy. The dynamic pressio-penetrometer probe is shown in Fig. 112.

The technology for such a probe has already been developed (3). The testing sequence would be as follows:

1. Drive the probe to the first testing depth and stop.
2. Push the probe 0.5 in. (1.3 cm) at a slow rate of penetration
3. Repeat 1 and 2 at the other testing depths.

The measurements would be the point and friction resistance on the penetrometer, the radial stress on the pressuremeter and the displacement at the surface. Recording of the measurements during step 1 would give valuable information for wave equation analysis. The measurements at the end of step 1 would give valuable information on residual stresses. Step 2 measurements would give the data necessary for static analysis: residual stresses would automatically be included because of the continuous record of point resistance with the electric cone. Every so often a pressuremeter test would be performed in order to

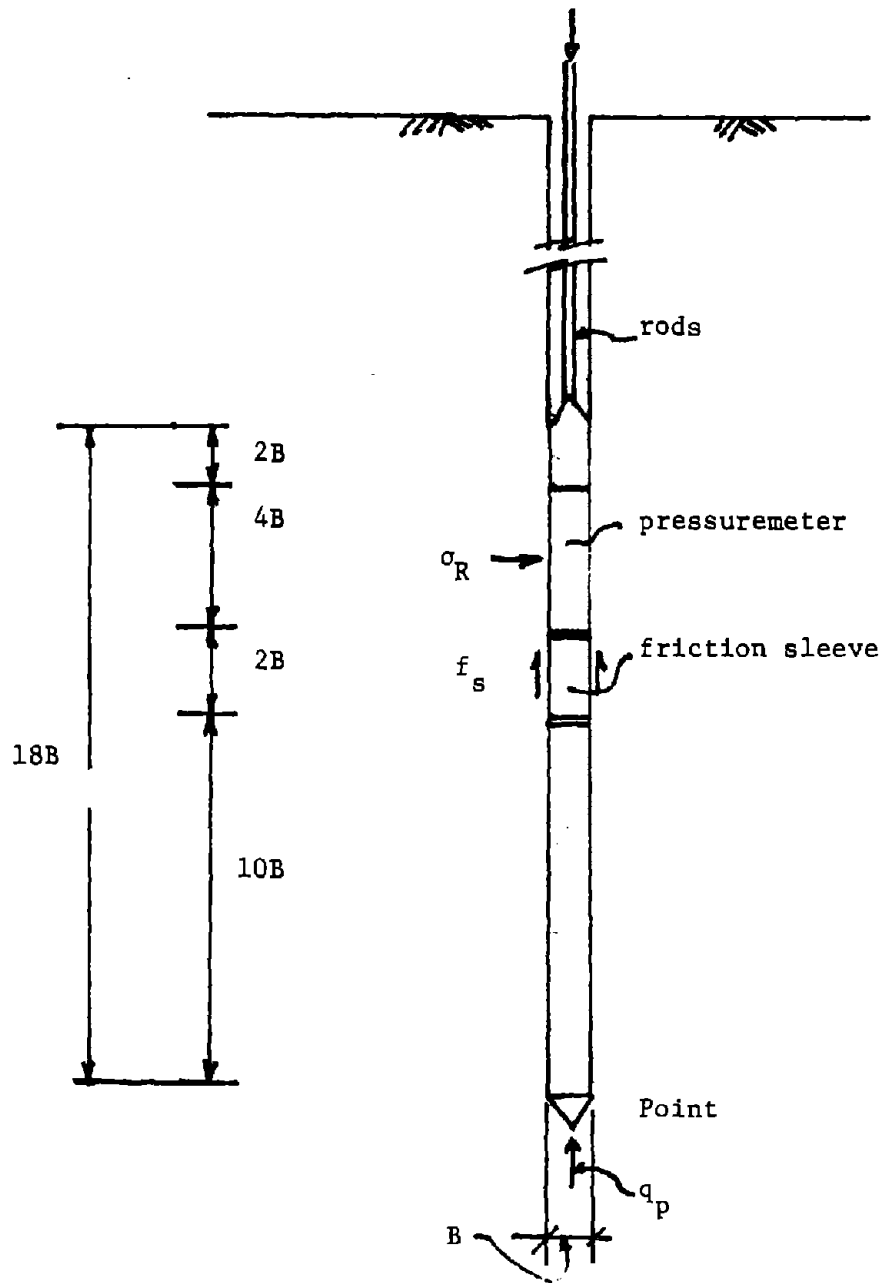


FIG. 112.- The Dynamic Pressure Penetrometer (DYPP)

obtain soil deformation characteristics and information for lateral loads if necessary. The fact that the probe is driven in the soil would allow to penetrate soils which would otherwise not be penetrated by a continuous push.

The precision of the design method is influenced by the soil heterogeneity, the precision of the soil test, the adequacy of the soil test. It is also influenced by the precision of the load tests results forming the data base for that method and by the adequacy of the design mechanism which links the measured soil parameter to the sizing of the pile. This mechanism is based either on theory, empiricism, analogy or a combination thereof. Theoretical methods rely on the undisturbed characteristics of the soil and simulate the driving process before predicting the load-displacement response of the pile. These methods present ultimately the most sound approach to the problem, and should be pursued. These methods are presently unsatisfactory however, because they require the knowledge of too many soil parameters which are difficult to measure accurately with current technology. Empirical methods are easy to develop and usually easy to use. Empirical methods which have the least number of intermediary steps have the least chance of error. However, methods which use the blow count  $N$  to obtain the relative density  $D_R$  to then obtain the friction angle  $\phi$ , to then obtain the bearing capacity factor  $N_q$ , to then obtain the value of  $q_{max}$  are accumulating imprecision in each of the steps using empirical correlations. Empirical methods are always questionable outside the data base on which they were developed.

Methods based on testing analogy present the best short term payoff for driven piles in sand. The SPT and CPT are tests which represent a partial testing analogy with the driven pile. The proposed dynamic pressio-penetrometer test represents a nearly complete analogy of the driven pile and includes all influencing factors.

Construction activities such as inadvertent batter, heave and subsequent re-driving of adjacent piles, method and order of driving will influence the accuracy of the pile capacity. It is very difficult to incorporate in a reliable fashion all those factors in the method of design. These factors can best be incorporated by making use of the pile driving records while construction proceeds in order to assess the

"as built" capacity of the foundation. The wave equation is very useful in this respect, especially if force time input are available and if the soil model is available from previous tests with the proposed dynamic pressio-penetrometer. As construction progresses, the engineer can evaluate the foundation capacity and may decide to decrease (or increase) the number of piles originally planned. This requires a flexibility in the pile driving contract which is not presently described in most specifications, but which has already been used in the offshore environment and has resulted in great savings to the client. This approach also requires a careful planning of the order of driving in a joint effort by the engineer and the contractor.

## CHAPTER XII - SUMMARY, CONCLUSIONS AND RECOMMENDATIONS

### SUMMARY AND CONCLUSIONS

The purpose of this study was to advance the state of knowledge on the behavior of piles and pile groups in cohesionless soils and to make recommendations for further research in this area. The project was limited to the study of existing data on instrumented piles, hammer driven and load tested vertically.

#### Pile Load Tests Selected

A total of 35 load tests at 10 different sites were selected as a data base (Table 1). The piles were of various types: steel pipe, steel H, prestressed concrete or timber. Their diameter averaged 1.29 foot and their length, 49.6 ft. The ultimate vertical load was determined by three criteria: Davisson's,  $0.1 \times D$  and hyperbolic asymptote (Table 2). The average ultimate load for all the piles considered, was 192 tons for Davisson's criterion, 228 tons for the  $0.1 \times D$  criterion, and 264 tons for the hyperbolic asymptote criterion. The maximum load applied during the tests averaged 222 tons.

Due to a lack of full scale group load tests in sand, much reliance has been made on model studies. These studies indicate that group efficiencies in sand are almost always equal to or greater than one. This conclusion is verified for driven piles by the full scale pile group tests available (29).

The only instrumented full scale load test reported in the literature used partially jettted timber piles (43,44). In addition to this the group was subjected to various preloading conditions which may have had a drastic effect on the load transfer behavior of the piles. The side friction for the group piles was significantly lower than the friction on the single pile and the point loads were much higher. The large model tests performed by Vesic (40) showed the opposite to this. On these groups the friction was more than twice the friction on the single piles and the point loads were approximately equal. These conflicting results point out the need for carefully performed load

tests on well instrumented full scale pile groups which include measurements of residual loads.

A preliminary report on the West Seattle Freeway Bridge Project (35) gives some measurements of residual point loads on driven piles. The residual point loads, on 92 ft (28 m) long piles immediately after driving were about 60 tons (598 kN). Subsequent driving of piles in the group did not reduce the residual point load on the pile.

### Conventional Load Transfer Analysis

Measurement of movements with strain rods and measurement of strains with strain gages lead to the calculation of loads in the pile at various depth along the pile. The slope of this discrete profile of load in the pile leads to values of mobilized friction. This derivation process introduces great scatter in the friction values which, cumulated with errors in the measurements, leads to meaningless friction transfer f-w curves. A curve fitting method on the load profile would lead to smoother f-w curves but would introduce an arbitrary massaging of the data. This problem and the overall lack of sufficient precision in the measurements lead to the choice of an average analysis (Chapter III) where an average friction value was calculated for the entire pile shaft. The hyperbolic model fits that f-w curve very well with most of the friction being mobilized at a pile movement of 0.15 in. or 1% of the pile diameter. The hyperbolic model also fits the point pressure transfer q-w curve very well with 50% of the point resistance being mobilized at a point movement of 0.3 in. or 2% of the pile diameter and 90% of the point resistance being mobilized at a point movement of 1.5 in. or 10% of the pile diameter. The equations for these hyperbolic transfer curves are:

$$f = \frac{w}{\frac{1}{K_t} + \frac{w}{f_{\max} + f_{\max}}}$$

$$q = \frac{w}{\frac{1}{K_p} + \frac{w}{q_{\max} - q_{\text{res}}}}$$

### Residual Stresses: Basic Considerations

The phenomenon of residual stresses in a pile takes place upon unloading of that pile after either a hammer blow, a compression test, or a tension test. A theoretical formulation of this unloading process, based on the fundamental differential equation, is presented. The solution indicates the following influence of various factors:

1. The longer the pile, the larger the residual point load.
2. The more compressible the pile, the larger the residual point load.
3. The steeper the unloading slope of the friction transfer curve, the larger the residual point load.
4. The softer the unloading slope of the point pressure transfer curve, the larger the residual point load.

It was shown that the distribution of residual loads and residual stresses in a pile is directly related to distribution of ultimate loads and ultimate stresses in that pile and that residual loads after a tension test are not zero but are much smaller than those after a compression test.

### Obtaining Residual Stresses From Load Tests

In conventional load tests the instrumentation is zeroed after the pile is driven thereby assuming that the pile is stress free before the start of the test. At least four methods exist to obtain residual loads from pile load tests. The first one consists of zeroing the instrumentation before driving and reading the instrumentation after driving. The three others consist of zeroing the instrumentation after driving the pile and before performing the compression test and then making use of various combination of instrumentation readings for the tension test and for the pile state of stress in the unloaded condition (Chapter V).

The results of this residual stress analysis are summarized in Table 7. These results indicate that the residual point load varies from 11% to 54% of the true ultimate point load and averages 36%. This means that on the average the true ultimate point load for those hammer



driven piles in sand is equal to 1.56 times the ultimate point load measured in a conventional load test. At the same time the true ultimate friction load averaged 0.81 times the ultimate friction load measured in a conventional load test.

This residual stress analysis also allowed to calculate the ratio of the true ultimate friction load in tension over the true ultimate friction load in compression. It was found (Fig. 28) that for short piles, tapered piles, and H piles this ratio is less than one, but that for straight shaft piles longer than about 50 ft this ratio may be more than one.

#### Obtaining Residual Stresses with the Wave Equation

The wave equation was used to predict residual stresses in the pile after driving. A multiple blow analysis was used together with the conventional linear elastic-plastic model ( $Q_{\text{side}} = Q_{\text{point}} = 0.1$  in.,  $J_{\text{point}} = 0.15$  sec/ft,  $J_{\text{side}} = 0.05$  sec/ft). A minimum of 5 blows with 1000 time steps per blow is necessary to obtain valid results. The residual point load  $Q_{p(\text{res})}$  is obtained by plotting  $Q_{p(\text{res})}$  versus time steps for all blows and determining the  $Q_{p(\text{res})}$  about which the oscillations take place.

This method was used on the piles where  $Q_{p(\text{res})}$  was measured. The ratio of  $Q_{p(\text{res})}$  predicted over  $Q_{p(\text{res})}$  measured had a mean of 1.12 and a coefficient of variation of 0.66.

#### Load Transfer Analysis by Finite Difference- Pattern Search Approach

This approach was taken in an effort to develop depth dependent friction and point transfer curves while minimizing the error made in the regression analysis. The general differential equation for the pile-soil system was developed and assumptions were made for the constitutive models for the pile and the soil. The pile model was linear elastic. The point soil resistance model and the friction model were hyperbolic models. For the friction model, the initial slope and the ultimate friction value were assumed to vary as a power law of the depth. The friction hyperbolic model was cut off at a limiting

friction value. The residual stresses after driving were assumed to have a damped sinusoidal distribution with depth. This led to a total of nine constants to be determined by a best fit regression on the load test data.

The finite difference method was used to solve the differential equation together with a powerful pattern search program to find the best fit values of the nine constants by minimizing in the 9 dimensional space the error between the pile loads calculated using the 9 constants models and the measured pile loads. A program was developed for this method and reasonable answers were obtained (Tables 8, 9, 10). More work is necessary however, to bring this method to the level of usefulness that it promises to be.

#### A New Design Method Considering Residual Stresses

Due to the lack of other soil data at the sites, only the SPT uncorrected blow count,  $N$ , was used in the correlations. The point residual pressure correlated best with the parameter,  $L\beta$ , a key parameter in the solution to the governing differential equation. This parameter is the product of the pile length  $L$  by the relative soil pile stiffness factor,  $\beta$ , (Chapter VII).

$$q_{res} = 5.57 L\beta \quad \text{in tsf}$$

where

$$\beta = \sqrt{\frac{K_t P}{AE_p}}$$

$P$  = perimeter of pile

$A$  = cross-sectional area of pile

$E_p$  = modulus of elasticity of the pile

The following correlations were also found

$$q_{max} = 19.75 (N_{pt})^{0.36} \quad \text{in tsf}$$

$$K_p = 5.05 (N_{pt})^{0.247} \quad \text{in tsf}$$

$$f_{\max} = 0.224 (N_{\text{side}})^{0.29} \quad \text{in tsf}$$

$$K_{\tau} = 5.01 (N_{\text{side}})^{0.27} \quad \text{in tsf/in.}$$

where  $q_{\max}$  and  $f_{\max}$  are the true ultimate point pressure and friction.

$q_{\text{res}}$  is the residual point pressure after driving

$K_p$  is the initial slope of the hyperbolic q-w curve

$K_{\tau}$  is the initial slope of the hyperbolic f-w curve

$N_{\text{pt}}$  and  $N_{\text{side}}$  are the average uncorrected SPT blow count values in the pile point and pile shaft respectively.

The precision of these correlations can be observed from the figures of Chapter VIII. These correlations were used to develop a new design method to predict the entire load settlement curve for the pile. This method is the first such method based on friction and point transfer curves, which include residual stresses. The equations for the hyperbolic f-w and q-w curves are:

$$f = \frac{w}{\frac{1}{K_{\tau}} + \frac{w}{f_{\max} + f_{\text{res}}}} - f_{\text{res}}$$

and

$$q = \frac{w}{\frac{1}{K_p} + \frac{w}{q_{\max} - q_{\text{res}}}} + q_{\text{res}}$$

The correlations above are used to find  $q_{\max}$ ,  $f_{\max}$ ,  $q_{\text{res}}$ ,  $K_{\tau}$  and  $K_p$ . The residual friction,  $f_{\text{res}}$ , is found by

$$f_{\text{res}} = q_{\text{res}} \frac{A_p}{A_s}$$

### Predictions by Conventional Methods

Conventional methods to predict the ultimate capacity of a driven pile in sand were used. These were Meyerhof method, API method, Coyle & Castello method. The results show that on the average the API method is 10% conservative, Meyerhof method is 37% unconservative, Coyle and Castello method is 2% conservative. The coefficient of variation for these methods is approximately 0.45 and the coefficient by which to multiply the mean predicted ultimate load to obtain a 90% confidence ultimate load averages 0.3. The detailed results are shown in Table 17 of Chapter IX.

A method developed by Coyle was also used to predict the load settlement curve for the pile. This method recommends the use of a very simple friction transfer and point load transfer curve (Tables 18 and 19) and gave reasonably accurate results for its simplicity (Figs. 54 to 76).

### Predictions by the Cone Penetrometer and the Pressuremeter Methods

Three pressuremeter methods and four cone penetrometer methods were used to predict the ultimate capacity of the piles at the few sites where PMT and CPT data was available. These methods were:

- |     |   |                           |
|-----|---|---------------------------|
| PMT | 1 | Menard                    |
|     | 2 | Baguelin-Jezequel-Shields |
|     | 3 | Bustamante-Gianeselli     |
| CPT | 1 | DeRuiter-Beringen         |
|     | 2 | Schmertmann               |
|     | 3 | Bustamante-Gianeselli     |
|     | 4 | Cone Method               |

The results are shown in Table 26 of Chapter X.

Pressuremeter data was available at two sites. The Bustamante-Gianeselli method gave the best predictions with the other two methods being unconservative. For the CPT predictions the Bustamante-Gianeselli method again gave the best results with a ratio of predicted total load over measured total load which averaged 1.06. The averages for the other methods are: DeRuiter-Beringen, 0.75; Schmertmann, 0.93;

Cone, 1.20. These methods however, underestimated friction and overestimated point load by a factor of about 2, whereas the Bustamante-Gianeselli method averaged 1.23 and 1.32 ratios for predicted overmeasured point and side load respectively.

Three pressuremeter methods and one cone penetrometer method were used to predict the load-settlement curve for the piles. These methods where

- |     |   |   |
|-----|---|---|
| PMT | 1 | Menard-Gambin   |
|     | 2 | Baguelin-Jezequel-Shields/<br>Baguelin-Frank-Jezequel |
|     | 3 | Bustamante-Gianeselli/<br>Frank-Zhao                  |
| CPT | 1 | Verbrugge   |

The CPT Verbrugge method gave good predictions of the load settlement curve. The closest PMT predictions were obtained with Bustamante methods.

#### Improving the State of the Practice

An optimum method of design is one that minimizes in a cost effective fashion. The behavior prediction errors due to soil heterogeneity, precision of the soil test, adequacy of the soil test, precision of the design method and construction activity. There is an optimum number of boring to characterize soil variability at a site. At Lock and Dam No. 26, this number was 6 borings for a 400 x 200 ft (122 m x 61 m) area. Beyond this number a pile load test would be more beneficial than added borings.

An analysis at Lock and Dam 26 site shows that at a given site the precision on the soil parameters measured with the SPT, PMT and CPT is approximately the same and that only the cross-hole shear wave velocity shear modulus shows an increased precision. However, the repeatability of the tests from one site to another and from one operator to another is not included in the above analysis and it is argued that the rating of repeatability of these tests would be; 1. Cross-hole shear wave velocity and cone penetrometer, 2. Pressuremeter, 3. Standard Penetration Test. Other factors not included in the above analysis and important to consider before choosing one test over another are whether the soil parameter measured is representative of the phenomenon to be

predicted, whether the test is cost effective and whether the test can be performed in all soil conditions.

It appears that the CPT is the more precise and repeatable test and offers the best potential for improved ultimate capacity predictions. Design methods based on testing analogy have the best potential for short term success for driven piles in sands. Therefore, a dynamic Pressio Penetrometer (DYPP) Test which would simulate the driving and then the loading of the pile, is proposed.

Residual stresses play an important role in pile design and must be considered in any future design method. The influence of construction activities and other uncertainties can best be incorporated by making use of the pile driving records while construction proceeds in order to assess the "as built" capacity of the foundation. This in turn may provide significant savings to the client.

#### RECOMMENDATIONS FOR FURTHER RESEARCH

Residual stresses play an important role in the behavior of driven piles in sands and appear to lead to shorter onshore pile lengths when they are properly considered. At the same time the current data base on precisely and reliably instrumented driven piles in sand is extremely weak. Therefore there is a need to perform full scale load tests on piles instrumented in such a way that residual stresses can be determined accurately. In this respect, more pile behavior case histories such as the West Seattle Freeway Bridge project must be encouraged. There is need at the same time for continuing to develop the theoretical analyses of the residual stress phenomenon such as the wave equation analysis.

For the immediate future, the method of design by analogy is the most promising method to predict the behavior of driven piles in sand. While awaiting the further development of theoretical methods, and because the SPT is not at present a sufficiently repeatable test, it is recommended to develop a dynamic pressio-penetrometer test which would be driven in place to simulate the driving of the pile and then pushed to record the load transfer characteristics of the sand. It would be driven and pushed in place by conventional drilling rigs.

More precise use of the pile driving and redriving records should be made to evaluate the "as built" capacity of the foundation while the piles are driven. There is evidence to show that flexibility in the pile driving contract, well planned order of driving, together with a close on site cooperation between the geotechnical engineer and the pile driving contractor, can lead to significant savings to the client.

The data on residual stresses in groups of piles is inexistent with the exception of the ongoing West Seattle Bridge project. There is a need to investigate whether residual stresses are released or if additional residual stresses are locked in during the driving of additional piles. No full scale test on groups of driven piles loaded to failure and sufficiently instrumented to determine the evolution of residual stresses exists.

## REFERENCES

1. American Petroleum Institute, Recommended Practice for Planning, Designing, and Constructing Fixed Offshore Platforms, API RP 2A, 13th Edition, 1982.
2. Baguelin, F., Frank, R., and Jezequel, J.F., "Parameters for Friction Piles in Marine Soils," Proceedings, Second Annual Int. Conf. on Numerical Methods in Offshore Piling, Austin, Apr., 1982, pp. 197-214.
3. Baguelin, F.J., and Jezequel, J.-F., "The LPC Pressiopenetrometer," Proceedings, ASCE Conference on Geotechnical Practice in Offshore Engineering, Apr., 1983, pp. 203-219.
4. Baguelin, F., Jezequel, J.-F., and Shields, D.H., The Pressure-meter and Foundation Engineering, Trans Tech Publications, Rockport, Mass., 1978.
5. Bjerrum, L., "Embankments on Soft Ground: State-of-the-Art Report," Proceedings, ASCE Specialty Conference on Performance of Earth and Earth Supported Structures, Vol. 2, 1972.
6. Bowles, J.E., Foundation Analysis and Design, 3rd Edition, McGraw-Hill, 1982
7. Briaud, J.-L, and Shields, D.H., "A Special Pressure Meter and Pressure Meter Test for Pavement Evaluation and Design," Geotechnical Testing Journal, ASTM, Vol. 2, No. 3, Sept., 1979.
8. Bustamante, X., and Gianceselli, L., "Prevision de la Capacite Portante des Pieux Isoles sous Charge Verticale," Bull. de liaison, Lab. des Ponts et Chaussees, No. 113, Paris, May-June, 1981.
9. Bustamante, X., and Gianceselli, L., "Portance Reelle et Portance Calculee des Pieux Isoles, Sollicites Verticalement," Revue Francaise de Geotechnique, No. 16, August, 1981.
10. Coyle, H.M., Unpublished Class Notes, Graduate Course on Deep Foundation Engineering - CE687, Texas A&M University, 1979-1983.
11. Coyle, H.M., Bartoskewitz, R.E., and Berger, W.J., "Bearing Capacity Prediction by Wave Equation Analysis - State of the Art," Research Report No. 125-8, Texas Transportation Institute, Texas A&M University, August, 1973.
12. Coyle, H.M., and Castello, R., "New Design Correlations for Piles in Sand," Journal of the Geotechnical Engineering Division, ASCE, Vol. 107, No. GT7, July, 1981, pp. 965-986



13. Coyle, H.M., and Reese, L.C., "Load Transfer for Axially Loaded Piles in Clay," Journal of the Soil Mechanics and Foundations Division, ASCE, Vol. 92, No. SM2, March, 1966.
14. Davisson, M.T., "High Capacity Piles," Proceedings, ASCE Lecture Series, Innovations in Foundation Construction, Illinois Section, 1972.
15. DeRuiter, J., and Beringen, F.L., "Pile Foundations for Large North Sea Structures," Marine Geotechnology, Vol. 3, No. 3, 1979.
16. Frank, R., and Zhao, "Estimation, par les Parametres Pressiométriques, de l'Enfoncement sous Charge Axiale de Pieux Fores dans des Sols Fins," Bull, de Liaison, Lab. des ponts et Chaussees, No. 119, Paris, May-June, 1982.
17. Fruco and Associates, "Pile Driving and Loading Tests," Report for Corps of Engineers, Little Rock, Arkansas, September, 1964.
18. Fruco and Associates, "Overwater Steel H-pile Driving and Testing Program," Report for Corps of Engineers, St. Louis, Missouri, September, 1973.
19. Gambin, M., "Calcul du Tassement d'une Foundation Profonde en Fonction des Resultats Pressiométriques," Sols-Soils, No. 30/31, 1979.
20. Gregersen, O.S., Aas, G., and DiBiaggio, E., "Load Tests on Friction Piles in Loose Sand," Proceedings of the VII International Conference on Soil Mechanics and Foundation Engineering, Moscow, Vol. 2.1, 1973, pp. 19-27.
21. Hirsch, T.J., Carr, L., and Lowery, L.L., Jr., "Pile Driving Analysis-Wave Equation Users Manual," Report No. 76-13.2, U.S. Dept. of Transportation, Wash., D.C., Apr., 1976.
22. Holloway, D.M., Clough, G.W., and Vesic, A.S., "The Mechanics of Pile-Soil Interaction in Cohesionless Soils," Report for Corps of Engineers, Vicksburg, Miss., Dec., 1975.
23. Hunter, A.H., and Davisson, M.T., "Measurements of Pile Load Transfer," Performance of Deep Foundations, ASTM STP 444, 1969, pp. 106-117.
24. Mansur, C.I., and Hunter, A.H., "Pile Tests - Arkansas River Project," Journal of the Soil Mechanics and Foundation Division, ASCE, Vol. 96, No. SM5, September, 1970, pp. 1545-1582.
25. Mansur, C.E., and Kaufman, R.I., "Pile Tests, Low-Sill Structure, Old River, Louisiana," Transactions of ASCE, Vol. 123, 1958, pp. 715-748.

26. Menard, L., "The Menard Pressuremeter: Interpretation and Application of Pressuremeter Test Results to Foundation Design," General Memorandum, Sols-Soils, No. 26, 1975.
27. Meyerhof, G.G., "Bearing Capacity and Settlement of Pile Foundations," Journal of the Geotechnical Engineering Division, ASCE. Vol. 102, No. GT3, Mar., 1976, pp. 197-228.
28. Peck, R.B., Hanson, W.E., and Thornburn, T.H., Foundation Engineering, 2nd Edition, Wiley & Sons, 1974.
29. O'Neill, M.W., "Group Action in Offshore Piles," Proceedings, ASCE Conference on Geotechnical Practice in Offshore Engineering, Apr., 1983, pp. 25-64.
30. Olson, R.E., and Dennis, N.D., "Review and Compilation of Pile Test Results - Axial Pile Capacity," Final Report Project 81-29, American Petroleum Institute, 1982.
31. Schmertmann, J.H., "Guidelines for Cone Penetration Test Performance and Design," U.S. Dept. of Transportation, FHWA, Report No. FHWA-TS-78-209, 1978.
32. Sellgren, E., "Friction Piles in Non-Cohesive Soils. Evaluation from Pressuremeter Tests," Thesis, Chalmers University of Technology, Goteborg, Sweden, 1982.
33. Shannon & Wilson, Inc., "Geotechnical Engineering Studies: West Seattle Freeway Bridge Replacement," Report for Anderson-Bjornstad-Kane-Jacobs, Inc., Vol. 2, August, 1980.
34. Shannon & Wilson, Inc., "Instrumentation Installation and Initial Monitoring Pier EA-31," Report for City of Seattle, FHWA (Progress Report 1), November, 1982.
35. Smith, E.A.L., "Impact and Longitudinal Wave Transmission," Transactions, ASME, August, 1955, p. 963.
36. Smith, E.A.L., "Pile Driving Analysis by the Wave Equation," Transactions, ASCE, Vol. 127, 1964, Part I, p. 1145.
37. Tavenas, F.A., "Load Tests on Friction Piles in Sand," Canadian Geotechnical Journal, Vol. 8, No. 7, 1971, p. 7-22.
38. Verbrugge, J.C., "Evaluation du Tassement des Pieux a Partir de l'Essai de Penetration Statique," Revue Francaise de Geotechnique, No. 15, May, 1981, pp. 75-82.
39. Vesic, A.S., "A Study of Bearing Capacity of Deep Foundations," Project B-189 (Final Report), Georgia Institute of Technology August, 1966.

40. Vesic, A.S., "Experiments with Instrumented Pile Groups in Sand," Performance of Deep Foundations, ASTM STP 444, 1969.
41. Vesic, A.S., "Tests on Instrumented Piles, Ogeechee River Site," Journal of the Soil Mechanics and Foundation Divisions, ASCE, Vol. 96, No. SM2, March, 1970, pp. 561-583.
42. Vesic, A.S., "Design of Pile Foundations," NCHRP Synthesis of Highway Practice, No. 42, Transportation Research Board, 1977, p. 10.
43. Woodward-Clyde Consultants, "Results and Interpretation of Pile Driving Effects Test Program," Phase IV Report for Corps of Engineers, Vol. III, St. Louis, Missouri, July, 1979.
44. Woodward-Clyde Consultants, "Axial Load Tests Monoliths M5 and M6," Supplemental Report to Corps of Engineers, St. Louis, Missouri, February. 1980.



## FEDERALLY COORDINATED PROGRAM (FCP) OF HIGHWAY RESEARCH, DEVELOPMENT, AND TECHNOLOGY

The Offices of Research, Development, and Technology (RD&T) of the Federal Highway Administration (FHWA) are responsible for a broad research, development, and technology transfer program. This program is accomplished using numerous methods of funding and management. The efforts include work done in-house by RD&T staff, contracts using administrative funds, and a Federal-aid program conducted by or through State highway or transportation agencies, which include the Highway Planning and Research (HP&R) program, the National Cooperative Highway Research Program (NCHRP) managed by the Transportation Research Board, and the one-half of one percent training program conducted by the National Highway Institute.

The FCP is a carefully selected group of projects, separated into broad categories, formulated to use research, development, and technology transfer resources to obtain solutions to urgent national highway problems.

The diagonal double stripe on the cover of this report represents a highway. It is color-coded to identify the FCP category to which the report's subject pertains. A red stripe indicates category 1, dark blue for category 2, light blue for category 3, brown for category 4, gray for category 5, and green for category 9.

### *FCP Category Descriptions*

#### **1. Highway Design and Operation for Safety**

Safety RD&T addresses problems associated with the responsibilities of the FHWA under the Highway Safety Act. It includes investigation of appropriate design standards, roadside hardware, traffic control devices, and collection or analysis of physical and scientific data for the formulation of improved safety regulations to better protect all motorists, bicycles, and pedestrians.

#### **2. Traffic Control and Management**

Traffic RD&T is concerned with increasing the operational efficiency of existing highways by advancing technology and balancing the demand-capacity relationship through traffic management techniques such as bus and carpool preferential treatment, coordinated signal timing, motorist information, and rerouting of traffic.

#### **3. Highway Operations**

This category addresses preserving the Nation's highways, natural resources, and community attributes. It includes activities in physical

maintenance, traffic services for maintenance zoning, management of human resources and equipment, and identification of highway elements that affect the quality of the human environment. The goals of projects within this category are to maximize operational efficiency and safety to the traveling public while conserving resources and reducing adverse highway and traffic impacts through protections and enhancement of environmental features.

#### **4. Pavement Design, Construction, and Management**

Pavement RD&T is concerned with pavement design and rehabilitation methods and procedures, construction technology, recycled highway materials, improved pavement binders, and improved pavement management. The goals will emphasize improvements to highway performance over the network's life cycle, thus extending maintenance-free operation and maximizing benefits. Specific areas of effort will include material characterizations, pavement damage predictions, methods to minimize local pavement defects, quality control specifications, long-term pavement monitoring, and life cycle cost analyses.

#### **5. Structural Design and Hydraulics**

Structural RD&T is concerned with furthering the latest technological advances in structural and hydraulic designs, fabrication processes, and construction techniques to provide safe, efficient highway structures at reasonable costs. This category deals with bridge superstructures, earth structures, foundations, culverts, river mechanics, and hydraulics. In addition, it includes material aspects of structures (metal and concrete) along with their protection from corrosive or degrading environments.

#### **9. RD&T Management and Coordination**

Activities in this category include fundamental work for new concepts and system characterization before the investigation reaches a point where it is incorporated within other categories of the FCP. Concepts on the feasibility of new technology for highway safety are included in this category. RD&T reports not within other FCP projects will be published as Category 9 projects.

B73  
~~11~~